THE UNIVERSITY OF MANITOBA

A STUDY OF DEVELOPING TURBULENT PIPE FLOW

by

J. K. REICHERT

A THESIS

SUBMITTED TO THE FACULTY OF GRADUATE STUDIES IN PARTIAL FULFILLMENT OF THE REQUIREMENTS FOR THE DEGREE OF DOCTOR OF PHILOSOPHY

DEPARTMENT OF MECHANICAL ENGINEERING

WINNIPEG, MANITOBA
MARCH, 1977

"A STUDY OF DEVELOPING TURBULENT PIPE FLOW"

by

J. K. REICHERT

A dissertation submitted to the Faculty of Graduate Studies of the University of Manitoba in partial fulfillment of the requirements of the degree of

DOCTOR OF PHILOSOPHY

ABSTRACT

An experimental investigation of the structure of steady, axisymmetric, incompressible developing turbulent pipe flow was undertaken. Profile measurements of the mean U velocity component exhibited nonasymptotic development. A U component peak which exceeded more developed values occurred along the pipe centerline. The Reynolds number behavior of the peak was determined. Hot wire measurements of turbulent energy and shear stress spectra and the terms in the axisymmetric Reynolds stress tensor were taken for a Reynolds number of 54900, based on bulk velocity and pipe radius. Contour plots were generated from the survey of the mean and turbulence fields. The results were compared with previous evidence for nonasymptotic development. The nonasymptotic turbulent field behavior appeared to be a response to the mean flow development. The terms appearing in the mean turbulent energy balance equation were calculated and their behavior over the developing flow field was presented in contour form. The complex development of small magnitude energy balance terms which are often neglected was exhibited by the contouring procedure. Contouring indicated the importance of the boundary layer interface for the nonasymptotic development. Hot wire measurements of statistical moments of u and v plus quadrant sampling of the Reynolds stress were presented for this region.

These measurements and the analysis of oscilloscope photographs of individual events were consistent with previous models. The presence of velocity fluctuations in the core, which were induced by turbulent bulges, suggested that the turbulent-nonturbulent interface acted as a contraction surface for the core flow, causing it to accelerate.

ACKNOWLEDGEMENTS

The author would like to thank Dr. R. S. Azad for the guidance and direction which he has provided during the course of this work. Special thanks are expressed to Mr. R. H. Hummel for helpful discussion and technical advice. The contribution of Mr. S. Arora is also gratefully acknowledged.

The assistance provided by Ms. J. Cook and Mrs. P. Giardino in preparing and typing the manuscript is appreciated.

The financial assistance of the taxpayers of Canada through the National Research Council of Canada Postgraduate Scholarship Program is gratefully acknowledged.

TABLE OF CONTENTS

Page

LIST OF TABLES

LIST OF FIGURES

NOMENCLATURE

A	Eulerian longitudinal integral scale
d	hot wire diameter
$\mathbb{C}$	pipe centerline
D	pipe diameter
E_i	one dimensional wave number spectra ($i = 1, 2,$ or 3)
f	frequency
F_u	flatness factor of u
F_v	flatness factor of v
G	nondimensional second derivative
H	shape factor
i	subscript; $i = 1, 2,$ or 3 for u, v, or w respectively
j	subscript; $j = 1, 2,$ or 3 for u, v, or w respectively
k	wave number
k_i	wave number component ($i = 1, 2,$ or 3)
l_w	sensitive length of a hot wire
P, p	total pressure
P_s	static pressure
$\overline{q^2}$	mean square of turbulent kinetic energy; $\overline{q^2} = \overline{u^2} + \overline{v^2} + \overline{w^2}$
R, r	pipe radius
Re	Reynolds number; $Re = \frac{U_B R}{\nu}$
R_λ	turbulence Reynolds number
S	skewness factor of $\frac{\partial u}{\partial t}$

S_u skewness factor of u

S_v skewness factor of v

$S(t)$ an indicator function; $S(t) = 0$ or 1

u fluctuating longitudinal velocity component

uv fluctuating Reynolds stress; $uv = u \cdot v$

u_+v_- contribution to uv from positive u and negative v quadrant of the u-v plane; $u_+v_- = uv$ if u is positive and v is negative, $u_+v_- = 0$ otherwise

u_+v_+ similar to u_+v_- but for u positive and v positive quadrant

u_-v_- similar to u_+v_- but for u negative and v negative quadrant

u_-v_+ similar to u_+v_- but for u negative and v positive quadrant

U mean longitudinal velocity component

U_B bulk velocity

U_c centerline velocity

$\overline{U_L}$ local mean velocity

U_m mean velocity ($= U_B$)

U_* friction velocity

v fluctuating radial velocity component

V mean radial velocity component

w fluctuating circumferential velocity component

x longitudinal co-ordinate; $x = 0$ at upstream edge of the trip

x_p mean longitudinal velocity overshoot position on the centerline

y radial co-ordinate; $y = 0$ on pipe axis

y' radial co-ordinate; $y' = 0$ at pipe wall ($y' = R-y$)

α_i one dimensional Kolmogorov inertial subrange constant; $\alpha_i = (k_1\eta)^{5/3}\ \Phi_i\ (k_1\eta)$

α_p angular direction of the greatest principal stress

γ intermittency factor

δ displacement thickness or a boundary layer thickness estimate

ε viscous dissipation

ε_T turbulent eddy viscosity

η Kolmogorov length scale; $\eta = \left(\frac{\nu^3}{\varepsilon}\right)^{1/4}$

Θ momentum thickness

μ dynamic viscosity

ν kinematic viscosity

ρ air density

τ_w wall shear stress

υ Kolmogorov velocity scale; $\upsilon = (\nu\varepsilon)^{1/4}$

Φ_i nondimensionalized one dimensional wave number spectra ($i = 1$, 2, or 3)

ω_i fluctuating vorticity component ($i = 1$, 2, or 3)

$\overline{\quad}$ overbar; denotes time average

$'$ prime; denotes root mean square value

NOTE: Equations are numbered (a.b) where a is the chapter and b is the equation within the chapter.

1.0 INTRODUCTION

1.1 General Background

The simplest example of a completely wall bounded flow, and perhaps the most commonly occurring in practise, is the flow in a circular pipe. When laminar flow enters a pipe and is of high enough Reynolds number or is artificially tripped, an annular turbulent boundary layer begins to grow from the walls of the pipe. After sufficient entry length the thickening turbulent boundary layer completely fills the pipe and eventually the flow structure becomes independent of downstream position. Generally, the fully developed structure occurs after about 60 pipe diameters.

The importance of developing turbulent flows is twofold. Bounded developing flows exist in virtually all turbomachinery, therefore their importance from an engineering design point of view is self-evident. Transitional flow in pipes is of special importance for the design of hydraulic piping systems, tubular heat exchangers and both wind and water tunnel test facilities. From a basic scientific point of view, the dynamics of turbulence in general may be better understood by observing how the turbulent boundary layer evolves and interacts.

A great deal of experimental and analytical effort has been directed towards the fully developed region, where the

turbulent energy transfer processes are in dynamic equilibrium. The experimental work on the developing region is somewhat meager in comparison. The flow development involves the complex interaction of many terms. An analytical treatment of the developing region is difficult since many terms which become zero in the mean in the fully developed region must be considered. The usual developing flow models assume an asymptotic flow development and a boundary layer structure analogous to the flat plate boundary layer. Various techniques have been suggested to handle the interaction of the merging boundary layer. The most recent is simple super-position. To date, numerical solutions have not been based on detailed experimentally determined data.

It is remarkable that so little experimental data is available to provide the appropriate boundary conditions and checks for the numerical work. The inadequacy of the analytic and numerical work has become evident as more experimental results become available. In particular, experimental results on bounded flows indicate a nonasymptotic development of the mean flow which was not predicted by the numerical work. Since the equations for the turbulent flow are non-linear, the association between the observed mean flow nonasymptotic development and the behaviour of turbulence quantities is difficult to anticipate. Small magnitude quantities may have a bearing on the developing flow structure and should

not be overlooked. Further insight into the physics of the nonlinear turbulence problem may be gained by the comparison of the relative behaviors of the various turbulent quantities with the mean flow in the developing region.

1.2 Objectives and Scope

The primary objective of the experimental work which follows was to characterize the mean and turbulent fields for the steady, axisymmetric, incompressible, developing flow in a pipe. An examination of both the survey results and the specialized measurements at the turbulent-laminar boundary layer interface has led to an experimentally based model for the flow development mechanism.

In many respects the work presented in this dissertation represents an outgrowth and extension of the experimental work initiated in 1972 while the author was proceeding towards the degree of Master of Science. The Master of Science thesis (Reichert; 1974) dealt with various techniques for the measurement of wall shear stress. The use of these measurement techniques in turbulent pipe flow suggested a nonasymptotic development. In particular, wall shear stress measurements made with a flush mounted hot film probe were observed to undershoot fully developed values in the entrance region. Pressure tube measurements of the axial component of the mean velocity were taken as a result of

these observations. The most apparent features of the mean axial velocity on the pipe axis and near the wall were reported in conjunction with the wall shear stress measurements.

The present work began with a detailed analysis of the mean velocity field based on the axial component pressure tube measurements. The Reynolds number dependence of the position and magnitude of the main mean flow nonasymptotic feature was determined. An experimental program was undertaken to measure the mean characteristics of the developing turbulent field using hot wire techniques. The behavior of each of the terms of the turbulent stress tensor was determined. These measurements and the results of computations of the terms in the turbulent kinetic energy balance equation have been presented in field contour form. The aim of this form of presentation was to make the spatial trends in the large amount of data easily comprehensible and to facilitate the identification of significant regions in the flow.

Some portions of the experimental work were reported in the scientific literature prior to the production of this dissertation. In this respect this dissertation attempts to provide a reiteration and collection of the results with more details and discussion.

The turbulent-nonturbulent interface was identified as a region of particular importance for the nonasymptotic flow behavior. A series of more specialized turbulence measurements were undertaken to study the detailed features of this region which were beyond the resolution of the contouring process. The behavior of these later measurements near the interface has suggested a mechanism for the nonasymptotic mean flow development. The nonasymptotic development can be viewed as an example of a "negative viscosity" phenomenon. A physical understanding of this more general class of flow problems may be indicated by the present results.

2.0 LITERATURE REVIEW

Some experimental data for developing, incompressible turbulent pipe flow has been presented by Deissler (1950) in support of his numerical work. However, the more recent and most often quoted results due to Barbin and Jones (1963) are probably the most accurate and detailed available. Barbin and Jones have reported mean longitudinal velocity profile measurements for a pipe length of 40 diameters and for a Reynolds number of 194000 (based on pipe radius and mean velocity). Although fully developed flow may not have been attained for this short pipe length, their centerline velocity data exhibited a maximum development which exceeded accepted fully developed values. This is in disagreement with Deissler's results which indicated asymptotic development. The earliest experimental evidence for nonasymptotic pipe flow development appeared in a study of the damping of entrance region perturbations by Buyuktur (1961). This study showed that the presence of large orifice plates at the pipe entrance greatly modified the flow development. In unobstructed flow a mean velocity maximum occurred along the pipe axis. When the flow was obstructed this mean velocity maximum disappeared. A similar study by Sharan (1969) supports this finding.

No direct measurements of the wall shear stress were attempted by Barbin and Jones or Buyuktur, although Barbin

and Jones presented values computed from static pressure measurements using a momentum balance equation. These values showed rapid asymptotic development of the wall shear stress within 15 diameters from the inlet. More recently Mizushina et al (1970) have used an electrochemical technique to obtain skin friction coefficients for developing axisymmetric flow, but the results showed rather large scatter. It is virtually impossible to determine details of the downstream velocity profile development from their work because the profile data was normalized by the centerline velocity. Reichert's (1974) measurements of skin friction coefficients using Preston tube and hot film techniques indicated that, contrary to Barbin and Jones results, the skin friction develops in a nonasymptotic manner with minimum values in the region 15 to 20 diameters from the entrance. A more detailed examination of the Barbin and Jones and Mizushina et al shear stress results has been given by Reichert (1974).

Barbin and Jones measurements of longitudinal and tangential turbulence intensity in the developing region of the 40 diameter pipe generally indicated asymptotic development. In contrast, the values measured near the pipe exit exceeded Laufer's (1954) fully developed values. This may be evidence of a nonasymptotic development of

the turbulence field, however, the short pipe length was inadequate to achieve fully developed flow. Details of the Reynolds stress measurements near the wall also indicated nonasymptotic behavior. In view of the present measurements these details appeared to be significant.

Recently, Dean (1974) has presented experimental evidence for a "mean flow overshoot" in developing rectangular duct flow which agrees with duct flow measurements by Byrne et al (1969). Preston tube measurements by Dean indicated that for the duct flow the wall shear stress exhibits a minimum at about 20 duct heights from the entrance. The "focusing effect" afforded by the circular cross-section of a pipe discussed by Sabot and Compte-Bellot (1976) with respect to fully developed flow and also the absence of secondary flow probably accounts for a more prominent nonasymptotic development in a pipe.

Several investigators have attempted to obtain solutions for incompressible turbulent flow development in pipes or ducts using numerical techniques (e.g., Richman and Azad 1973; Bradley and Cockrell 1970; Bowlus and Brighton 1968; Filippov 1958; Ross and Whippany 1956; Holdhusen 1952; Latzko 1944). A brief but fairly complete review of these studies has been presented by Tullis and Wang (1972). Perhaps due to simplifying assumptions or inadequate boundary condition specifications, none of

the above numerical work successfully predicted non-asymptotic behavior. Recent numerical work by Bradshaw et al (1973), using nonasymptotic boundary conditions supplied by Dean's (1974) experimental work, showed that nonasymptotic mean flow behavior could be predicted for two dimensional interacting boundary layers. The method used simple superposition of computed stress profiles for the interacting boundary layers. Further, it was assumed that the turbulence properties appearing in a simplified form of the turbulent kinetic energy balance equation were uniquely related to the computed stress profiles. To date, a similar analysis for pipe flow, which involves a more complex form of boundary layer interaction, has not appeared. A physical basis for the success of the technique has not been adequately established.

3.0 EXPERIMENTAL APPARATUS AND TECHNIQUE

3.1 Wind Tunnel Facility

The experiments were conducted in The University of Manitoba Turbulence Laboratory low speed, open circuit wind tunnel shown diagrammatically in figure 1. As is illustrated, two experimental set-ups were used. Briefly, for the basic flow survey, air was blown through an 89:1 contraction cone and allowed to develop along a 76 diameter length of 101.6 mm. inside diameter pipe before being exhausted through an 8° included angle diffuser (test Section A). The straight pipe set-up (test Section B) was used for a check of the diffuser's effects on flow development. The pipe material was honed stainless steel with a 6.35 mm. wall thickness. The smooth laminar flow at the entrance of the pipe was tripped by a .089 m length of grade 4F floor sanding paper. The choice of trip was based on the thorough work of Klebanoff and Diehl (1952). The conical diffuser was machined from cast aluminum. Details of the flow in the diffuser have been given by Okuwobi and Azad (1973).

Measurements at longitudinal intervals of about 5 pipe diameters were facilitated by rearrangements of the available pipe sections and the traversing mechanism. Although no disturbances due to the joints were discernable, pipe arrangements were chosen to minimize the number of joints upstream of the traversing position and maximize

the length of unbroken straight pipe immediately ahead of the traversing position.* The various pipe arrangements maintained the overall pipe length within 5 cm.

3.2 Basic Instrumentation

The mean longitudinal velocity component was measured using a traversing total head pressure tube and static pressure taps in the pipe wall. Turbulence measurements were made using a Disa 55P51 gold plated X probe (1.2 mm. wire length; 5 μm. wire diameter) and a Disa 55H01 mounting tube, guide tube and traversing mechanism system. The probe extended 6 cm. into the end of the upstream pipe section. The electronic equipment included the following: Disa 55M01 anemometers, 55D10 linearizers, 55D26 signal conditioner, 55D71 linearizers, 55D71 dual summing unit, 55D70 correlator, 55A06 differentiator, 55D35 rms meters and a true integrating digital voltmeter.

The standard procedures recommended in the Disa technical literature for the instrumentation and X probe operation were followed to obtain the linearized hot wire turbulence signals. The circumferential (w) component was obtained by turning the probe in its support by 90°. The probe was calibrated on the pipe axis in the vicinity of $x/D = 65$. Pressure tube measurements of the center line

* Further details concerning pipe joints etc. are given by Reichert (1974).

velocity near x/D = 65 and for different static pressure differences across the contraction cone formed the basis of the hot wire calibration. Periodic checks of the probe calibration were performed several times. The linearized outputs from the X probe wires were matched to within 1.5% over the required operation range. The thermal stability of the electronic equipment was maintained by allowing the units to remain powered during the course of the experimental work. A gradual decrease in the calibration sensitivity of 4% was observed over the period of the turbulence survey. This was probably due to the combined effects of dust deposition on the wires and linearizer drifts. The particular wire sensitivities used for the raw data reduction of a trial were estimated from the nearest calibration checks made before and after the trial.

No corrections were applied to the turbulence measurements to account for wire length effects or variations of the inclined wire response from the cosine law. As a result, the magnitudes of the radial and circumferential turbulence velocity components were slightly underestimated. Appropriate correction factors are given in Sec. 5.4.

The instrumentation mainly used for spectra measurement consisted of two Krohn-Hite model 3550 active filters and the Disa rms voltmeters. Most spectra were measured using turbulence signals from the X probe. Some additional

spectra were measured for comparison using an H.P. model 3590 A spectrum analyser and a 55P01 single wire. The H.P. analyser has very sharp and narrow, fixed bandwidth filters, while the Krohn-Hite filters have a variable bandwidth equal to 43% of the center frequency. Measurements of cross spectra (shear stress spectra) were performed using the Disa 55D70 correlator to multiply the filtered u and v signals.

3.3 Aquisition of Survey Data

Profiles of the axial component of the mean velocity were calculated from dynamic pressure profile measurements obtained with a traversing total pressure tube. The dynamic pressure was taken as the pressure differential between the total pressure tube and a ring of static pressure taps in the same plane. The primary pressure measuring device employed was a Betz projection manometer with 0.1 mm. of water scale intervals. No corrections were applied to account for turbulence or displacement effects on the pressure tube.* Details of the pressure tube construction and the procedures and errors associated with its use were given by Reichert (1974).

Pressure tube velocity profile data were taken at 15 longitudinal positions along the pipe and for 7 Reynolds numbers. Measurement positions were equally spaced at

* See Appendix A for further discussion.

approximately 5 diameter intervals. The Reynolds numbers ranged from 54000 to 153000 based on mean velocity and pipe radius. At the position $x/D = 72.3$, a more detailed study using 13 Reynolds numbers was undertaken. A total of 60 differential pressure measurements were recorded for each traverse of the pipe. Data were recorded at 2 mm. intervals in the central region of the pipe while near the walls a 1 mm. spacing was used. The reproducibility of the Reynolds numbers for successive profile positions was $\pm$ 2%.

Initially the dynamic pressure measurements exhibited some asymmetry. This was most noticable near the wall on either end of a traverse where large velocity gradients occurred. This effect was traced to mechanical slippage errors in the traversing mechanism (locally constructed) used for the pressure tube movement. When modifications were made so that the Disa 55H01 traversing mechanism could be used to position the pressure tube, smoother more symmetric profiles were measured.

Profile measurements of turbulent quantities were obtained by slowly moving the probe along the pipe diameter. The rms voltmeter analog output voltage for the turbulent signal and an analog voltage proportional to the probe radial position were continuously recorded on an H.P. model 7004 A XY plotter. By using the plotter and the

continuous traverse technique, the data could be taken in a relatively short time compared with discrete positioning and manual recording. Small radial trends which might otherwise be missed due to data point spacing or drifts in either the tunnel or hot wire operating conditions could be discerned in this manner.

A complete traverse of the pipe diameter was completed in about 5 minutes using the continuous recording method. The slowest probe movement was used near the walls where the radial derivatives of turbulent quantities were generally greatest. The rms voltmeter time constant which was used for continuous recording (typically 3 or 10 seconds) was inadequate to prevent large recorder pen chatter. A 2200 μf capacitor was placed across the recorder input to reduce this problem. The recording delay introduced by the overall time constant of the recording system was evident as a shift between the plotter traces which resulted when the probe was moved rapidly back and forth across the pipe. No shifts were evident for traverse times greater than 2 minutes. The traverse time of 5 minutes was therefore ample for the recording system to track the probe voltage and position accurately.

After each continuous record was made, the probe was positioned at several different radial positions and conventional voltage measurements were taken. These values

were written directly onto the traverse record. A linear regression of these voltage measurements with the corresponding heights of the plotter trace above a base line provided a check of the scaling parameters required for the quantitative analysis of the plotter record.

The plotter technique was used to gather survey data of the developing turbulence field at approximately the same longitudinal spacing used for the mean flow measurements. Over most of the developing field the differences in the measurements at adjacent stations using the 5 diameter spacing were significantly greater than the errors usually associated with hot wire anemometry. The spacing was therefore appropriate for the detection of the main features of the longitudinal behavior.

The hot wire traversing support presented an asymmetrical blockage to the flow. This was not the case for the total pressure tube measurements for which a thin support spanning the pipe diameter was used. Figure 2 presents a comparison of mean velocity profiles at $x/D = 60$ computed from the dynamic pressure measurements and those continously recorded using the plotter connected to the linearized output of one of the X probe wires. The results for the second hot wire were similar. Measurements of turbulent intensity and time derivative profiles also showed this characteristic. This tendency was taken into account when extracting numerical data from the continuous hot wire

traverse records by giving more weight to the side of the profile for which there was less flow blockage.*

Survey data were gathered using the plotter technique for u', v', w', $\frac{\partial u'}{\partial t}$ and (uv)'. The linearized signals from each of the hot wires were added and subtracted using the Disa 55D71 dual summing unit in conjunction with the inverting function of a Disa 55D26 signal conditioner. In this manner the basic u and v turbulent components were generated. Measurements of $\frac{\partial u'}{\partial t}$ were obtained using a Disa 55A06 differentiator set for a time constant $\tau = .5 \times 10^{-3}$ msec., providing a nearly linear frequency response to 30 kHz (manufacturer's specification). Because of the linearly increasing gain for higher frequencies which was inherent in the electronic differentiation process, the presence of high frequency noise in the input to the differentiator was very detrimental to the resultant signal to noise ratio at the differentiator output. The effect of high frequency noise in the anemometer circuitry was eliminated by pre-filtering the differentiator input using a Krohn-Hite 3550 filter with a low pass cut-off of 20 kHz. It was evident from subsequent spectra measurements that little of the turbulence signal was lost by this procedure. The internal noise of the differentiator preamplifiers was limited by the differentiator time constant adjustment. After the pipe flow survey was completed an improved solid state,

* Typical U differences at y/R = .6 were approximately 3%.

low noise differentiator (Tri Met Instruments model TM-TD1) became available. Measurements with this instrument in the fully developed region using prefiltering cut-off frequencies of 20 and 28 kHz gave identical results indicating that little turbulence signal was lost by filtering at 20 kHz. The results obtained with the original differentiator which included some background preamplifier noise were 10% higher in the pipe axis and approximately 7% higher near the wall. The newer differentiation equipment was employed for the subsequent specialized inlet region measurements.

3.4 Processing of Survey Data

The analog traverse records obtained by the plotter technique were digitized for analysis and presentation. The record for a traverse was folded along the co-ordinate corresponding to the pipe centerline. Using a light table, a single curve was faired through the record. In drawing the curve an attempt was made to incorporate only those characteristics common to both halves of the traverse record thereby using the symmetry of the pipe geometry to enhance the data. In most cases the curve drawing process was very straight-forward with little chance of bias being introduced by the analyst. The resulting curves were scaled and then measured at approximately 40 appropriately

spaced radial positions from the centerline towards the wall. The closest spacing was used where the measurements changed most rapidly with radial position. The data was punched in formatted form on computer cards. Simple Fortran computer programs were written to handle the scale factors introduced by the instrument gains and the probe sensitivity. Data values were generated at 101 equally spaced radial positions between the centerline and the wall using Aitken's interpolation method. Data points which were generated near the wall, outside the range of the actual hot wire traverse were ignored.

The processing of the mean flow pressure tube survey measurements was performed in a similar manner. Mean velocity profile results were calculated from the pressure tube measurements and were plotted on a large scale. Obvious outliers were eliminated. The plotted profiles were folded along the pipe axis symmetry co-ordinate and a smooth continuous curve was drawn through the profile data. These faired, symmetric curves were then scaled and evaluated at about 35 radial positions. High density, equally spaced profile data was generated by interpolation. Pressure tube data in the region nearest the wall ($y/R>.95$) were subject to the greatest errors and were eliminated from further analysis.

3.5 Contouring Technique

The difficulty of presenting the large amount of experimental data gathered in a survey study and the problem of assimilating the data into a meaningful picture was overcome by producing computer generated contour plots of the flow field for each of the measured and calculated quantities. The contour form of presentation has been commonly used to represent flow fields in meteorology and geophysics but its use in turbulence research has appeared to be limited. Researchers have tended to avoid the interpretive judgements and general subjectivity associated with manual contouring. The computer procedures which were used to smooth the data and generate the contours avoid this subjectivity.

An analytic description of the longitudinal behavior of each measured quantity for a particular radial position was obtained by applying the least squares technique to data extracted from the interpolated profiles at successive longitudinal positions. Approximately 100 fifth order polynomial fits were generated in this manner, each for a different radial position. A high density rectangular grid of data representing the flow field between the centerline and the wall and suitable for computer manipulation was generated by evaluating each polynomial at many longitudinal positions. These data grids also provided the

basic data for the subsequent evaluation of spatial derivatives of the turbulence survey measurements required for the turbulent kinetic energy balance.

The selection of a fifth order polynomial was based on the examination of plotted results for the longitudinal mean velocity measurements using polynomials of different orders. While lower order polynomials tended to smooth out the obvious features of the profile development, higher order polynomials tended to introduce spurious oscillations while co-locating with the measurements. Comparison of the fifth order results with the original data showed them to be sufficient to include the principal characteristics while providing adequate data smoothing.

For contouring purposes the flow field was represented by a 735 point matrix contouring data at 35 equally spaced longitudinal positions and 21 equally spaced radial positions. The contouring program which was used to produce the contour plots generates smooth contour lines but honours the specified value at each grid point. In this way the contouring process was sufficiently controlled to avoid smoothing out small but significant trends.

It should be pointed out that the polynomial technique which was employed tended to extrapolate measurements to zero in regions where a low but non-zero background measurement existed. This occurred for turbulence intensity

measurements in the non-turbulent entrance region core. This tendency to extrapolate must be considered when interpreting zero value contours in the entrance region. A similar problem was found to occur for the survey data of the $\overline{uv}$ Reynolds stress component.

3.6 Spectra Measurement and Processing

One dimensional spectra measurements were made by filtering the turbulence signal with the Krohn-Hite 3550 filter and measuring the rms of the filter output. This measurement provided an estimate of the power in the turbulence signal at a frequency corresponding to the filter setting. Data were collected for 25 frequencies, f, logarithmically distributed between 2Hz and 30 kHz and were converted to one dimensional wave number spectra $E_i(k_1)$ (where i is 1,2, or 3 for u, v, or w respectively) using Taylor's hypothesis in the form $k_1 = \frac{2\pi f}{\overline{U}}$. $\overline{U}$ was the longitudinal mean velocity at the location of the spectra measurement and was determined from the hot wire probe d.c. voltage and calibration. Taylor's hypothesis is premised on the assumption that the sequence of changes in velocity at a fixed location are simply due to the passage of an unchanging pattern of turbulent motion over the point. The assumption was valid for pipe flow since the mean velocity of the flow which carried the turbulent

eddies was generally much greater than the turbulent velocity fluctuation.

The wave number spectra $E_i\ (k_1)$ were normalized so that the integral of the spectra equalled the overall mean square of the bandpassed signal between 2Hz and 30 kHz. The wave number spectra were nondimensionalized using the dissipation

$$\varepsilon = 15\,\nu \int_o^\infty k_1^2\, E_i\ (k_1)\ dk_1 \tag{3.1}$$

to obtain

$$\Phi_i\ (k_1) = E_i\ (k_1)/\eta\upsilon^2 \tag{3.2}$$

where η was the Kolmogorov length scale,

$$\eta = (\nu^3/\varepsilon)^{1/4} \tag{3.3}$$

and υ was the Kolmogorov velocity scale,

$$\upsilon = (\nu\varepsilon)^{1/4}. \tag{3.4}$$

4.0 MEAN VELOCITY FIELD SURVEY

4.1 Mean Longitudinal Velocity Component

4.1.1 Flow Survey Results

Mean velocity survey measurements were taken for a total of 7 Reynolds numbers between 55000 and 153000. Initially, the results for Re = 76000 and 153000 were selected for detailed analysis and presentation. A decision was made at a later stage of experimentation to perform the turbulence survey measurements at the lowest Reynolds number of the mean flow survey, Re = 54900. This was desirable because improved experimental accuracy could be achieved with the reduced high frequency content (less than 20 kHz) of the lower Reynolds number turbulence. Both the high frequency signal to anemometer noise ratios and the wire length attenuation were less important for turbulence with reduced high frequency content. To provide a complete picture of both the mean and turbulent fields at this lower Reynolds number, the mean velocity measurements for Re = 54900 were analysed and contoured. The contours for this subsequent analysis are presented in this section along with the results for the higher Reynolds numbers that were initially selected.

A summary of the bulk flow parameters occurring at x/D = 60.3 for Re = 54900 and with the test section terminated with the diffuser (experimental setup A) appears as Table 1. At this lower Reynolds number the operating speed and test section diameter were nearly identical with those used for the recent fully developed flow study of Sabot and Compte-Bellot (1976). The friction velocity for this Reynolds number was determined by measurement of the pressure gradient between x/D = 62 and 72. It agreed well with the value of .78 m/sec reported by Sabot and Compte-Bellot.

The symmetric velocity profiles obtained after interpolation and curve fairing of the dynamic pressure measurements for Re = 76000 and 153000, appear as figures 3 and 4 respectively. The profiles were normalized using mean velocities calculated by numerical integration of each profile. The difference between these two Reynolds numbers was sufficient to demonstrate the nature of the Reynolds number effect on the mean flow. Qualitative study of the raw data for the intermediate Reynolds number experiments verified that the effect was gradual. The main characteristics of the flow development shown by these selected Reynolds numbers were typical of all the results.

An analytic description of the profile development was obtained by fitting fifth order least squares polynomials

to data extracted from the profiles at successive longitudinal positions, in the manner previously described. Curves for several of the polynomial fits are presented in figures 5 and 6, although for the actual analysis over 100 radial positions were used. The high accuracy with which the set of parametric (in radial position) polynomials described the flow development was apparent from these figures. Differentiation and evaluation of these polynomials provided the longitudinal velocity gradient data required for the computation of the radial component of mean velocity. Employing the technique discussed in Section 3.5, the polynomials were used to generate velocity values for a rectangular grid of points representing the flow field. The grid data were contoured by computer to produce figures 7, 8, and 9 which represent the longitudinal mean velocity fields for Re = 54900, 76000, and 153000 respectively. The interpolation scheme involved in the production of these plots developed difficulties in the high gradient wall region where profiles were most subject to error. Contours in the immediate vicinity of the wall were omitted for this reason.

The plots of the longitudinal velocity showed the tendency of the flow near the centerline of the pipe to accelerate to velocities (at about x/D = 34) which exceeded those achieved farther downstream (eg. near x/D = 60) after further development. This mean velocity behavior was

called "mean velocity overshoot". This velocity overshoot was most evident on the contour plots of the axial velocity where it appeared as an organized region of concentric contours. The U contour plots were all characterized by a narrowing core of accelerating fluid which disappeared after 30 - 40 pipe diameters. Outer regions were characterized by decelerating axial flow over approximately the first 20 diameters. This wall region behavior was called a "mean velocity undershoot". The contours in the first 20 diameters reflected the gradual disappearance of the flat profiled non-turbulent core as the turbulent boundary layer grew from the wall. The contours at $x/D = 60$ were parallel to the pipe wall in accordance with the fully developed condition $\frac{\partial U}{\partial x} = 0$, but the effects of the flow truncation with the diffuser were apparent downstream. The flow in the core was accelerated and flow near the wall decelerated by the diffuser. This was most evident for the lowest Reynolds number. Examination of the higher Reynolds number contours showed that the extent of the effective upstream virtual origin for the diffuser diminished for higher Reynolds numbers and, as was evident from the work of Okwuobi and Azad (1973), was not detectable for higher Reynolds numbers.

Near the pipe wall, where the viscous shear component $\mu \frac{\partial U}{\partial y}$ of the total shear stress becomes important, it

was hypothesized that the radial gradient of the U velocity would be a reasonable trend indicator for the wall shear stress. On this basis, crude estimates of the shear stress were obtained by examining the axial velocities for radial positions near the wall ($y/R > .75$). The axial velocity undershoot near the wall thus led to the expectation of a wall shear stress minimum. This provided qualitative corroboration of the hot film measurements of wall shear stress made previously (Reichert; 1974). In particular, the skin friction coefficient determined in that study showed an undershoot occurring for positions $20 < x/D < 30$.

4.1.2 Overshoot Peak Analysis

Comparison of the axial velocity contour plots for the different Reynolds numbers, showed that the centerline overshoot peak was most pronounced for the lowest Reynolds number. Maximum values of U/U_B approached 1.28 for $Re = 54000$, while for $Re = 153000$ maximum U/U_B values just exceeded 1.24. An analysis of the centerline velocities was undertaken to determine the peak position as a function of Reynolds number. For each of the 7 Reynolds numbers of the flow survey, centerline velocities were plotted against the profile mean velocities with longitudinal position as a parameter. The nearly linear curves which resulted were

interpolated to obtain centerline velocities at different longitudinal positions and for several selected mean velocities. The interpolated centerline velocity and longitudinal position data were fitted by fifth order polynomials and overshoot peak positions for the selected mean velocities were determined by analytic differentiation. The peak position as a function of Reynolds number is presented as figure 10. The peak position decreased (moved towards the pipe entrance) approximately 3 diameters for increasing Reynolds numbers from 54900 to 153000. An equation suitable to describe this behavior was

$$x_p/D = 30.80 + .89\ (Re \times 10^{-5})^{-1} + 0.79\ (Re \times 10^{-5})^{-2} \qquad (4.1)$$

This equation implied a limit of $x/D \simeq 31$ for the peak position at the highest incompressible Reynolds numbers. On the other hand, the analysis implied that rather long entrance lengths would be required for low Reynolds number flows to become fully developed.

It may be significant to note that the overshoot peak positions were nearly the same as the pipe length (40.5 diameters) which Barbin and Jones (1963) used. Thus, while both centerline overshoot and wall region undershoot of usually accepted fully developed pipe flow values were indicated by their axial velocity data near the exit,

it could not be resolved whether these were characteristic of pipe flow development or were a manifestation of the short pipe length and possible exit effects. The problem was further complicated by their calculation of wall shear stresses from static pressure gradient measurements. Because of the difficulty in obtaining sufficiently accurate static pressure measurements, their stresses erroneously exhibited rapid asymptotic development.

4.1.3 Integral Parameters

Integral boundary layer parameters, such as the displacement (δ) and momentum (θ) thicknesses, are correctly calculated only where a well defined free stream velocity exists. For bounded duct or pipe flows, corresponding integral parameters can be calculated using the centerline velocity. Following this procedure, axial displacement and momentum thicknesses were computed by numerical integration of the smoothed U velocity profiles for Re = 76000, and Re = 153000. The equations used for calculation were

$$\theta = R \int_0^1 \frac{U}{U_c} \left(1 - \frac{U}{U_c}\right) \left(\frac{y}{R}\right) d\left(\frac{y}{R}\right) \qquad (4.2)$$

and

$$\delta = R \int_0^1 \left(1 - \frac{U}{U_c}\right) \left(\frac{y}{R}\right) d\left(\frac{y}{R}\right) \qquad (4.3)$$

where U_c was the centerline velocity.

The behavior of these scalar integral boundary layer parameters is significant because the parameters are related to momentum flux terms appearing in the Von Karman boundary layer momentum balance equation. The calculated thicknesses are presented in figure 11 where they have been normalized by the pipe diameter. The observation that the longitudinal derivatives of these integral parameters did not become zero monotonically provided clear evidence for the nonasymptotic character of the flow development. The dashed lines on figure 11 are for a rectangular duct and were taken from work by Byrne et al (1969) and Dean (1974). The lines showed the same behavior as the present pipe data and suggested that the nonasymptotic development occurs for bounded flows in general.

The results of the calculation of shape factors (H) for the developing flow are shown in figure 12. The shape factor is the nondimensional ratio of the displacement and momentum thickness. Its insensitivity to the flow development structure and the rather large errors associated with the ratio were obvious. It was not found to be a satisfactory parameter to describe the development and therefore its rather widespread use in numerical methods should be cautioned.

The data in figures 11 and 12 also illustrated the Reynolds number dependency of the thickness parameters.

The results implied that more rapid boundary layer growth occurred for the lower Reynolds number since thicknesses for the lower Reynolds number were largest. This is the usual trend observed for turbulent boundary layer growth in other flows such as on a flat plate. Remembering that the analysis of the behavior of the longitudinal velocity component indicated overshoot positions nearer to the entrance for increasing Reynolds numbers, the present results indicated that the mean boundary layer merge point was not simply related to the overshoot position.

4.2 Mean Radial Velocity Component

The mean radial velocity profiles were computed using the continuity relation

$$\frac{V|_{(y = r)}}{U_m} = - \frac{1}{r} \int_o^r \frac{\partial}{\partial x} \left(\frac{yU}{U_m} \right) dy. \qquad (4.4)$$

Data for the longitudinal derivative of U was obtained by evaluation of the fourth order polynomials which resulted from analytic differentiation of the fifth order least square polynomial fits of the U data of Sections 3.5 and 6.3.2 Before integration, the data for the derivative of U was smoothed numerically using a Hamming convolution filter. This process tended to eliminate small irregularities which appeared in the computed derivative profiles but were

inconsistent with expected resolution. The normalized radial velocity profiles for the Reynolds numbers 76000 and 153000 are plotted as figures 13 and 14 respectively. According to the sign convention which was adopted, a negative radial velocity indicated a motion toward the pipe axis. Contour plots of the radial mean velocity fields were generated from these profiles by the processes of polynomial fitting and interpolation to obtain a rectangular data grid. The results for Reynolds numbers of 54900, 76000 and 153000 are presented as figures 15, 16 and 17 respectively.

The radial velocity components were about three orders of magnitude smaller than the longitudinal components. In the entrance the accelerating core region flow was supported by a radial movement of fluid towards the core. Farther downstream the radial velocity was directed back towards the wall. The fully developed condition that $V = 0$ corresponded with a zero value contour which crossed the flow near the pipe exit. A second zero value contour was associated with the region of maximum longitudinal velocity between $x/D = 30$ and 40.

5.0 TURBULENT STRESS TENSOR SURVEY

As a first step towards an understanding of the physical processes involved in the nonasymptotic mean flow development, a program was initiated to survey the behavior of the turbulent Reynolds stress tensor for the developing region for a Reynolds number of 54900. The turbulent stress tensor, when written in matrix form, consists of terms involving the intensities of velocity fluctuations and correlations between pairs of the fluctuating velocity components:

$$\rho \begin{vmatrix} \overline{u^2} & \overline{uv} & \overline{uw} \\ \overline{vu} & \overline{v^2} & \overline{vw} \\ \overline{wu} & \overline{wu} & \overline{w^2} \end{vmatrix} \qquad (5.1)$$

Physically, the presence of fluctuating velocities superimposed on the mean flow introduces additional mean momentum fluxes within the fluid. By Newton's law these additional momentum fluxes appear as additional stresses within the fluid. The Reynolds stress tensor is symmetric and for axisymmetric pipe flow the terms $\overline{uw}$ and $\overline{vw}$ are also equal to zero. The stress tensor therefore reduced, for the present study, to the three normal stress terms on the diagonal and the tangential $\overline{uv}$ stress. Each of the stress terms was measured by a separate traverse of the pipe with the hot wire X probe using the XY plotter recording technique.

Dean (1974) examined simplified fully developed momentum equations for duct flow and showed that the Reynolds stress and mean velocity longitudinal behavior were related. This suggested that the nonasymptotic behavior could be characteristic of both the mean velocity and turbulent stresses and could be expected to show up in the stress measurements. As given by Laufer for fully deveoped pipe flow,

$$\frac{1}{\rho}\frac{\partial P}{\partial x} = -\frac{1}{r}\frac{d}{dr}\, r\left(\overline{uv} - \nu\frac{\partial U}{\partial r}\right). \qquad (5.2)$$

Writing the total pressure P as a sum of static (P_s) and dynamic ($1/2\ \rho U^2$) components and considering only core region flow ($U \approx U_c$) for which the viscous term can be ignored, the following results:

$$U_c\ \frac{\partial U_c}{\partial x} = -\frac{1}{r}\frac{d}{dr}\,(r\ \overline{uv}) + \text{constant} \qquad (5.3)$$

Dean's result for the duct geometry is similar. The implication of the above equation (although formally it should only apply to the fully developed state because several fully developed approximations are involved) is that the shear stress radial gradient and also the shear stress magnitude are closely related to the mean flow adjustment.

5.1 Normal Stresses

5.1.1 Contoured Results

The contoured results for the intensities of the longitudinal, radial, and circumferential turbulence components are presented as figures 18, 19, and 20 for the nominal Reynolds number of 54900. Each of the terms exhibited a nonasymptotic development, with a distinct core region maximum like the longitudinal component of the mean velocity. The position along the pipe axis for these intensity maxima occurred approximately 15 diameters downstream of the mean velocity peak position for the same Reynolds number. For radial positions near the wall ($y/R > .7$) all of the turbulence intensities generally increased with downstream position up to about $x/D = 30$. Beyond this point the intensities decreased with the u' and w' intensities exhibiting an undershooting of the values for the more developed flow downstream.

Comparison of the mean radial velocity component contours (figure 15) with the turbulence intensity figures showed that the region of mean radial velocity towards the wall was associated with more widely spaced intensity contours in the region $.8 < y/R < .4$ and $32 < x/D < 54$. This suggested that the existence of a mean velocity component towards the wall attenuated the turbulence intensity. This qualitative correlation appeared to be

maintained in detail for the contours. Considering that a mean velocity component towards the wall could be expected to produce elevated static pressures and modification of the pressure gradient, this observation is probably more than coincidental.

5.1.2 Contour Evidence for a Superlayer

Over the bulk of the flow field the longitudinal intensity u' was greater than either w' or v'. However, comparison of the intensity contours in the vicinity of the inlet showed that in a region likely associated with the intermittent interface between the nonturbulent core and turbulent boundary layer, the radial and circumferential components exceeded the magnitude of the longitudinal intensity. The relative magnitudes of these fluctuations appeared to satisfy the theoretical criteria for a superlayer established by Phillips (1955) and Stewart (1956):

$$v'^2 = u'^2 + w'^2 \qquad (5.4)$$

This condition was satisfied over a much wider region than is actually the case for the superlayer which exists at a flat plate turbulent-nonturbulent interface. The effect of the pipe geometry may have contributed to this. Barbin and Jones (1963) have referred to some unpublished results which also indicated radial fluctuations exceeding longit-

udinal fluctuations in the interface region. However, in his thesis, Barbin (1961) assumed that the larger than expected radial intensities that he measured were due to unknown errors. Dean (1974) has observed a similar behavior in a rectangular duct and suggested that it was due to irrotational fluctuations induced in the free stream by the convoluting edge of each turbulent boundary layer. The present results suggest that a similar magnified version of the superlayer exists for pipe flow.*

Details of the superlayer region could not be accurately determined from the contoured results. This was due to the polynomial smoothing which was used to pre-condition the data before generation of the data matrices for contouring. The very high gradients associated with the relatively narrow interface region were not well represented by the longitudinal fifth order polynomial fits. The polynomial technique was more appropriate for features with longitudinal spatial extents of the order of 5 pipe diameters. In particular, the polynomials tended to extrapolate the turbulence measurements to zero in the interface region even though a nonzero background existed in the nonturbulent core (see Section 3.5). More detailed measurements in the interface region were required to examine the superlayer mechanism.

* While possessing similar qualities, this region is much too large to be considered as identically the same superlayer as discussed by Phillips (1955) or Stewart (1956).

5.1.3 Stress Tensor Trace

The trace of the Reynolds stress tensor $q'^2 = u'^2 + v'^2 + w'^2$ is directly proportional to the total turbulence kinetic energy. The values of the stress tensor trace were computed from the normal stress measurements and are presented in figure 21. The contours have been nondimensionalized by the bulk velocity. As expected, the total turbulence kinetic energy exhibited the same basic features common to the normal stresses. Along the pipe centerline the maximum turbulent kinetic energy occurred at x/D = 50. Turbulent kinetic energy generally increased toward the wall except for a small region near y/R = .9 between x/D = 10 and 20 where a tendency to decrease appeared. Fully developed conditions appeared to be satisfied at x/D = 64 where tangents to the contours became parallel to the pipe wall. However, the anomalous contour spacing near the wall indicated some diffuser effects.

5.1.4 Turbulent Boundary Layer Growth

The rate of turbulent boundary layer growth in the developing region was roughly estimated from the shape of the contours for small values of the stress tensor trace. The growth was characterized by three regions. Initially, perhaps due to the presence of the trip, rapid boundary layer thickening occurred. For $10 < x/D < 20$, the boundary

layer thickness increased at a nearly linear rate. Beyond this point and presumably where intermittent interaction from opposite halves of the flow became important, the boundary layer rapidly thickened to fill the pipe. This accelerating boundary layer thickening stage was unlike the smooth asymptotic thickening for a flat plate and suggested a complexity for merging boundary layers that could not be accounted for by simple superposition theory. Re-examination of the momentum and displacement thicknesses, which were computed from mean velocity measurements at higher Reynolds numbers (figure 11). also suggested the same trends for the boundary layer growth.

5.2 Tangential Stresses

5.2.1 Contoured Results

Contours of the measurements of the tangential Reynolds stress component appear as figure 22. While contours near the centerline conformed to the symmetry condition $\overline{uv} = 0$, the contours away from the core clearly exhibited a non-asymptotic development. Peak values near the pipe axis were again downstream of the mean longitudinal velocity peak position. Slack radial gradients were also associated with mean radial velocity components towards the wall. The position of maximum stress for a given radius appeared to be nearest to the pipe entrance for radial positions farthest

from the axis. Contrary to what might be expected on the basis of superposition of boundary layer stress profiles from opposite halves of the flow, the radial stress gradient in the central region, where the mean velocity component U was accelerating and overshooting, was lower than the central region gradients farther downstream.

The $\overline{uv}$ stress generally increased with distance from the centerline except for a region near the wall for $x/D \simeq 20$ where the contours indicated a tendency to level off and even decrease. The longitudinal behavior of $\overline{uv}$ through this region agreeded with the minimum exhibited by flush mounted hot film measurements of the wall shear stress in developing pipe flow (Reichert; 1974). The tendency of the tangential Reynolds stresses away from the axis to develop rapidly and overshoot was first observed by Barbin and Jones (1963) although their pipe length of 40 diameters was inadequate to achieve fully developed flow. The significance of their observation as an aspect of an overall nonasymptotic development was not appreciated.

5.2.2 Principal Stress Angle

In analogy with the stresses in a solid, there is no fundamental difference between the normal and shear stresses in turbulence. Whether a given arrangement of stresses is normal, or shear, or both, depends solely on the choice of

axes. A set of principal axes can always be found for which only normal stresses remain. As given by Dryden (1947), the angular direction of the greatest principal stress is given by α_p where

$$\tan 2\,\alpha_p = 2\,\overline{uv}/(\overline{u^2} - \overline{v^2}) \qquad (5.5)$$

and α_p is measured in the uy plane from the mean flow direction. Dryden's measurements on a flat plate boundary layer were made with what is now outdated equipment, but the results agree with the recent measurements by Charnay et al (1976). The findings indicated that for most of the boundary layer width $\alpha_p \approx 20°$. This corresponds to a direction inclined at 20° from the plane of the plate. The α_p angle was slightly lower for cases with greater free stream turbulence above the boundary layer.

The results for developing pipe flow at selected longitudinal positions are presented in figure 23. The findings showed that within the turbulent boundary layer, in the entrance, α_p was high. As the flow developed the values decreased. The flow at x/D = 60 exhibited maximum α_p values of 19.5° for y/R = .4. The values decreased gradually by about 6° as the wall region was approached. A similar decreasing trend of about 3° was evident in the flat plate results (Charnay et al; 1975). The centerline symmetry condition for the $\overline{uv}$ stress was illustrated by values of $\alpha_p = 0$

on the pipe axis. The trends of the results at x/D = 60 were similar to those calculated from Laufer's (1954) measurements in fully developed flow, although Laufer's results were from 6° to 8° higher. The sensitivity of the expression for α_p to errors in v intensity probably accounts for this. Inclusion of first order correction terms to account for deviations of the X probe behavior from the cosine law for inclined wires would typically increase the present α_p estimates by 4°. Further, longitudinal intensity measurements by Perry and Abell (1975) have shown that Laufer's longitudinal intensity measurements may be of the order of 15% too high over a considerable region. This consideration alone could shift the α_p magnitudes to values similar to the present x/D = 60 results.

5.3 Correlation Coefficients

The character of the $\overline{uv}$ contours was considerably modified when the stress was nondimensionalized by the longitudinal and radial turbulence intensities (figure 24). The most striking feature introduced by the normalization are the regions of increasing correlation coefficient associated with the turbulent boundary layer in the inlet region. The numerical difficulties encountered when computing the ratios of very small quantities, such as

occurred in the laminar core region, were overcome by arbitrarily setting the correlation coefficient to zero when $u'v'$ was the order of its background value in the nonturbulent core. It should be appreciated, therefore, that the high gradient region of the contour plot bounding the nonturbulent core and of width comparable to the grid point spacing was an artifact introduced by this computational convenience. While zero was the natural lower bound for the correlation coefficient due to the axis symmetry, one could hypothesize that within nonturbulent eddy structures associated with the boundary layer interface, nonzero correlations could exist. Because of the intermittency of the boundary layer interface, a cautious approach must be taken to physical interpretation of mean correlation coefficients. However, the existence of higher correlations within the boundary layer near the interface would be consistent with the concept of an interface controlled mainly by large scale turbulent eddies (Corrsin and Kistler; 1955). Considering the magnification of the boundary layer interface apparently provided by the pipe geometry, it appeared that the effects of the large eddies controlling the interface were evident in the mean measurements well within the boundary layer.

In the region downstream of $x/D = 30$ the correlation coefficients rapidly adjusted to a fully developed pattern

characterized by a wall region with approximately constant correlation, and a core region with a large radial gradient. Sabot and Compte-Bellot (1976) showed that the small correlations in the centerline region were due to the flow symmetry rather than a tendency towards isotropy.

5.4 Comments on Flow Development

The addition of a diffuser after 80 pipe diameters provided the advantage of a previously documented (Okwuobi and Azad; 1973) flow regime as a controlled, known, boundary condition against which the trends of the analysis of the present results in the exit region could be compared. Terms such as the mean flow convection of turbulent energy, which exist in the developing pipe flow but would be zero in fully developed flow, are important in the diffuser. Since the behavior of these terms in the developing inlet region was of particular interest, it was a valuable check on the analysis procedure to observe the appropriate trends towards the known diffuser characteristics as the diffuser was approached. The exit region trends of the previous mean velocity and turbulence stress tensor contours showed that the diffuser provided a smooth and gradually more effective termination of the pipe flow. The effect of the diffuser on the pipe flow was evident several diameters upstream of the diffuser and appeared to affect different quantities by

different amounts.

As a check on the effect of the diffuser on the flow development, measurements of u', v', $\left(\frac{\partial u}{\partial t}\right)'$, and the center-line velocity defect obtained at x/D = 60.3 using experimental setup A (diffuser on) were compared with results at x/D = 65.2 and 85.4 using setup B (diffuser off) (figure 25). To illustrate the magnitude of the experimental errors associated with the equipment and XY plotter record digitization, the results of two separate trials at each of the positions x/D = 60.3 and x/D = 65.2 were included in the figure. Measurements at intermediate positions between x/D = 65.2 and 85.4 using setup B were similar. Since normalization can often tend to hide differences in the actual measured values, the turbulence results were plotted in dimensional form. The data compared reasonably well. The largest spread in values appeared in the measurements of the longitudinal turbulence intensity. The differences appeared to be largely systematic and were similar in both character and magnitude to the hot wire errors reported by Lawn (1971). The results showed that, for the quantities presented, the effect of the diffuser on the flow at x/D = 60.3 was marginal, if present at all. Further, these results showed that the measurements at x/D = 60.3 with the diffuser attached were ostensibly the same as measurements which repeated over the final 20 pipe diameters when the diffuser

was not present. The extent of the flow development occurring in the first 60 diameters of the pipe was further examined by comparing profiles of both the longitudinal turbulence intensity and the correlation coefficient (extracted from the contour plot of the survey measurements at x/D = 60) with the thorough fully developed pipe flow results of Perry and Abell (1975) and the more recent results of Sabot and Compte-Bellot (1975) (figure 26). Aside from showing the rather large discrepency between accepted fully developed results, the figure shows that after 60 diameters some basic characteristics of fully developed flow had evolved.

A characteristic usually expected of developed turbulent pipe flow is that the streamwise spatial derivatives of measured quantities be zero. A zero value of the streamwise derivative of a quantity occurs where the tangent to a contour line becomes parallel to the pipe axis. An extended region of zero value streamwise derivatives was not evident on the contours of the basic measured quantities because the developing region nearly merged with the region of upstream diffuser effects for experimental setup A. The situation was further complicated since different quantities seemed to exhibit different susceptibility to the diffuser effects. The upstream influence of the flow truncation appeared to preclude the existence

of an extended dynamic equilibrium region for the pipe lengths involved.

The static pressure gradient was not a sensitive indicator of pipe flow development and hardly changed over the last 50 pipe diameters. The value of $\tau_w/\rho = .62\ m^2/sec^2$ from Table 1 was determined from measurements of the static pressure gradient at 10 positions between x/D = 62 and 72. A standard test often used for hot wire measurements in pipe flows considers the linear extrapolation of $\overline{uv}$ measurements to the wall. In developed flow the extrapolated value should compare with pressure gradient measurements of the wall shear stress. Based on this criterion, an indication of the flow development could be acquired from the examination of $\overline{uv}$ survey results.

Profiles of $\overline{uv}$ data extracted from the XY plotter records are plotted as figure 27. Since the hot wire yaw calibration was assumed to follow a simple cosine law, the hot wire measurements tended to underestimate the true v' and $\overline{uv}$. Champagne and Sleicher (1967) have shown that for a hot wire with l/d = 200 and k = .20, which is very close to the Disa 55P51 X probe configuration, the following corrections apply:

$$\begin{aligned} (u')_c^2 &= (u')_m^2 \\ (v')_c^2 &= 1.17\ (v')_m^2 \\ \overline{uv}_c &= 1.08\ \overline{uv}_m \end{aligned} \tag{5.6}$$

(c denotes corrected value, m denotes measured value). On this basis, the uncorrected $\overline{uv}$ measurements might be expected to extrapolate to a value of $\tau_w/\rho = .57\ m^2/sec^2$ at the wall, rather than the value $.62\ m^2/sec^2$ from Table 1. The general behavior of the $\overline{uv}$ measurements of figure 27 and in particular, the nonlinearity of the measurements near the wall, is consistent with the data presented by Lawn (1971). While Laufer's (1954) results are linear to $y/R \simeq .95$, an extrapolation of $\overline{uv}$ measurements to the wall appeared to be best based on the $\overline{uv}$ gradient near the centerline. The extrapolation of measurements for $x/D > 60$ gave values of τ_w/ρ somewhat smaller than the expected fully developed value of $.57\ m^2/sec^2$. However, measurements as little as 5 diameters further upstream extrapolated to considerably higher τ_w/ρ values. The dashed line indicates the extrapolation to the expected uncorrected fully developed value $\tau_w/\rho = .57$. On the basis of this extrapolation criterion it appears that the $\overline{uv}$ results exhibited the characteristics of fully developed flow at $x/D = 54.86$. Beyond this position the occurrence of lower extrapolated stresses can most probably be attributed to the effect of the diffuser.

6.0 TURBULENT KINETIC ENERGY BALANCE

6.1 The Energy Equation

The turbulent kinetic energy budget for the developing pipe flow was obtained from experimental evaluation of the terms in the time averaged turbulence energy equation. Assuming stationarity, the equation may be written in the form

$$I + II + III + IV + V = 0 \tag{6.1}$$

and for axisymmetric flow the five terms were identified as follows:

Mean flow convection:

$$I = \frac{1}{4}\frac{U}{U_B}\frac{\partial(\overline{q^2}/U_B^2)}{\partial(x/2R)} + \frac{1}{2}\frac{V}{U_B}\frac{\partial(\overline{q^2}/U_B^2)}{\partial(y/R)} \tag{6.2}$$

Convective diffusion by kinetic and pressure effects:

$$II = \frac{1}{2}\overline{\frac{\partial}{\partial(x/2R)}\{uq^2/2U_B^3 + up/\rho U_B^3\}} + \frac{1}{(y/R)}\overline{\frac{\partial}{\partial(y/R)}\{(y/R[vq^2/2U_B^3 + vp/\rho U_B^3]\}} \tag{6.3}$$

Turbulent kinetic energy production:

$$III = \frac{\overline{uv}}{U_B^2}\frac{\partial(U/U_B)}{\partial(y/R)} + \frac{\{\overline{u^2} - \overline{v^2}\}}{2U_B^2}\frac{\partial(U/U_B)}{\partial(x/2R)} \tag{6.4}$$

$$+ \frac{\overline{uv}}{U_B^2}\frac{\partial(V/U_B)}{\partial(y/R)} + \frac{1}{(y/R)}\frac{V}{U_B}\frac{\{\overline{w^2} - \overline{v^2}\}}{U_B^2}$$

Work done by viscous shear stresses (viscous transport):

$$IV = \frac{-1}{2Re(y/R)} \frac{\partial}{\partial(y/R)} \{(y/R) \frac{\partial(\overline{q^2}/U_B^2)}{\partial(y/R)}\}$$

$$- \frac{1}{8Re} \frac{\partial}{\partial(x/2R)} \{\frac{\partial(\overline{q^2}/U_B^2)}{\partial(x/2R)}\} - \frac{\nu R}{U_B^3} \overline{\left(\frac{\partial u_i}{\partial x_j}\right)\left(\frac{\partial u_j}{\partial x_i}\right)} \quad (6.5)$$

Dissipation (ε):

$$V = \frac{R}{U_B^3} \{\nu \overline{\left(\frac{\partial u_i}{\partial x_j} + \frac{\partial u_j}{\partial x_i}\right) \frac{\partial u_i}{\partial x_j}}\} \quad (6.6)$$

In the above terms the overbar indicates a time averaged quantity. The turbulent kinetic energy budget is a conservation equation for the quantity $\frac{1}{2} \rho \overline{q^2}$ and as such each term describes a rate of appearance or disappearance of turbulent kinetic energy at a point.

In dimensional form each term of the above turbulent kinetic energy balance equation would have the dimensions of power per unit mass but for presentation the normalizing factor R/U_B^3 was incorporated into the equation.

The terms of the energy equation can be divided into two classes: those dealing with the local creation or the annihilation of turbulent kinetic energy within the control volume and those dealing with the movement of kinetic energy into or out of the control volume. It is the

presence of these later transport and convective terms which limit the usefulness of eddy viscosity concepts. The structure of the flow both upstream and downstream of a particular point determines the behavior of the turbulent kinetic energy and therefore the normal stresses at that point. This is implicit in the energy balance equation because these quantities appear in spatial derivative terms which would require integration over the whole flow field for analytic solution.

The fundamental starting points for the development of the turbulent kinetic energy balance equation are the Navier-Stokes and the continuity equation which are respectively statements of Newtons law (a force balance) and mass conservation. Multiplication of the sum of these two equations by the total velocities yields an energy equation. By the usual processes of Reynolds decomposition and time averaging followed by subtraction of the mean energy equation, the dimensional form of the above equation is obtained. The detailed derivation of the turbulent kinetic energy equation is available in several sources {e.g. Hinze; 1959 (in rectangular co-ordinates) and Huffman; 1968 (in mixed cylindrical and rectangular co-ordinates as given here)} and the details will not be unnecessarily repeated here. The genealogy of the turbulent kinetic energy equation is summarized diagrammatically in figure 28. In fully developed turbulent

pipe flow the energy equation becomes much simpler as both the longitudinal space derivatives and the mean radial velocity are zero. In particular, the mean flow convection term disappears entirely. The derivation of the simplified fully developed equation is given by Laufer (1954).

The sign convention adopted for the energy equation was such that a term was negative within a certain volume element in the flow field if the effect of the term was to cause a net increase in the turbulent kinetic energy of the volume element. This is the usual convention and is consistent with that used by Laufer (1954) and Hinze (1959) (but not Rotta; 1962) although it leads to the seemingly paradoxical statement that a gain in turbulence energy is associated with a negative turbulence production term.

6.2 Comments on Interpretation

The assignment of names to the individual terms in the energy equation and the implied physical interpretation is essentially conventional. As pointed out by Brodkey et al (1973), the terminology is vague and the physical implications of the terms have never really been clear. The historical basis for the convention is the dynamic flow model which developed out of work on grid flow and pure shear flow. Strictly speaking, the equation can only be regarded as a mathematical expression describing a

functional relationship between the physical properties of the fluid, the pressure, and the velocity. The subsequent identification of specific terms with particular physical mechanisms implies the conception of a flow model. Caution must therefore be exercised in applying these classic names to the terms when examining a different flow case. As an example, to assign a particular grouping of terms a name such as "production" and hypothesize a physical mechanism to account for the relationship of the quantities in this term and then, on the basis of its behavior in grid flow, expect it to be always of one sign would be the erroneous elevation of the flow model to the status of a physical law. A subsequent observation of changing signs in some other flow regime does not imply a contradiction but would rather serve to demonstrate the inadequacy of the original model and may imply that other mechanisms may be involved. The main point is that the terminology applied to the various terms do not preclude the existence of other phenomena or different interpretations of the terms for new flow regimes. Lindsay and Margenau (1956) have given a detailed discussion of these concepts relating physical models and mathematical symbolism.

A further point concerning the interpretation of the energy balance terms is that the equation involves only overall time averaging of turbulent quantities. It can be argued

(Bradshaw; 1974) that the equation is therefore too crude to support the development of physical models of the detailed flow mechanism. Brodkey et al (1975) have considered this problem of interpretation and suggested the examination of the instantaneous behavior of individual terms. In particular, they reformulated the production as the mean of the instantaneous stress-velocity gradient product. This procedure showed that the triple velocity products in the diffusion term could be considered as production terms and that the work term due to viscous shear stress of the turbulent motion was similar to an expression for molecular diffusion. This demonstrated the ambiguities of interpretation. Brodkey et al (1975) suggested the need for conditional analysis of the turbulence to resolve these difficulties. This is particularily true for the present results in the entrance region where intermittency exists.

6.3 Evaluation Techniques

6.3.1 Closure and Dissipation

Each term in the energy balance equation, except term II which contains pressure-velocity correlations, could be calculated from the experimental results. Term II which was not available experimentally was obtained by closure. The dissipation term combined with the last part of term IV was estimated from the root mean square measurements

of the time derivative of the longitudinal velocity fluctuations, assuming small scale isotropy and Taylor's frozen turbulence hypothesis such that:

$$-\nu\overline{\left(\frac{\partial u_i}{\partial x_j}\right)\left(\frac{\partial u_j}{\partial x_i}\right)} + \nu\overline{\left(\frac{\partial u_i}{\partial x_j} + \frac{\partial u_j}{\partial x_i}\right)\left(\frac{\partial u_i}{\partial x_j}\right)}$$

$$= \nu\overline{\left(\frac{\partial u_i}{\partial x_j}\right)^2} = 15\overline{\left(\frac{\partial u}{\partial x}\right)^2} = \frac{15\nu}{\overline{U}^2}\overline{\left(\frac{\partial u}{\partial t}\right)^2} \qquad (6.7)$$

The expediency of this method of dissipation measurement for a survey study of the energy balance was obvious because of the relative ease with which $\partial u/\partial t$ profiles could be measured. A comparison of the dissipations determined using time derivative measurements with those evaluated from one dimensional spectra measurements using equation 3.1 indicated that the estimates from the derivative measurements were lower than those obtained from the spectra.* As shown by figure 29 the values were linearly related. The estimates using derivatives were approximately 30% lower. Lawn (1969) has done a comparative study of dissipation measurement techniques in developed turbulent pipe flow. Lawn's findings indicated that for a Reynolds number of 9×10^4 (based on centerline velocity and diameter), the ε from his spectra measurements was systematically in error by -29% when compared with estimated values determined by closure of

* Calculations of the high turbulence intensity shear flow correction for the spectra estimate of ε (Lumley; 1965) indicated that the ε values were approximately 1% too high.

the fully developed energy balance equation. Thus, while the magnitude of the dissipation may have been systematically underestimated by as much as 60%, the trends which were indicated by the $\partial u/\partial t$ results were most probably correct.*

6.3.2. Spatial Derivatives

The longitudinal and radial derivatives of the basic turbulence measurements appearing in the energy equation were obtained by a process similar to that originally developed to get the longitudinal derivatives of U required for the evaluation of V from continuity (Section 4.2). The high density data grids of the survey measurements (Section 3.5) provided the input data for the computation of these spatial derivatives. Longitudinal derivatives of turbulence quantities were obtained by analytic differentiation of fifth order least square polynomial fits of the data at each radial position. The resulting fourth order derivative polynomials were evaluated at two diameter intervals. As with the derivatives of the mean velocity, the resulting derivative data was smoothed numerically in the radial direction using a Hamming convolution filter. This eliminated small irregularities which were inconsistent with expected smoothness. Data was then extracted from the smoothed, high density data grids to fill a matrix of sixe 21 x 35 representing the

* An estimate of length correction for the X probe $\partial u/\partial t$ results based on Wyngaard's (1969) analysis for parallel wires indicated that an underestimate of ε between 50% and 70% was possible for the typical range of η values encountered. These were assumed to be appropriate for the X probe since Wyngaard found that the parallel wire corrections also applied to the 45° slant wires of a vorticity probe.

previously described for the basic measurements. Computations of the various energy equation terms were performed with a series of computer routines designed to handle the 21 x 35 point matrices.

Radial derivatives were obtained by an analogous procedure but with numerical smoothing in the longitudinal direction. Centerline zero values for the derivatives (a symmetry condition for mean quantities) were forced by reflecting five data points for radial positions nearest the centerline, around the centerline, before fitting the fifth order polynomials and analytic differentiation.

Both longitudinal and radial second order derivatives were obtained by application of the same procedures to the data for the first derivatives except no virtual points about the centerline were used.

The techniques for producing the spatial derivatives were developed as Fortran computer programs. The polynomial technique required much more computer time to determine the derivatives than a finite difference technique would require. Its use in iterative computational procedures would therefore be inappropriate. However, differencing techniques are very sensitive to errors in the data and can produce unacceptably large fluctuations in the computed derivatives. The polynomial technique produced smooth mean results which were both physically reasonable and appropriate for contouring.

6.4 Spatial Derivative Contours

Contour plots of the longitudinal and radial derivatives generated for U, V and $\overline{q^2}$ appear as figures 30 - 35. The success of the fifth order polynomial fits for the data was supported by the finding that the contoured derivatives which were produced did not contain unexpected zero contours inconsistent with the original data. Such spurious zeros might have been introduced had the order of the fitted polynomials been too high, allowing oscillation of the fitted curve between data points.

The behavior of the spacial derivative plots was generally more complex than for the contours of the original data. As expected, zero derivative contour lines corresponded with the ridges and troughs (lines of maximum or minimum values) on the original data contours. More detailed features of the original contoured data such as changes in contour spacing were emphasized by the derivative contours. In particular a region of maximum longitudinal spatial gradient for U was apparent in the nonturbulent entrance region core (Figure 30). This may indicate the spatial location where the mechanism causing overshoot was most effective. Details of the wall region turbulence structure were also highlighted by the closed patterns of the turbulence intensity spatial derivative contours in that region (Figures 34 and 35).

6.5 Energy Balance Contours

6.5.1 Production

The total turbulent kinetic energy production (Figure 36) had a general behavior similar to the Reynolds stress terms, with a ridge of high production extending from the wall region into the core region for $30 < x/D < 42$. For a fixed radial position, the region of maximum production was upstream of the position of maximum Reynolds stresses. According to the sign convention adopted for the energy balance equations, a negative term corresponded to a gain of turbulence energy for a unit mass. Production was therefore greatest near the walls. The production describes the action of Reynolds stresses to extract energy from the mean flow. While the production term III is a grouping of four terms only the first term was significant. The others were approximately two orders of magnitude smaller over the contoured region. This was especially true for the parts involving the differences of normal stresses. While the smaller magnitude parts did not affect the total production appreciably, their contoured behavior was quite complex (Figures 37, 38, and 39). In each case the predominant contour features appeared to divide the flow field into three regions: a region associated with the growing turbulent boundary layer upstream of the mean flow overshoot positions, a second region associated with the flow downstream

of the mean flow peaks where the turbulent stresses peaked and fully developed flow was established, and a region near the pipe exit where diffuser effects were identified.

In the usually observed situation, the production terms bear a sign indicating an increase in the turbulent kinetic energy at the expense of the mean flow energy. However, Tennekes and Lumley (1972; p. 62) have pointed out that the reverse situation can occur over restricted flow regions. This admits the possible existence of a mechanism by which the mean flow may be accelerated at the expense of the turbulent energy. Individually, the smaller magnitude production terms exhibited regions where this reverse turbulent production could be occurring. The reverse production terms which appeared in the entrance region were of particular interest since they could play a role in the nonasymptotic mean flow development.

While the usual dynamic processes involve transfer of kinetic energy to higher wave numbers and eventual dissipation, theoretical work on two dimensional turbulent flow (Novikov; 1974) indicates that the transfer of turbulent energy to the lower wave numbers will occur. It seems plausible that in the region of the boundary layer - core interface the turbulent structure may tend towards two dimensionality and be distiguished by a special energy transfer mechanism tending to accelerate the mean flow at the expense of the turbulent kinetic energy.

In connection with the turbulence production term, the behavior of the mean flow vorticity contours, $\frac{1}{2}\left[\frac{\partial(V/U_B)}{\partial(x/R)} - \frac{\partial(U/U_B)}{\partial(y/R)}\right]$ (Figure 40) was examined. According to recent theoretical work at Stanford (Ferziger and Shaanan; 1976), the presence of mean flow vorticity in a turbulent field should inhibit production. A comparison of the vorticity with total production contours seemed to bear this out insofar as the ridge of high vorticity extending from the wall region in the vicinity of x/D = 25 could be associated with the ridge of total turbulence kinetic energy production in the same area. The only component of mean vorticity which exists for the axisymmetric pipe flow may be attributed to fluid tending to roll, like donut-shaped toroids, about the pipe axis. Over most of the contoured region the positive vorticity indicated a tendency of the mean flow to turn towards the pipe wall. The core region exhibited a small region of opposite tendency.

6.5.2 Mean Flow Convection

Term I in the turbulent kinetic energy balance describes how the mean flow moves turbulence energy in the field. The mean flow convection contours exhibited a radical nonasymptotic behavior (Figure 41). In this case the second part of the mean flow convection term was of opposite sign and it

was typically an order of magnitude smaller than the first part (Figures 42 and 43). This indicated that the general pattern of the total mean flow convection was largely due to the interrelation of the U and turbulence intensity fields rather than the computed V field which it appeared to resemble. The mean flow convection contours indicated a region of general turbulence kinetic energy loss, followed downstream by a region of kinetic energy gain.

As the flow became fully developed, the magnitude of the mean flow convection diminished. A zero value contour traversed the flow near x/D = 65. Since the mean flow convection was zero only if both the longitudinal derivative of the turbulent kinetic energy and the mean radial velocity component were zero, the convection term was a sensitive indicator for fully developed flow. Closer to the pipe exit the variation of the mean flow convection across the pipe reproduced the same trends as those measured independently by Okwuobi and Azad (1973) in the diffuser.

6.5.3 Viscous Transport

Term IV of the turbulent kinetic energy balance is the viscous transport term. Only the part of the term involving the Laplacian of the turbulent kinetic energy was calculated

and of these two terms only the first was significant (figure 44). The remaining part of the viscous transport term was included in the dissipation estimate. The viscous transport term represents the transport of turbulence energy due to viscous effects and as such would be expected to be important only where viscous effects are important such as near a solid boundary. Throughout the major portion of the developing field away from the pipe axis the viscous transport term is about an order of magnitude smaller than the mean flow convection. In the fully developed region away from the pipe axis the viscous work term was small and showed a small energy loss as the wall was approached. This was similar to Laufer's (1954) findings for fully developed pipe flow.

The appearance of cells of decreasing absolute magnitude along the centerline was unexpected. In these cells, the viscous transport approached values comparable in magnitude to the mean flow convection term. These cells tended to delineate the regions of acceleration and deceleration of the longitudinal mean velocity component which did not enter into the calculation for the viscous transport at all. This suggested that when the mean flow was accelerating or decelerating, even though this was not due to the local presence of a solid body, viscous effects became more important.

6.5.4 Dissipation

The appearance of the nondimensionalized dissipation contours, as determined from $\partial u/\partial t$ (Figure 45), was similar to the behavior for the total production term, although the longitudinal peak positions were farther downstream, closer to those of the Reynolds stress terms. Examination of the contour magnitudes for $.7 < y/R < .9$ indicated that dissipation values were approximately 1/3 to 1/2 of the production. Considering that dissipation may have been underestimated by as much as 60% and that the relative magnitudes of the mean flow convection and viscous transport terms were small in this region, it appears that production and dissipation approximately balanced near the wall. Further, the high gradient wall region which appeared in the contours for the convective diffusion term, which was calculated by closure (Figure 46), was apparently caused by this underestimate of the dissipation measurements.

6.5.5 Closure Term

The closure term which involves triple velocity products and pressure-velocity correlations divided the flow field into two regions. The term was positive in a large area of the flow field near the wall. This indicated a loss of turbulent energy due to convective diffusion. The term was negative near the pipe axis and in the region of the boundary layer-core interface. The zero contour line dividing these

regions ostensibly coincided with the limits of the region of nearly constant correlation coefficient previously observed. In the centerline region, for $38 < x/D < 54$, where total production was small, the convective diffusion achieved its largest negative values to balance the turbulent kinetic energy losses due to all of the other energy terms. The convective diffusion also appeared to be an important energy term at the top of the boundary layer in the entrance region where the production was small. Convective diffusion becomes the only significant term to balance the mean flow convection in this region.

6.6 Tentative Flow Classification

Based on the approximate spatial locations of the contour features of the measured and calculated quantities, an overall impression was created that the flow field could be divided into two broad areas (Figure 47). The contoured behavior of quantities such as the mean radial velocity, mean flow convection, mean vorticity, viscous transport, and correlation coefficients segregated the part of the flow field in the entrance which was with the top of the growing turbulent boundary layer and the acceleration of the mean flow field. The nonasymptotic development of the mean flow was identified with this "interaction" region. Further downstream where the total production, dissipation, and Reynolds stress tensor contours peaked, it was hypothesized

that the response of the turbulent quantities to the mean flow nonasymptotic development was in evidence. This area was called a "recovery" region. The additional classifications which are shown in the figure are based on more detailed contour features within these two regions.

7.0 SPECTRA RESULTS

7.1 Preliminary Checks

A comparison of normalized spectra results for u, using the Disa 55P51 X probe and the 55P01 single wire probe at 3 radial positions for x/D = 65, showed that the single wire gave slightly higher spectral estimates in regions of high turbulence intensity (Figure 48). A check of the nondimensionalizing factor ε from equation (3.1) also gave comparable values for both probes and it was concluded that the use of the X probe for further spectra measurements was justified. Spectra results obtained with the Krohn-Hite 3550 filter (constant 43% of mid-frequency bandwidth) were compared with those obtained using the extremely sharp 10 and 100 Hz bandwidth filters of the H.P. 3590-A wave analyser (Figure 49). Even at the highest wave numbers, the results were nearly identical, verifying that the Krohn-Hite filter was adequate for the measurement of the smooth spectra. As a second check, the spectra results for u at x/D = 60 and y/R = .5 were compared with those of Lumley and Takeuchi (1976) measured in fully developed pipe flow at nearly the same Reynolds number. Excellent agreement was found for α coefficients in the 5/3 decay region of each spectrum (see Section 7.5).

7.2 Wave Number Spectra

One dimensional wave number spectra ($E_i(k_1)$) (where i = 1, 2, or 3 for u, v, or w respectively) were obtained for 3 radial positions at 7 axial positions. Radial positions in the inlet region, where a nonturbulent core existed, were selected so that $y/R = .9$, $y'/\delta \approx .5$ and .9 ($y' = R-y$) using the contours of the total turbulence intensity to estimate δ. Beyond $x/D = 30$, δ was taken to be the pipe radius. The nondimensionalized ($\Phi_i(k_1\eta)$) spectra results for u, v and w appear as figures 50, 51, and 52. The pertinent experimental parameters and calculated scales for the spectra appear in Table 2. In general, all of the spectra collapsed in the high wave numbers. Exceptions were the data for x/D = 10 and 20 at $y'/\delta = .9$ where intermittency of the turbulent boundary layer existed. For axial positions in the inlet region a trend for increasing low wave number energy with downstream position existed. This trend was least pronounced for v spectra. The detailed behavior of the spectra for $x/D > 30$ seemed to suggest a maximum of low wave number energy for $x/D \approx 40$ or 50. This would be consistent with the nonasymptotic turbulent field development, but the large data scatter, especially at the lowest wave numbers, made a definite statement impossible. The appearance of a high wave number "hook" in spectra results for $y'/\delta = .9$ was attributed to the decreasing signal to anemometer noise ratio for the higher Kolmogorov miscroscales, η, of the core region turbulence. The Kolmogorov microscales

were computed using ε determined from the spectra and varied from approximately 1.3×10^{-4}m near the pipe axis, to $.7 \times 10^{-4}$m at y/R = .9. This effect of noise on the high frequency character of the spectra has been described by Wyngaard and Lumley (1967).

All of the u spectra were characterized by a -5/3 slope region over about a decade of wave numbers. This range was not as extensive for the v and w spectra. The turbulence Reynolds number $R_\lambda = 15^{1/2} (u'\eta/\nu)^2$ was calculated for each u spectra using the Kolmogorov length scale (see Table 2). Values ranged between 140 and 250 with maximum values near the wall. In the intermittent region near the inlet some lower values of R_λ occurred. Bradshaw (1967) has suggested that $R_\lambda = 140$ can be taken as a lower limit for the existence of an inertial subrange for pipe flow. On this basis, it was expected that the major portion of the turbulent field would exhibit some form of local isotropy for higher wave numbers.

7.3 Dissipation Spectra

To facilitate examination of the high wave number spectra behavior, dissipation spectra were computed from the wave number spectra. While a log-log presentation of the dissipation spectra (after Kistler; 1964) gave the impression of general convergence of the measurements, a linear plot (Monin and Yoglam; 1975) was chosen to magnify the details

(Figures 53, 54 and 55). Scatter of the data points at the dissipation spectra peaks was least for the measurements at $y'/\delta = .5$ compared with the results either closer to the wall or pipe axis. Frenkiel and Klebanoff (1975) pointed out that the appropriate region for study, when investigating the small scale structure of a boundary layer, is located at an intermediate position, away from the intermittency effects associated with both the wall and the outer regions of the boundary layer. The appearance of the present spectra results at $y'/\delta = .5$ seem to bear this out.

The physical significance of the dissipation spectrum peak has been given by Monin and Yoglam (1975). The peak position defines the high wave number limit of the -5/3 decay region and therefore, if it exists, the upper limit of the inertial subrange. While Monin and Yoglam suggested a value of $k_1\eta = .125$ for this limit, the present results peaked near $k_1\eta = .10$. Similar dissipation spectra peak positions at $k_1\eta = .10$ were found by Champagne et al (1976) in a two-dimensional mixing region. Lumley and Takeuchi's (1976) pipe flow results were similar. Bradshaw (1967) has suggested $k\eta \leq .1$ as an upper limit for the -5/3 region. For one-dimensional spectra he has modified the limit to $k_1\eta \leq .07$ but, when compared to the present results, this figure appeared to be conservative.

Qualitative comparison of the heights of the spectral peaks for $y'/\delta = .5$ showed that those for v and w were nearly the same. Using .37 as a crude representative value of the height, a ratio of the radial and circumferential peak heights to the u height of $\simeq 1.5$ was estimated. The results of detailed calculations with the maximum spectral value for each spectrum gave a mean ratio within 10% of 4/3, the theoretical value for a locally isotropic structure. The satisfaction of this local isotropy condition at the high wave number limit of the -5/3 law region was considered as evidence for the existence of an inertial subrange.

7.4 Wire Length Effects

The present spectra results were obtained using a wire with a sensitive length $l_w = 1.25$ mm. For the dissipation spectra of u at $y'/\delta = .5$, the l_w/η values were all within 5% of 12.1. This ratio was considerably higher than those of Champagne et al (1976) and Lumley and Takeuchi (1976) (reporting $l_w/\eta = 4$ and 4.1 respectively), but surprisingly, the dissipation spectra compared well and did not appear to show significant attenuation effects for $k_1\eta < .5$. Wyngaard (1969) has shown that for wave numbers greater than l_w^{-1} ($k_1\eta \simeq .08$ for the present results), the effects of wire length attenuation become increasingly important until at $k_1\eta = 1$ the attenuation is about 30%. Champagne et al (1976) compared dissipation spectra results obtained using wires

with l_w/η = 12 and 4, using $\partial u/\partial t$ measurements with the l_w/η = 4 wire to estimate ε, and demonstrated a relative attenuation consistent with Wyngaard's calculations. The wave number spectra nondimensionalization and the calculation of dissipation spectra for the present results were carried out using ε computed by integration of the wave number spectra rather than from $\partial u/\partial t$ measurements, although both methods assume isotropy. Consideration of the effects of using an underestimated ε value to process a given set of $E_i(k_1)$ spectral measurements indicated that dissipation spectra would appear to be shifted to higher $k_1\eta$ values by a factor related to $\varepsilon^{-1/4}$ and would be amplified by a factor related to $\varepsilon^{-3/4}$. The apparent agreement between the present measurements and the previously mentioned l_w/η = 4 results indicated, therefore, that the ε value estimated from the spectral results significantly underestimated the true ε value and was not as good as values estimated by the $\partial u/\partial t$ measurements with the smaller l_w/η ratio. It was concluded that the attenuation of spectral measurements which must occur because of the high l_w/η ratio, was somewhat compensated by the corresponding low values of ε which arose. Had the ε values calculated from the present $\partial u/\partial t$ measurements with l_w/η = 12.1 been used, an even larger underestimate of ε would have resulted (Figure 29). It becomes evident, that in the absence of $\partial u/\partial t$ measurements with l_w/η of at most 4, the best estimate of ε was derived from spectra results rather than $\partial u/\partial t$ measurements with the

same wire. This is in agreement with Lawn's (1969) findings and implies that any comparison of spectra results must include careful consideration of the source of the nondimensionalizing terms.

7.5 Alpha Plots

Details of the spectra behavior for intermediate wave numbers was obtained by plotting α_i vs $k_1\eta$ (Figures 56, 57, and 58) where α_i was the one dimensional Kolmogorov inertial subrange constant defined by:

$$\Phi_i(k_1\eta) = \alpha_i(k_1\eta)^{-5/3}. \qquad (7.1)$$

The extent of the -5/3 decay region for each spectrum was delineated by a region of approximately constant α_i value. The upper $k_1\eta$ limit of the constant α_i region corresponded favorably with respective peak positions of the dissipation spectra. As expected on the basis of the appearance of the $\Phi_i(k_1\eta)$ plots, the range of constant α_2 and α_3 was very narrow. For reasons presented above, the analysis of the α_i plots was restricted to those for $y'/\delta = .5$. These exhibited the least data scatter. For the limited range of $k_1\eta$ for which all of the u, v and w spectra at a position had a constant α_i value, the isotropic condition $\alpha_3 = \alpha_2 = (4/3)\alpha_1$ was found to hold. This condition was satisfied for a range of $k_1\eta$ extending about 1/3 decade below the upper

limit of the inertial subrange. Thus, for a considerable range of $k_1\eta$ the u spectra exhibited a -5/3 power law behavior even while anisotropic conditions existed. This feature was also present in Lawn's (1969) pipe flow results. The values for α_i in the dissipation region of the spectra progressively deviated from the isotropic ratio relationship with increasing $k_1\eta$. This was undoubtedly a reflection of the wire length attenuation.

The constant α_1 regions for the u spectra at $y'/\delta = .5$ showed a considerable range of scatter for α_1. An average value of .57 was calculated which was in fair agreement with Bradshaw's (1967) value of .55 for the outer layer of a shear flow. In particular, the data for x/D = 60 within the constant region indicated an average α_1 value of .57, in agreement with the value at $y'/\delta = .5$ measured by Lumley and Takeuchi (1976), in what they have considered to be fully developed pipe flow, at x/D = 60, for a Reynolds number of 60000 (radius = 1.26 cm, mean velocity = 7.6 m/sec.). The spectra which they measured were obtained by digital methods. The agreement between their digital results and the present analog results indicated that the filters which were used were adequately sharp.

7.6 Integral Scale Estimation

Using the present u spectra results and the method recommended by Builtjes (1975), the value of the Eulerian

longitudinal integral scale (A) was estimated. As given by Builtjes,

$$\lim_{k_1 \to 0} E_1(k_1)/(u')^2 = 2A/\pi. \qquad (7.2)$$

The approximately constant low wave number region of the $E_1(k_1)$ spectra was extrapolated graphically to $k_1 = 0$ to obtain the values appearing in Table 2. Except for the inlet regions, the largest values of A were associated with the $y'/\delta = .5$ measurements. Typical values of A ranged between .3 and .5 D. A similar radial trend for the integral scale has been given by Sabot and Comte-Bellot (1976). Smaller integral scales were measured in the inlet region, consistent with the occurrence of a thinner boundary layer. In this region ($x/D \leq 30$), the largest integral scales occurred for $y/R = .9$. The intermittency of the boundary layer can be expected to decrease the value of the integral scales determined from the low wave number spectra behavior.

7.7 Cross Spectral Density

Measurements of the cross spectral density of u and v, that is the shear stress spectra, appear in nondimensional form in figure 59. In contrast to the one dimensional spectra, the least data scatter occurred for $y/R = .9$ which was within the region of constant correlation

coefficient as indicated by contouring (Figure 24). Because the mean $\overline{uv}$ values and hence, the spectral estimates were smallest near the pipe axis due to the flow symmetry, experimental accuracy diminished and may have contributed to the larger data scatter for $y'/\delta = .9$. This is in addition to the intermittency effects in the entrance region. The anomalous results for $x/D = 1.8$, $y/R = .9$ due to the presence of the flow trip were included because of the interesting relationship which they bear to the one dimensional v and u spectra. It was evident that the predominent effect of the trip roughness elements was to introduce radial velocity fluctuations over a rather restricted range of $k_1\eta$ centered approximately at $k_1\eta = .01$. Using the u spectral estimate of ϵ, this $k_1\eta$ corresponded to a wave number of $\approx 200\ m^{-1}$ which compared with a rough estimation of the linear distribution of sand grains on the trip. As evidenced by the stress spectra for $y/R = .9$, the effects of the amplified shear were quickly dissipated. The absence of marked trip effects in the u spectra agrees with the spectra measurements of Klebanoff and Diehl (1952), who studied the same trip in a flat plate geometry.

Klebanoff (1955) pointed out that the shear spectra provide a direct test of local isotropy since local isotropy can exist only for $k_1\eta$ values for which the shear spectrum is zero. Thus, extrapolation of the shear stress spectra to zero provides a lower $k_1\eta$ limit for local isotropy. The

shear stress spectra for $y'/\delta = .5$ indicated a limit of $k_1\eta \approx .08$ while those for $y/R = .9$ and $y'/\delta = .9$ gave values nearer $k_1\eta = .1$. The observation that, for $k_1\eta$ values below these limits, the isotropic ratio for the energy of the velocity components held and yet shear was nonzero, was characteristic of the condition termed "second class isotropy" by Bradshaw (1967). It appears that true local isotropy was achieved only at the upper $k_1\eta$ limit of the -5/3 region. It should be noted however, that the requirement that the cross spectrum actually vanish for local isotropy is unnecessarily strong. The discussion given by Tennekes and Lumley (1972; p 262) indicates that local isotropy is a state that is achieved asymptotically and begins when the time scales of the dissipative eddies are short relative to those of the mean strain rate. On this basis, it is not necessary for the cross spectrum to vanish at a particular wave number for locally isotropic conditions to hold.

8.0 THE TURBULENT-NONTURBULENT INTERFACE

8.1 Motivation For Study

The contoured results of the turbulent kinetic energy balance survey focused attention on the zone associated with the turbulent-nonturbulent interface in the pipe inlet region. The appearance of production terms which suggested a mean loss of turbulent energy to the mean flow was especially intriguing. The possibility that these results were a clue to the mean flow overshoot mechanism and overall nonasymptotic development warranted further, more detailed, turbulence measurements. It was hypothesized that the focusing effect of the pipe geometry could accentuate some details of the turbulent-nonturbulent interface mechanism. This could perhaps cause an acceleration of the mean flow. The primary objectives of this further series of experiments were to examine the interface region and study the nature of the free stream fluctuations above the interface.

The spectra measurements were not particularily indicative of the nonasymptotic development and suggested that this behavior was mainly a characteristic of the low frequency turbulence. Considering this, and the reasonable assumption that effects of an interaction between the mean flow and boundary layer would probably be most evident for large scale turbulent structures, it was decided to include an experimental investigation of low pass filtered

turbulence.

8.2 Description of Experiments

Basic quantities which were measured in this specialized series of experiments included the second, third, and fourth moments (intensity, skewness and flatness factor) of the u and v turbulence signals. Detailed measurements were also made of the $\overline{uv}$ Reynolds stress and the percentage contribution to the total stress due to u and v fluctuations in each of the four quadrants of the uv plane. First and second order time derivatives of the u signal were produced and estimates of the intermittency factor in the inlet region were made by a visual analysis of these signals on a Tektronics model 466 dual trace storage oscilloscope. Only "overall" characteristics of the flow were measured. That is, no discrimination was made between the random motion occurring inside and outside the bulges.

The special analog turbulence processing equipment required to produce the various moments, stresses and derivatives were designed and built by Mr. R.H. Hummel in association with Tri Met Instruments Ltd. of Winnipeg. The circuits were of standard design employing high quality solid state multipliers and amplifiers. The instrumentation consisted of a model TM-377 turbulence processor, TM-TD1 differentiator and TM-276 quadrant correlator. The function

of the quadrant correlator was to select the positive or negative parts of the u and v fluctuating signals and produce a product signal. The linearized signals from a Disa 55P51 X probe provided the inputs to the turbulence processor. The anemometers, linearizers, probe supports and traversing mechanism were as described previously for the survey measurements. Filtering of the signals for the large scale turbulence measurements was performed with Krohn-Hite model 3770 filters set at a low pass frequency of 500 Hz. The operational effectiveness of the various analog devices was verified by visual observation of the simultaneously stored input and output traces on the storage oscilloscope. In particular, by using the scope in an XY plot mode, the transfer function of the various square, cube and fourth power circuits could be checked directly and the amplifier gains could be readily adjusted for maximum signal levels without exceeding the dynamic range of the instrumentation.

Profile measurements were made at approximately 5 diameter intervals in the first 20 pipe diameters where a discrete potential core existed. Measurements were continued at 10 diameter intervals further downstream. Most of the measurements were made in the half of the flow opposite to the position where the traversing mechanism entered the pipe. The asymmetrical probe support slightly displaced the symmetry of the flow from the pipe axis.

8.3 Experimental Results

8.3.1 Turbulence Intensities

Profiles of the longitudinal turbulence intensity, which were measured using the turbulence processor, are presented in figure 60. The measurements were normalized by the local mean velocity. This normalization was appropriate for showing the background turbulence levels and the boundary layer thickening in the inlet, but it confused the developing behavior downstream. Thus, the collapse of the results for x/D = 40.1 and 50.4 does not imply that the flow structures were the same. The results in the entrance region core showed a background turbulence level of ≈ .25% for the tunnel. This low value demonstrated that the long settling sections and the screens upstream of the contraction cone were very effective. The high values of $u'/\overline{U_L}$ near the wall, for x/D = 1.71, indicated that increased longitudinal turbulence levels or decreased local mean velocities existed in the "shadow" of the trip element. The position x/D = 1.71 was located approximately 8 cm. downstream of the trip. The measurements further downstream did not exhibit this wall region anomaly. The results on the pipe axis generally increased with downstream distance. The constant $u'/\overline{U_L}$ values, which were characteristic of the nonturbulent core region for each profile, disappeared between x/D = 20 and 30.

A comparison of the relative energies associated with the longitudinal and radial turbulence components in the entrance region ($\overline{u^2}/\overline{v^2}$) is presented in figure 61. The existence of a region associated with the interface, where radial intensities exceeded longitudinal intensities, was clearly indicated by values of $\overline{u^2}/\overline{v^2}$ less than 1.0. Evidence for the existence of this region was indicated by the contours of u' and v' but the details of its magnitude and spatial extent could not be determined. In this region, at x/D = 4.66, the present measurements showed radial turbulence energy levels ≈ 46% larger than the longitudinal levels. This percentage decreased with downstream position. The spatial extent of the region appeared to be largest for x/D = 10.21. The low ratios for radial positions near the wall, at x/D = 1.71, suggested that the trip disturbed the flow proportionately more in the radial direction than in the longitudinal direction. This agreed with the indications of longitudinal and radial spectral measurements in the inlet (Section 7.7).

The anomalies that appeared in the curves between y/R = .5 and .7 for x/D = 10.21, 15.49 and 20.41 (particularily 15.49) correlated with u' contour anomalies in the same region (Figure 18). The reason for this feature was unclear, but it appeared to be related to a local mechanism which tended to decrease longitudinal turbulence energy.

8.3.2 Correlation Coefficients

Measurements of correlation coefficients, $\overline{uv}/u'v'$, in the interaction and recovery regions, are given in figures 62 and 63 respectively. The same general trends were present in both the unfiltered and filtered (low pass at 500 Hz) results, but the filtered correlations were higher in magnitude. This similarity suggested that the main contributions to the correlation were due to relatively large scale flow features.

The symmetry condition which required zero correlation on the pipe axis was satisfied in the recovery region, but the measurements on the centerline in the nonturbulent core showed considerable scatter about zero. Very high amplifier gains were required to measure the small fluctuations in this region. As a result, correlation coefficient measurements were very sensitive to a slight mismatch in the adjustments and linearization of X probe wires. These errors were proportionately much less important closer to the wall, where velocity fluctuations were larger.

The main trends of the correlation profiles in the recovery region compared well with the contoured survey results (Figure 24), although the magnitudes of contoured values were slightly lower than the non-filtered profile values. In the interaction region, both filtered and non-filtered correlation profiles exhibited peak values within

the turbulent boundary layer. The contour correlations also showed peaks, however, they were sharper, higher and located closer to the interface than were those indicated by the profile measurements. The correlation coefficients which were contoured to produce figure 24, were calculated from the smoothed $\overline{uv}$, u', and v' contour data matrices. As outlined in Section 3.5, the data smoothing process using polynomials tended to extrapolate decreasing trends to zero, where a small but non-zero background value existed. Considering this, the discrepancy between the direct profile measurements and the contour behavior, where $\overline{uv}$, u', and v' were small, was understandable.

The most unusual feature of the correlation profiles was the region of positive correlation associated with the area above the turbulent interface. The characteristics of the uv signal which caused this sign reversal were examined using the quadrant correlation technique.

8.3.3 Quadrant Correlations

Conditional measurements of the fluctuating uv signal were made which determined the contribution to the uv signal from each quadrant of the u-v plane. The technique was similar to that described by Willmarth and Lu (1971), and independently by Wallace et al (1972) but no conditioning based on signal amplitude was used (Lu's "hole size" = 0).

The function of the quadrant correlation circuit was to form the instantaneous product of the u and v signals and provide a conditional uv signal for the quadrant selected. Possible conditional uv signals were u_+v_-, u_-v_+, u_+v_+, u_-v_- where the conditional signals were typically defined as

$$u_+v_- = uv\ S(t) \tag{8.1}$$

where $S(t) = 1$ if u is positive and v is negative

$= 0$ otherwise.

According to the sign convention appropriate for the probe orientation and co-ordinates of the present measurements, a positive radial velocity fluctuation corresponded to a movement of fluid towards the pipe axis. Positive u fluctuations indicated movements of fluid in the downstream direction which were superimposed on the mean flow. The occurrence of u_-v_+ events therefore corresponded to the movement of relatively low speed fluid away from the wall. This type of turbulent motion has been called a "burst" or "ejection". Similarily, u_+v_- corresponds to the movement of high speed fluid towards the wall and has been called the "sweep" event. The remaining events have been called "outward" (u_+v_+) and "wallward" (u_-v_-) interactions. Recently, many studies of these kinds of turbulent events in regions near the wall have appeared (e.g., Kline et al; 1967, Kim et al; 1968, Grass; 1971, Brodkey et al; 1974, Willmarth and Lu; 1971, Nychas et al; 1973, among others).

The behavior farther from the wall has been studied by Lu and Willmarth (1973), and Blackwelder and Kovasznay (1972). A recent review article by Willmarth (1975) has summarized the main findings.

The mean value of each of the quadrant conditional signals was measured. To compare the relative contribution of each quadrant to the total uv signal, the absolute values of the means were used to compute a percentage. For example, the percentage contribution of the u_+v_+ signal was calculated using

$$\text{Percent } u_+v_+ = \frac{100 \quad \overline{u_+v_+}}{\overline{u_+v_+} + \overline{u_-v_-} + \overline{u_+v_-} + \overline{u_-v_+}} \tag{8.2}$$

During the measurements, periodic checks verified that

$$\overline{uv} = \overline{u_+v_+} + \overline{u_-v_-} + \overline{u_+v_-} + \overline{u_-v_+} \tag{8.3}$$

within about 5%. The quadrant results for successive longitudinal positions are presented in figures 64 to 72. Each figure contains the data for both the total uv signal and the low pass filtered uv signal.

As with the correlation coefficients, both the filtered and non-filtered quadrant correlation results showed similar behaviors. Within the turbulent boundary layer, the burst

events (u_-v_+) were largest. The sweep events (u_+v_-) were less important. Both the wallward and outward interactions were small and of nearly the same magnitude. These findings were in agreement with Lu's (1972) boundary layer results. The large negative contributions to the uv signal by the burst and sweep events accounted for the negative correlation coefficients in the boundary layer. The results in the first 30 diameters showed a tendency for the burst and outward interaction events to increase in the turbulence near the interface, while sweep events became less important. A rapid change was observed in the intermittent region such that, further towards the nonturbulent core, the u_+v_+ interaction event became most important. This coincided with the measurements of a positive correlation in this region. Near the centerline, in the nonturbulent core, all of the events tended to become equally important. Kovasznay et al (1970), Blackwelder and Kovasznay (1972), and more recently, Charnay et al (1976) have shown that overall (not conditional) measurements in the intermittent region are nearly a linear combination of conditional turbulent and nonturbulent zone measurements which are weighted by the intermittency factor. The behavior of the quadrant profiles up to $x/D = 10.21$, in the intermittent interface region, appeared to be the superposition of two trends; one associated with important u_+v_+ events on the

nonturbulent side of the interface, and one associated with important u_-v_+ burst events on the turbulent side of the interface. The later u_-v_+ burst events are known to be associated with the turbulent bulges of the boundary layer (for example, Blackwelder; 1970). The presence of an important u_+v_+ event on the nonturbulent side of the interface was of considerable interest. Physically, the u_+v_+ event corresponded to the movement of high velocity fluid (relative to the local longitudinal mean velocity) towards the pipe axis. This fluid movement would cause a radial transport of longitudinal momentum towards the pipe axis. The nonasymptotic development of the mean flow field required that some mechanism with this momentum transfer characteristic exist.

Further downstream where the nonturbulent core did not exist, the region of u_+v_+ maximum did not exist. The relative contributions of each event remained nearly constant in the turbulence near the wall. In the centerline region the turbulent cross stream mixing of fluid was apparent. Since the sign of v changed on the pipe axis, symmetry required that the u_+v_- and u_+v_+ events (or u_-v_- and u_-v_+ events) be equal on the pipe axis. Thus, the movement of fluid associated with a u_-v_+ burst from one-half of the flow across the centerline contributed to the u_-v_- interaction event in the other half of the flow. The examination

of the burst event results at x/D = 50.43 and 60.27 showed that this cross stream mixing occurred in a region of radius y/R = .2 about the centerline. This agreed with Sabot and Comte-Bellot's (1975) developed pipe flow observations.

8.3.4 Skewness Coefficients

The skewness coefficient is the nondimensional third order moment of a distribution. For the longitudinal fluctuating velocity component, the skewness was defined by $S_u = \overline{u^3}/(\overline{u^2})^{3/2}$. The profile measurements of S_u, for longitudinal positions in the interaction and recovery regions, appear as figures 73 and 74 respectively. The corresponding measurements for the low pass filtered u signal appear as figures 75 and 76. Filtered and unfiltered results had similar trends, but the filtered results were smaller. This attenuation was expected to occur for the filtered, higher order, moment measurements. This was because the filtering of the u signal removed short duration signal fluctuations which were potentially very large (and therefore significant contributors to the mean) when the higher order powers of the unfiltered signal were formed.

The skewness and all other odd moments are zero for a Gaussian distribution. This implies that a Gaussian distribution is symmetric and that the mean and most probable

value are the same. The skewness of u was negative in the turbulent flow. This implied that the mean value of the longitudinal velocity was lower than the most probable value. The skewness became more negative with increasing distance from the wall. The most negative skewness measurements occurred on the turbulent side of the intermittent region. Like the quadrant correlations, the profile measurements in the entrance region of the pipe appeared to exhibit distinct turbulent and nonturbulent region trends. The data for $x/D \leq 20.41$ clearly showed a trend for increasing positive skewness values in the nonturbulent core as the boundary layer was approached. Hence, in this region, the mean value of the longitudinal velocity fluctuation exceeded the most probably value. A possible reason for this could be the occurrence of relatively rare but large longitudinal velocities.

Few independent results in the nonturbulent region were available to confirm the existence of this positive S_u region. Recent measurements in the intermittent boundary layer on a flat plate given by Charnay et al (1976) do show this feature; however, they have not discussed the result. The overall skewness measurements which they present for a free stream intensity level of .3% have the same character as the present inlet region measurements. Their data also demonstrated that the occurrence of the positive skewness region is highly dependent on the free stream intensity level. Positive

skewness regions do not occur for their measurements at background intensity levels of 1.8% or higher. As reported in Section 8.3.1, the background intensity level for the present results was less than .3%. The conditional skewness measurements made by Charnay et al indicate that the trend towards positive skewness is definitely a characteristic of the nonturbulent zones. Their conditional skewness results in the nonturbulent zones show positive values for background turbulence levels as high as 3.2%. Conditional skewness measurements given by Dean (1974), at a position 26.5 duct heights from his trip, also show positive values in the nonturbulent zone. Dean's results were obtained digitally. Unfortunately, the measurements are not extensive and exhibit considerable scatter.

The trend towards positive u skewness did not appear for profiles measurements for $x/D \geq 30.25$, where presumably the nonturbulent core had disappeared. The maximum negative skewness measurements gradually decreased. Between $y/R \approx .2$ and the wall, the measurements for $x/D \geq 40.10$ collapsed. Near the wall, the measurements were in good agreement with Lawn's (1969) fully developed skewness results. Towards the centerline region, the values were somewhat more negative than Lawn's values.

Overall measurements of the skewness of the fluctuating radial velocity component, S_y, are presented in figures 77 -

80 for both the unfiltered and filtered signals in the interaction and recovery regions. The main feature of the measurements was the high positive skewness peak which occurred near the turbulent-nonturbulent interface. The maximum peak values occurred for the unfiltered results at x/D = 10.21, where S_y values greater than 1.2 were measured. The skewness peaks decreased farther downstream. Aside from a tendency for slightly increased skewness values near the wall, the unfiltered results for x/D = 50.43 agreed with Lawn's (1969) fully developed results. While the filtered results at x/D = 60.27 agreed with those at 50.43, the unfiltered values were lower. Generally, the skewness was near zero on the pipe axis; however, the measurements in the very low intensity core near the entrance (x/D = 1.71 and 4.66) were exceptions. As discussed in Section 8.3.2, the measurements in this region were very sensitive to wire mismatch.

The occurrence of positive S_v values over the turbulent boundary layer indicated that the mean radial velocity was greater than the most probable velocity. Considering that positive v fluctuations were due to motions towards the pipe axis, this skewness suggested that radial velocity fluctuations towards the axis were larger in magnitude and/or more frequent than fluctuations towards the wall. The u_-v_+ burst event and the u_+v_+ outward interaction event are involved with positive v fluctuations. Significantly, the quadrant correlation results showed that through the

turbulent, intermittent, and well out into the nonturbulent flow, it was generally a quadrant result involving v_+ which predominated. S_v peak positions in the entrance region also appeared to be nearer to the pipe axis than the corresponding negative S_u peaks. It therefore seemed plausible to conclude that the special flow dynamics in the intermittent and nonturbulent regions, which were associated with the observations of both positive S_u and predominant u_+v_+ percentages, were also characterized by positive S_v.

A natural way to interpret triple velocity correlations is as a transport or flux. This concept is embodied in the usual grouping of the triple velocity correlations into the convective diffusion term (eqn. 6.3). In particular, Snyder and Margolis (1967) have shown that the skewness of a turbulent velocity component can represent the transfer of the intensity of that component by itself. Further, it is normally expected that the turbulent intensity would be transfered down the intensity gradient. Since the v intensity is decreasing in the direction of positive v (decreases towards the pipe axis), this leads to the expectation of positive S_v. This is consistent with the present S_v results. The S_u results generally indicate the expected upstream intensity transfer, except in the interface region.

The effects of the boundary layer trip were apparent in the S_v results at $x/D = 1.71$ as a secondary peak near the wall. Both the filtered and unfiltered results showed this. Presumably, the flow along the wall was often sharply deflected away from the wall when a trip element was encountered. By this

mechanism, the trip elements could introduce a significant positive skewness to the v fluctuations which they generated. Evidently, the longitudinal extent of this perturbation was limited, since it was not present at x/D = 4.66.

8.3.5 Flatness Factors

The flatness factor of the fluctuating u component is defined by $F_u = \overline{u^4}/(\overline{u^2})^2$ and is a nondimensional measure of the fourth moment of the probability density function for u. Large flatness factors imply that the probability of fluctuations quite different from the mean is large; that is, the normalized probability density function appears relatively wide. For comparison, the flatness factor for a random signal with a Gaussian probability density function is 3.0, while a sine wave has a flatness factor of 1.5. Large amplitude, intermittent signals produce high flatness factors. Profiles of F_u for filtered and unfiltered signals, in both the interaction and recovery regions, are given in figures 81 - 84. Similar measurements for the flatness factor of the radial fluctuating velocity component, F_v, are given in figures 85 and 86. The results in the interaction region all showed peaks associated with the intermittent region. The largest F_u values ($F_u \simeq 20.0$) occurred for unfiltered signals at x/D = 4.66, while the largest F_v values ($F_v \simeq 14.0$) occurred for unfiltered signals at x/D = 15.49. F_u were slightly less than Gaussian near the wall but F_v was larger. Downstream, at x/D = 50.43, the measurements agreed reasonably well with Lawn's (1969) fully developed measurements, although Lawn's results were considerably more scattered.

The high flatness factors, F_u, which occurred in the intermittent region, have also been shown by Charnay et al (1976). They suggest that these flatness factors are related to the spatial distribution of the turbulent structures which exhibit the largest uv values. Their results showed that the maximum flatness factors occurred very near the mean boundary layer thickness position. Sizeable flatness factors occur well out into the nonturbulent region in both the present results and Charnay's results.

8.3.6 First and Second Time Derivatives

Measurements have been made of the first and second time derivatives of the filtered and unfiltered u fluctuation. The initial purpose of the measurements was to calculate the nondimensional factors S and G,

$$\text{where } S = \overline{\left[\frac{\partial u}{\partial t}\right]^3} \Big/ \left[\overline{\left[\frac{\partial u}{\partial t}\right]^2}\right]^{3/2} \quad \left(\text{ie. skewness of } \frac{\partial u}{\partial t}\right), \tag{8.4}$$

$$\text{and } G = \overline{u^2} \cdot \overline{\left[\frac{\partial^2 u}{\partial t^2}\right]^2} \Big/ \left[\overline{\left[\frac{\partial u}{\partial t}\right]^2}\right]^2 . \tag{8.5}$$

Batchelor and Townsend (1946) showed that for isotropic turbulence the factor S is related to the rate of production of vorticity by the process of vortex stretching, and the factor G/R_λ is related to the rate of decay of vorticity

due to viscosity. A complete derivation of the results from the vorticity equation has been given by Panchev (1972). The form of the relationship utilized by Batchelor and Townsend is

$$\frac{d\overline{\omega^2}}{dt} = \frac{7}{3\sqrt{5}} \overline{\omega^2}^{3/2} S - \frac{14}{3\sqrt{5}} \overline{\omega^2}^{3/2} \frac{G}{R_\lambda} \qquad (8.6)$$

where $\overline{\omega^2}$ is the mean square of the fluctuating vorticity. The non-isotropic shear flow occurring in the pipe was not expected to follow the above isotropic relation; however, the expression did suggest a physical interpretation which could be applied to the S and G parameters in the non-isotropic flow. Measurements of S and G in pipe flow have not been available and the particular expressions relating S and G with vorticity production in shear flow are unknown. The decay rate of vorticity by viscosity must certainly have a major bearing on the rate of re-adjustment of the turbulence downstream of the overshoot. Similarily, the generation of vorticity in the interaction region is a fundamental process for boundary layer development. Since direct measurements of the fluctuating vorticity were unavailable, the behavior of S and G were worth investigation. Further, since both S and G were higher order turbulence quantities, they were potentially sensitive indicators of the nonasymptotic development mechanism.

The mean cube of the $\frac{\partial u}{\partial t}$ signal was directly available using the TM377 turbulence processor. The second derivatives of u, which were required for the G calculation, were obtained by using the differentiator section of the TM377 turbulence processor to differentiate the output of the TM-TD1 differentiator unit. The accurate measurement of the second derivatives was limited by the deteriorating signal to noise ratios which occurred at successive differentiation and amplification stages. This was particularily a problem at low values of turbulence intensity. Krohn-Hite model 3770 filters, adjusted to a L.P. cutoff frequency of 28 kHz, were used before and after the differentiation stages to minimize the noise. Measurements of G in the nonturbulent region were not possible. Nevertheless, the present measurements which employed modern, solid state, microcircuit technology, represent a vast improvement in noise and frequency response characteristics over the vacuum tube circuits used originally by Batchelor and Townsend.

The unfiltered and filtered results for S are given in figures 87 and 88 respectively. The unfiltered results within the turbulence showed a trend towards a constant S value of $\approx$ .15 while filtered results were nearer to .35 or .40. The isotropic results given by Batchelor and Townsend are scattered about .4. Townsend's (1948) measurements in the wake of a cylinder indicate a constant S value

of .36. The closer agreement of these older results with the present filtered results may be an indication of the limited high frequency response of the older equipment. The relative magnitudes of the filtered and unfiltered results suggested that the presence of higher frequency components decreases the rate of vorticity production.

A trend towards negative S values was characteristic of the intermittent region. Negative S values were measured in the nonturbulent region. This feature of the $\frac{\partial u}{\partial t}$ profiles was undoubtedly related to the anomalous positive S_u measurements reported in Section 8.3.4.

The profiles of G and $\frac{G}{R_\lambda}$ which were computed from the unfiltered measurements of the first and second time derivatives of u are presented for 7 longitudinal positions in figures 89 and 90 respectively. The measurements of G at x/D = 1.71, 4.66, and 15.49 increased sharply for radial positions where the boundary layer became intermittent. Generally, within the turbulence, the G values appeared to decrease towards the pipe axis. For longitudinal positions in the recovery region, the longitudinal behavior of G at a given radial position showed a trend similar to that exhibited by the dissipation contours

(Figure 45). Specifically, G values for x/D = 50.43 were largest and the values for x/D = 30.25 and 60.27 were lower by nearly the same amount (except near the pipe axis). This similarity between G and dissipation was not due to the common appearance of the term

$$\overline{\left(\frac{\partial u}{\partial t}\right)^2}$$

in both the normalization of the second derivative for G and the calculation of ε. This follows because the term appears in the denominator of the G calculation but in the numerator of the ε calculation.

G measurements of filtered u signals are also included in figure 89 for completeness. Little can be said relating these to vorticity decay. The small value and uniformity of the filtered G emphasized that G is predominantly a fine structure parameter.

The $\frac{G}{R_\lambda}$ profiles (Figure 90) generally increased towards the pipe axis. Large values were again associated with the intermittent boundary layer region. Near the wall, and for x/D > 30, the curves were nearly linear, however, the data as far down the pipe as x/D = 40.10 indicated the trend for sharply increased $\frac{G}{R_\lambda}$ values toward the centerline.

8.4 Visual Studies

Perhaps the most significant progress towards an under-

standing of specific wall and intermittent region turbulent mechanisms has been achieved only recently, by using direct visual studies of individual events and by sampling the turbulence upon detection of a specific event. Thus, while overall statistical measurements provide a convenient method for quantization of the turbulent structure, it is becoming more apparent that their utility for determining the dynamics of a specific turbulence mechanism is limited. For this study, the main ideas concerning a mechanism near the interface which might account for the nonasymptotic flow development were derived from the observation of specific events on the oscilloscope. In addition, qualitative corroboration for several of the statistical characteristics which were presented in Section 8.3 was available through direct observation of the turbulent signals. The storage capability of the oscilloscope was an invaluable asset for the visual studies.

8.4.1 Intermittency Estimates

The intermittency factor, γ, is a measure of the fraction of the time that an intermittent flow is turbulent at a particular location. In fully turbulent flow $\gamma = 1$. The measurement of γ therefore involves some process by which a decision is made as to whether turbulent or nonturbulent flow exists at a particular time. For the present γ estimate,

this decision was based upon a visual assessment of the appearance of $\frac{\partial u}{\partial t}$ signals which were displayed on the storage oscilloscope. If the $\frac{\partial u}{\partial t}$ signal appeared to consist of relatively large amplitude, high frequency fluctuations, it was decided that the flow had been turbulent over that period. During nonturbulent periods $\frac{\partial u}{\partial t}$ was characterized by relatively low frequency, small amplitude, smoothly changing fluctuations. While obviously a large degree of subjectivity entered into the process, it is questionable whether the results would be any less accurate than those obtained by electronic techniques which require the adjustment of discriminator levels. As with most intermittency measurement techniques, the most difficult measurements were for γ near 1, when short nonturbulent regions became lost in the turbulent signal. Fiedler and Head (1966) have discussed this point and show that their optical detection scheme can provide superior high γ measurements.

Intermittency factor estimates for 5 longitudinal positions in the inlet region of the pipe are presented in figure 91. Each point in the figure represents a composite average of measurements on between 30 and 40 oscilloscope traces. The typical cumulative sampling time for the traces was of the order of 1.5 sec. For comparison, the dashed lines are the usual error function curves for a flat plate. These were calculated using

$$\gamma\left(\frac{y'}{\delta}\right) = 1/2\left[1 - \text{erf}\left(\frac{\frac{y'}{\delta} - \alpha}{\beta\sqrt{2}}\right)\right] \qquad (8.7)$$

where $y' = y-R$ and δ = mean boundary layer position. On the basis of Charnay et al (1976), the α and β coefficients were assigned the values .83 and .22 respectively. Mean boundary layer positions, δ, were estimated from the positions of maximum flatness factor of u (Figure 81). Comparison of the flat plate and pipe results suggests that the intermittent region is narrower for a pipe.

8.4.2 Photographic Results

Photographs of oscilloscope traces of the u, v, and $\frac{\partial u}{\partial t}$ signals were taken at the longitudinal position x/D = 10.21. A well defined nonturbulent core existed at this position. The mean thickness of the turbulent boundary layer at this point was $\approx$ 2.5 cms. Photographs were taken at 3 distances from the wall; 2.5, 3.0, and 3.5 cms. The object was to observe the nature of the flow in the outer intermittent region and nonturbulent regions where the unique behavior of S_u, S, and u_+v_+ occurred. Significantly, this was also a region of maximum longitudinal mean velocity acceleration (Figure 30).. The photographs which are presented were selected because they showed particular features more clearly than others would; however, they are

not unique. They are good examples of events which were generally characteristic of the signals. The six photographs appear as figures 92(A) to 92(F). The identification and scaling information for the figures is summarized in Table 3. For all photographs the signal was a.c. coupled to the oscilloscope and ground levels were set at positions 30% and 70% (see left hand scale of photographs) for the lower and upper traces respectively.

Photograph A: (upper trace = u, lower trace = v, $y/R = .5$). At the radial position for this photograph $\gamma \approx .45$. The photo recorded the passage of two large turbulent bulges over the probe at $t \approx 4$ msec and $t \approx 15$ msec (considering $t = 0$ at the left side of the photograph). Within the bulges u was generally negative and v was generally positive. This was characteristic of the "burst" event and implied that the turbulent bulges carried low longitudinal momentum fluid outward towards the core. Turbulent fluctuations with a frequency the order of 10 times that associated with the period of the large bulges appeared to be superimposed on the bulges. This finer turbulent bulge structure also appeared to be characterized by u_-v_+ type events at the higher frequency. Single events with this higher time scale occurred at $t = 1.8$ msec and $t = 9.7$ msec. The overall character u and v traces showed why u_-v_+ were predominate at this position and why negative S_u and positive S_v measurements

occurred. On a finer scale, the photograph suggested that the large turbulent bulges were groupings of higher frequency "burst" events.

Photograph B: (upper trace = filtered u, lower trace = filtered v, y/R = .5). The flow conditions for this photograph were similar to those for photograph A but the total time for the trace was 2.5 times longer. The high frequency turbulent fluctuations which occurred within the large bulges shown on photograph A were attenuated by the filtering (L.P. filtering at 500 Hz). Photograph B showed five large $u_- v_+$ events at times t = 4, 12, 14, 23, and 37 msec respectively. Smaller magnitude $u_- v_+$ events may also have occurred. In several regions the signals appeared to oscillate 180° out of phase, which suggested the presence of successive burst and sweep events. Again, the rather large negative skewness of the u signal was apparent but the filtered v signal did not appear to be significantly skewed. This photograph illustrated that the low pass filtering at 500 Hz was appropriate for the study of the features associated with the large bulge structure of the interface.

Photograph C: (upper trace = u, lower trace = y, y/R = .4). In the position where this photograph was taken, γ was less than .05. A larger vertical scale than that used

for photographs A or B was required to amplify the lower intensity, nonturbulent region fluctuations. The horizontal time scale was the same as for photograph A. The photograph recorded three significant events at times t = 4, 12, and 17 msec. The events had a time scale comparable to that observed for the turbulent bursts of photograph A. The first two events are nonturbulent in character, but the appearance of high frequency fluctuations in the last event indicated that the top of a turbulent bulge was encountered. Each event was characterized by a positive u motion. The corresponding v signal was nearly zero at the u peak position. It appeared that the positive u fluctuation was preceeded by a negative v and followed by a positive v (particularly the second event). Kibens (1968), Blackwelder (1970), Paizis (1973) and Charnay et al (1976), among others, have shown that the turbulent boundary layer structure is convected downstream at a lower velocity than the nonturbulent fluid at the same level. Charnay has shown this difference to be between 3 and 4 percent for nonturbulent background intensity levels of .03%. This finding implies that, with respect to a frame of reference moving with a turbulent bulge, the nonturbulent fluid flows over and around the bulge, somewhat like potential flow around an obstacle (Kibens; 1968). The nonturbulent fluid motions indicated by the events on

photograph C, were consistent with this concept if these events could be associated with nearby turbulent bulges. This association was obvious for the third event. It appears that upon encountering a turbulent bulge the following sequence of events occurred; (1) the nonturbulent fluid was deflected towards the pipe axis, (2) a rather large, rapid longitudinal acceleration followed by rapid deceleration occurred over the bulge, (3) the fluid moved back towards the wall. The absence of turbulent bursts in the first two events suggests that the bulges may influence the nonturbulent flow well above the interface.

Photograph D: (upper trace = u, lower trace = v, $y/R = .3$). Turbulent events were very rare at the position $y/R = .3$ and none were apparent in photograph D. Three distinct nonturbulent events were visible at times $t = 1.2$, 5.0, and 8.5 msec. The sequence of events suggested by photograph C were quite apparent on this photograph. In particular, maximum u values were associated with zero value v fluctuations. The tendency of the u signal to have relatively large positive peaks accounted for the positive S_u values which were measured in this region. Events 1 and 3 were not as large nor as distinct as event 2. Considering only event 2 and the portion of the record for t between 3.0 and 7.0 msec associated with it, a

character of the v signal consistent with the S_v results was observed. Specifically, the positive part of the v signal oscillation was larger and suggested that v was indeed positively skewed. The larger positive v peaks associated with the positive u signal probably indicated the mechanism responsible for the maximum of u_+v_+ events in this region. The infrequency of turbulence events in this region was further evidence that the interface effected the nonturbulent flow a considerable distance above it.

Photograph E: (upper trace = filtered u, lower trace = filtered v, y/R = .3). The flow conditions for this figure were similar to those for figure D, but a slower sweep rate was used. Again the positive skewness of u was evident. The v fluctuations were also suggestive of a positive skewness due to more frequent and larger positive fluctuations. While photograph B had indicated u and v fluctuations which were 180° out of phase, photograph E had the appearance of signals 90° out of phase. This change in character indicated a fundamental difference between the fluctuations associated with the turbulent and nonturbulent regions, and probably accounted for the change from u_-v_+ prominence to u_+v_+ prominence in the quadrant measurements.

Photograph F: (upper trace = u, lower trace = $\frac{\partial u}{\partial t}$, y/R = .3). Photograph F illustrates the operation of the differentiator equipment and shows how the previous measurements of positive skewness of $\frac{\partial u}{\partial t}$ in this region could arise from the positive u fluctuations. The signal which appears in the photograph was filtered at 5 kHz to eliminate the effects of the anemometer noise in the u signal. It was evident from the photograph that the differentiation signal was delayed by approximately .2 msec.

Two positive u peaks were captured on the photograph at times t = 2.1 msec. and 4.2 msec. The second event was particularly large for this radial position and the peak behavior indicated that some turbulence may have actually been encountered. The larger amplitude negative $\frac{\partial u}{\partial t}$ fluctuations were characteristic of negative skewness and were likely the reason for the negative S results of figure 88. The large negative $\frac{\partial u}{\partial t}$ fluctuations indicated a fundamental asymmetry in the u fluctuation peak. It appeared that a more rapid change in the u component of velocity occurred upstream of the turbulent bulge than downstream. (Note that the downstream edge of a turbulent bulge reaches the probe before the upstream edge so that the action at the downstream edge is associated with the left hand side of the u peak on the photographs.) It was unclear whether or not this was due to the shape of the

turbulent bulges. If it were due to the bulges, it would appear to indicate steeper interfaces on the upstream parts of the turbulent bulges. This would not agree with LaRue and Libby's (1976) measurements of interface slopes.

9.0 REMARKS ON THE NONASYMPTOTIC MECHANISM

9.1 Speculative Model

The experimental evidence has generally indicated that the nonasymptotic development of the turbulent pipe flow was associated with a mechanism occurring at the turbulent-nonturbulent interface. The survey measurements of turbulent quantities have shown that the turbulent development occurs in response to the mean flow development.* The mean velocity survey results showed that, in the region near the turbulent-nonturbulent interface, the mean flow was accelerated. The results for various energy terms also focused attention on the interface region. In particular, the acceleration of the mean flow in this region was associated with a negative production term, which could imply a transfer of kinetic energy from the turbulent to the mean flow field. The more detailed measurements reported in Chapter 8 showed that positively skewed u fluctuations existed in the nonturbulent region. It was also observed that u_+v_+ Reynolds shear components, which could cause the transfer of longitudinal momentum against the mean velocity gradient, were important. The study of photographs of individual events in the nonturbulent region has suggested that the measured statistical behavior of the nonturbulent fluctuations was due

* "Response" is used in terms of the streamwise distribution of the mean and turbulent flow features.

to the proximity of turbulent bulges. The visual studies agreed with the interface model suggested by Kibens (1968) and Kovasznay et al (1970). The nonturbulent fluid appeared to flow over the bulges in an irrotational manner. The studies showed that the turbulent bulges influence the nonturbulent flow over a wide region. The induced free stream fluctuations appear to be central to the mechanism causing the mean flow acceleration.

From a simplified and mechanistic point of view, the core region flow appears to be squeezed by the growing turbulent boundary layer. Within the turbulent boundary layer, the production of turbulent fluctuations using energy extracted from the mean flow near the top of the boundary layer, combined with viscous dissipation to heat, results in a growing, decelerating annular flow region which extends from the wall. The core region accelerates to maintain a constant mass flow rate, as though being squeezed by the growing boundary layer. Obviously the entrainment of core region fluid into the boundary occurs, but the rate may not be sufficient to prevent the surface from acting as a contraction surface for the core flow. The decreased overshoot behavior for higher Reynolds numbers may be due to higher entrainment rates. The behavior of the nonturbulent fluctuations far from the interface also suggest that the interface acts as a wavy

boundary for the core fluid.

The character of the nonturbulent fluctuations suggests a mechanism by which part of the longitudinal momentum deficit of the turbulent boundary layer could be compensated by the acceleration of the mean flow. A high velocity (positive u) nonturbulent fluctuation was associated with the nonturbulent movement of fluid over the bulge, as if the bulge were simply a flow blockage. Statistically, these individual accelerations over the bulges introduced a net positive skewness to the u component of the nonturbulent region fluctuations. The superposition of these skewed fluctuations on the core flow would tend to increase the mean velocity of the core fluid. While the net effect due to the bulges over a particular part of the wall may be small, the circular geometry of the boundary would tend to concentrate the contributions from each part of the boundary layer at a given cross section. Further, the effects would be cumulative with distance down the pipe.

The positive v skewness of the nonturbulent fluctuations was very suggestive. It could indicate that higher radial velocities, and/or a shorter time interval, were associated with the flow of nonturbulent fluid up the bulges rather than down the bulges. This could be due either to the bulge shape (steeper in the upstream direction) or to the effects of the outward propagation of the

interface itself. Point average velocity results given by Kovasznayet al (1970) for a detector probe at a level where $\gamma = .1$ show that the positive radial velocities in the nonturbulent region for the "backs" (upstream edge) of turbulent bulges are larger than the absolute magnitude of the corresponding measurement at the "front" (downstream edge) of the turbulent bulge. It may be conjectured that, through viscous effects at the upstream interface of the bulge, a part of the overall positive radial momentum of the turbulent bulge is imparted to the induced nonturbulent fluctuation. By this process, the outward movement of the turbulent bulge would appear to be resisted by the nonturbulent fluid. Such a mechanism would constitute a reverse energy transfer process from the turbulence to the mean flow.

The Reynolds number behavior of the mean flow overshoot phenomenon appeared to be consistent with the concept of a nonturbulent interface mechanism. The magnitude of the mean flow overshoot on the center line was smaller for higher Reynolds numbers. Charnay et al (1976) observed positive u skewness in the nonturbulent region only for a low background turbulence level. The background turbulence level of the wind tunnel can certainly be expected to increase at higher operating speeds. It appears that for higher background turbulence levels the more organized

nonturbulent fluctuations induced by the boundary layer become less effective. On this basis, the expected effect of increased Reynolds numbers was a less pronounced non-turbulent region acceleration. The measurements made by Buyuktur (1961), Sharan (1969), and Weir et al (1974) have indicated that for large inlet disturbances, the velocity profiles become less peaked. For large disturbances (Buyuktur's toothed oriface plates) overshoot does not occur. Presumably the gross disturbances would produce large entrainments and would destroy the sharp interface.

The mean flow overshoot position appeared to move upstream for increasing Reynolds numbers, even though the mean boundary layer merge point moved downstream. It seems reasonable to speculate that the transfer of mean flow energy of the peak to the turbulent flow in the recovery region would be more efficient at higher Reynolds numbers. This could cause more rapid re-adjustment for higher Reynolds numbers once the boundary layers have merged. A more rapid recovery combined with smaller peaks could account for the higher Reynolds number peak behavior.

Further experimental investigation would be required to put the qualitative model, which has been speculated here, on a more analytic footing. In particular, detailed quantitative measurements using conditional techniques to obtain point velocity measurements are required for the

nonturbulent region fluctuations. When combined with statistical information on the interface wrinkling, an estimate of the overall effect that the phenomenon could have on the mean flow would be possible. A theoretical analysis of the focusing effect which the core regions of bounded flows must experience may be possible. The reason for the negatively skewed v for the nonturbulent fluctuation also requires further investigation. This implies a need for further studies of bulge shapes, entrainment rates, and the radial propagation velocity of the interface.

The existence of an interface mechanism for developing pipe flow suggests a more general problem for investigation. Perhaps, wherever a sharp wrinkled interface exists between two fluids moving with different relative velocities, a similar mechanism may exist which appears to accelerate the flow on the high speed side of the interface. The "negative viscosity" phenomenon, discussed by Starr (1968), may be examples of this process.

9.2 "Negative Viscosity"

As speculated in Section 9.1, the nonasymptotic development of turbulent pipe flow may be a laboratory example of a more general class of fluid behavior called "negative viscosity" phenomena. The purpose of this section is to examine this class of phenomena and further explore this

speculation.

A brief explanation of the terminology is in order. The definition of a turbulent eddy viscosity is based on the attempt to draw an analogy between the effects of momentum exchange due to turbulent mixing and momentum exchange due to the molecular viscous effects of a Newtonian fluid. While there is little physical basis for the analogy between dissimilar molecular and continuum scale phenomena, such simplification, at the expense of obscured physics, is expedient for certain engineering purposes. For the case of molecular stresses caused by the cross stream mixing and transfer of momentum by molecular motion, it is observed that momentum is transfered from regions of high mean velocity towards regions of lower mean velocity, or "down the velocity gradient". The molecular viscous action tends to decrease the mean shear in the flow and defines a positive viscosity, μ, by the expression

$$\tau \equiv \mu \frac{\partial U}{\partial y} , \qquad (9.1)$$

where τ is the shear due to molecular motion. The effect of turbulent mixing by the Reynolds stress $-\rho\overline{uv}$ is usually similar, but on a much greater scale. The Reynolds shear stresses in a turbulent flow usually cause a mean cross stream transfer of momentum so that the mean

shear in the flow tends to decrease. Under certain special flow conditions the Reynolds shear stress appears to be less efficient in decreasing the mean flow shear or can actually appear to increase the mean shear by transfering momentum "up the velocity gradient". The term "negative eddy viscosity" describes a turbulent regime which is characterized by an effective turbulent eddy viscosity which is negative. The constant of proportionality ε_T relating the local Reynolds shear stress to the local gradient of mean velocity, such that

$$- \rho\overline{uv} = \varepsilon_T \frac{\partial U}{\partial y}, \qquad (9.2)$$

becomes negative. In this case, the main turbulent kinetic energy production term (which is the product of the Reynolds shear stress and velocity gradient) has a sign opposite to the usual sense.

An example of this type of special situation occurs for the turbulent flow between two annular pipes. Bradshaw (1971) has briefly considered this flow. It is observed experimentally that the mean Reynolds stress and velocity profiles are both asymmetric and are not coincident. This asymmetry causes the appearance of a region of negative turbulent production. A fundamental question is raised by the situation; namely, by what process is the mean velocity shear increased to support the relative asymmetries

of the stress and mean velocity profiles. There appears to be a mechanism which accelerates the mean flow associated with the outside pipe.

Another laboratory example of negative viscosity was studied by F. Erian (1967). Detailed measurements of mean velocity and turbulent stresses for a turbulent wall jet flow were found to exhibit a region of mean opposing shears due to turbulence and viscosity, with concomitant reduced turbulent kinetic energy production (the term $(-\rho\overline{uv})\ \frac{\partial U}{\partial y}$ was negative but was offset by positive normal stress production terms). No explanation of the phenomenon was offered.

Several geophysical and astrophysical examples of turbulent flows which also appear to have a turbulent transfer of momentum towards regions of higher mean velocity have been given by V. Starr (1968).

The designation "negative" for the anomalous Reynolds stress behavior has resulted from the negative eddy viscosities which must be used to relate the mean shear and Reynolds shear stress in these special flow examples. The presence of an anomalous momentum transfer process would of course be most apparent where actual sign changes in various turbulence parameters occur. This is the case for the above examples and notably the regions of interest are all associated with critical points $\left(\frac{\partial U}{\partial y} = 0\right)$ of the

mean velocity profiles.* If this process transferring momentum to regions of higher mean velocity was coexisting with the more usual momentum exchange processes, or were occurring at a position other than a mean velocity profile critical point, actual sign reversal of turbulence parameters need not occur. Negative viscosity physics must be present when the mean velocity shear increases while the turbulent stresses are such that momentum transfer down the shear gradient would be expected. Thus, the negative viscosity phenomenon could be associated, not only with critical points of the velocity profile, but also with inflection points

$$\left(\frac{\partial^2 U}{\partial y^2} = 0\right)$$

where anomalous turbulent momentum transfer is indicated. In this sense the appearance of negative production is a sufficient indicator for negative viscosity physics, but is not necessary. A broader criterion would be the occurrence of increases in the mean velocity gradient inconsistent with the direction of mean turbulent momentum transport.

It is in the scope of this wider criterion that developing turbulent pipe flow can be viewed as a negative viscosity phenomenon. The coexistence of mean Reynolds stresses, tending to transport momentum towards the wall, with the increasing mean velocity gradients associated with the

* Dr. J. Lumley has suggested (private communication) that "the 'negative viscosity phenomenon' can occur only in the vicinity of a peak, and not elsewhere".

accelerating mean flow prior to overshoot, satisfied the criterion. This appeared to occur in the intermittent region of the turbulent boundary layer. A mechanism which could cause this apparent anomalous momentum transport has been discussed in Section 9.1. It can be speculated that an analogous interface mechanism is responsible for the other negative viscosity phenomenon.

It appears that a universal aspect of the negative viscosity phenomenon is the presence of some type of irregular interface region. In the annular duct flow this interface may be the boundary between the turbulence associated with the opposite walls of the flow. Sabot and Comte-Bellot (1976) have shown that such an interface exists even in fully developed pipe flow. Turbulent shear stress fluctuation structures on the centerline can be identified with opposite halves of the flow. Similarily in the wall jet geometry, an interface must exist between the jet turbulence and free stream turbulence structure. The developing pipe flow involves the turbulent-non-turbulent flow interface. The geophysical examples given by Starr (1968) also occur in the interaction regions between large flow structures (jet stream, Gulf stream). Considering that wake flows and jet flows also involve irregular flow interfaces which are similar to the developing pipe flow boundary layer, these flows may also

exhibit steepened mean velocity gradients in the vicinity of the interface due to "negative viscosity" effects.

10.0 SUMMARY AND CONCLUSIONS

The mean flow survey results have indicated that the development of the mean velocity field for developing turbulent pipe flow is nonasymptotic. Regions of overshoot and undershoot of fully developed axial component velocity profiles were discernable in the developing region. These regions were related to radial component velocity features. The nonasymptotic mean flow development was consistent with previous results, which indicated a nonasymptotic wall shear stress development.

The centerline axial velocity maxima were less pronounced and moved forward towards the pipe entrance for higher Reynolds numbers. This Reynolds number behavior was contrary to the behavior of the average boundary layer merge point that was indicated by the calculations of integral boundary layer parameters.

The similarity between the present mean flow results for the pipe and recent independent measurements in ducts, has implied that nonasymptotic behavior may be characteristic of bounded developing flows in general.

The turbulent stress tensor survey results have indicated that the development of the turbulent quantities was also nonasymptotic. This was expected on the basis of the known behavior of the mean flow field. Pipe axis

maxima and wall region minima of the Reynolds stress tensor terms were downstream of those for the longitudinal mean velocity component. This spatial distribution of mean and turbulent nonasymptotic features suggested that the turbulent behavior was in response to the mean flow behavior. Results indicated a qualitative correlation between a mean radial velocity component towards the wall and the attenuation of turbulence. The behavior of the turbulence intensity in the inlet region suggested three phases of boundary layer growth, with rapid growth occurring where cross stream boundary layer interaction was expected. The mean turbulence intensities near the turbulent boundary layer surface, in the entrance region, suggested the existence of a magnified form of superlayer for developing pipe flow. High Reynolds stress correlation also occurred in this region. The contour patterns for several of the measured and calculated quantities have focused attention on the intermittent boundary layer interface region. The maximum mean flow acceleration of the core region appeared to be associated with this region and led to the conjecture that the overall nonasymptotic structure is due to the turbulent-nonturbulent energy exchange mechanism at the interface.

The calculations for the turbulent kinetic energy balance showed that production and dissipation approximately

balanced in the wall region. In the region of the boundary layer surface the convective diffusion of turbulent energy increased to balance the loss of turbulent kinetic energy due to mean flow convection. The results for the mean flow convection term in this region could be interpreted as indicating an energy transfer process which accelerates the mean flow at the expense of the turbulent kinetic energy. Contours of the viscous transport term displayed a behavior related to the acceleration of the mean flow. Generally, the viscous transport term was small, but in cells along the pipe axis the term approached magnitudes comparable with the mean flow convection.

The ease of conceptualization of the flow structure provided by using the contouring procedure for the presentation of the survey measurements was evident. Contouring facilitated the comparison of terms which differed widely in magnitude. The important role that small magnitude quantities could play in a nonlinear process was emphasized by the appearance of the contours of small terms. The contouring technique was not accurate in the narrow, high gradient regions near the turbulent interface.

The contouring has suggested that the flow may be classified into general regions. The flow associated with the mean flow acceleration and turbulent boundary layer

growth in the entrance was designated as an interaction region. Further downstream, in the recovery region, the mean and turbulent flow fields adjusted to the fully developed state. A region of upstream diffuser effects was observed in the vicinity of the pipe exit, but these were expected to diminish for higher Reynolds numbers.

Spectra measurements were not particularly indicative of the nonasymptotic development and suggested that this behavior was mainly a characteristic of the low frequency turbulence. Larger scatter in spectra results near the wall and pipe axis agreed with the finding that the small scale structure is best studied at an intermediate position. The effects of the intermittency of the turbulent boundary layer in the interaction region were evident. A 5/3 region existed for about a decade of wave numbers for u spectra but for a smaller range for v and w spectra. The isotropic 4/3 ratio for energy densities held only for the upper 1/3 decade. This implied that anisotropy existed over a considerable range of the 5/3 region. Shear stress spectra indicated nonzero shear stresses within this 1/3 decade. This suggested the existence of "second class" isotropy. The lower limit of the normal isotropic region (as indicated by extrapolation of shear stress spectra to zero) was nearly coincident with the upper wave number limit of the 5/3 region. Nondimensionalization using underestimated

dissipation values tended to hide the effects of wire length attenuation in the dissipation spectra. Typical values of the integral scales obtained by extrapolation of spectra results were .3 to .5 D.

Specialized turbulence measurements have indicated several interesting features associated with the non-turbulent side of the boundary layer interface. In particular, quadrant measurements of the Reynolds stress have shown that u_+v_+ events become important in the nonturbulent region. Nonturbulent longitudinal and radial velocity fluctuations appeared to be positively skewed. The behavior of filtered signals was generally the same as for unfiltered signals. This suggested that the nonturbulent fluctuations were due to large scale turbulent structure. A visual analysis of individual events on photographs of oscilloscope traces qualitatively confirmed the findings for the statistical measurements. A flow model similar to that given by Kibens (1968) and Kovasznay et al (1970) was indicated. Irrotational fluctuations induced in the free stream by the presence of the turbulent boundary layer bulges appeared to cause an increase in the mean velocity of the nonturbulent region. The irrotational flow was accelerated as it moved over a turbulent bulge. The overall effect was that the interface acted as a contraction surface for the nonturbulent core fluid. The interface mechanism which was speculated to cause

the nonasymptotic pipe flow development may also explain the behavior of a more general class of "negative viscosity" phenomenon which occur when a wrinkled interface exists between fluid moving at different mean velocities.

The following main conclusions can be drawn from the present work:

1. Turbulent pipe flow develops in a nonasymptotic manner. Both the mean and turbulent behavior was nonasymptotic. The nonasymptotic turbulent features appear downstream of the mean flow features. Non-asymptotic effects decrease at higher Reynolds numbers.

2. The nonasymptotic development is reflected most dramatically by the convection and diffusion terms in the kinetic energy balance. The structure of small magnitude terms indicated that a very complex dynamic balancing was occurring in response to the nonasymptotic development.

3. Smoothing and contouring were useful techniques for the presentation and analysis of the flow measurements where flow changes were gradual. Abrupt changes, such as occurred at the turbulent interface, were not represented well.

4. The diffuser can cause fairly extensive upstream effects, which are most important at lower Reynolds

numbers.

5. On the basis of contouring the developing flow can be divided into two broad regions; interaction and recovery. Contoured results indicated that the region associated with the top of the growing turbulent boundary layer was singularly important for the nonasymptotic development.

6. The nonasymptotic development is associated with large scale, low frequency turbulent structures. This was indicated by spectra results and the character of filtered statistical measurements.

7. Nonturbulent fluctuations exist in the nonturbulent core. These fluctuations appear to be induced by turbulent bulges. The flow model proposed by Kibens (1968) and Kovasznay et al (1970) appears to be valid. The turbulent-nonturbulent interface appeared to act as a contraction surface for the nonturbulent core fluid.

It has been speculated that the overall nonasymptotic development occurs as a specific result of the interface mechanism. It has further been speculated that nonasymptotic development is characteristic of all bounded developing flows. It has been suggested that the present findings may have implications for a wider class of flows.

BIBLIOGRAPHY

Barbin, A. R., 1961, Ph.D. thesis, Purdue University.

Barbin, A. R. and Jones, J. B., 1963, Am. Soc. Mech. Eng. Trans., 85, D, 29.

Batchelor, G. K. and Townsend, A. A., 1947, Proc. Roy. Soc., A, 190, 534.

Bowlus, D. A. and Brighton, J. A., 1968, Am. Soc. Mech. Eng. Trans. 90, D, 431.

Blackwelder, R. F., 1970, Ph.D. thesis, The Johns Hopkins University, Baltimore, Md.

Blackwelder, R. F. and Kovasznay, L. S. G., 1972, Phys. Fluids, 15, 1545.

Bradley, C. I. and Cockrell, D. J., 1970, Proc. Heat Transfer Fluid Mech. Inst., Stanford Univ. Press, Calif.

Bradshaw, P., 1967, N.P.L. Aero Rep., 1220.

Bradshaw, P., 1971, "An Introduction to Turbulence and Its Measurement", Pergamon Press, Oxford.

Bradshaw, P., 1974, Phys. Fluids, 17, 11, 2149.

Bradshaw, P., Dean, R. B. and McEligot, D. M., 1973, Trans. A.S.M.E. I, 40, 214.

Brodkey, R. S., Nychas, S. G., Taraba, J. L., 1973, Phys. Fluids, 16, 11, 2010.

Brodkey, R. S., Wallace, J. M. and Eckelmann, H., 1974, J. Fluid Mech. 63, 209.

Brodkey, R. S., Taraba, J. L., 1975, Phys. Fluids,17, 11, 2150.

Builtjes, P. J. H., 1975, Appl. Sci. Res., 31, 397.

Buyuktur, A., 1961, O.N.E.R.A. Rep. no. 378.

Byrne, J., Hatton, A. P. and Marriot, P. B., 1969, Proc. Inst. Mech. Eng., London, 184, 39, 697.

Champagne, F. H., Pao, Y. H. and Wyganski, I. J., 1976, J. Fluid Mech., 74, 2, 209.

Champagne, F. H. and Sleicher, C. A., 1967, J. Fluid Mech., 28, 177.

Charnay, G., Mathieu, J. and Compte-Bellot, G., 1976, Phys. Fluids, 19, 9, 1261.

Corrsin, S. and Kistler, A. L., 1955, N.A.C.A. Rep. no. 1244.

Dean, R. B., 1974, Ph.D. thesis, University of London, London.

Deissler, R. G., 1950, N.A.C.A. Tech. Note No. 2138.

Dryden, H. L., 1947, N.A.C.A. Tech. Note, 1168.

Erian, F., 1967, Ph.D. thesis, Syracuse University, Syracuse, N.Y.

Ferzieger, J. H. and Shaanan, S., 1976, Phys. Fluids, 19, 4, 596.

Fiedler, H. and Head, M. R., 1966, J. Fluid Mech., 25, 719.

Fillipov, G. V., 1958, Sov. Phys.-Tech. Phys. 3, 1681.

Frenkiel, F. N. and Klebanoff, P. S., 1975, Bdry-Layer Meteor., 8, 2, 173.

Grass, A. J., 1971, J. Fluid Mech., 50, 2, 233.

Hinze, J. O., 1959, "Turbulence", McGraw-Hill Book Co., New York, N.Y.

Holdhusen, J.S., 1952, Ph.D. thesis, University of Minnesota, Minneapolis, Minn.

Huffman, G. D., 1968, Ph.D. thesis, Ohio State University.

Kibens, V., 1968, Ph.D. thesis, The Johns Hopkins University, Baltimore, Md.

Kim, H. T., Kline, S. J. and Reynolds, W. C., 1971, J. Fluid Mech., 50, 133.

Kistler, A. L., 1964, The Mechanics of Turbulence, Gordon and Breach Science Publishers Inc., New York, N.Y.

Klebanoff, P. S., 1955, N.A.C.A. Rep. no. 1247.

Klebanoff, P. S. and Diehl, Z. W., 1952, N.A.C.A. Rep. no. 1110.

Kline, S. J., Reynolds, W. C., Schraub, F. A. and Runstadler, P. W., 1967, J. Fluid Mech. 30, 741.

Kovasnay, L. S. G., Kibens, V. and Blackwelder, R. F., 1970, J. Fluid Mech., 41, 283.

LaRue, J. C. and Libby, P. A., 1976, Phys. Fluids, 19, 12, 1864.

Lawn, C. J., 1971, J. Fluid Mech., 48, 477.

Latzko, H., 1944, N.A.C.A. Tech. Memo No. 1068.

Laufer, J., 1954, N.A.C.A. Rep. no. 1174.

Lu, S. S., 1972, Ph.D. thesis, University of Michigan, Ann Arbor, Mich.

Lu, S. S. and Willmarth, W. W., 1973, J. Fluid Mech., 60, 481.

Lindsay, R. B. and Margeneau, H., 1956, "Foundations of Physics", Dover Publications, New York, N.Y.

Lumley, J. L., 1965, Phys. Fluids, 8,6,1056.

Lumley, J. L. and Takeuchi, K., 1976, J. Fluid Mech., 74, 433.

Mizushina, T., Ito, R., Hiromasa, U., Tsubata, S. and Hayashi, H., 1970, J. Chem. Eng., Japan, 3, 34.

Monin, A. S. and Yaglom, A. M., 1975, Statistical Fluid Mechanics, Vol. II, MIT Press, Cambridge, Mass.

Novikov, E. A., 1974, Arch. Mech. 26, 4, 741 Warsaw.

Nychas, S. G., Hershey, H. C. and Brodkey, R. S., 1973, J. Fluid Mech., 61, 513.

Okwuobi, P. A. C. and Azad, R. S., 1973, J. Fluid Mech., 57, 3, 603.

Paizis, S. T., 1973, Ph.D. thesis, The Johns Hopkins University, Baltimore, Md.

Panchev, S., 1971, "Random Functions and Turbulence", Pegamon Press, Oxford.

Perry, A. E. and Abell, C. J., 1975, J. Fluid Mech., 67, 257.

Phillips, O. M., 1955, Proc. Camb. Phil. Soc., 51, 220.

Reichert, J. K., 1974, M.Sc. thesis, University of Manitoba, Canada.

Reichert, J. K., and Azad, R. S., 1976, Can. J. Phys., 54, 268.

Richman, J. W. and Azad, R. S., 1973, Appl. Sci. Res., 28, 419.

Ross, D. and Whippany, N. J., 1956, Am. Soc. Mech. Eng. Trans., 78, 915.

Rotta, J. C., 1962, "Turbulent Boundary Layers in Incompressible Flow", Vol. 2, Pergamon Press, Oxford.

Sabot, J. and Comte-Bellot, G., 1976, J. Fluid Mech., 74, 433.

Sharan, V. K., 1969, M.Sc. thesis, University of Salford.

Starr, V., 1968, "Negative Viscosity Phenomenon", McGraw-Hill Book Co., New York, N.Y.

Stewart, R. W., 1956, J. Fluid Mech., 1, 593.

Tennekes, H. and Lumley, J.L., 1972, "A First Course in Turbulence", M.I.T. Press, Mass.

Tullis, J. P. and Wang, J. S., 1972, Naval Ship Research and Development Center, Bethesda, Md., Report No. CER72-73JPT-JSW-2.

Townsend, A. A., 1948, Aust. J. Sci. Res., 1, 2, 161.

Wallace, J. M., Eckelmann, H. and Brodkey, R. S., 1972, J. Fluid Mech., 54, 39.

Weir, J., Priest, A. J. and Sharan, V. K., 1974, J. Mech. Eng. Sci., 16, 3, 211.

Willmarth, W. W., 1975, "Structure of Turbulence in Boundary Layers", Advances in Applied Mechanics, Vol. 15, Academic Press, New York, N.Y.

Willmarth, W. W. and Lu, S. S., 1971, J. Fluid Mech., 55, 481.

Wyngaard, J. C., 1969, J. Sci. Instr. ser. 2, 2, 983.

Wyngaard, J. C. and Lumley, J. L., 1967, J. Appl. Meteor., 6, 592.

Appendix A: Comments on errors

Considerable theoretical and experimental work has been directed towards the study of the errors involved in flow measurements made with both pressure tube and hot wire equipment. Discussions of these findings can be found for example, in Pankhurst and Holder (1952), Hinze (1959), and Bradshaw (1971). The errors involved in the electronic processing equipment and measuring instruments are straightforward to assess, but, the errors involved in the response of the basic sensor to the measured quantity are themselves the subject of continuing research. The assignment of an error to a particular measurement is further complicated since the turbulent flow structure is generally different at each measurement position. Measurements are generally less accurate in regions of high mean velocity gradient and high turbulence intensity.

The measurements of the mean velocity by the total pressure tube technique involves errors due to the effective displacement of the pressure tube in high mean velocity gradients, the variation of static pressure across the pipe, and the effect of the turbulence on the total pressure readings. Using Patel's (1965) estimate of the displacement effects, the maximum effective pressure tube displacement would be approximately 0.15 mm. Reichert (1974) has determined that the static pressure is constant to within about 2%. Maximum errors in the total pressure measurements due

to turbulence were approximately 1.2% (Goldstein; 1936). Likley the most important source of error was the changes in Reynolds number due to variations in the tunnel operation (approximately $\pm$ 2%). While individual mean velocity measurements may be the order of say 5% in error, the values obtained after numerical smoothing of the velocity profile trends are considerably improved and are more probably of the order of 2%.

The sources of errors for hot wire measurements are numerous and are described in the first references given above. The cumulative effect of the various errors can be very large. However, while hot wire anemometry may not give accurate absolute results, it is the ability of the equipment to give reproducible results and indicate proper trends which is most important. This is particularily true since often the measurements are nondimensionalized by a quantity computed from themselves (eg. U/U_B) or it is the spatial gradients which are of primary importance. A more detailed discussion of this point is given by Trupp (1973; p. 78). Typical approximate errors in the reproducibility of u', v', and w' hot wire measurements is $\pm$ 3%, while for $\overline{uv}$ the error is $\pm$ 5%.

References for Appendix A:

Pankhurst, R.C. and Holder, D.W., 1952, "Wind Tunnel Technique", Pitman Press, London.

Goldstein, S., 1936, Proc. Roy. Soc. (A), 155, 570.

Hinze, J.O., 1959, "Turbulence", McGraw-Hill Book Co., New York, N.Y.

Bradshaw, P., 1971, "An Introduction to Turbulence and Its Measurement", Pergamon Press, Oxford.

Patel, V.C., 1965, J. Fluid Mech. 23, 185.

Reichert, J.K., 1974, M.Sc. thesis, University of Manitoba, Canada.

Trupp, A.C., 1973, Ph.D. thesis, University of Manitoba, Canada.

Appendix B: Comments on the TM-377 turbulence processor

The TM-377 multifunction turbulence processor used for the majority of the measurements concerned with the turbulent-nonturbulent interface (reported in Chapter 8) was the prototype model of this instrument. As a result of the experience gained with this instrument, an improved model is now under development. Only minor changes are anticipated in the basic electronic configuration of the instrument. The modifications are expected to greatly improve the thermal stability of the instrument. Output voltage drifts as great as 10 mv/°C were observed for the prototype processor. These were especially significant when measuring the higher order turbulence moments and required that the offset voltages be noted at very frequent intervals. Some improvement was obtained by insulating the electronics cabinet and allowing very long warm-up times. Aside from this offset voltage drift, the high linearity of the circuit components (the multiplier network and squaring circuits employed Burr Brown 4205-K multipliers) provided the various transfer functions with an overall precision estimated to be better than 1% for reference voltages between .1 and 10 volts.

A system block diagram for the prototype is given below. An increased number of BNC outputs from the multiplier network is proposed for the improved system allowing the

simultaneous measurement of the skewness and flatness factors of the u and v signals. Further details concerning the electronic design of the instrument can be obtained from the manufacturer (Tri Met Instruments Ltd., 1792 St. Mathews Avenue, Winnipeg, Canada).

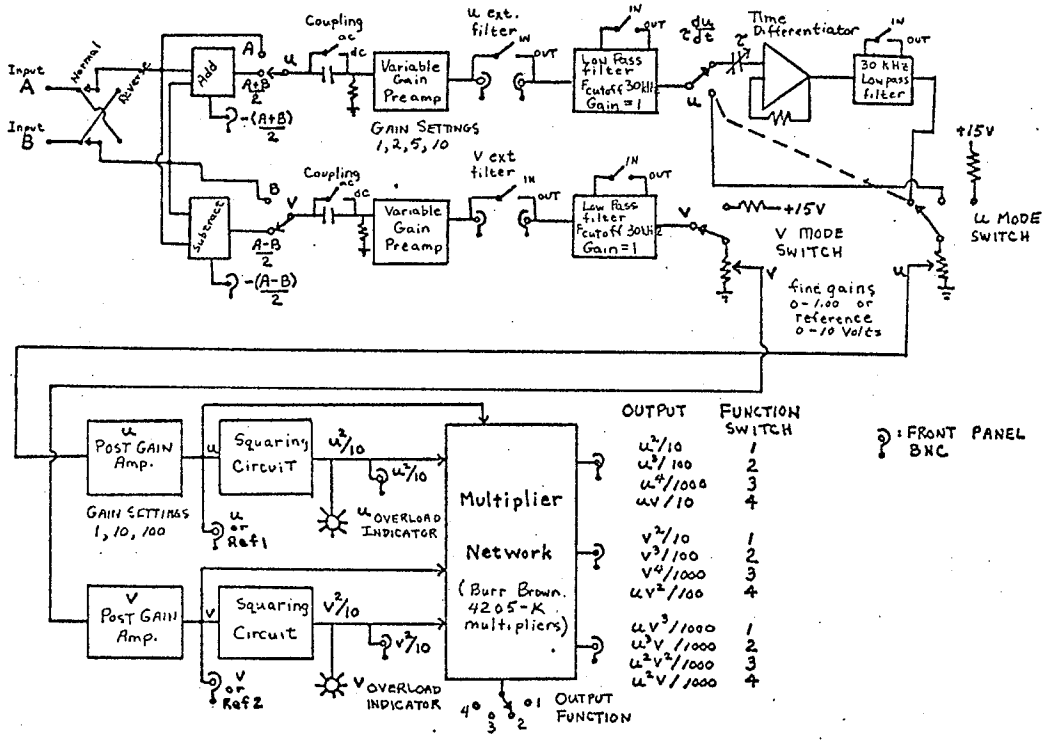

Figure B-1: Multifunction turbulence processor TM-377 system block diagram.

TABLE 1

MEAN FLOW PARAMETERS (x/D = 60.3)

Bulk flow velocity, U_B	17.3 m/sec
Centerline velocity, U_c	20.7 m/sec
Friction velocity, U_*	.79 m/sec
Wall shear stress, τ_w/ρ	.62 m^2/sec^2
Pipe radius, R	.0508m
Kinematic viscosity, ν	1.59×10^{-5} m^2/sec
Density, ρ	.118 kg/m^3
Reynolds number, $Re = U_B R/\nu$	54900

TABLE 2

TURBULENCE PARAMETERS FROM SPECTRA MEASUREMENTS

x/D	y/R	u' (m/sec)	ε m^2/sec^3 (eqn. 3.1)	$\eta \times 10^4$(m)	R_λ	$A \times 10^3$(m) (eqn. 7.2)
1.8	.90	1.74	396.	0.56	147.	7.30
10.6	.90	1.41	132.	0.74	167.	20.7
	.65	0.94	34.7	1.04	146.	16.1
	.40	0.25	2.9	1.93	35.1	10.2
20.5	.90	1.48	112.	0.77	201.	27.9
	.55	0.97	30.5	1.07	166.	23.3
	.25	0.40	3.9	1.79	77.0	20.0
30.3	.90	1.56	137.2	0.74	200.	29.2
	.50	1.04	38.4	1.01	169.	26.2
	.10	0.65	11.0	1.38	123.	24.9
40.2	.90	1.61	113.	0.77	238.	30.2
	.50	1.21	43.6	.98	214.	37.8
	.10	0.81	19.3	1.20	143.	29.0
50.5	.90	1.75	147.	0.72	245.	38.6
	.50	1.26	38.4	1.01	247.	39.7
	.10	0.91	22.0	1.16	169.	38.3
60.3	.90	1.72	162.	0.71	225.	39.9
	.50	1.21	36.3	1.02	235.	48.0
	.10	0.87	20.1	1.19	162.	39.9
65.2	.90	1.69	162.5	0.71	218.	33.0
	.50	1.13	28.9	1.09	233.	42.9
	.10	0.84	18.4	1.22	159.	42.7

TABLE 3

PARAMETERS FOR FIGURES 92(A) - 92(F)

Photograph	A	B	C	D	E	F
x/D	10.2	10.2	10.2	10.2	10.2	10.2
y/R	.5	.5	.4	.3	.3	.3
Upper trace	u	filtered u	u	u	filtered u	u
Vertical Scale (m/sec)/div.	.69	.52	.23	.23	.23	.23
Lower trace	v	filtered v	v	v	filtered v	$\frac{\partial u}{\partial t}$
Vertical Scale (m/sec)/div.	.69	.52	.23	.23	.23	1150 (m/sec^2)/div.
Horizontal Scale msec/div.	2.0	5.0	2.0	1.0	2.0	1.0

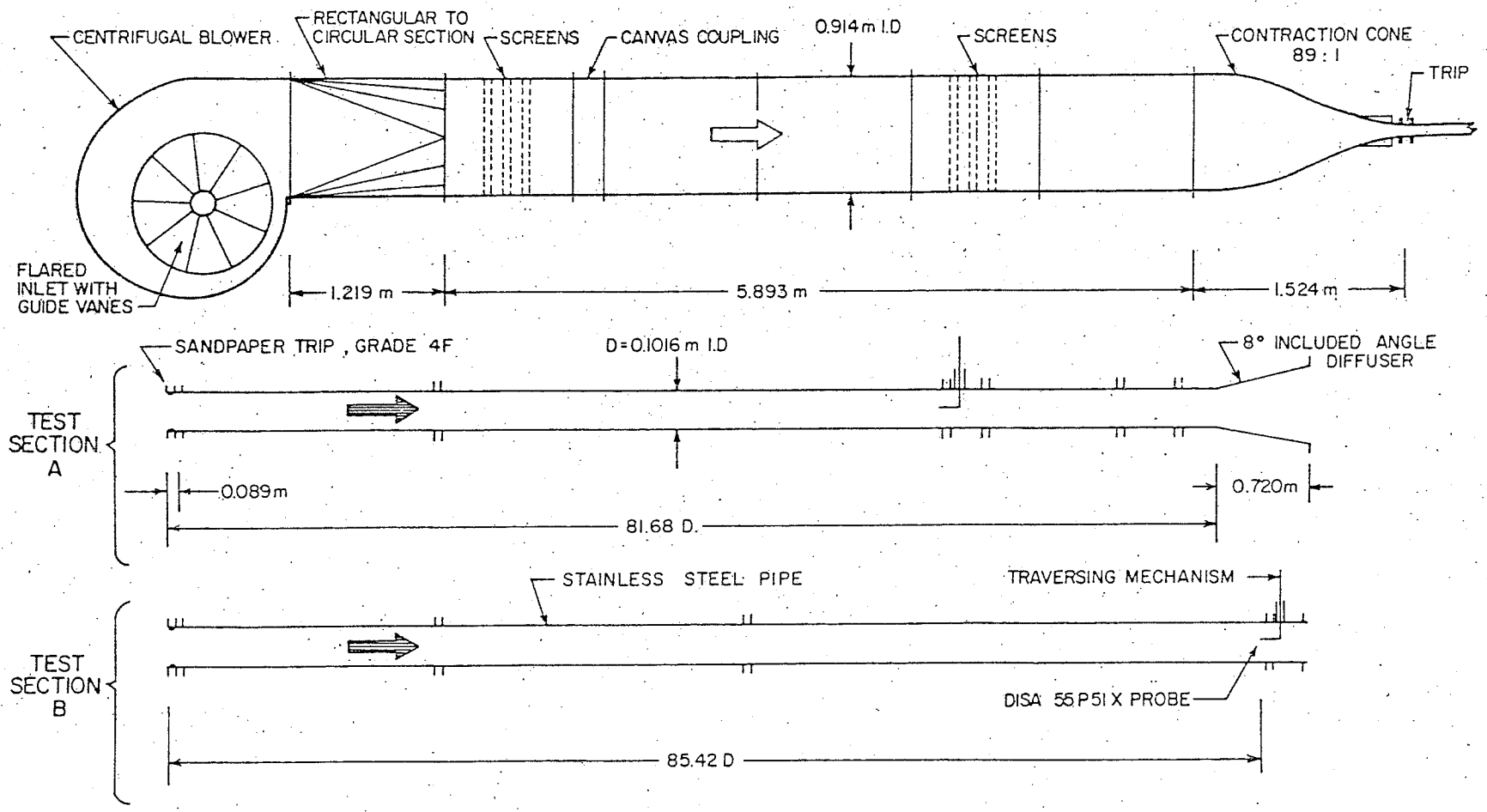

Figure 1. Open circuit wind tunnel facility.

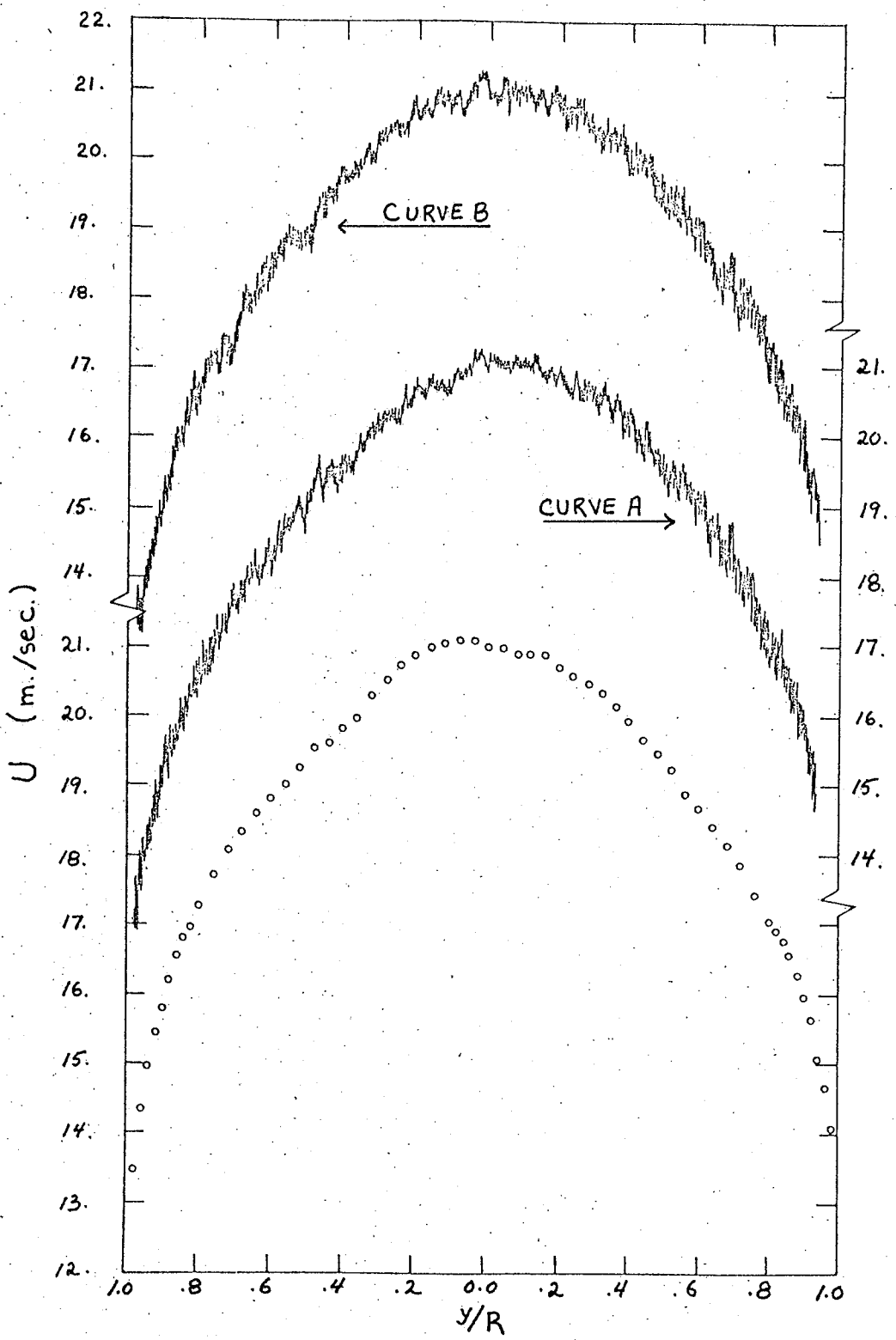

Figure 2. Comparison of mean velocity profiles. O, x/D = 61.9, Pitot tube traverse; curve A, x/D = 60.3, continous hot wire traverse, set-up A; curve B, continuous hot wire traverse, setup B.

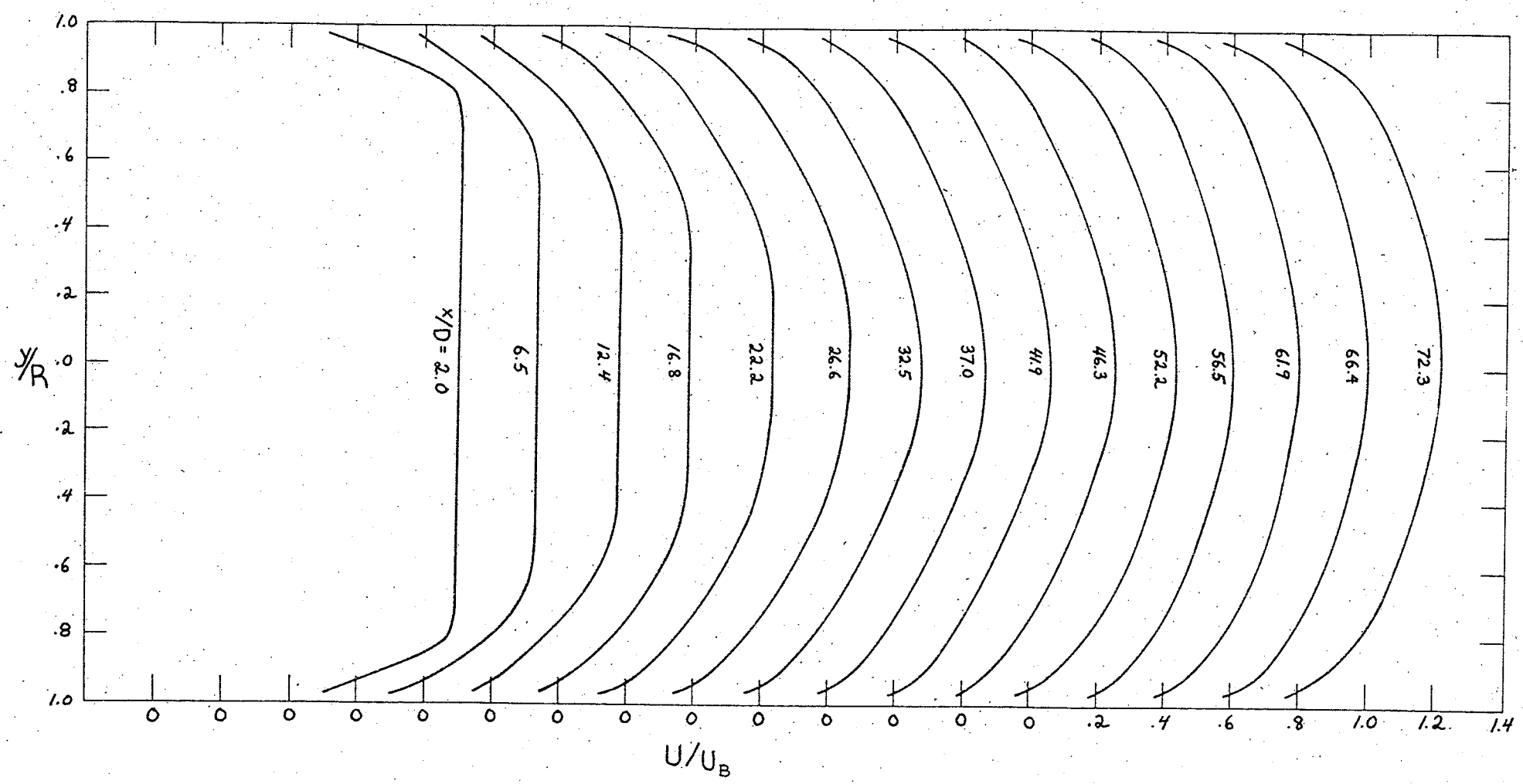

Figure 3. Mean axial velocity profiles U/U_B; Re = 76000.

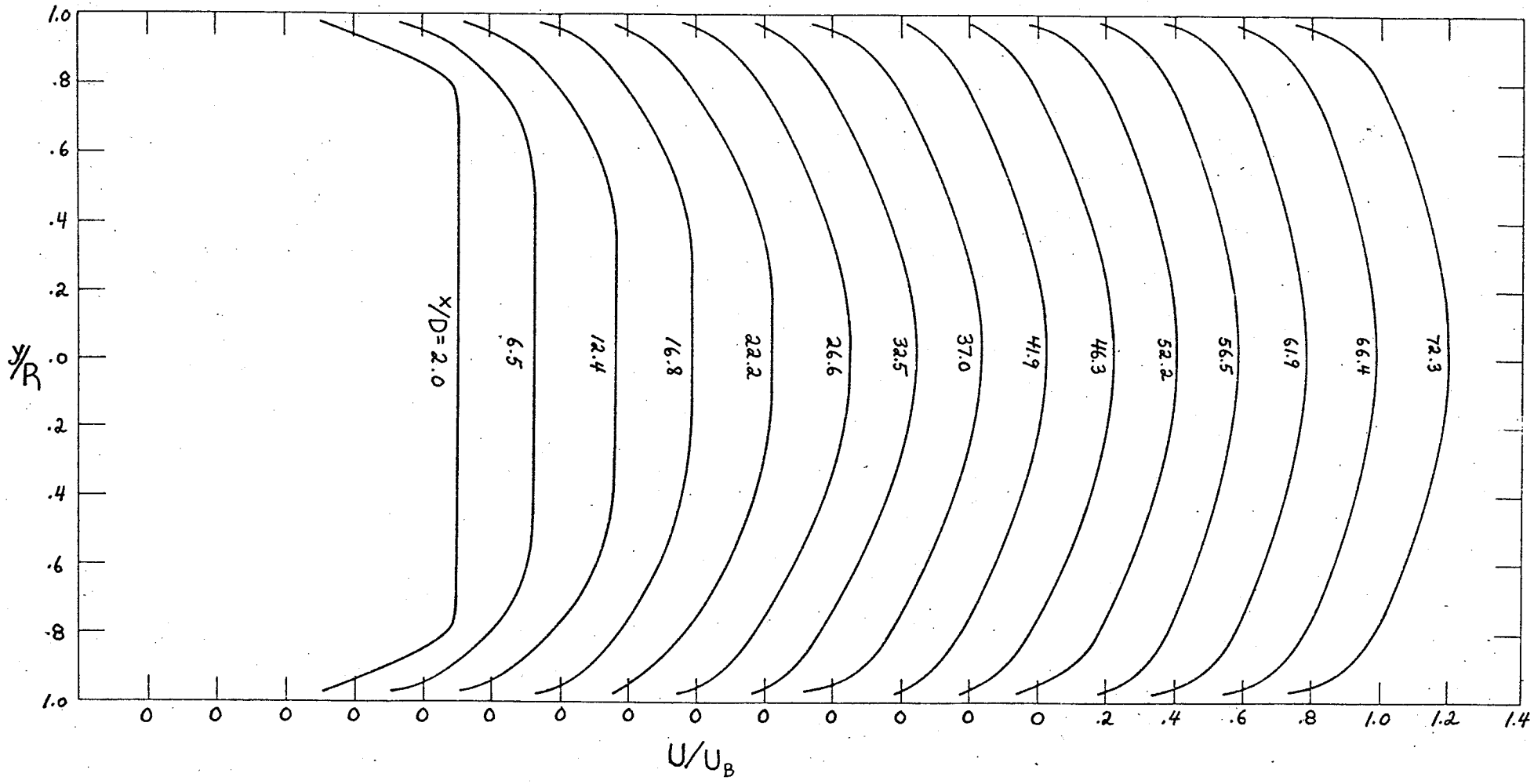

Figure 4. Mean axial velocity profiles U/U_B;Re = 153000.

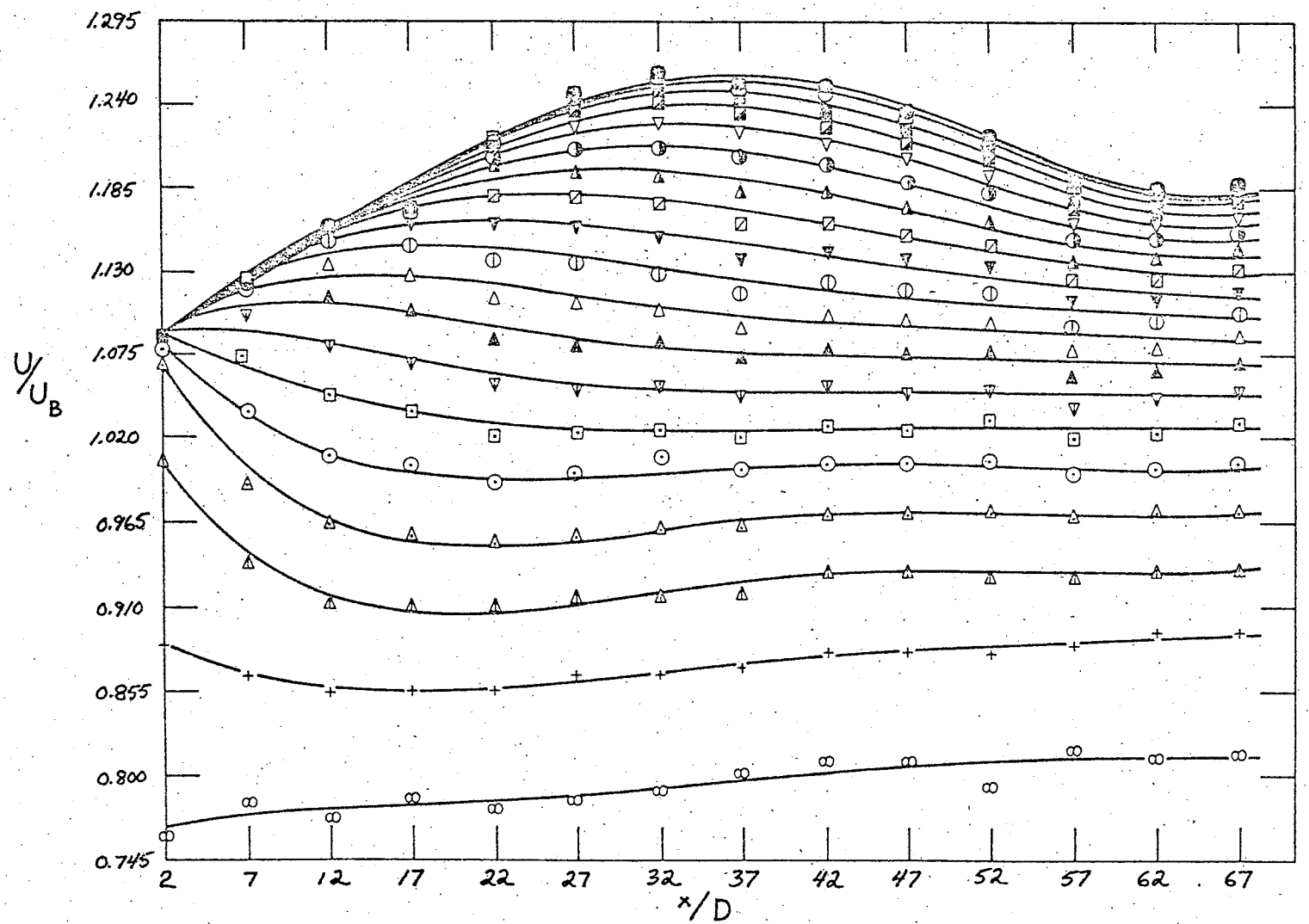

Figure 5. Radial distribution of mean axial velocity, U/U_B; Re = 76000. y/R = 0.00, □ ; y/R = 0.05, ◍; y/R = 0.10, ○; y/R = 0.15 ◪ ; y/R = 0.20, ■ ; y/R = 0.25, ▽; y/R = 0.30, ◑; y/R = .35, ◭; y/R = .40, ◪; y/R = .45, ▼; y/R = .50, ⊕; y/R = .55, ◬; y/R = .60, ▲; y/R = .65, ▼; y/R = .70, ⊡ ; y/R = .75, ⊙; y/R = .80, △; y/R = .85, ◬; y/R = .90, +; y/R = .95, ∞.

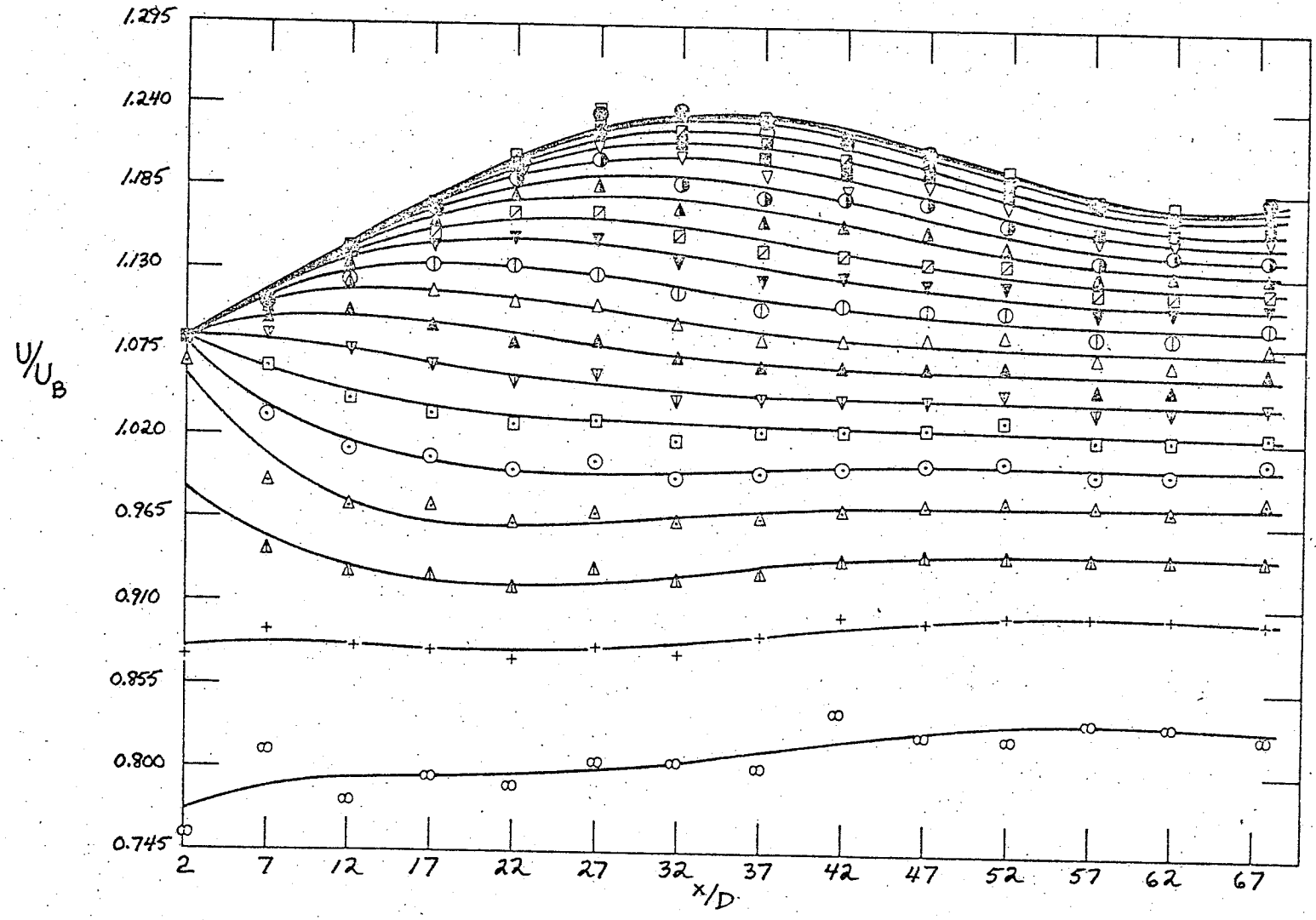

Figure 6. Radial distribution of mean axial velocity, U/U_B; Re = 153000; symbols as for figure 5.

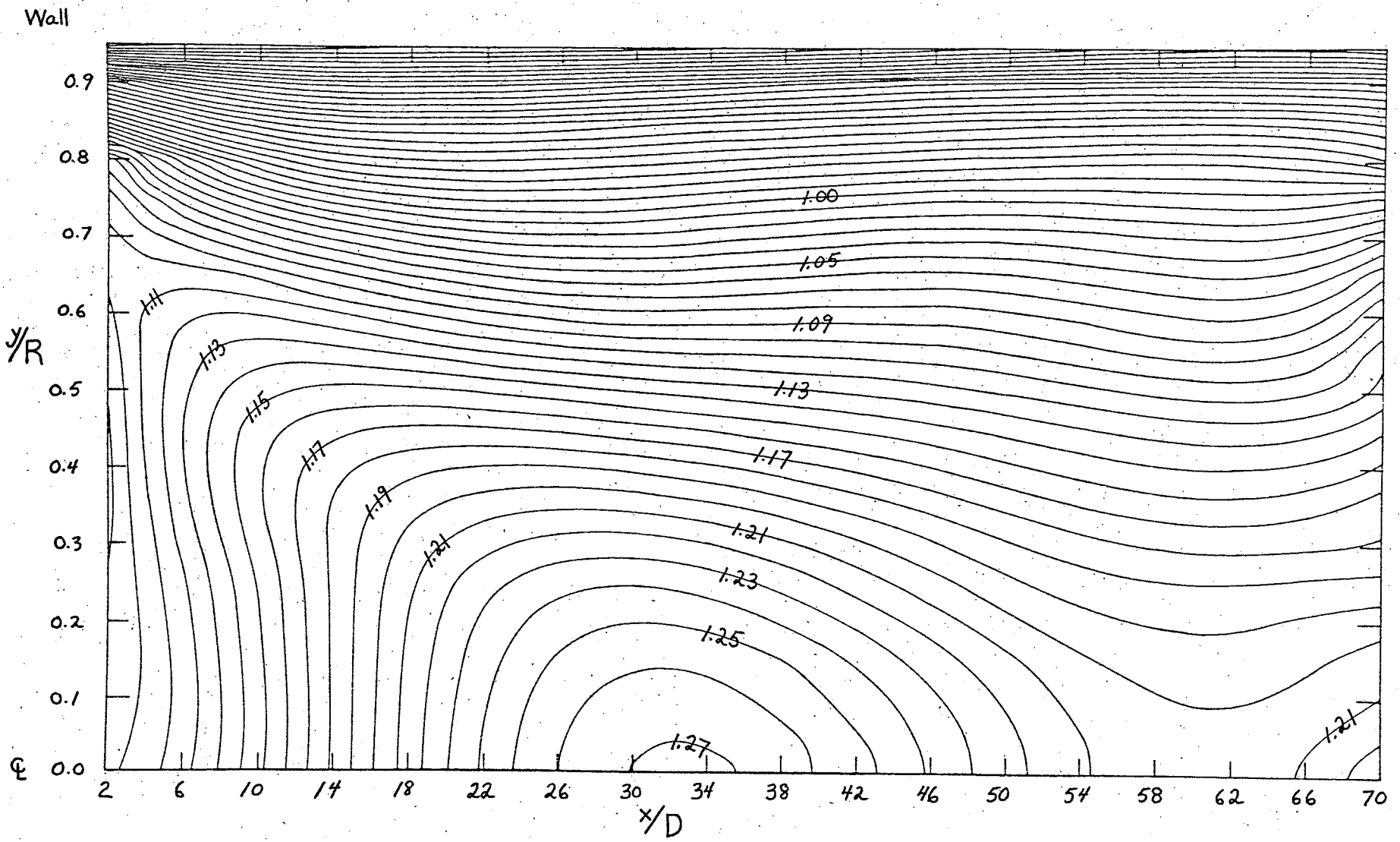

Figure 7. Longitudinal mean velocity field contours, U/U_B; Re = 54900; contour interval = 0.01.

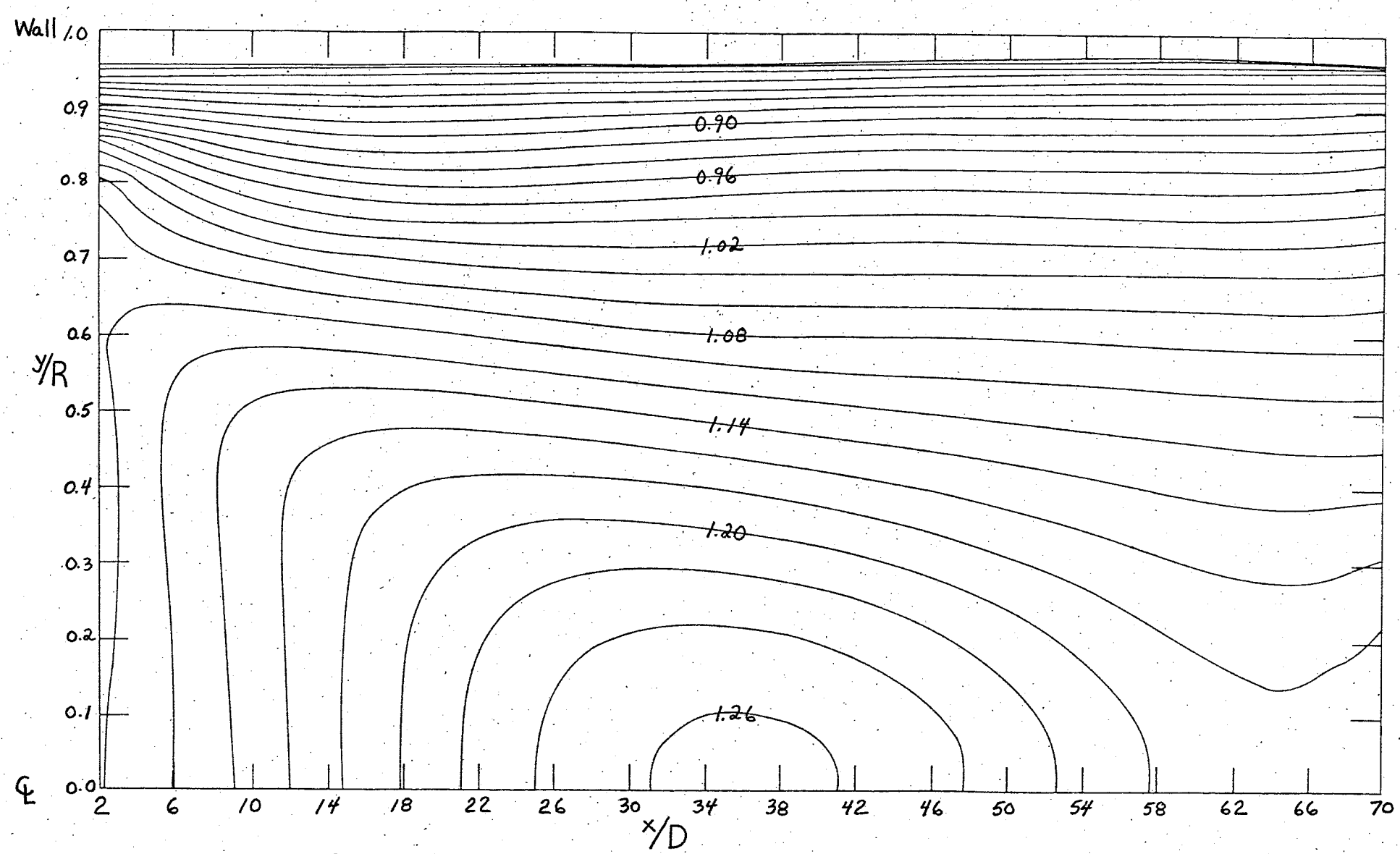

Figure 8. Longitudinal mean velocity field contours, U/U_B; Re = 76000; contour interval = 0.02.

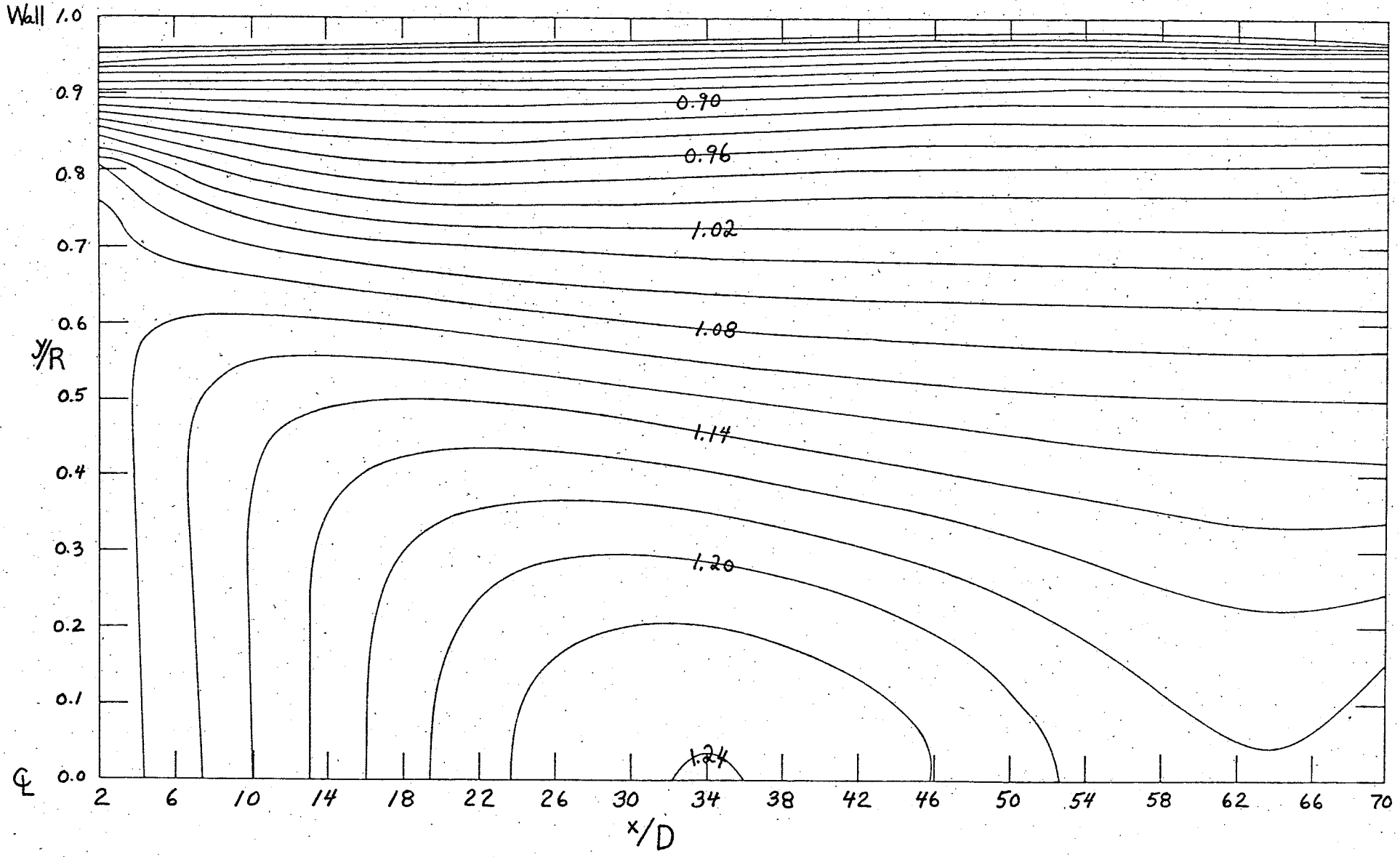

Figure 9. Longitudinal mean velocity field contours, U/U_B; Re = 153000; contour interval = 0.02.

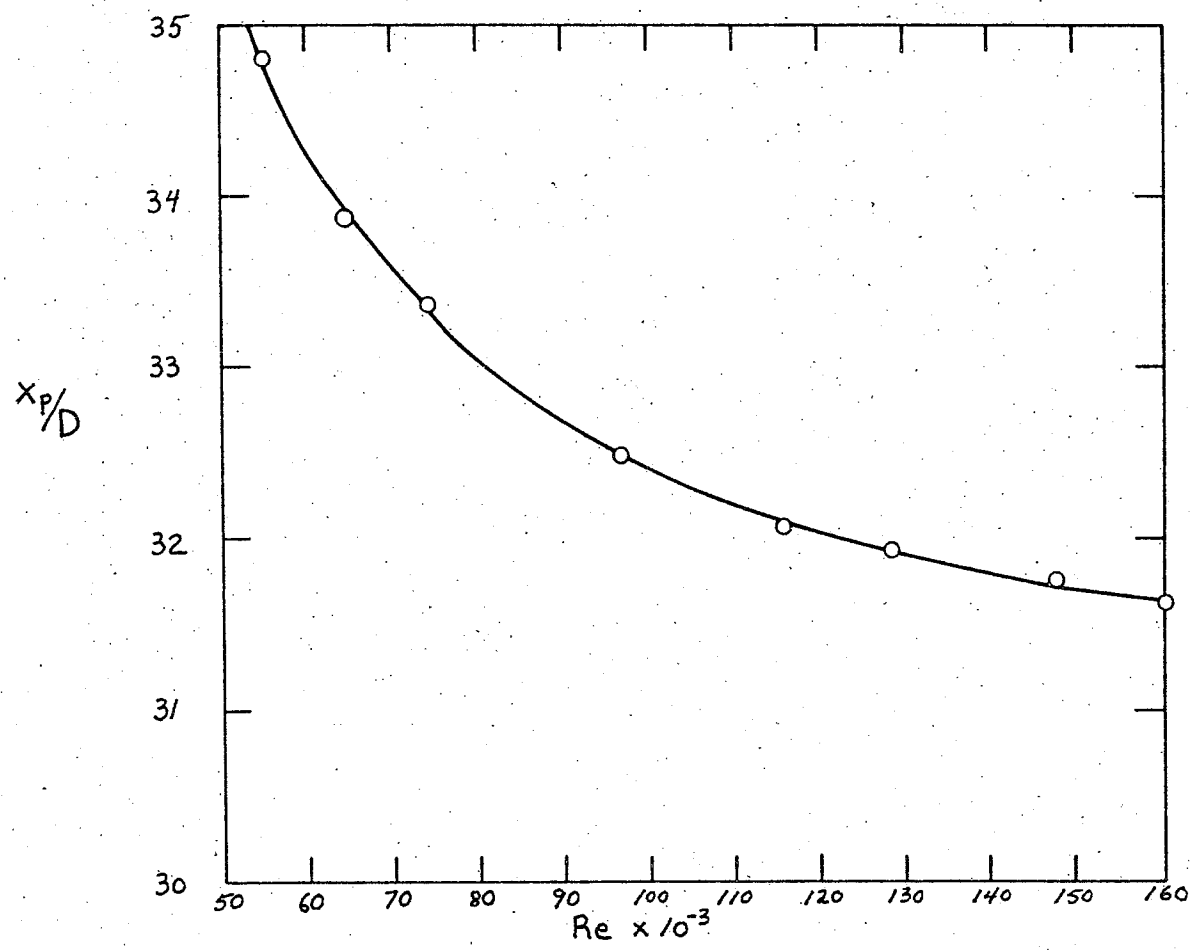

Figure 10. The effect of Reynolds number on the location of the centerline overshoot peak position, x_p/D. (—— fitted equation;

$x_p/D=30.80+.89(Re \times 10^{-5})^{-1}+.79(Re \times 10^{-5})^{-2})$.

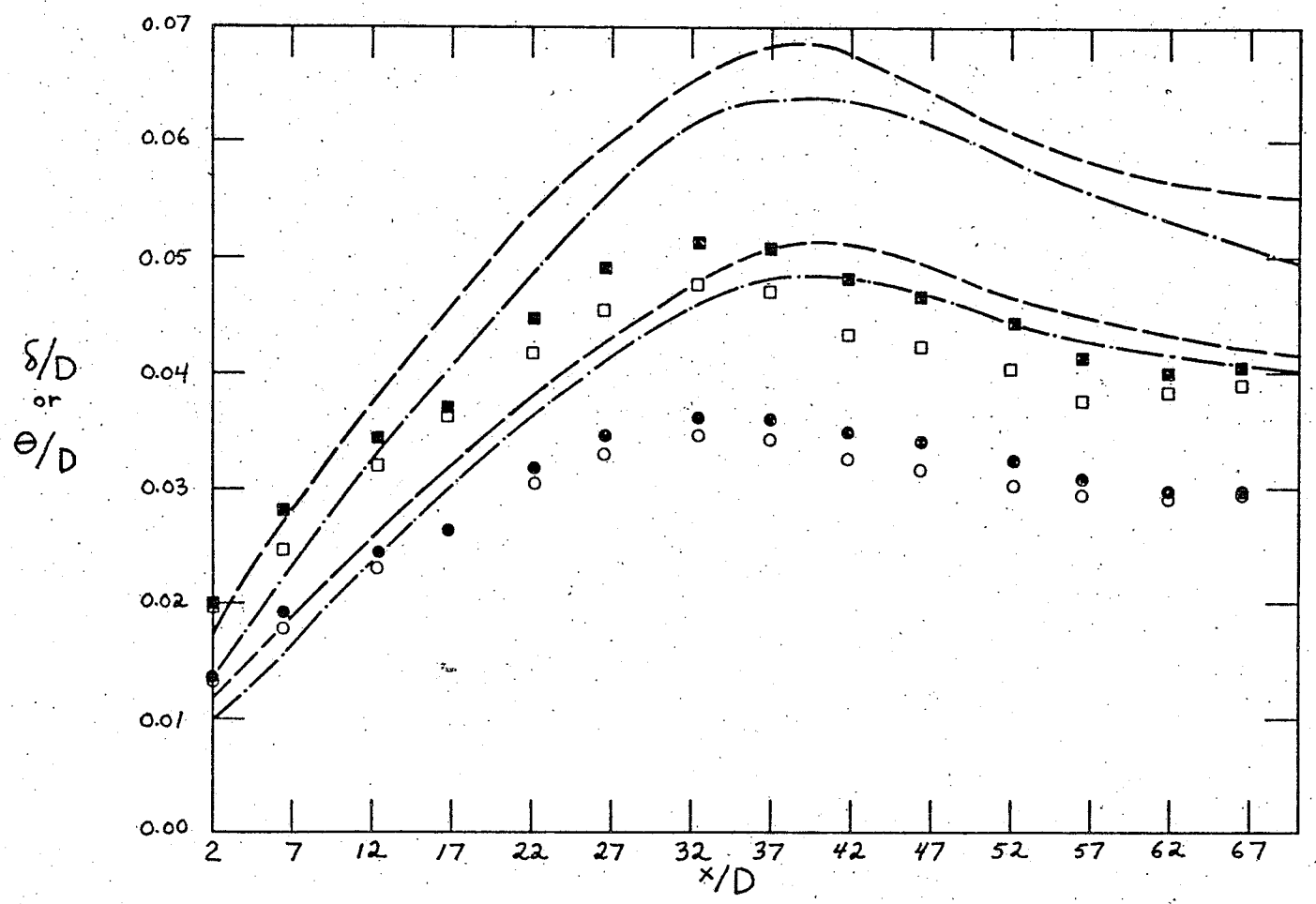

Figure 11. Normalized displacement (δ) and momentum (θ) thicknesses. (— — — Dean; 1974 rectangular duct; —·—·—·— Byrne et al; 1969 rectangular duct; ● momentum thickness Re = 76000; ○ momentum thickness Re = 153000; ■ displacement thickness Re = 76000; □ displacement thickness Re = 153000).

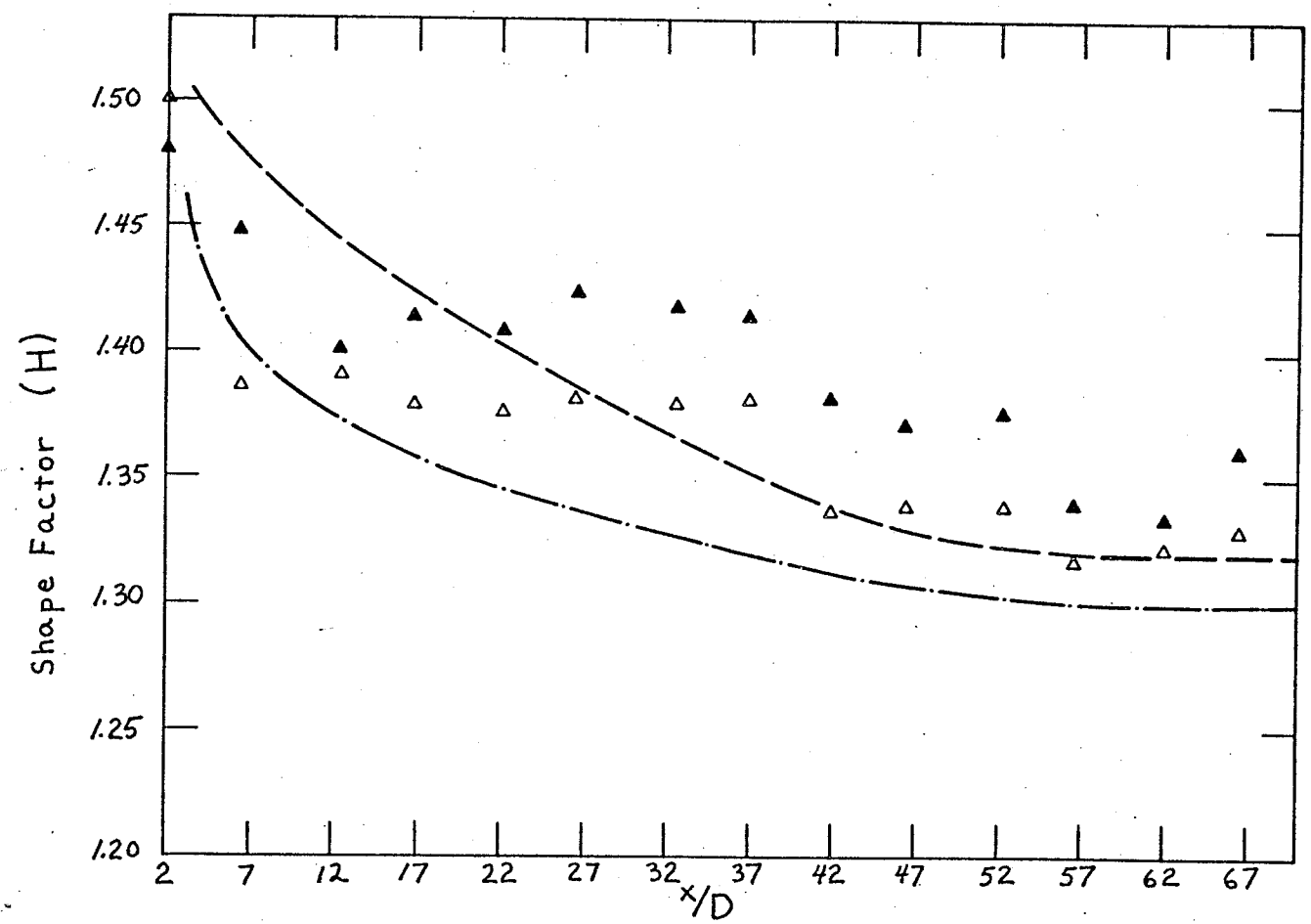

Figure 12. Shape factors for developing pipe flow.
(——— ——— ———Dean; 1974 rectangular duct;
———·———·——Byrne et al; 1969 rectangular duct;
▲ , Re = 76000; △ , Re = 153000).

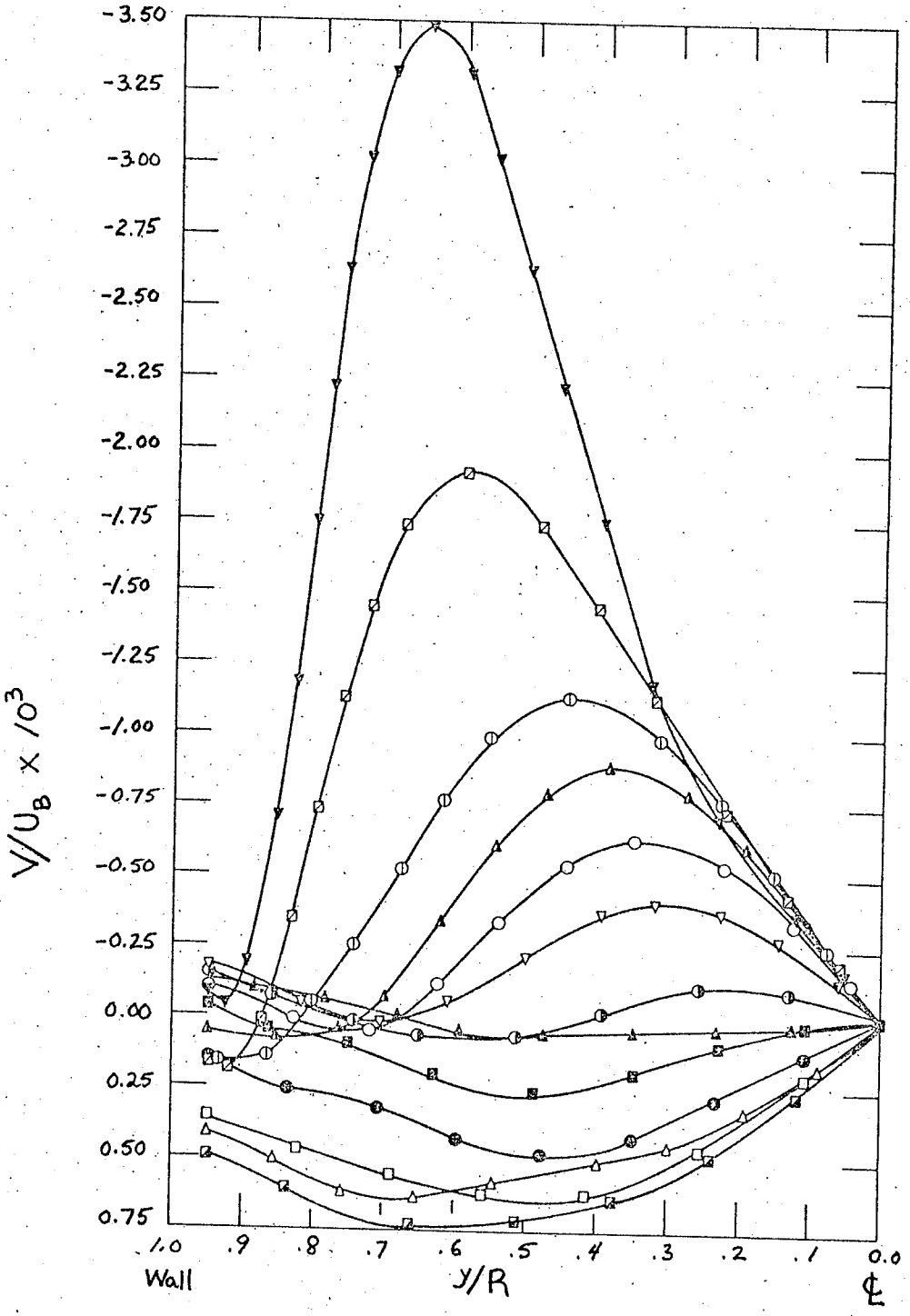

Figure 13. Mean radial velocity profiles V/U_B; Re = 76000. x/D = 2.0, ▼; x/D = 6.5 ◪; x/D = 12.4 ⦶; x/D = 16.8 ◭; x/D = 22.2, ○; x/D = 26.6 ▽; x/D = 32.5 ◑; x/D = 37.0 ■; x/D = 41.9 ◐; x/D = 52.2 ◪; x/D = 56.5 △; s/D = 61.9, ▲.

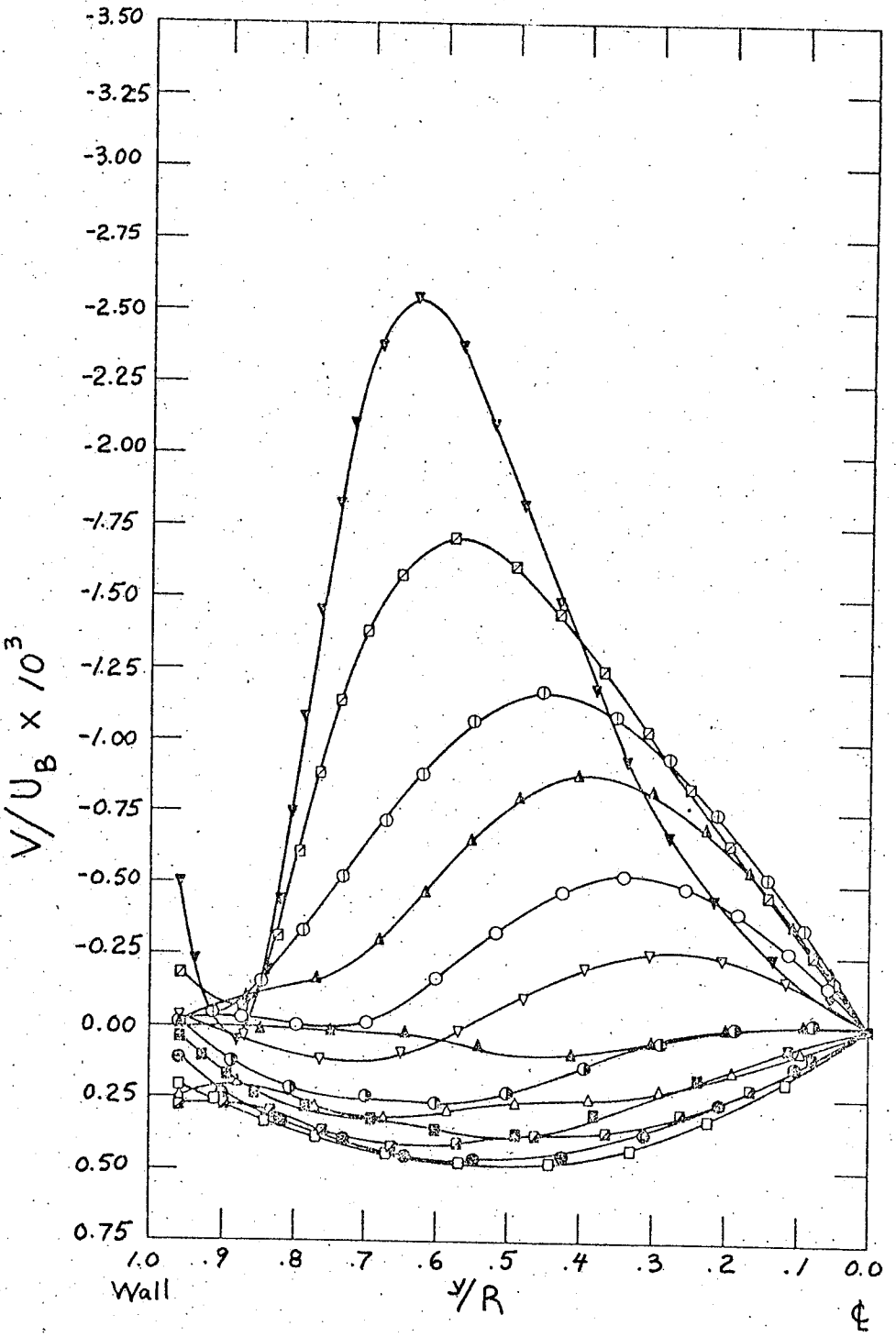

Figure 14. Mean radial velocity profiles, V/U_B; Re = 153000; symbols as for figure 13.

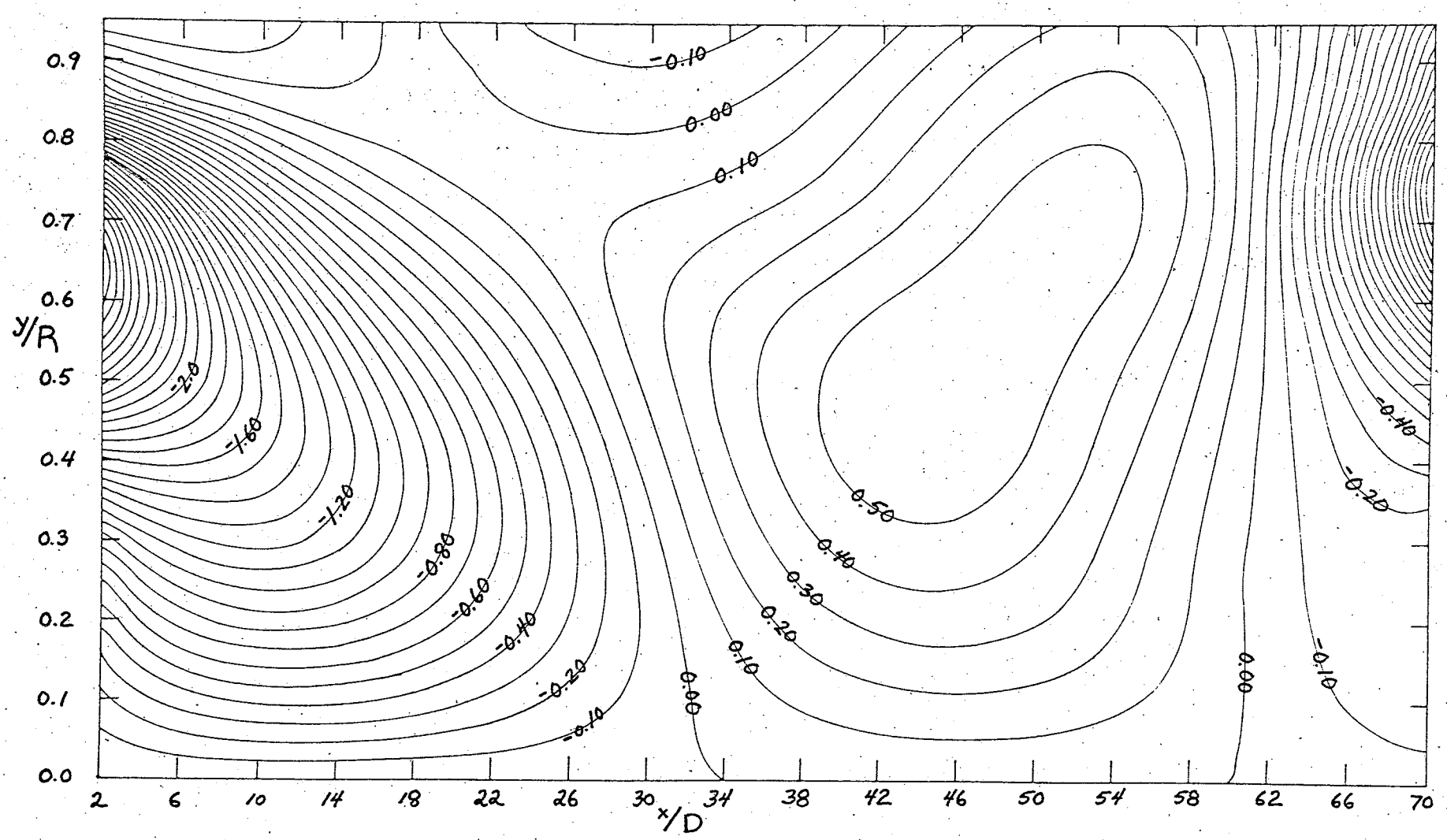

Figure 15. Radial mean velocity field contours, V/U_B; Re = 54900; contour interval = 0.10×10^{-3}.

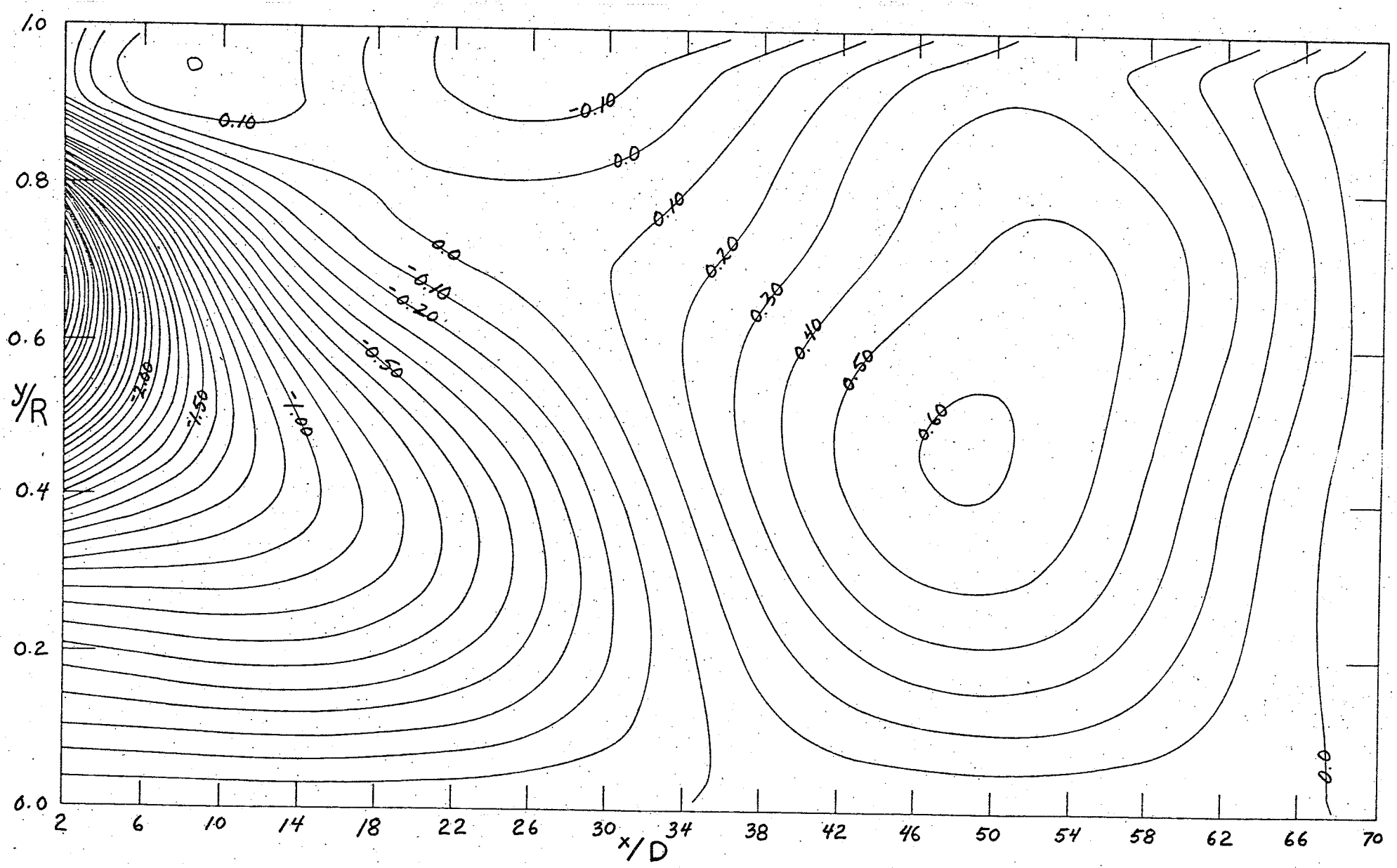

Figure 16. Radial mean velocity field contours, V/U_B; Re = 76000; contour interval = 0.10×10^{-3}.

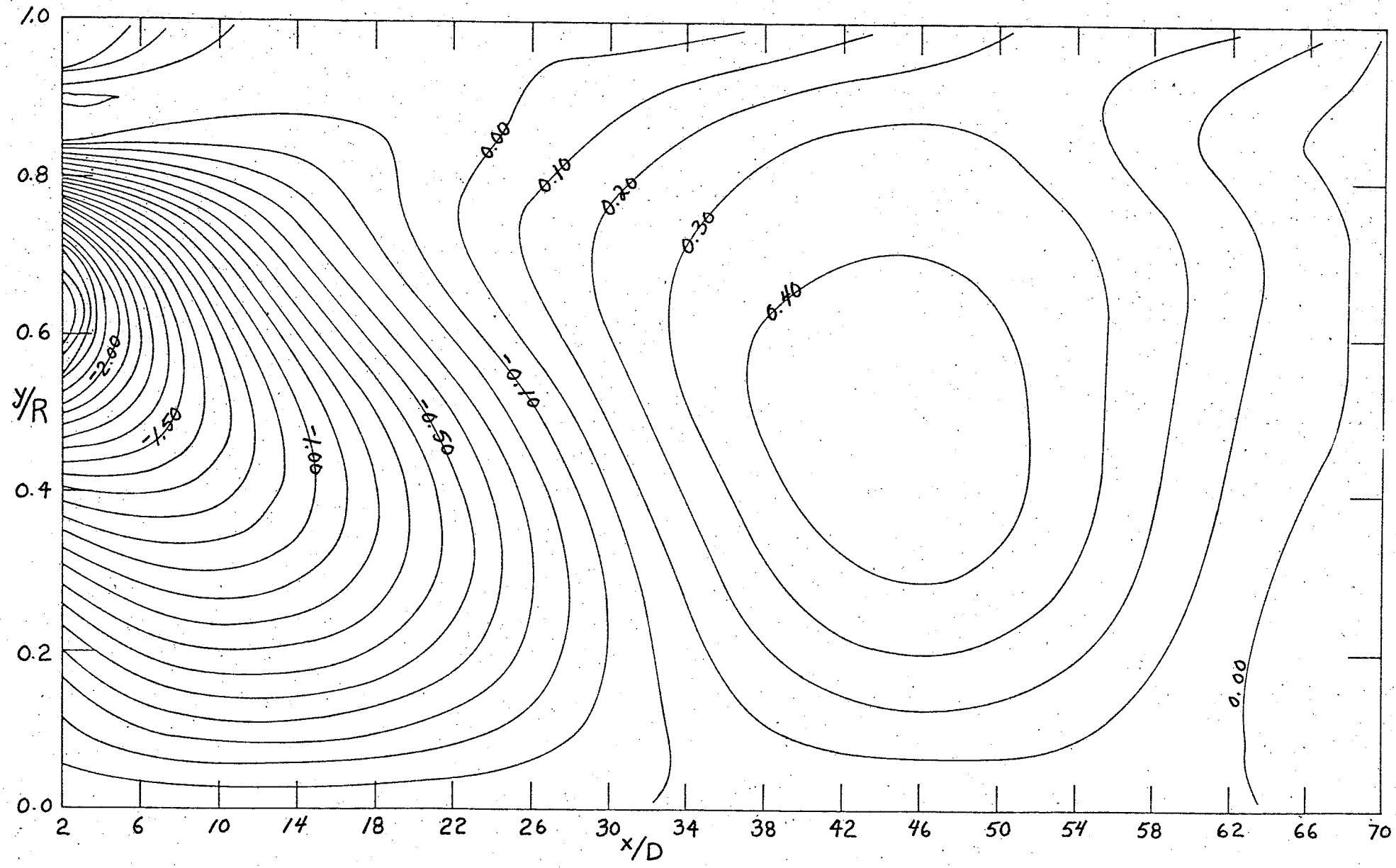

Figure 17. Radial mean velocity field contours, V/U_B; Re = 153000; contour interval = 0.10×10^{-3}.

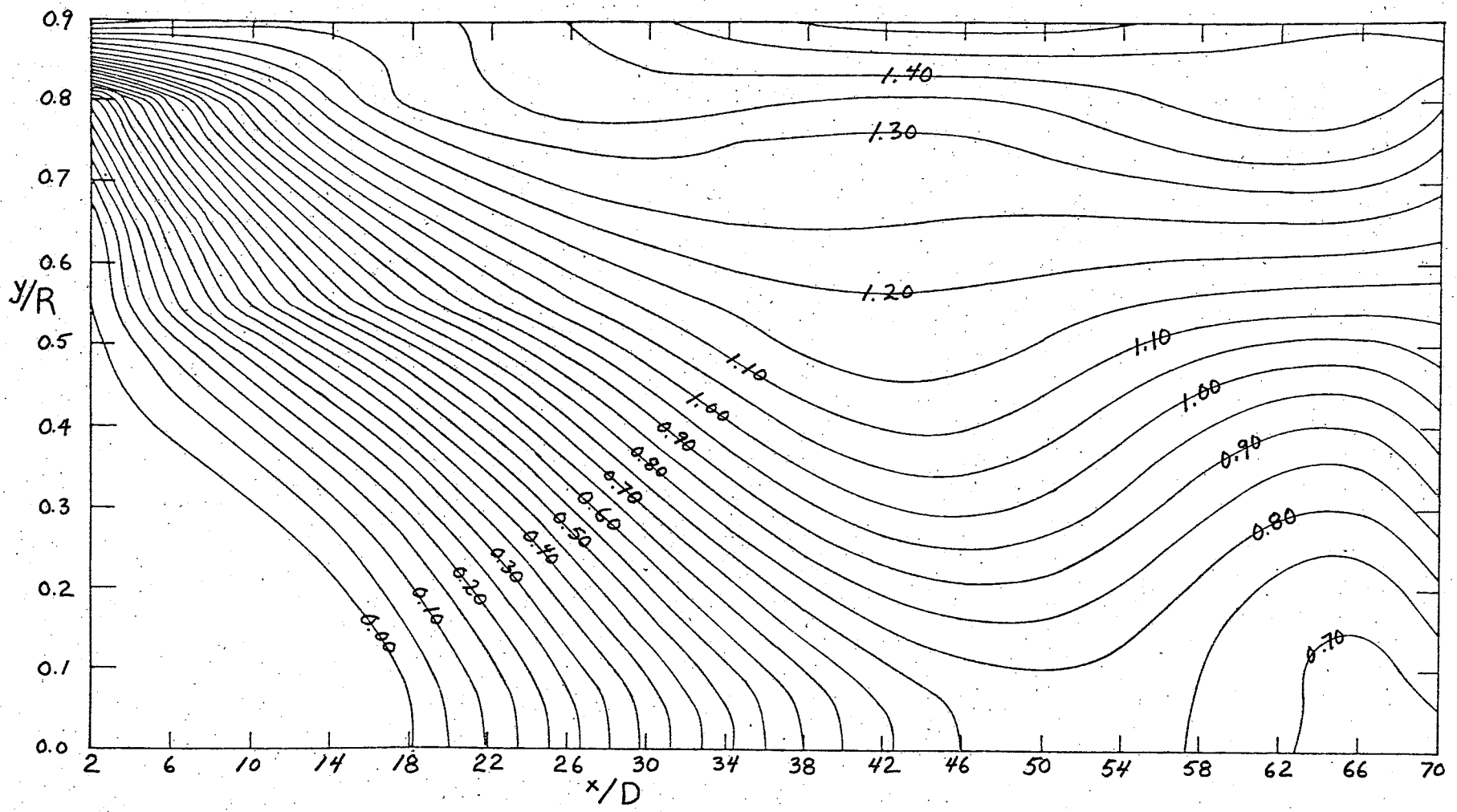

Figure 18. Contours of the longitudinal turbulence intensity field, u'; Re = 54900; contour interval = 0.05 m/sec.

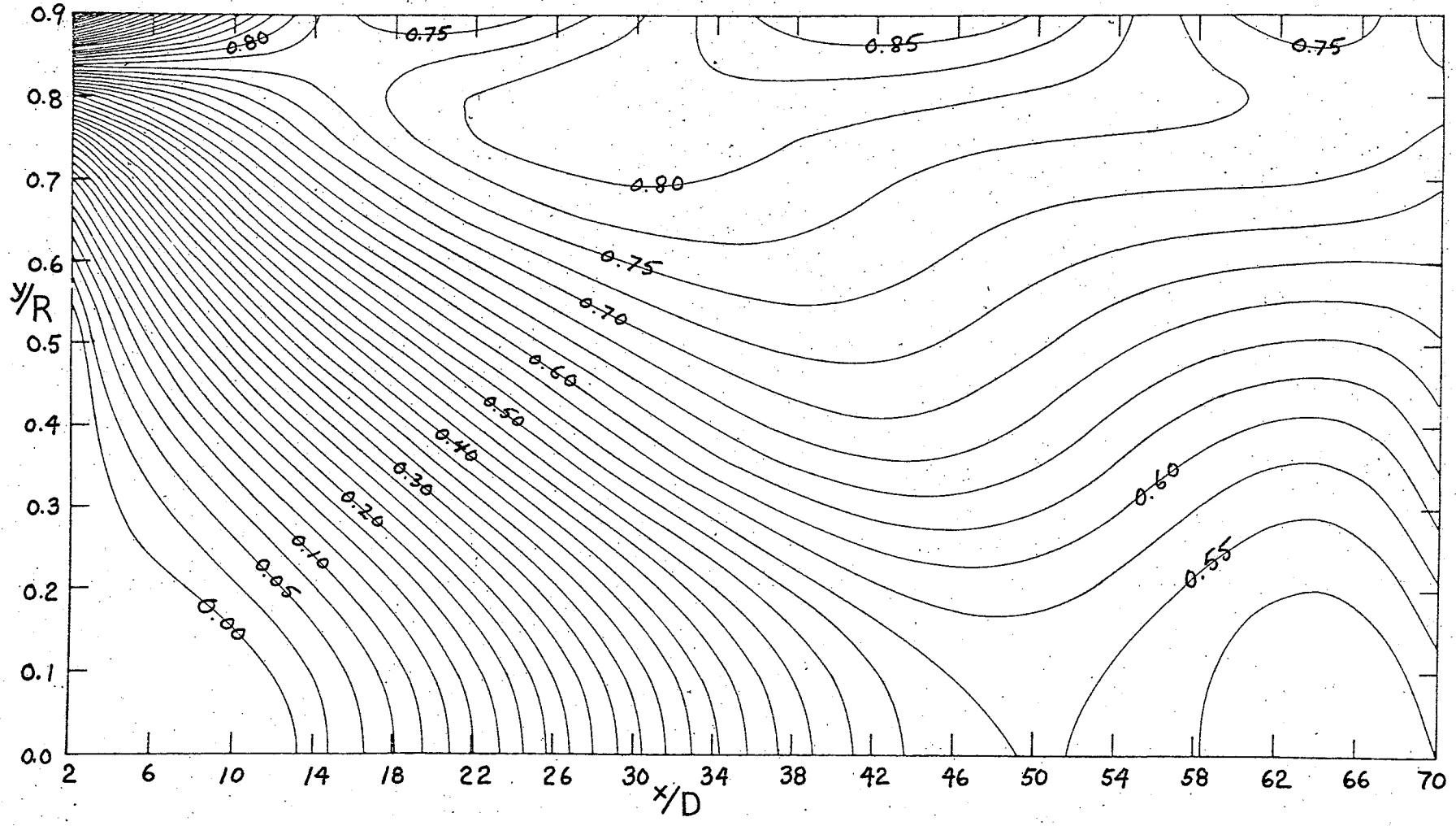

Figure 19. Contours of the radial turbulence intensity field, v'; Re = 54900; contour interval = 0.025 m/sec.

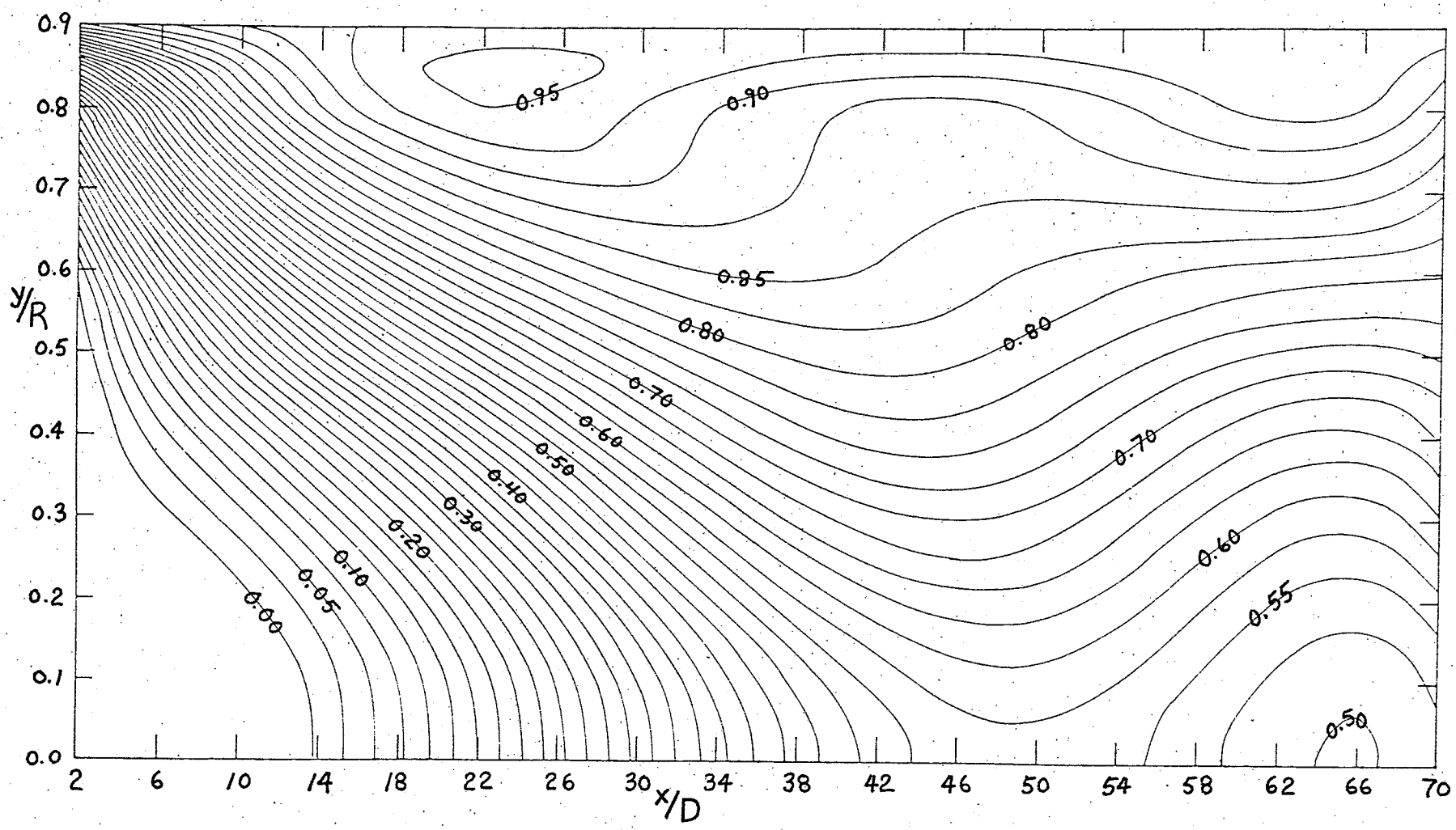

Figure 20. Contours of the circumferential turbulence intensity field w'; Re = 54900; contour interval = 0.025 m/sec.

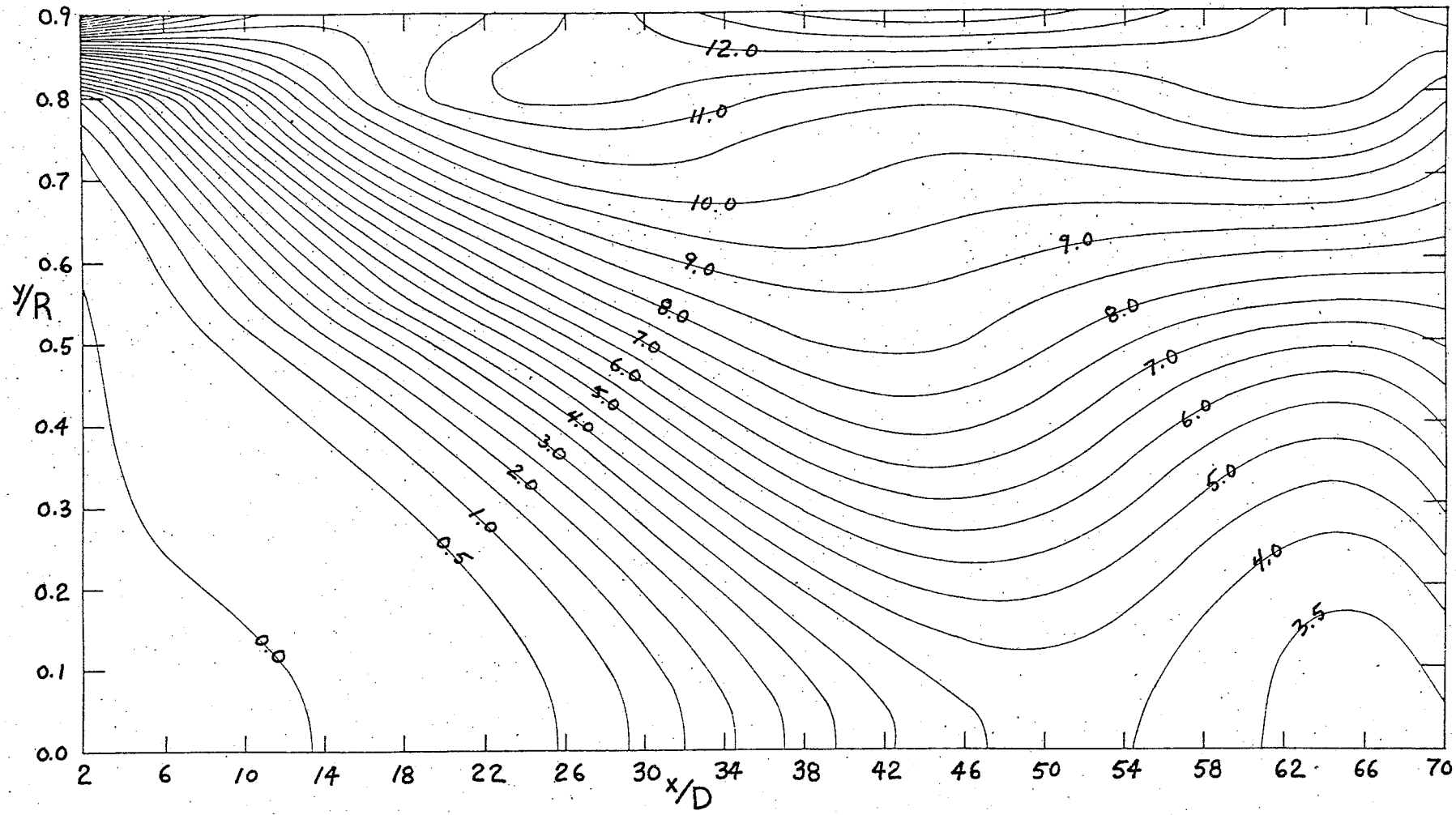

Figure 21. Contours of the nondimensionalized Reynolds stress tensor trace $\overline{q^2}/U_B^2 = (\overline{u'^2} + \overline{v'^2} + \overline{w'^2})/U_B^2$; Re = 54900; contour interval = 0.5×10^{-3}.

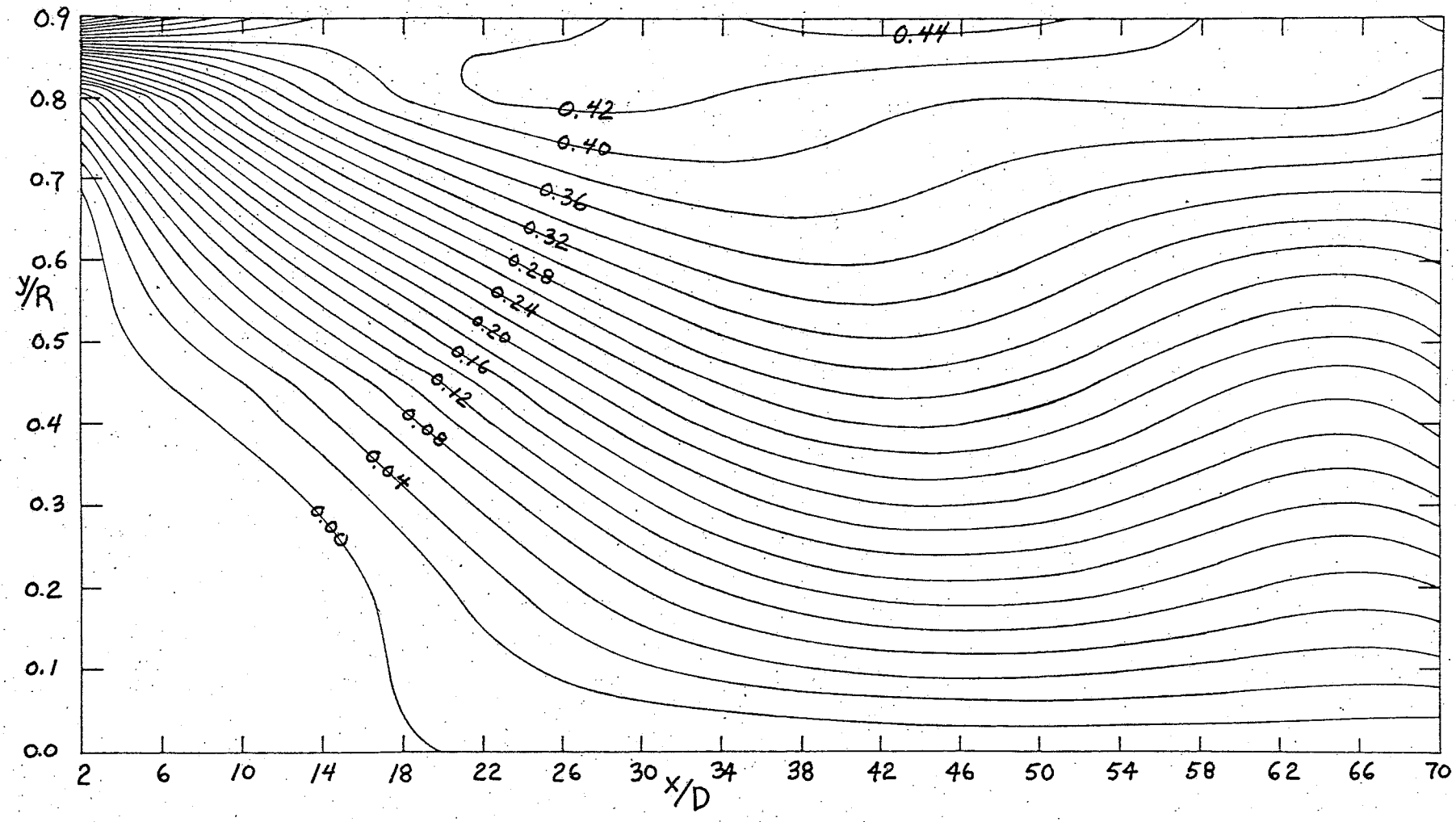

Figure 22. Contours of the tangential Reynolds stress component, $\overline{uv}$; Re = 54900; contour interval = 0.02 m^2/sec^2.

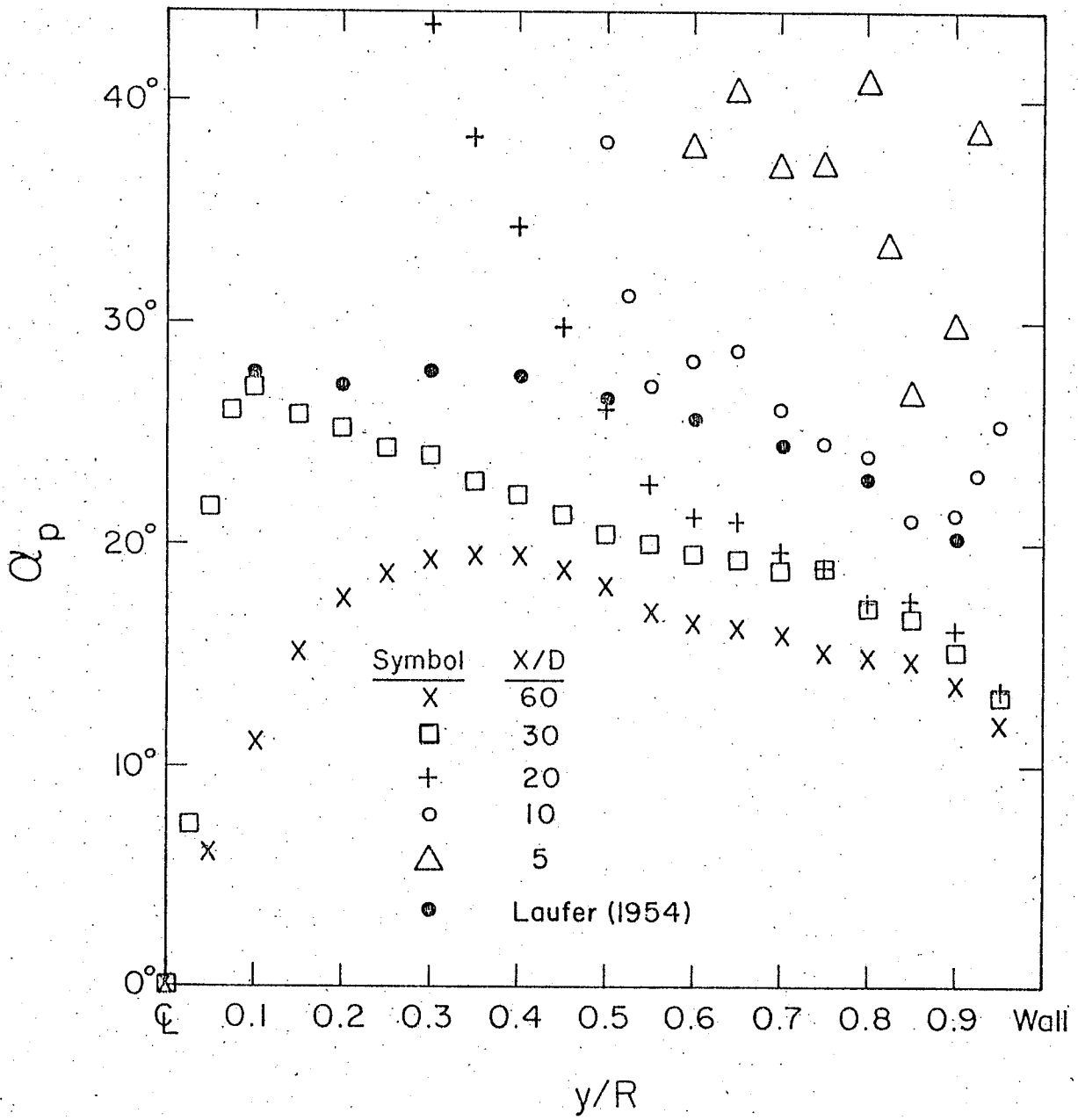

Figure 23. Angular direction of the greatest principal stress, α_p; Re = 54900.

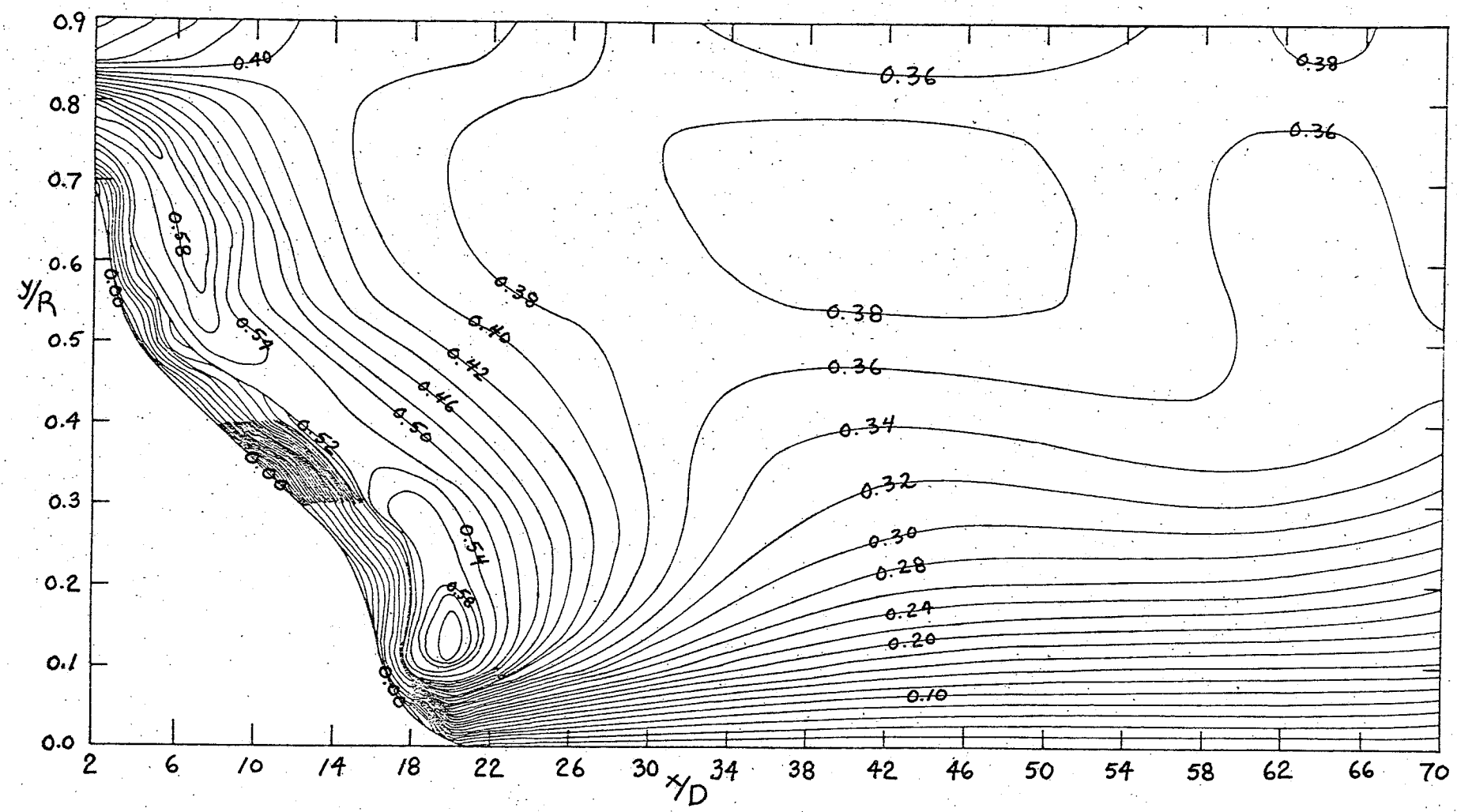

Figure 24. Contours of the computed correlation coefficient $\overline{uv}/u'v'$; Re = 54900; contour interval = 0.02.

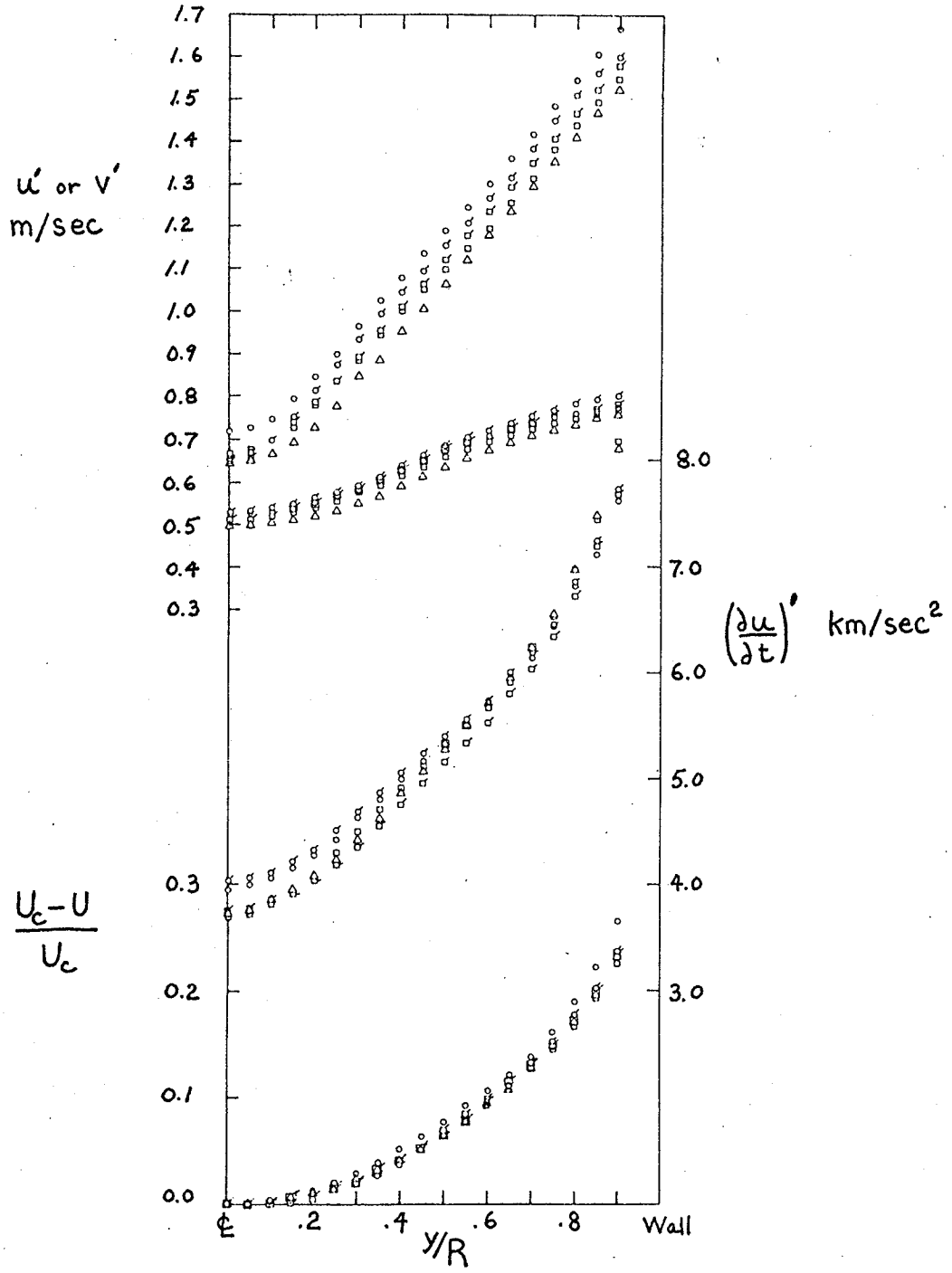

Figure 25. Comparison of results with experimental setups A and B. O, x/D = 60.3, setup A, trial 1; ◠, x/D = 60.3, setup A, trial 2; □ , x/D = 65.2, setup B, trial 1; ◠ , x/D = 65.2, setup B, trial 2;△x/D 85.4, setup B. All results for Re = 54900.

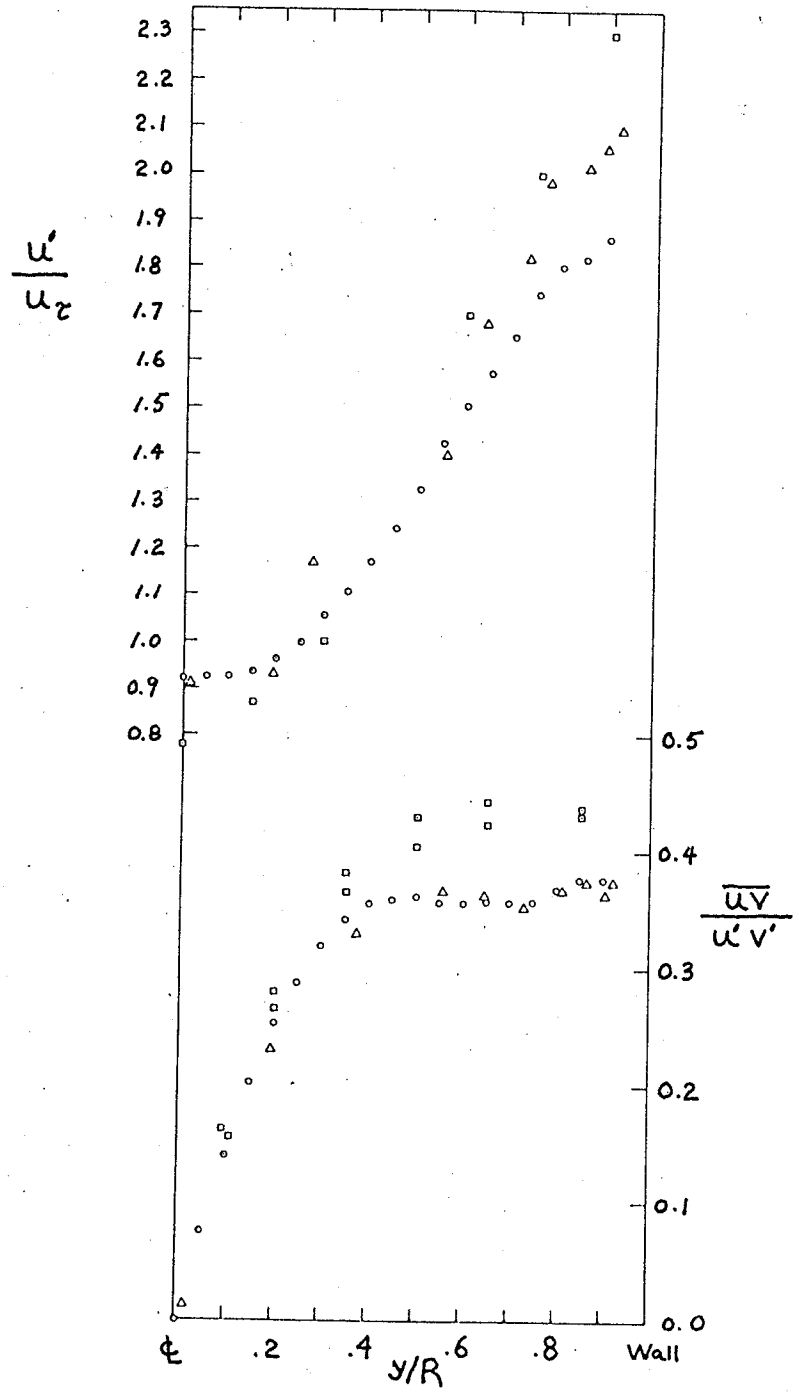

Figure 26. Comparison of longitudinal u' and correlation coefficient $\overline{uv}/u'v'$ with other investigators. ○, present results from contours at x/D = 60, Re = 54900; Δ, Perry and Abell (1975); □, Sabot and Compte-Bellot (1976).

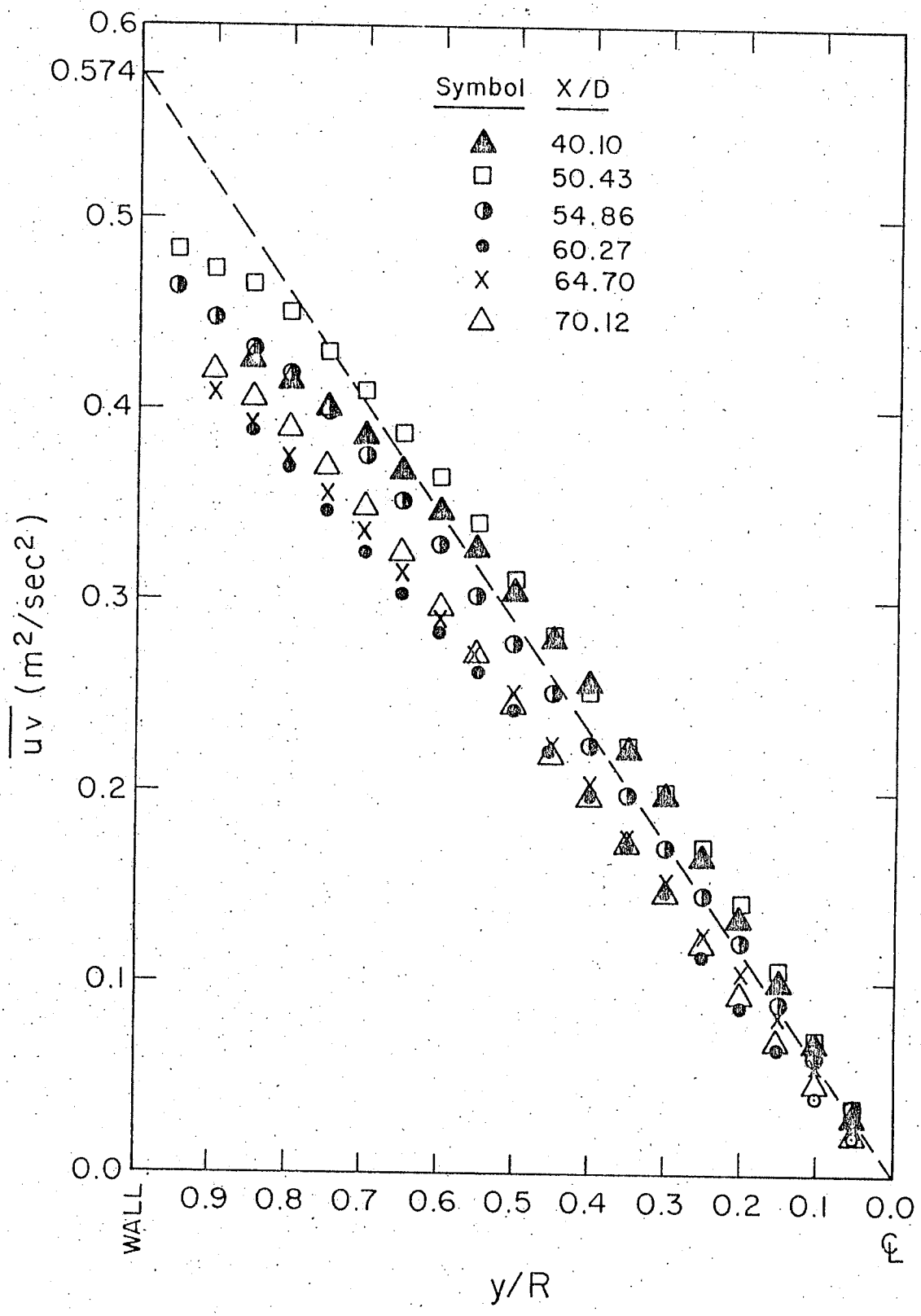

Figure 27. Profile data for $\overline{uv}$ extracted from XY plotter records, Re = 54900. ($\overline{uv}$ = .574 m^2/sec^2 expected fully developed value based on pressure gradient).

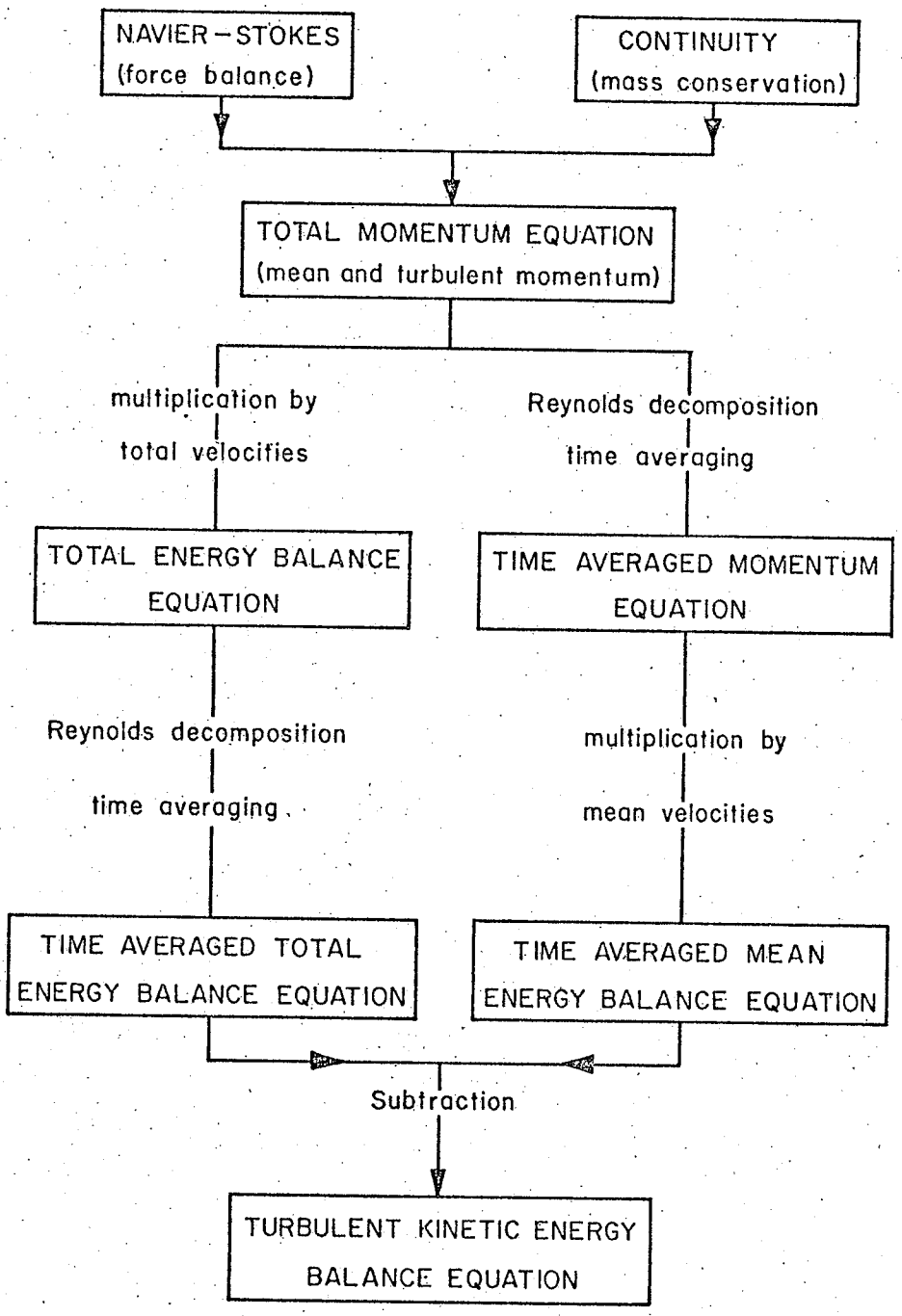

Figure 28. Genealogy of turbulent kinetic energy balance equation (eqn 6.1).

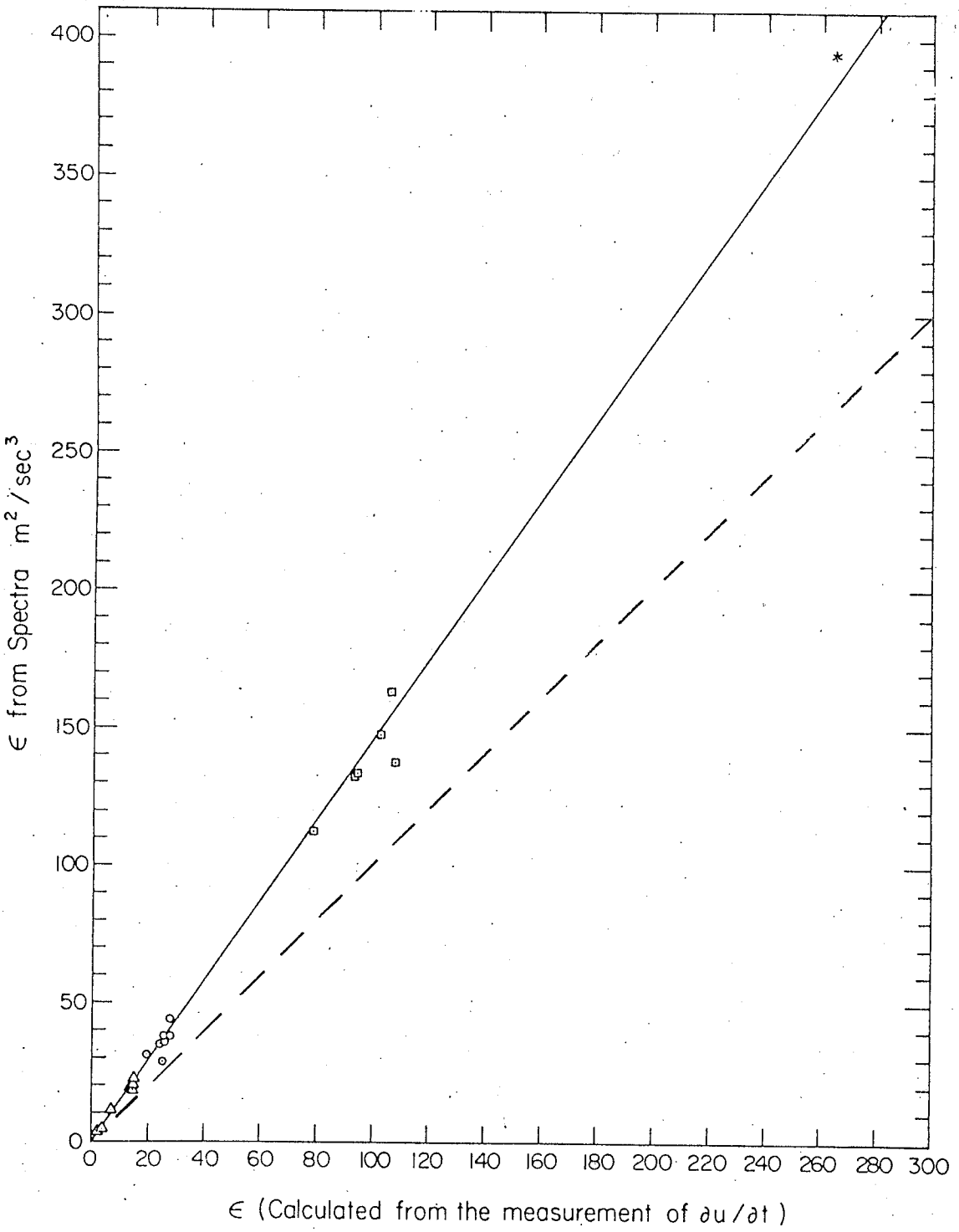

Figure 29. Comparison of dissipation estimates ε from spectra (eqn. 3.1) and $\frac{\partial u}{\partial t}$ (eqn. 6.7) measurements.

$10.6 \geq x/D \geq 65.2$: Δ, $y/\delta = .9$; O, $y/\delta = .5$; □ $y/\delta = .1$

($x/D = 1.8$: *, $y/R = .1$).

— — —: Reference line if ε estimates were equal.

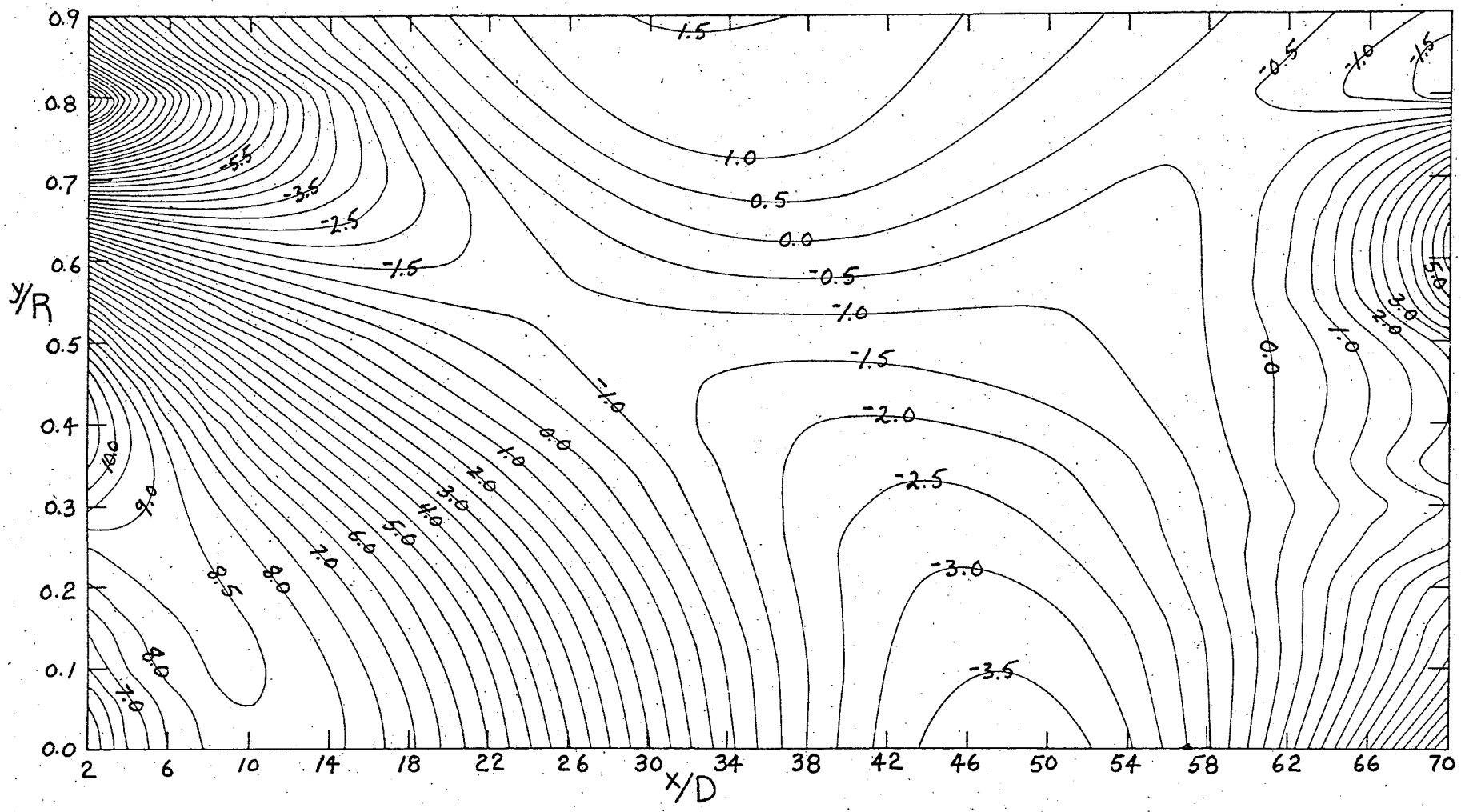

Figure 30. Contours of calculated longitudinal derivatives of the axial mean velocity component, $\partial(U/U_B)/\partial(x/2R)$; Re = 54900; contour interval = 0.5×10^{-3}.

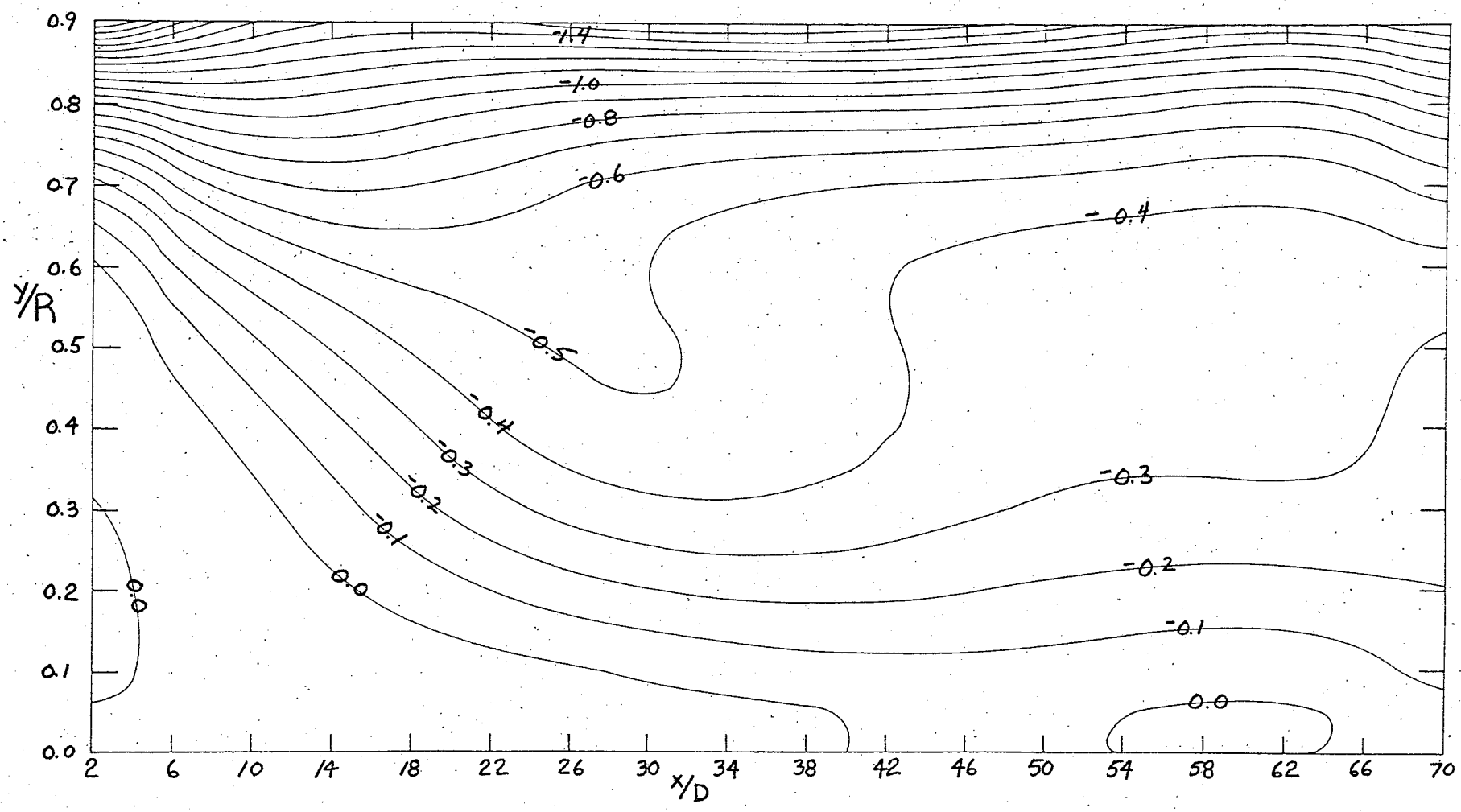

Figure 31. Contours of calculated radial derivatives of the axial mean velocity component, $\partial(U/U_B)/\partial(y/R)$; Re = 54900; contour interval = 1.0×10^{-1}.

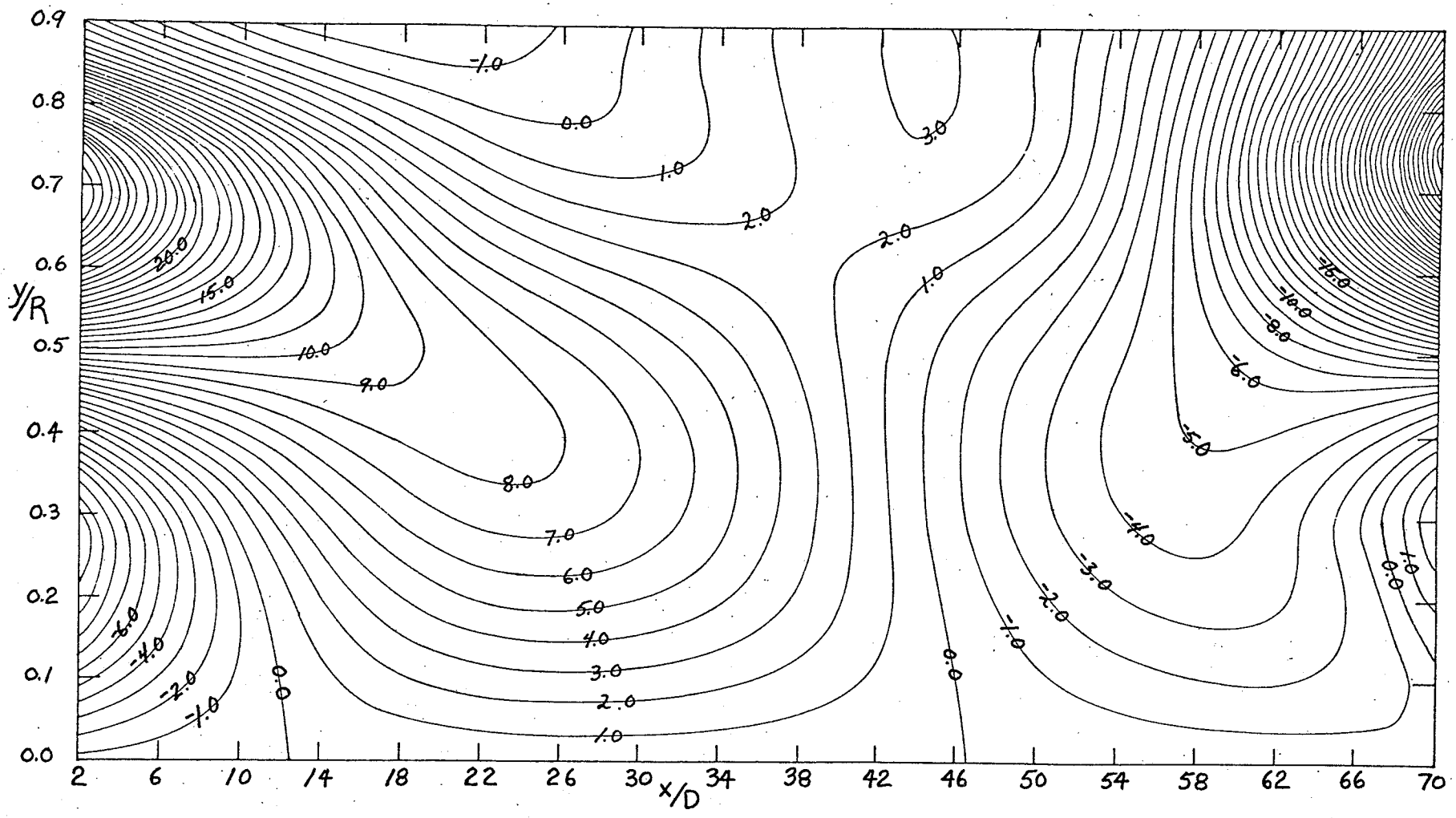

Figure 32. Contours of calculated longitudinal derivatives of the radial mean velocity component, $\partial(V/U_B)/\partial(x/2R)$; Re = 54900; contour interval - 1.0×10^{-5}.

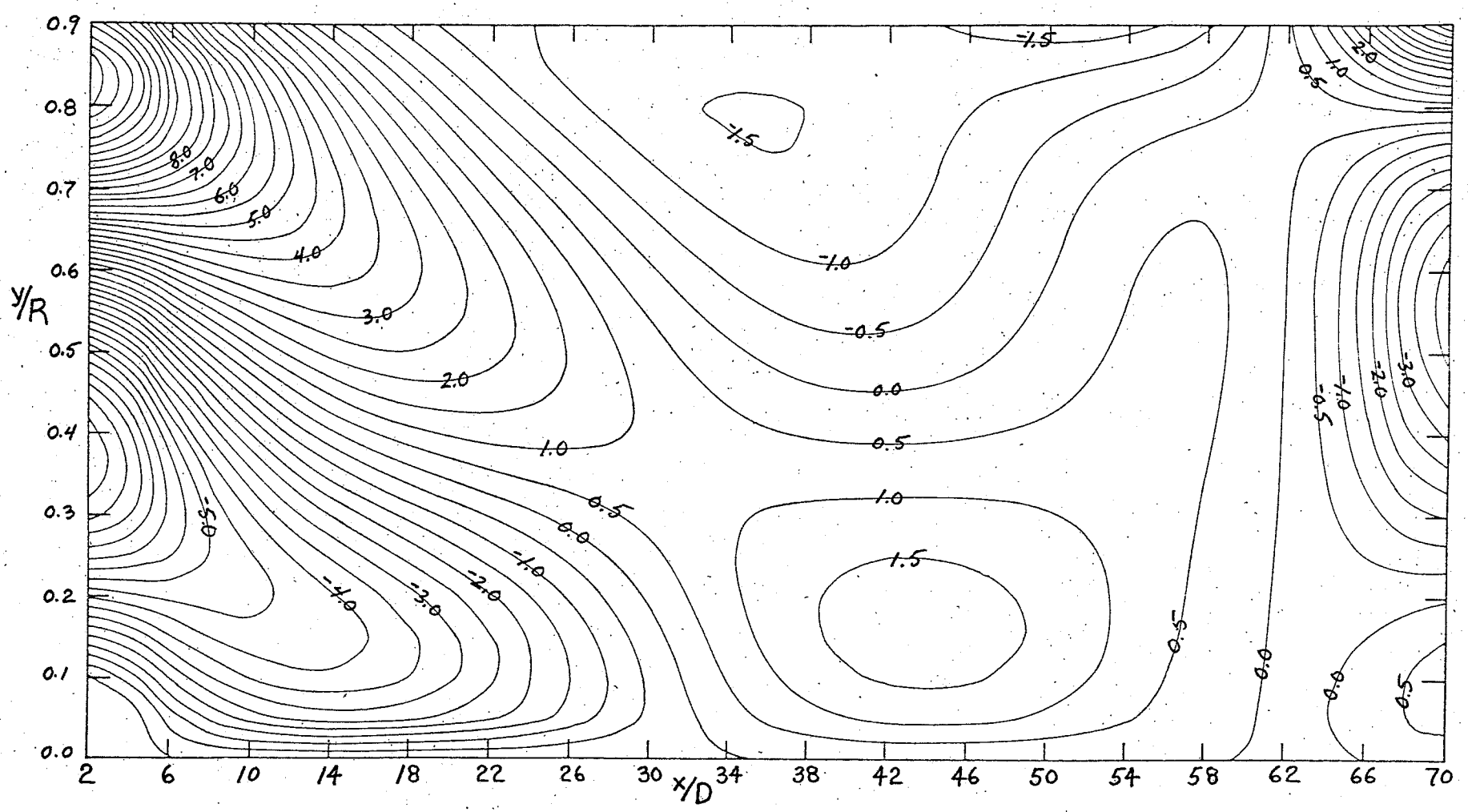

Figure 33. Contours of calculated radial derivatives of the radial mean velocity component, $\partial(V/U_B)/\partial(y/R)$; Re = 54900; contour interval = 0.5×10^{-3}.

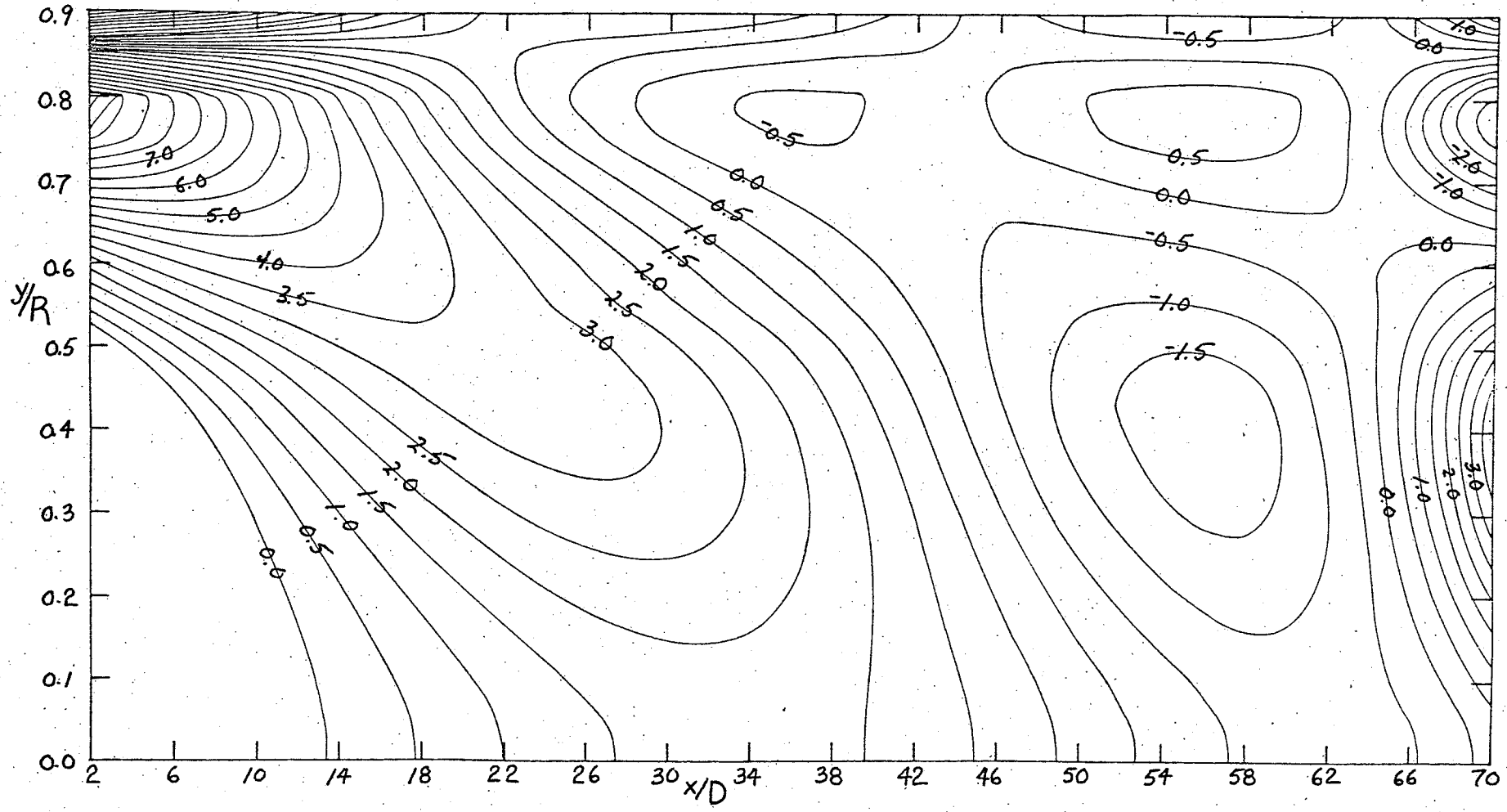

Figure 34. Contours of calculated longitudinal derivatives of the total turbulence intensity, $\partial(\overline{q^2}/U_B^2)/\partial(x/2R)$; Re = 54900; contour interval = 0.5×10^{-4}.

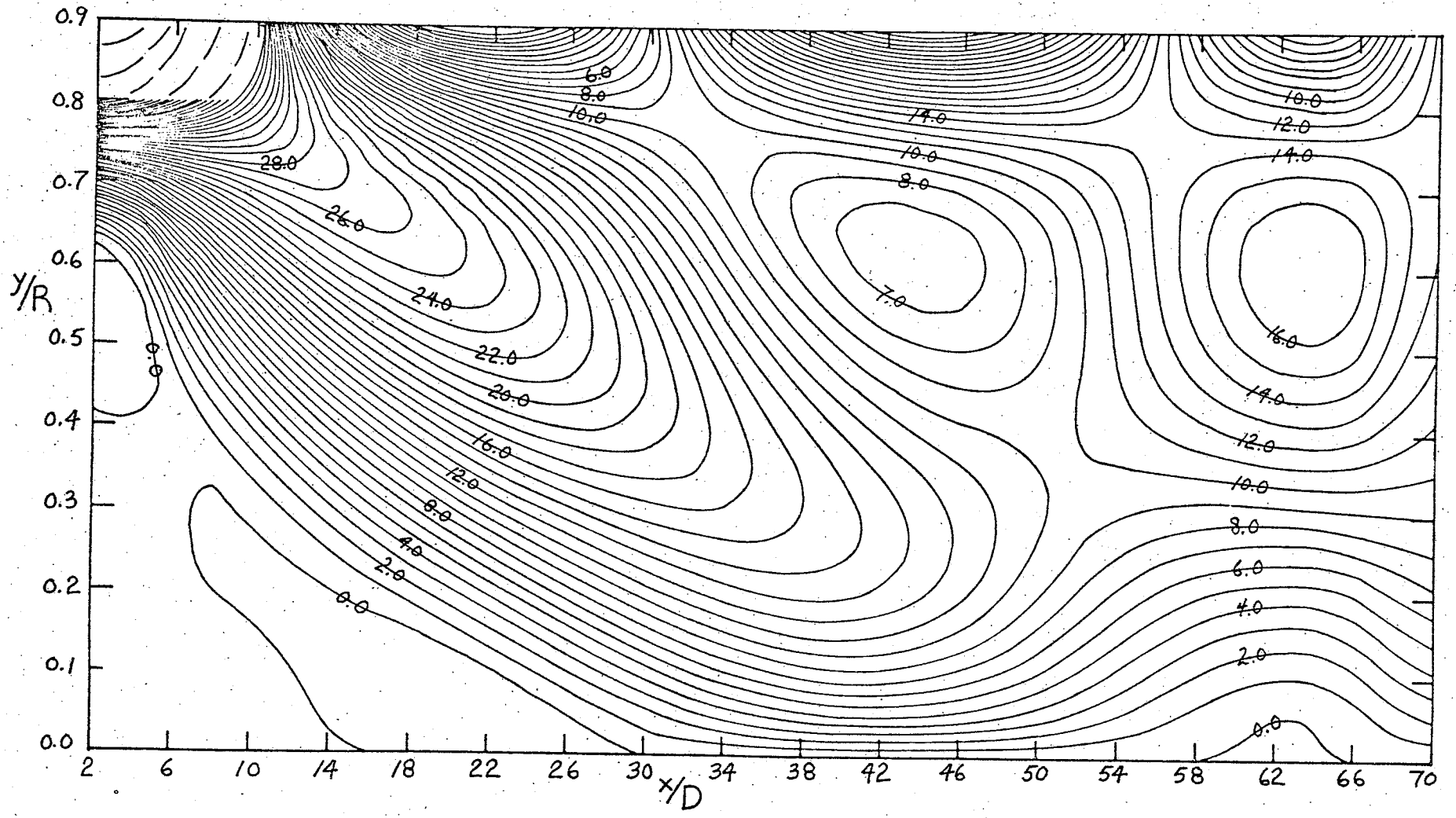

Figure 35. Contours of calculated radial derivatives of the total turbulence intensity, $\partial(\overline{q^2}/U_B^2)/\partial(y/R)$; Re = 54900; contour interval = 1.0 x 10^{-3}.

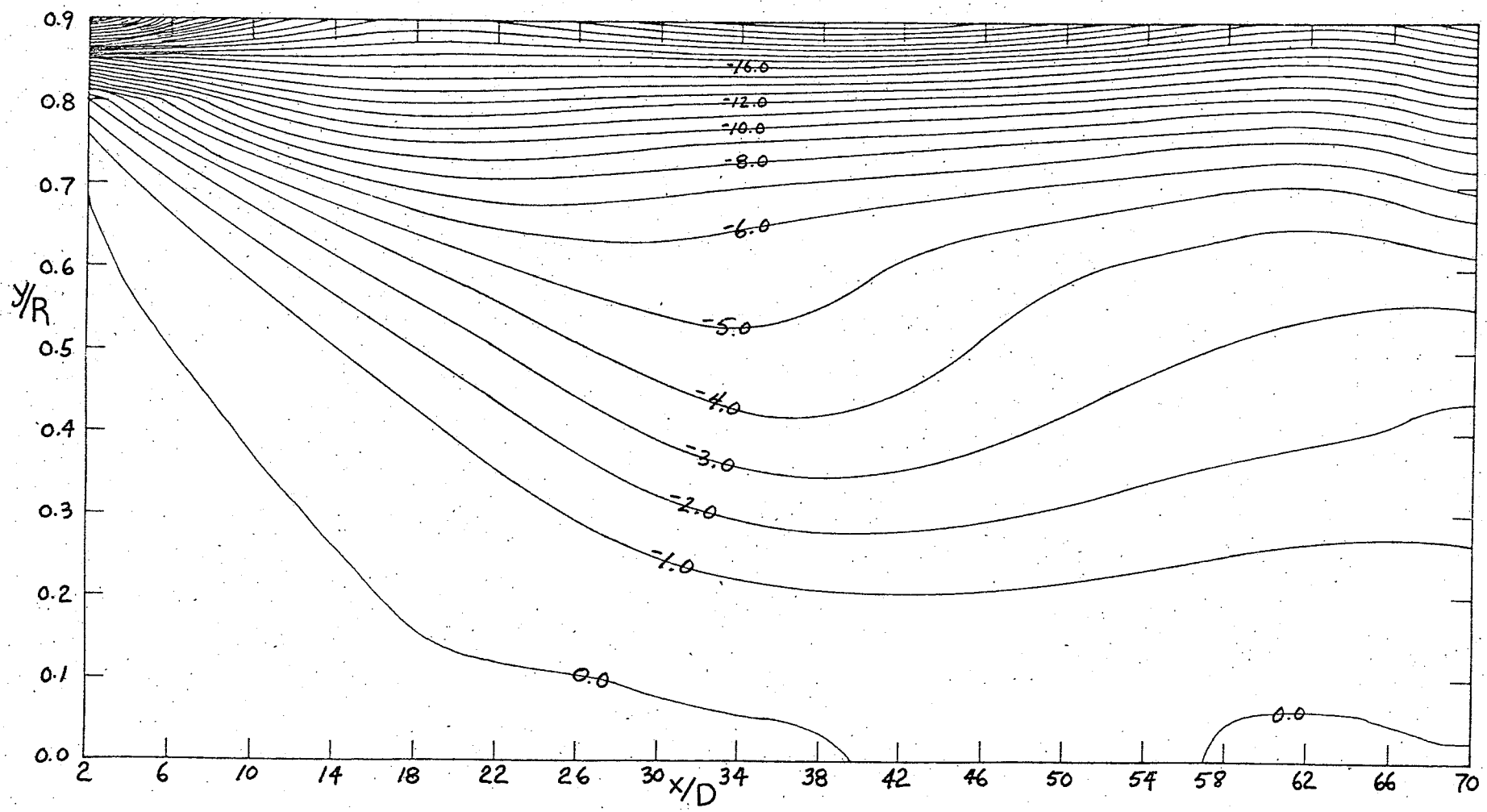

Figure 36. Contours of the total turbulent kinetic production (eqn. 6.4); Re = 54900; contour interval = 1.0×10^{-4}.

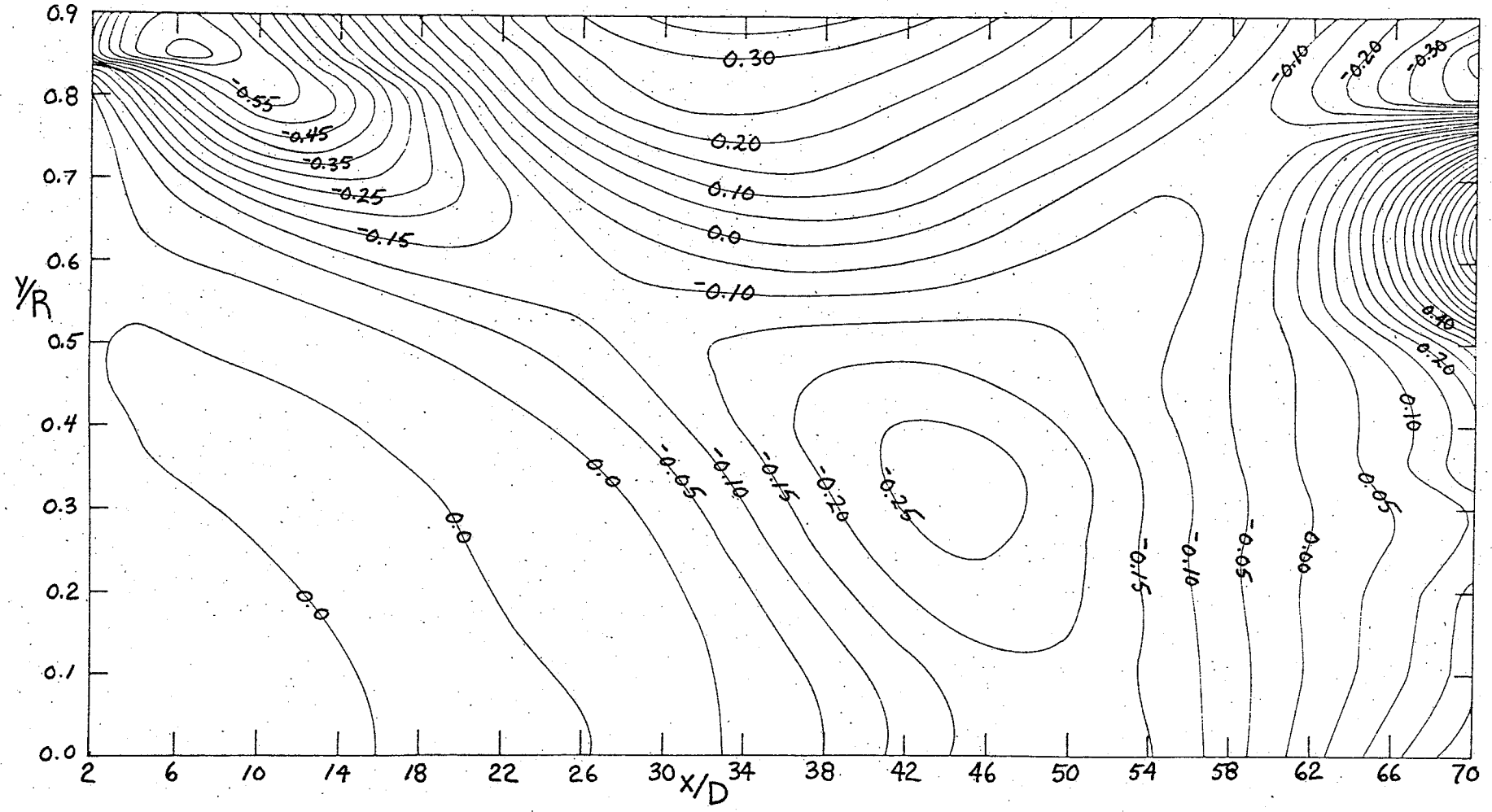

Figure 37. Contours of the turbulent kinetic energy production term, $\frac{\overline{u^2} - \overline{v^2}}{2U_B^2} \frac{\partial(U/U_B)}{\partial(x/2R)}$; Re = 54900; contour interval = 0.5×10^{-6}.

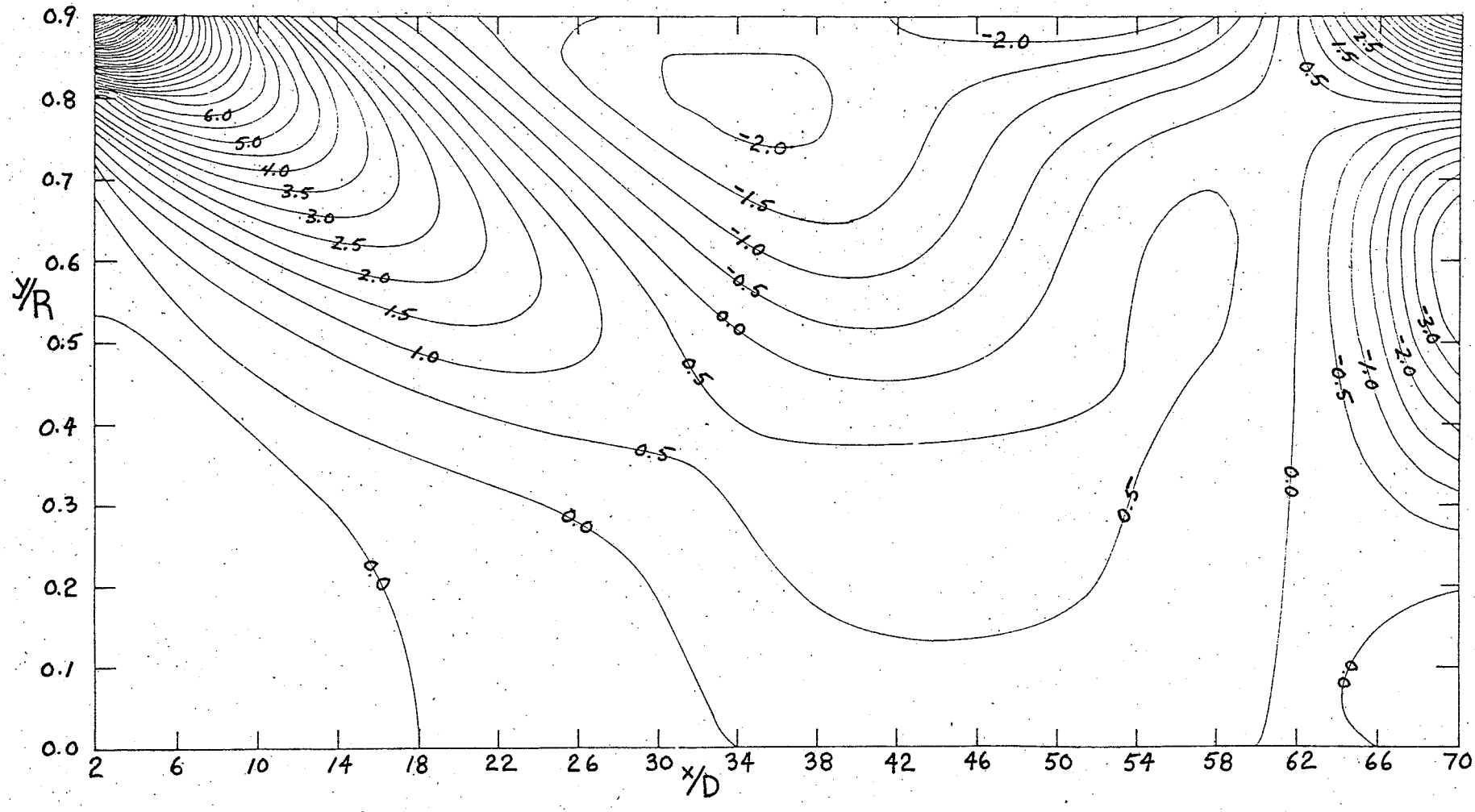

Figure 38. Contours of the turbulent kinetic energy production term, $\frac{\overline{uv}}{U_B^2} \frac{\partial(V/U_B)}{\partial(y/R)}$; Re = 54900; contour interval = 0.5 x 10^{-6}.

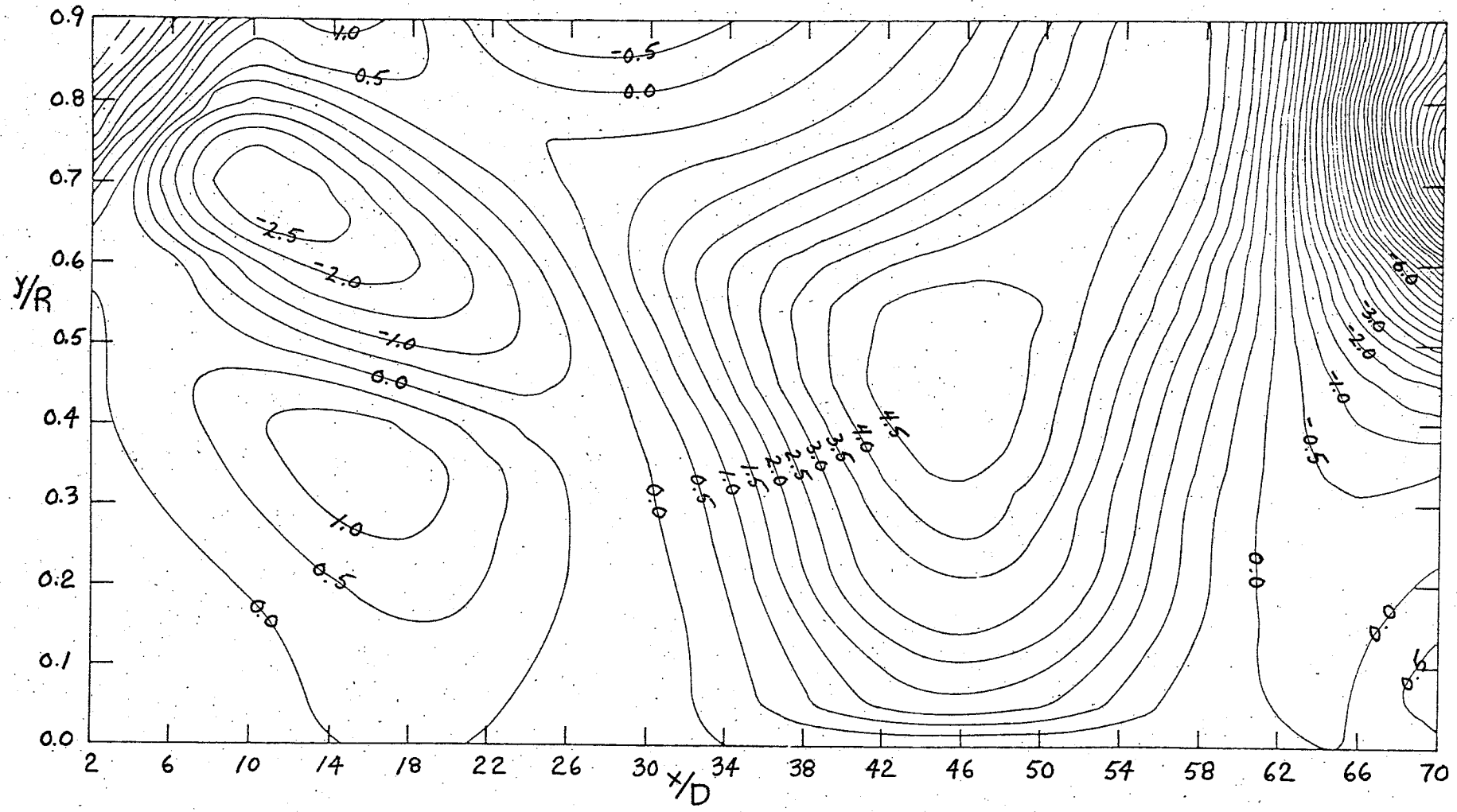

Figure 39. Contours of the turbulent kinetic energy production term,

$$\frac{1}{(y/R)} \frac{V}{U_B} \frac{\overline{w^2} - \overline{v^2}}{U_B^2}$$; Re = 54900; contour interval = 0.5×10^{-7}.

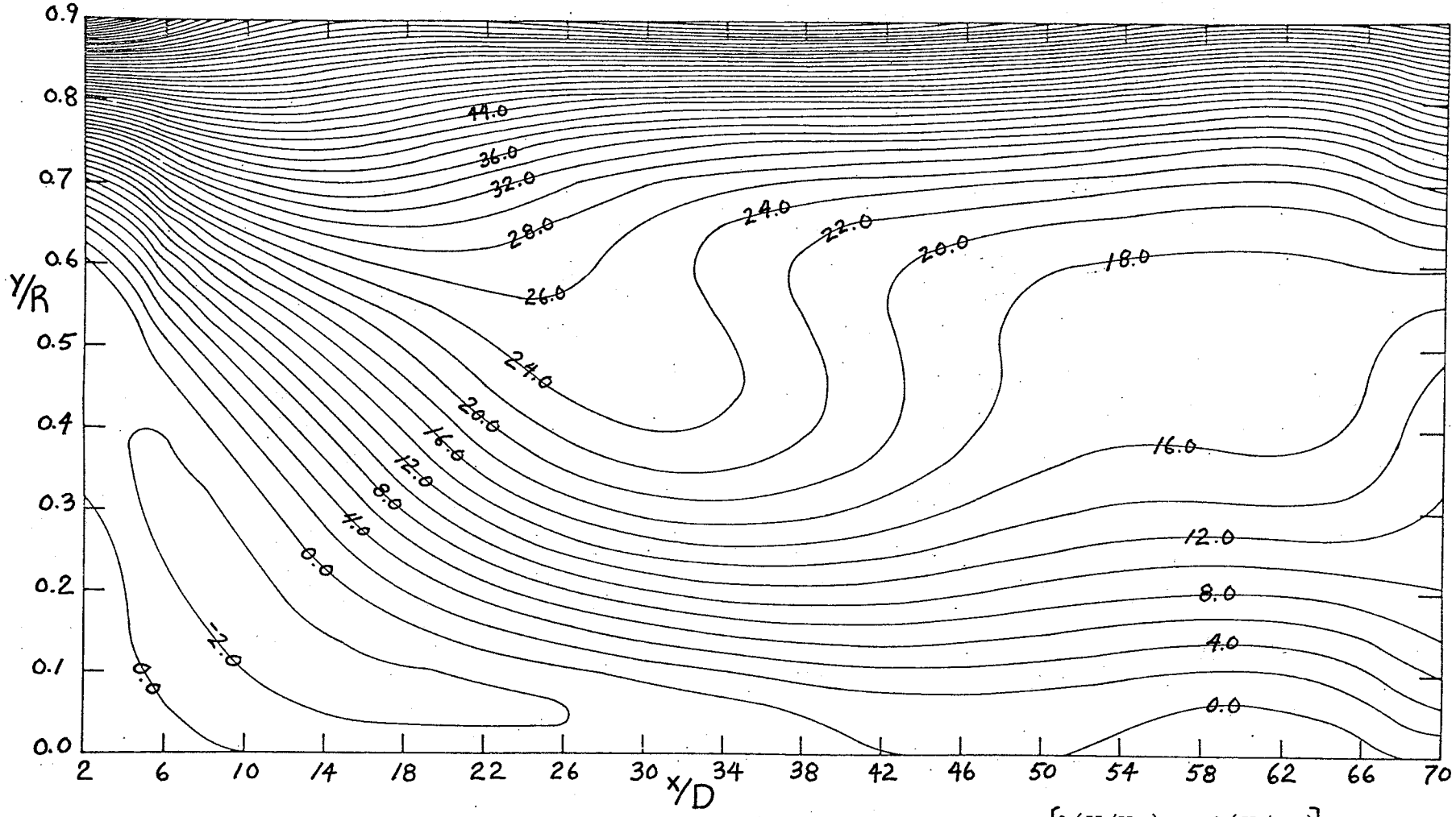

Figure 40. Contours of the mean flow vorticity, $\frac{1}{2}\left[\frac{\partial(V/U_B)}{\partial(x/R)} - \frac{\partial(U/U_B)}{\partial(y/R)}\right]$; Re = 54900, contour interval = 2.0×10^{-2}.

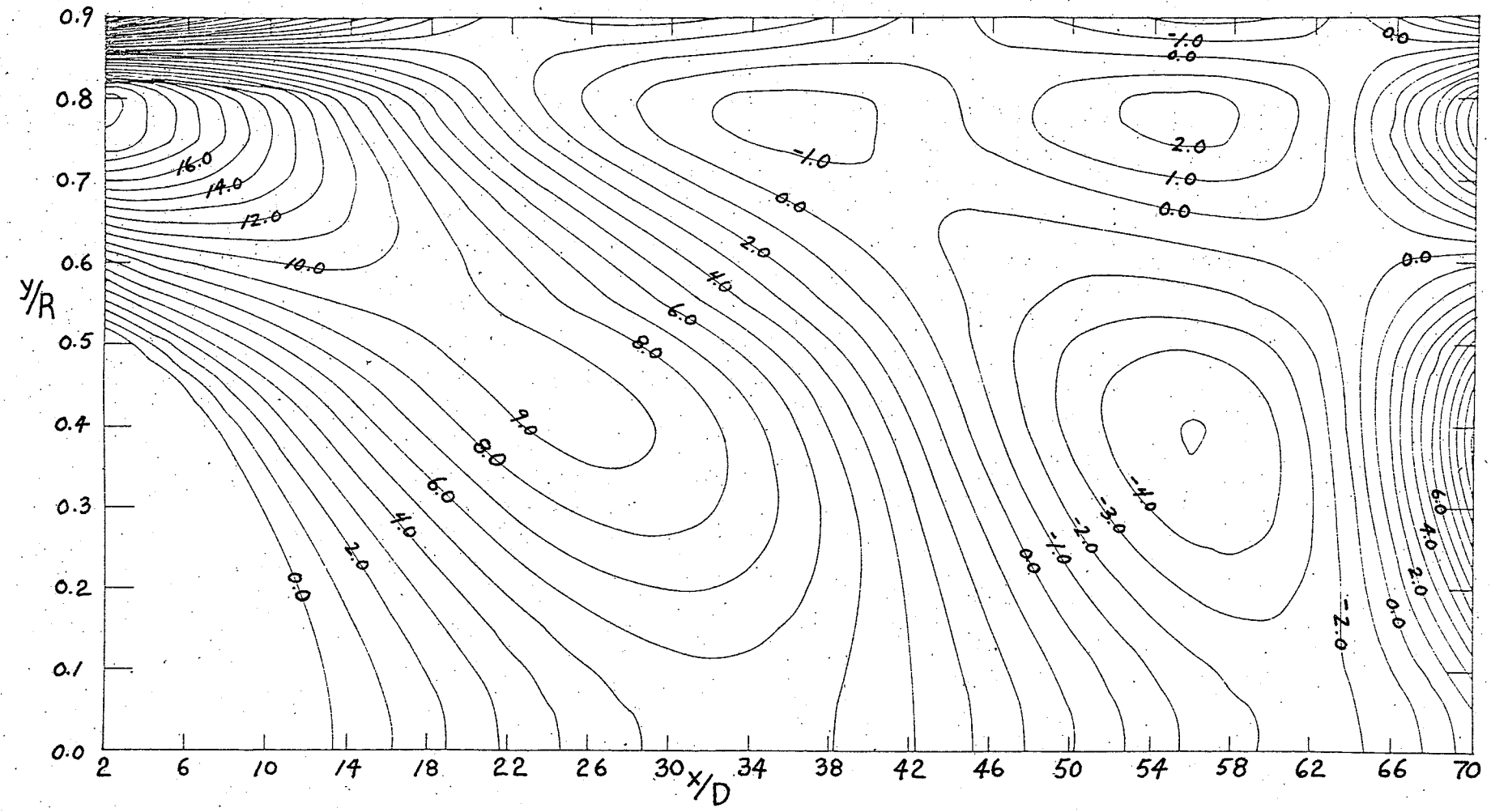

Figure 41. Contours of the total mean flow convection, (eqn. 6.2); Re = 54900; contour interval = 1.0×10^{-5}.

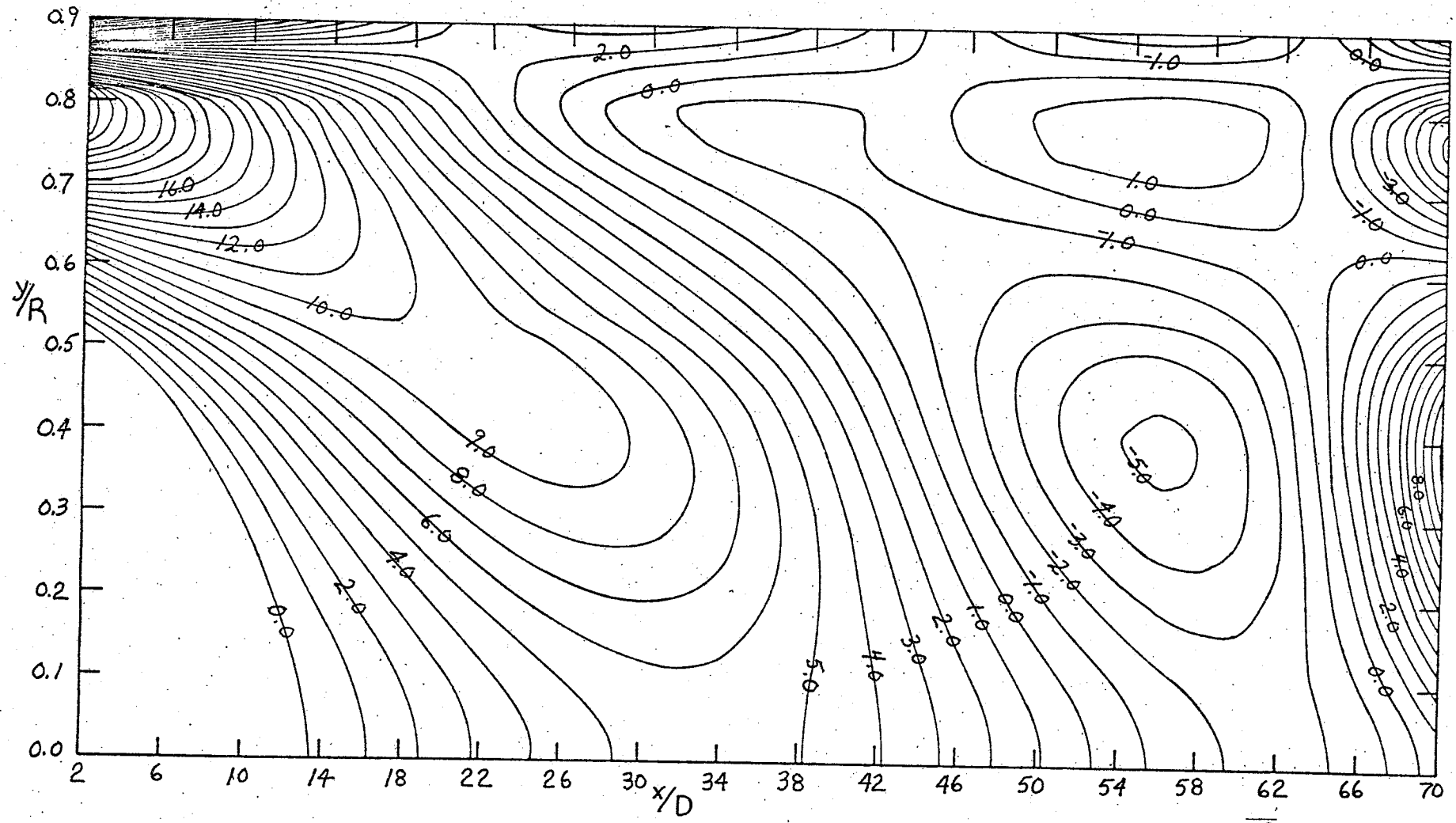

Figure 42. Contours of the mean flow convection term, $\frac{1}{4}\frac{U}{U_B}\frac{\partial(\overline{q^2}/U_B^2)}{\partial(x/2R)}$; Re = 54900; contour interval = 1.0×10^{-5}.

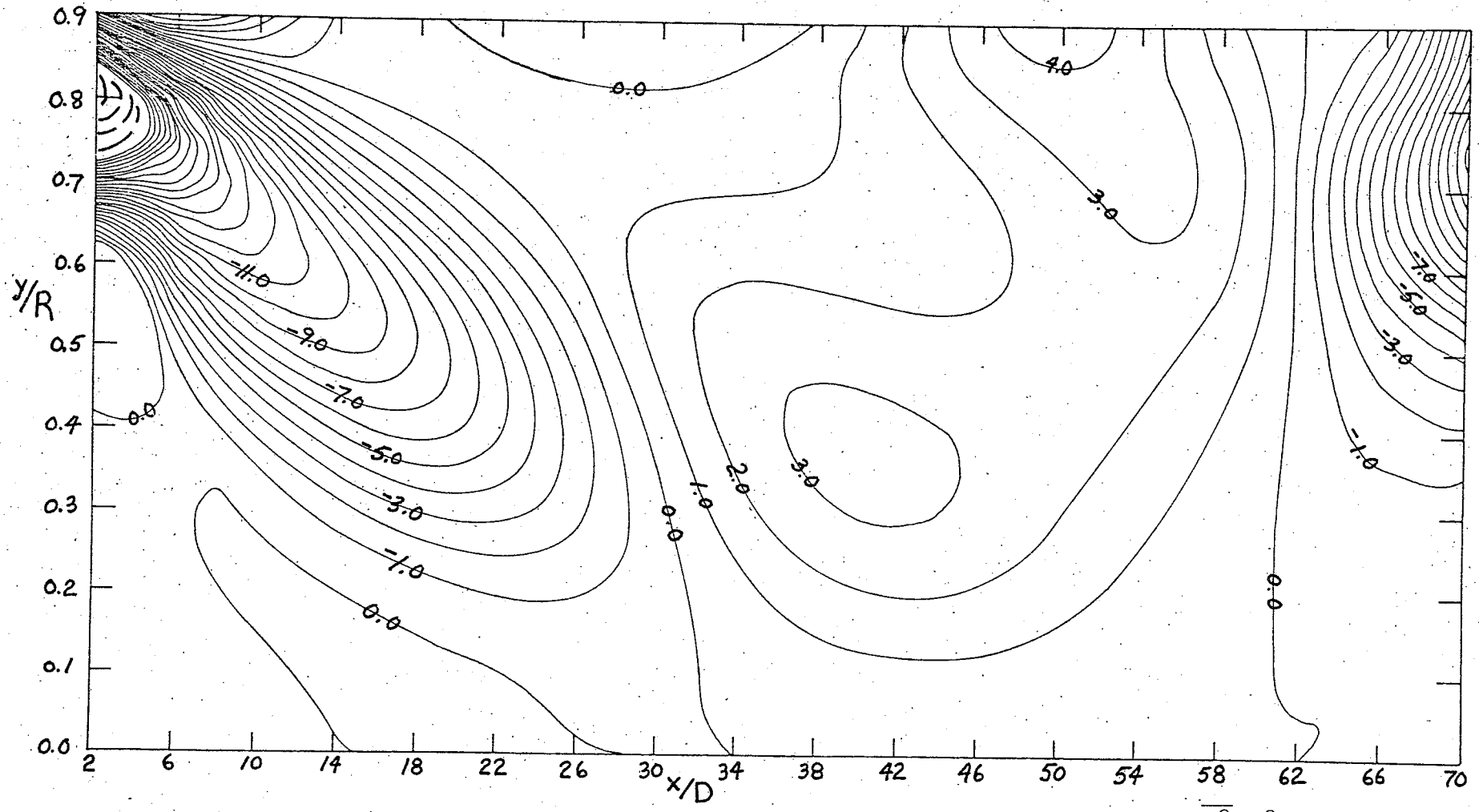

Figure 43. Contours of the mean flow convection term, $\frac{1}{2}\frac{V}{U_B}\frac{\partial(\overline{q^2}/U_B^2)}{\partial(y/R)}$; Re = 54900; contour interval = 1.0×10^{-6}.

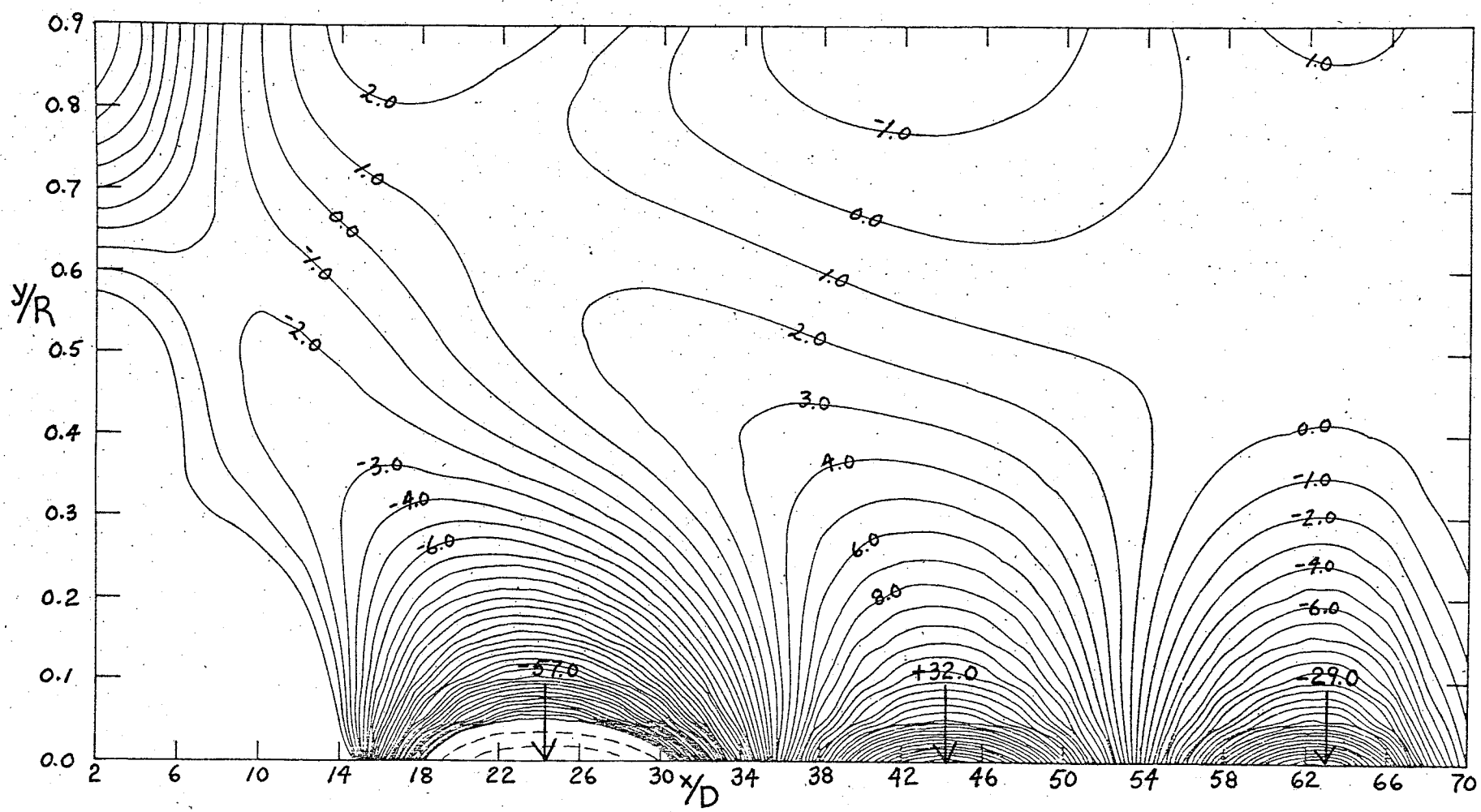

Figure 44. Contours of the computed viscous transport term,

$$-\frac{1}{2Re(y/R)}\frac{\partial}{\partial(y/R)}\left[y/R\frac{\partial(\overline{q^2}/U_B^2)}{\partial(y/R)}\right]-\frac{1}{8Re}\frac{\partial}{\partial(x/2R)}\left[\frac{\partial(\overline{q^2}/U_B^2)}{\partial(x/2R)}\right];$$

Re = 54900; contour interval = 1.0×10^{-7}.

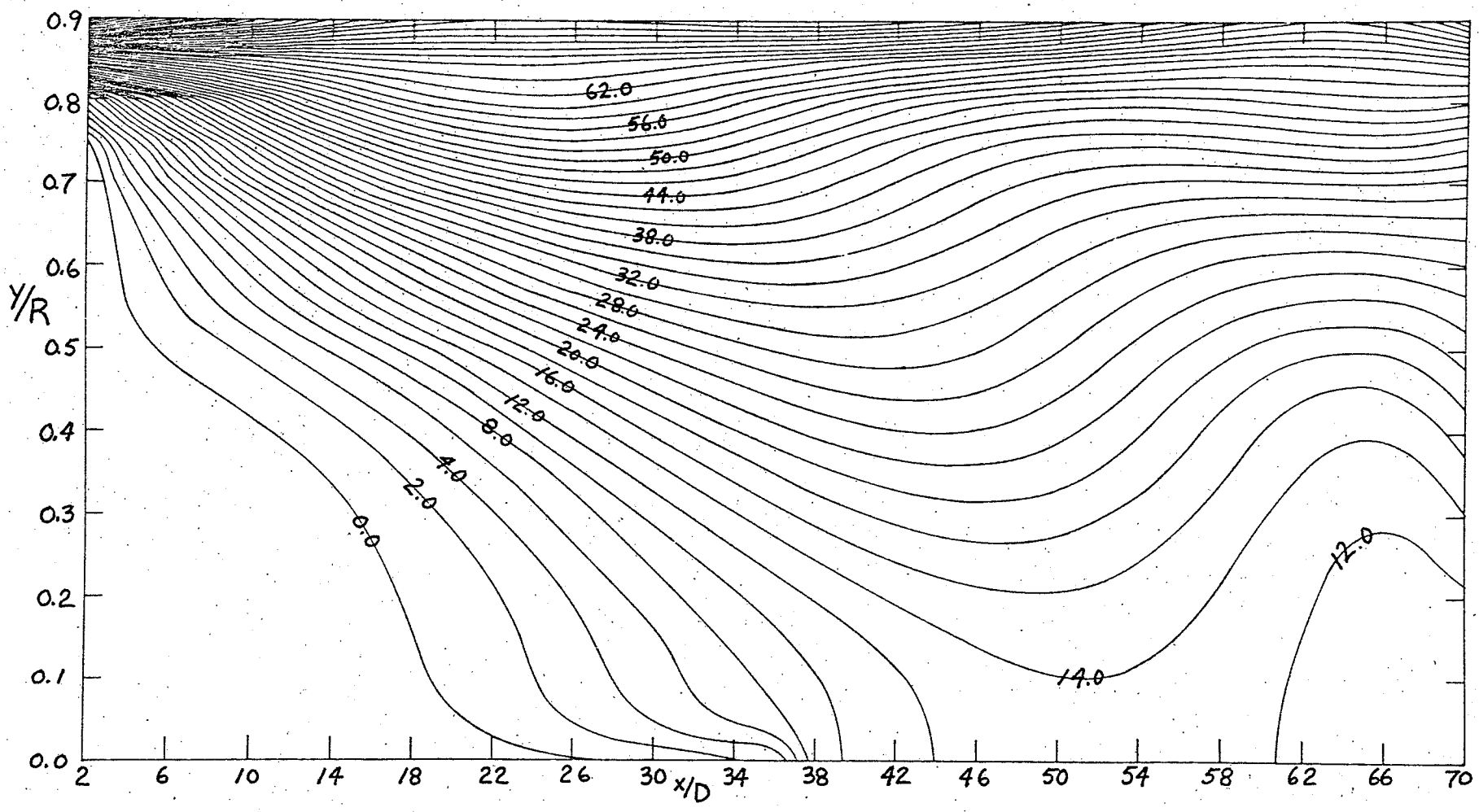

Figure 45. Contours of nondimensionalized dissipation, $\frac{R}{U_B^3}\frac{15\nu}{\overline{U_L}^2}\overline{\left(\frac{\partial u}{\partial t}\right)^2}$; Re = 54900; contour interval = 2.0×10^{-5}.

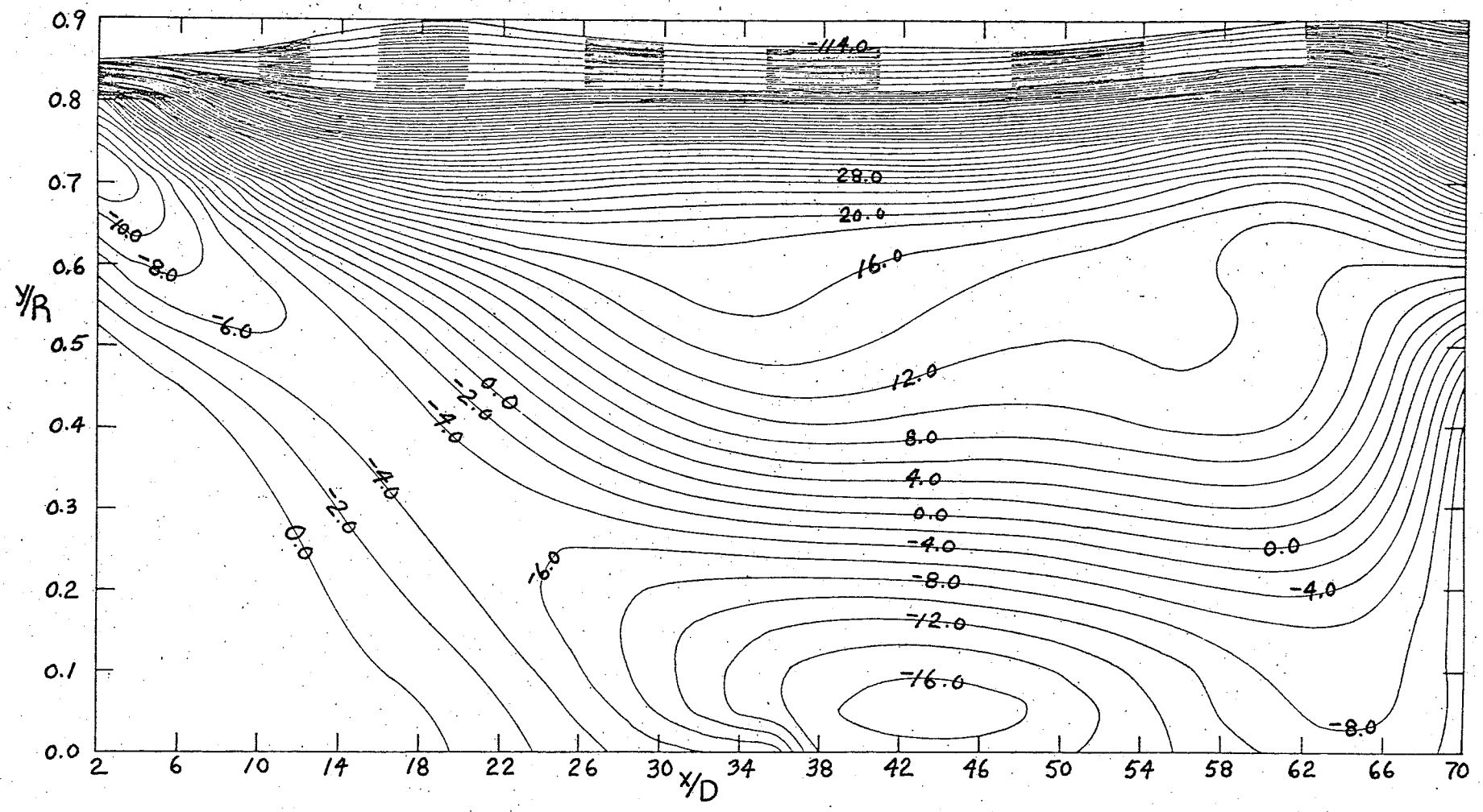

Figure 46. Contours of the convective diffusion term obtained by closure (eqn 6.3); Re = 54900; contour interval = 2.0 x 10-5.

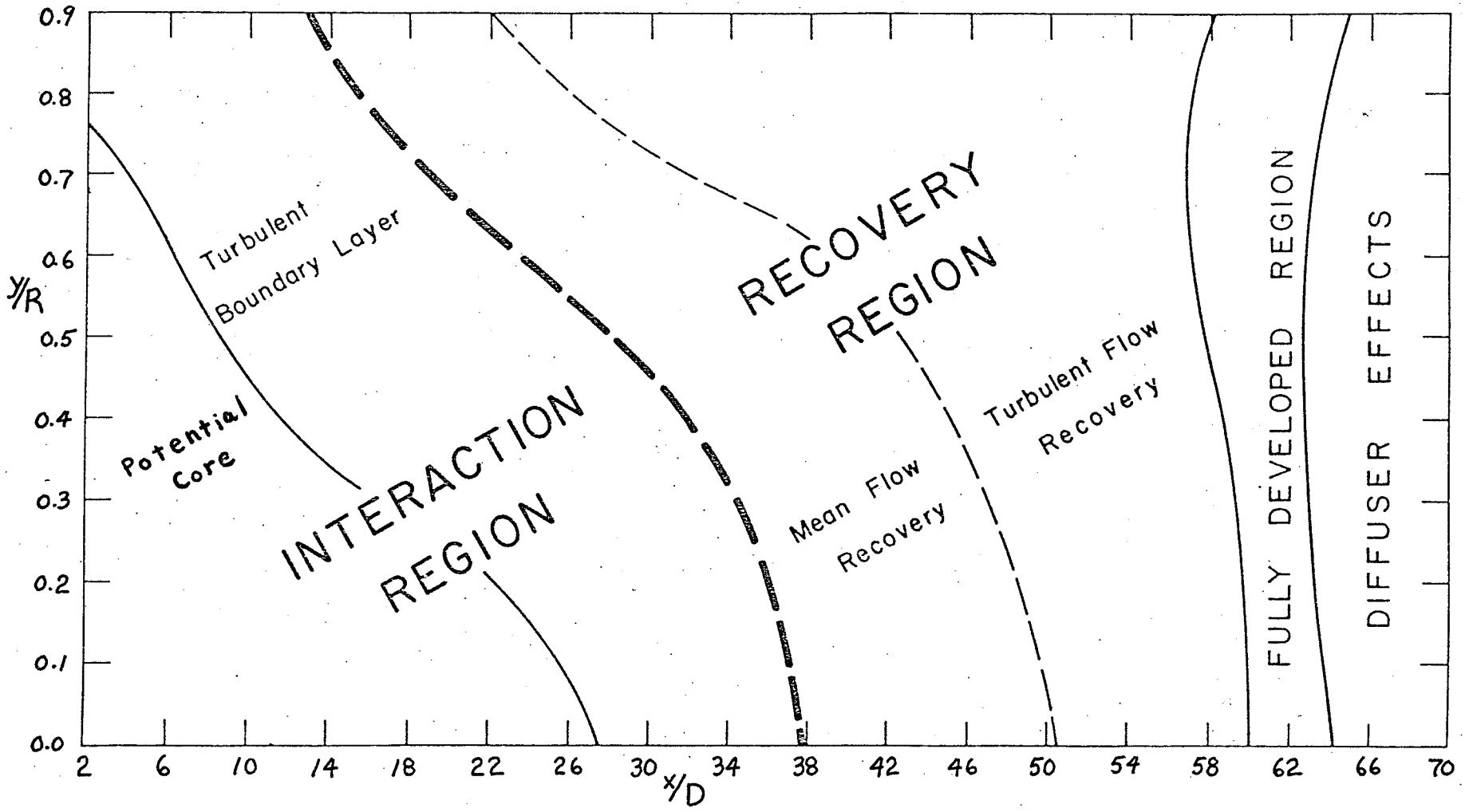

Figure 47. Classification of the flow regime.

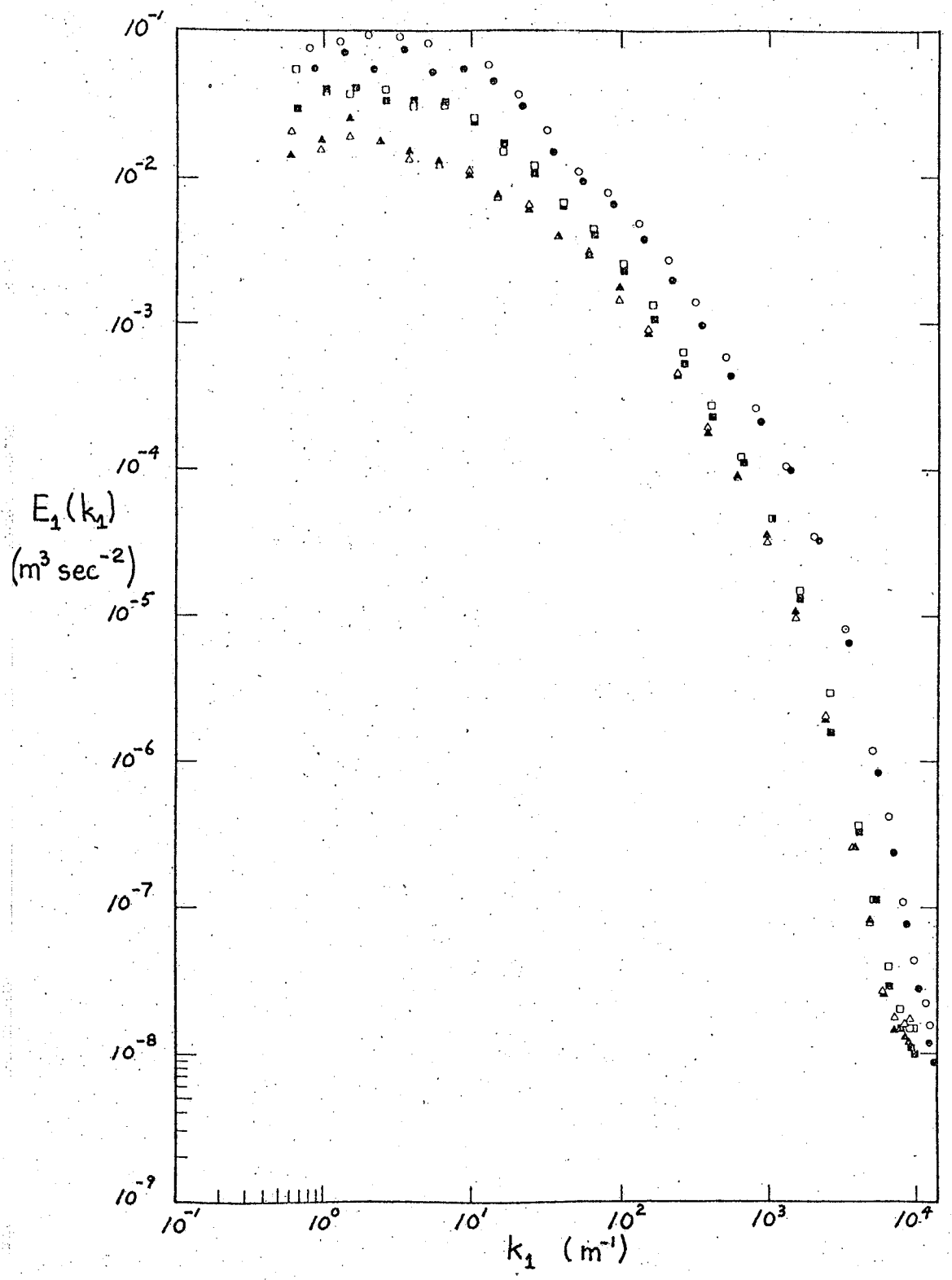

Figure 48. Comparison of single wire and X probe spectra results $E_1(k_1)$ at x/D = 65.2 for setup A; Re = 54900.
X wire (55P51): ●, y/R = 0.1; ■, y/R = 0.5; ▲, y/R = 0.9
Single wire (55P01): ○, y/R = 0.1; □, y/R = 0.5, Δ, y/R = 0.9.

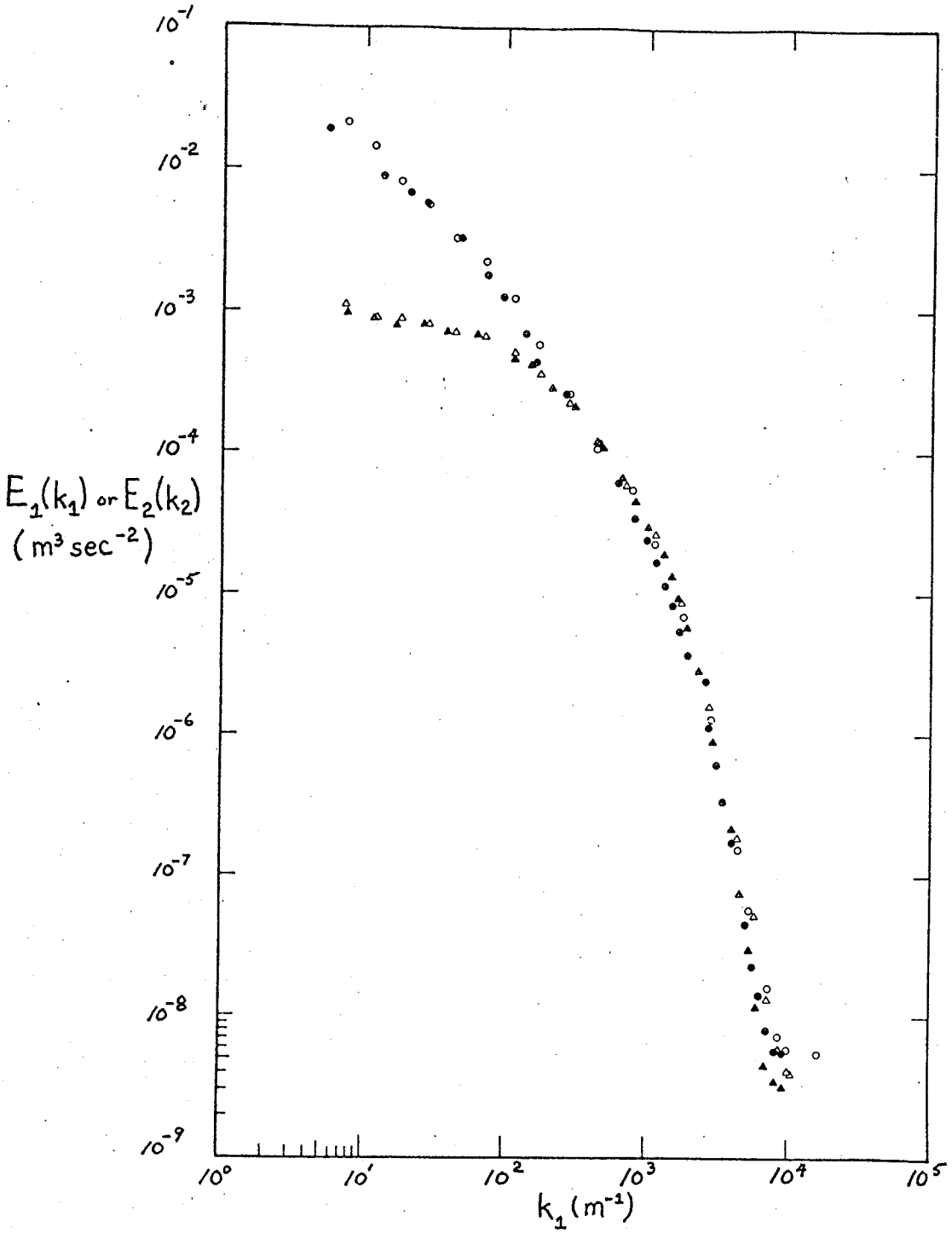

Figure 49. Comparison of u and v spectra measurements $E_1(k_1)$ and $E_2(k_2)$ at x/D = 65.2 for setup B; $Re_\lambda = 54900$.
H.P. 3590A: ●, u spectra; ▲, v spectra.
Krohn-Hite 3550: ○, u spectra; △, v spectra.

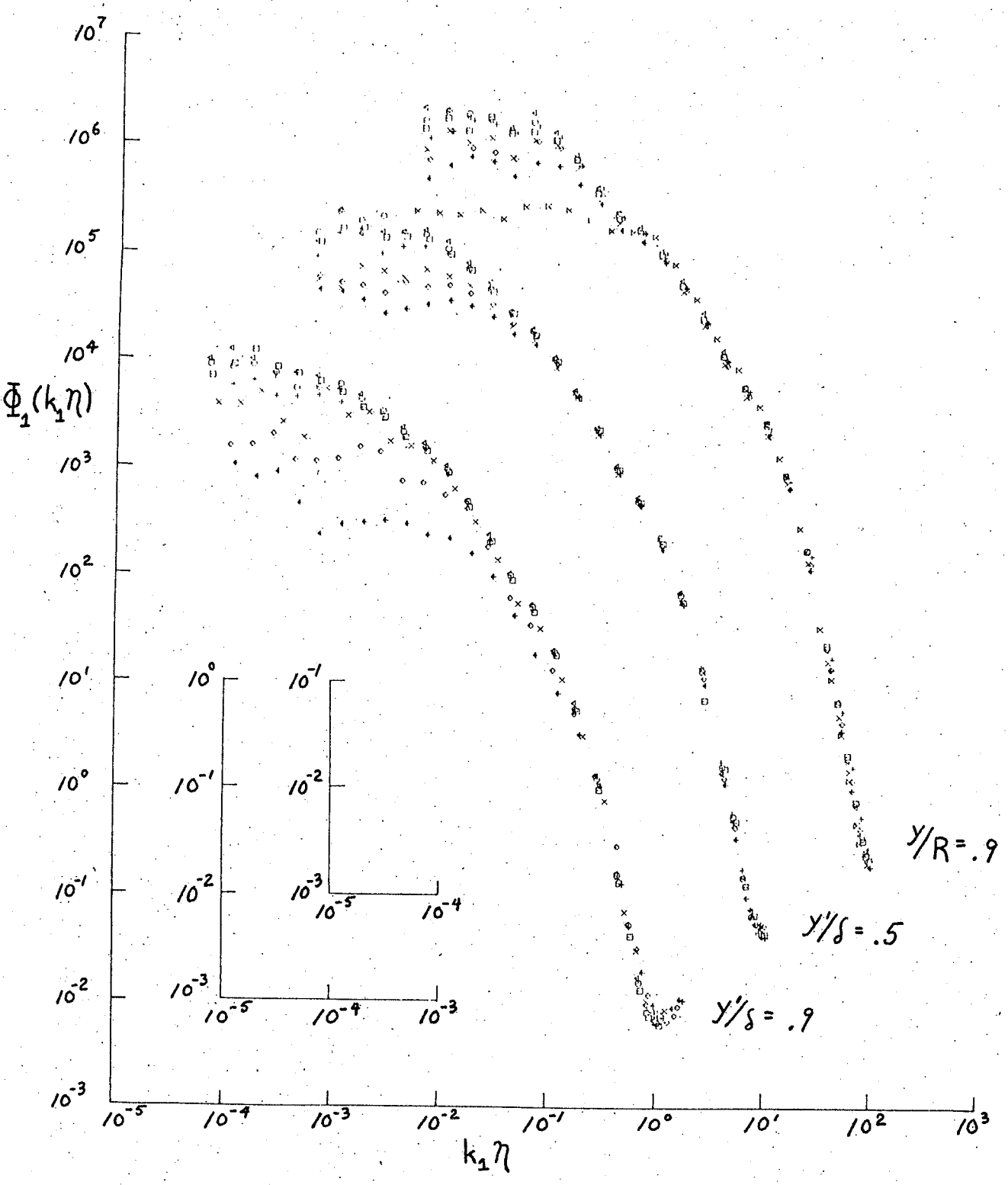

Figure 50. Normalized longitudinal component one dimensional spectra results, $\Phi_1(k_1\eta)$; Re = 54900; □, x/D = 65.2; ⊖, x/D = 60.3; ◁, x/D = 50.5; +, x/D = 40.2; X, x/D = 30.3; ◇, /D = 20.5; ⊣, x/D = 10.6; ⋉, x/D = 1.8.

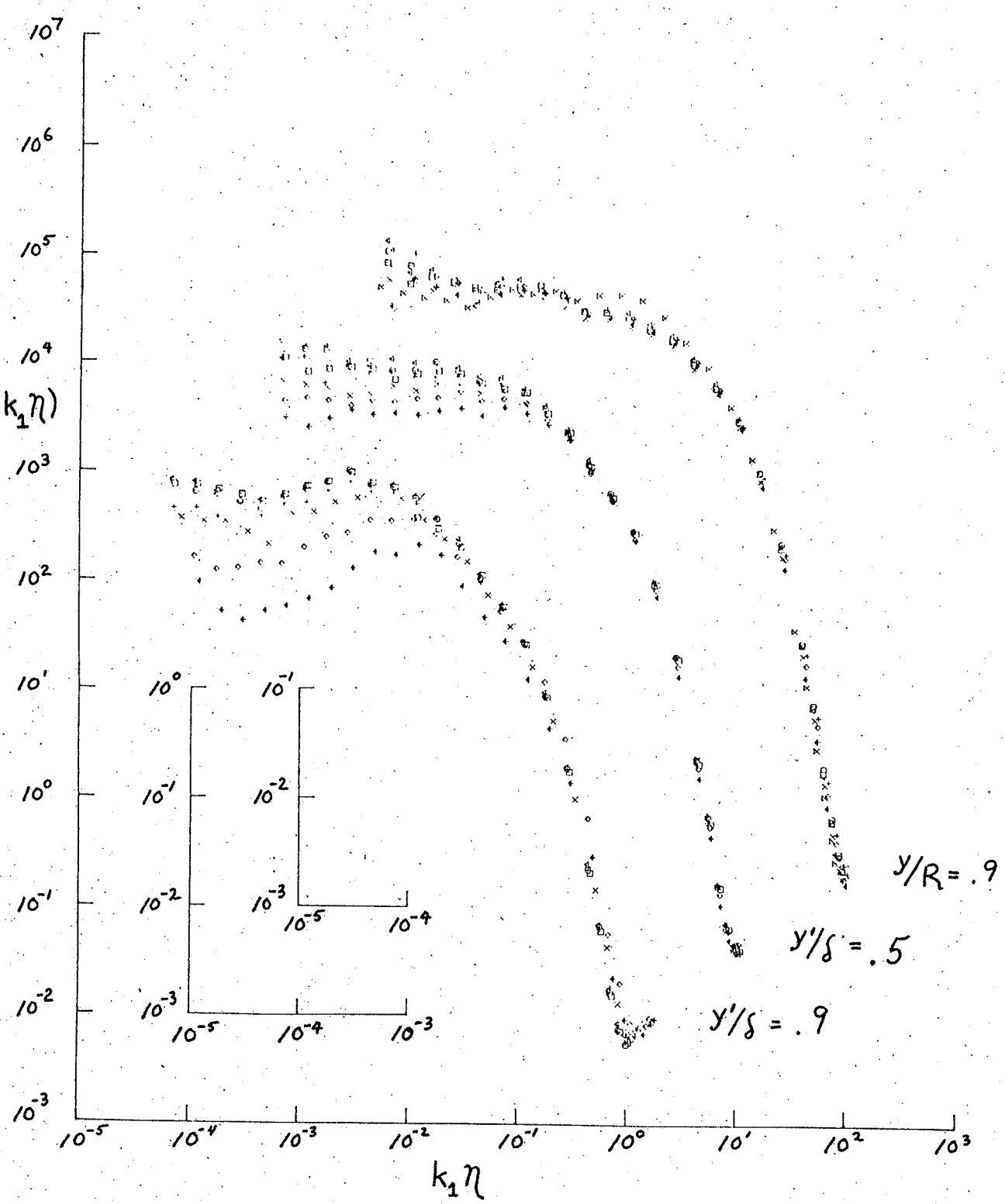

Figure 51. Normalized radial component one dimensional spectra results, $\Phi_2(k_1\eta)$; Re = 54900; symbols as for figure 50.

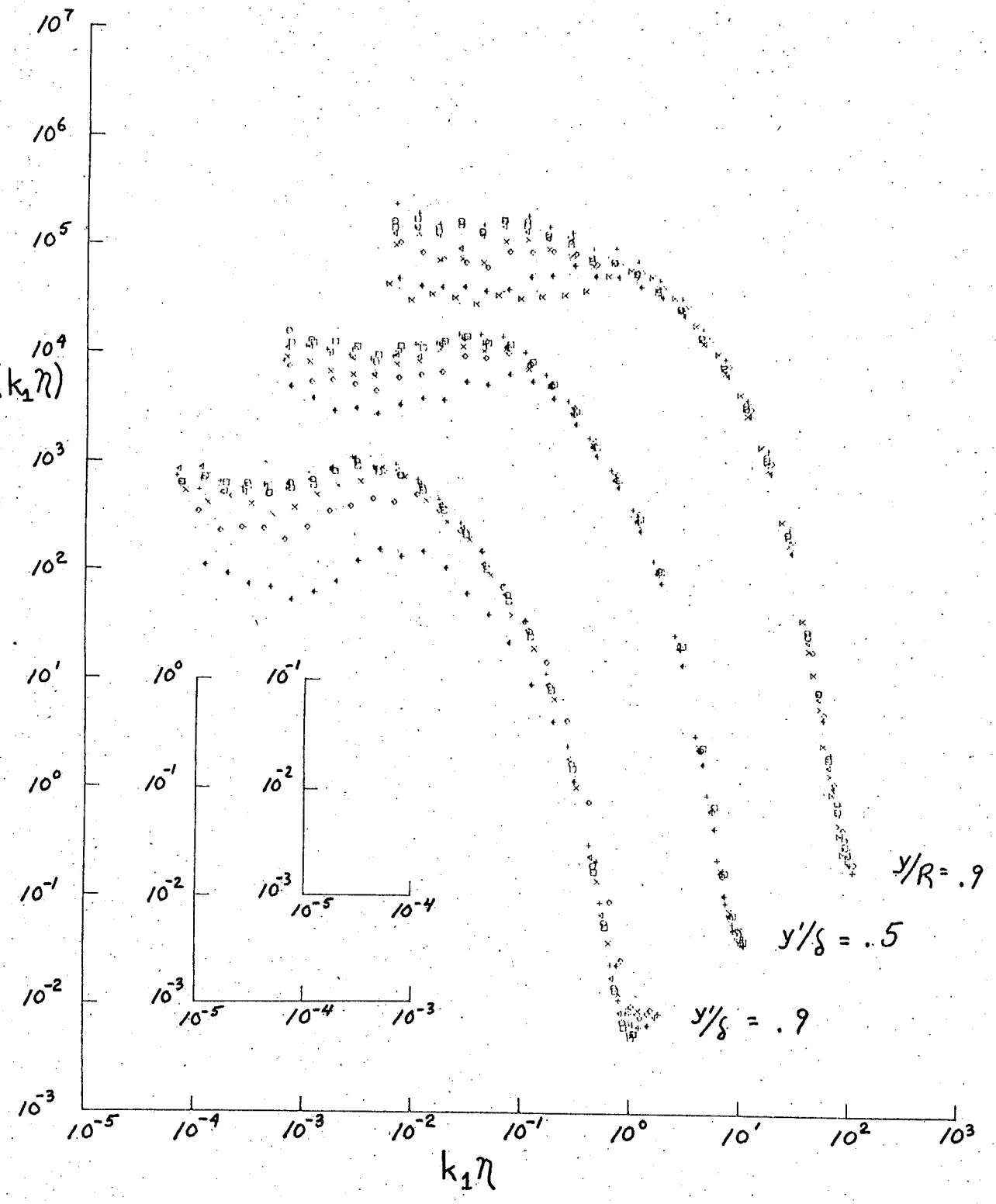

Figure 52. Normalized circumferential component one dimensional spectra results $\Phi_3(k_1\eta)$; Re = 54900; symbols as for figure 50.

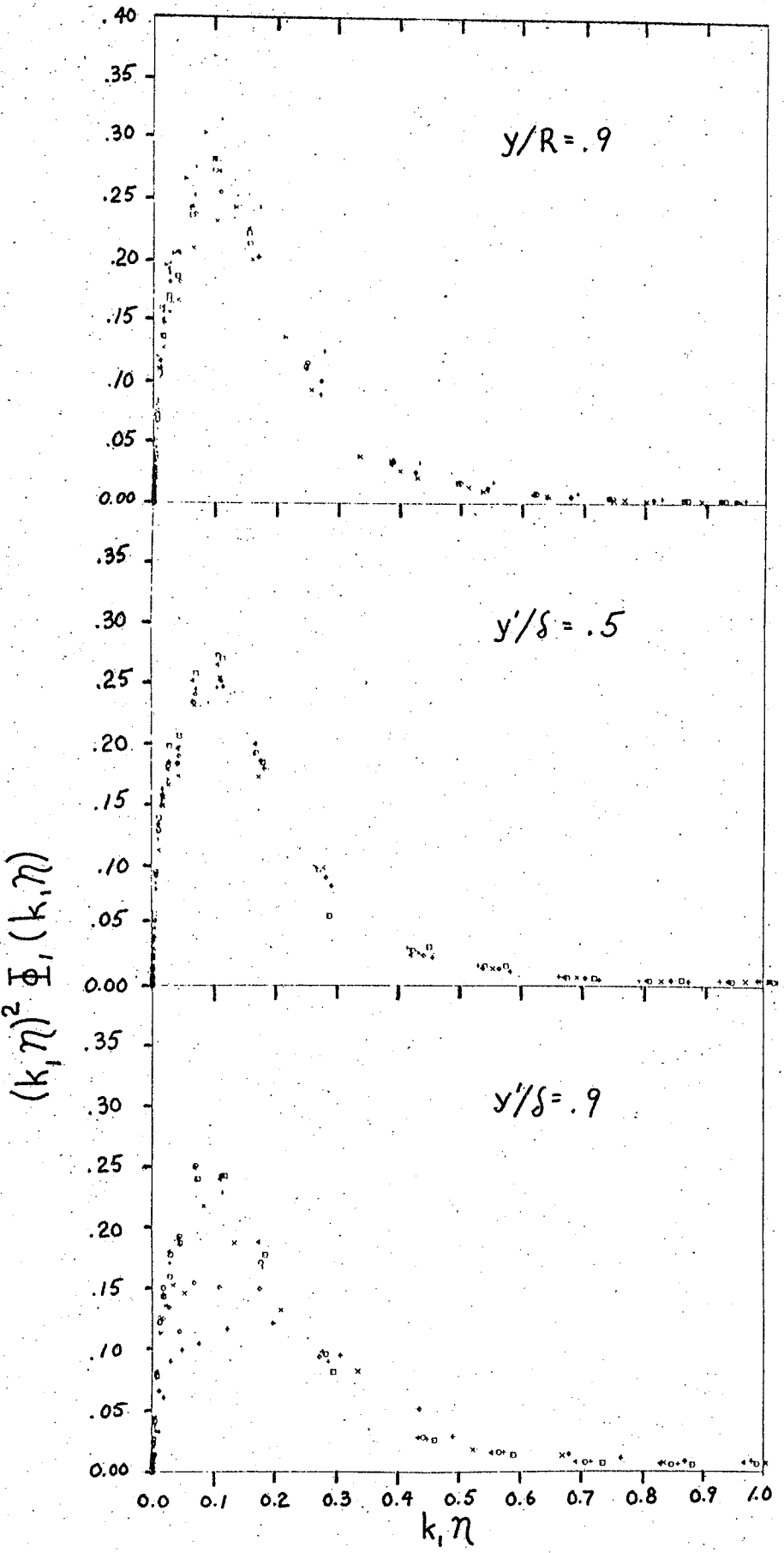

Figure 53. Normalized longitudinal component one dimensional dissipation spectra results, $(\eta k_1)^2 \Phi_1(k_1\eta)$; Re = 54900; symbols as for figure 50.

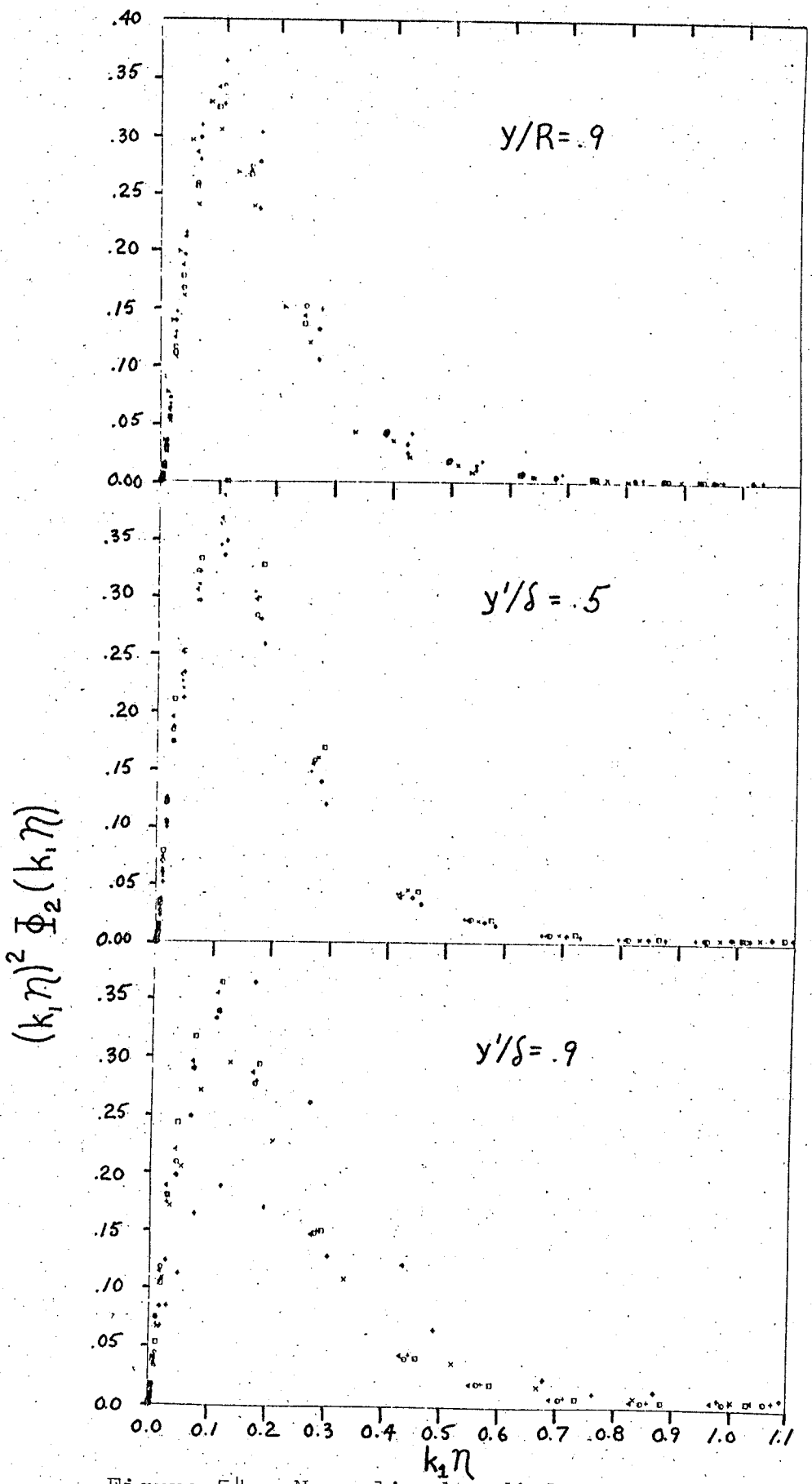

Figure 54. Normalized radial component one dimensional dissipation spectra results, $(\eta k_1)^2\ \Phi_2(k_1\eta)$; Re = 54900; symbols as for figure 50.

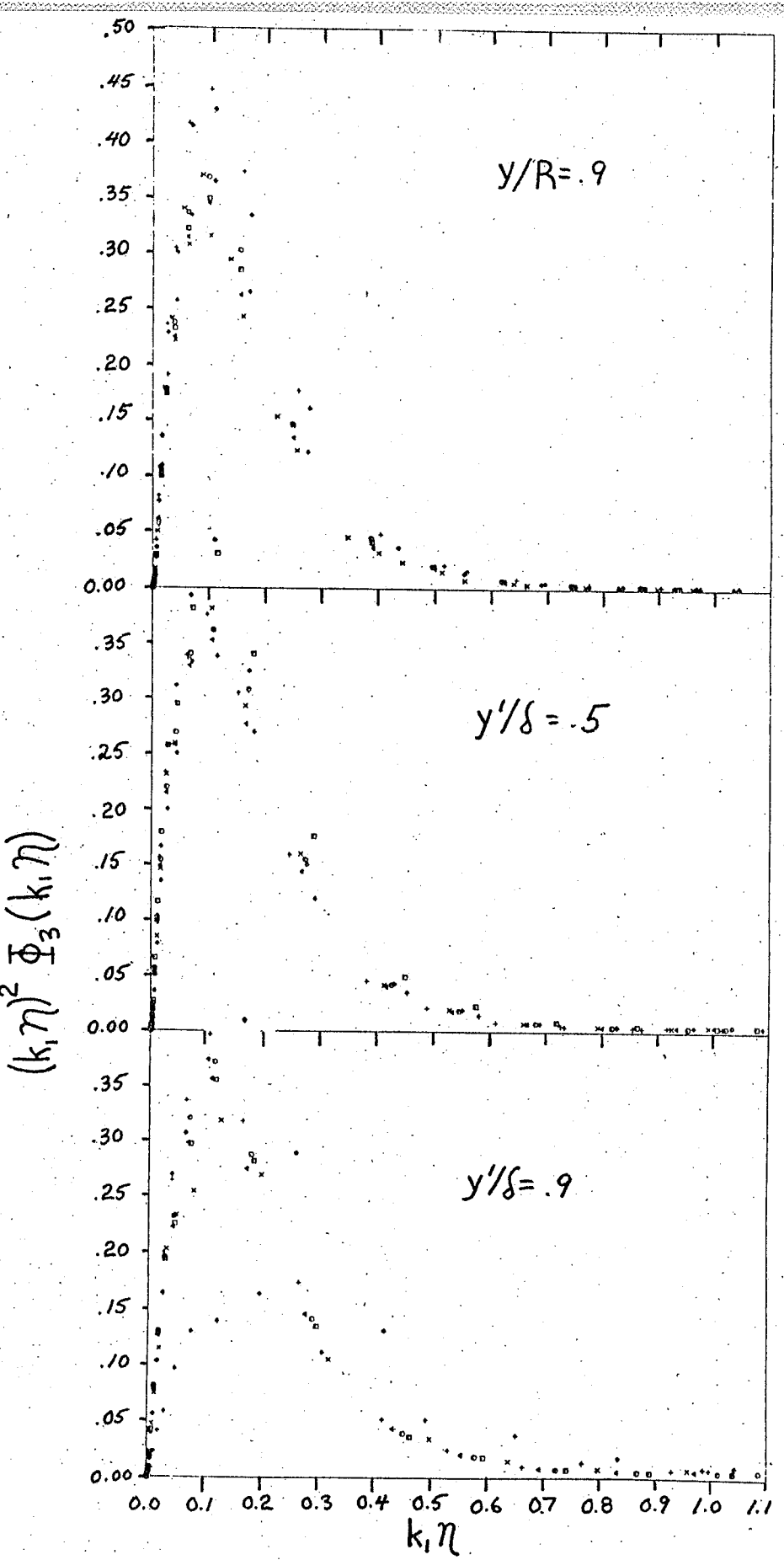

Figure 55. Normalized circumferential component one dimensional dissipation spectra results, $(\eta k_1)^2\ \Phi_3(k_1\eta)$; Re = 54900; symbols as for figure 50.

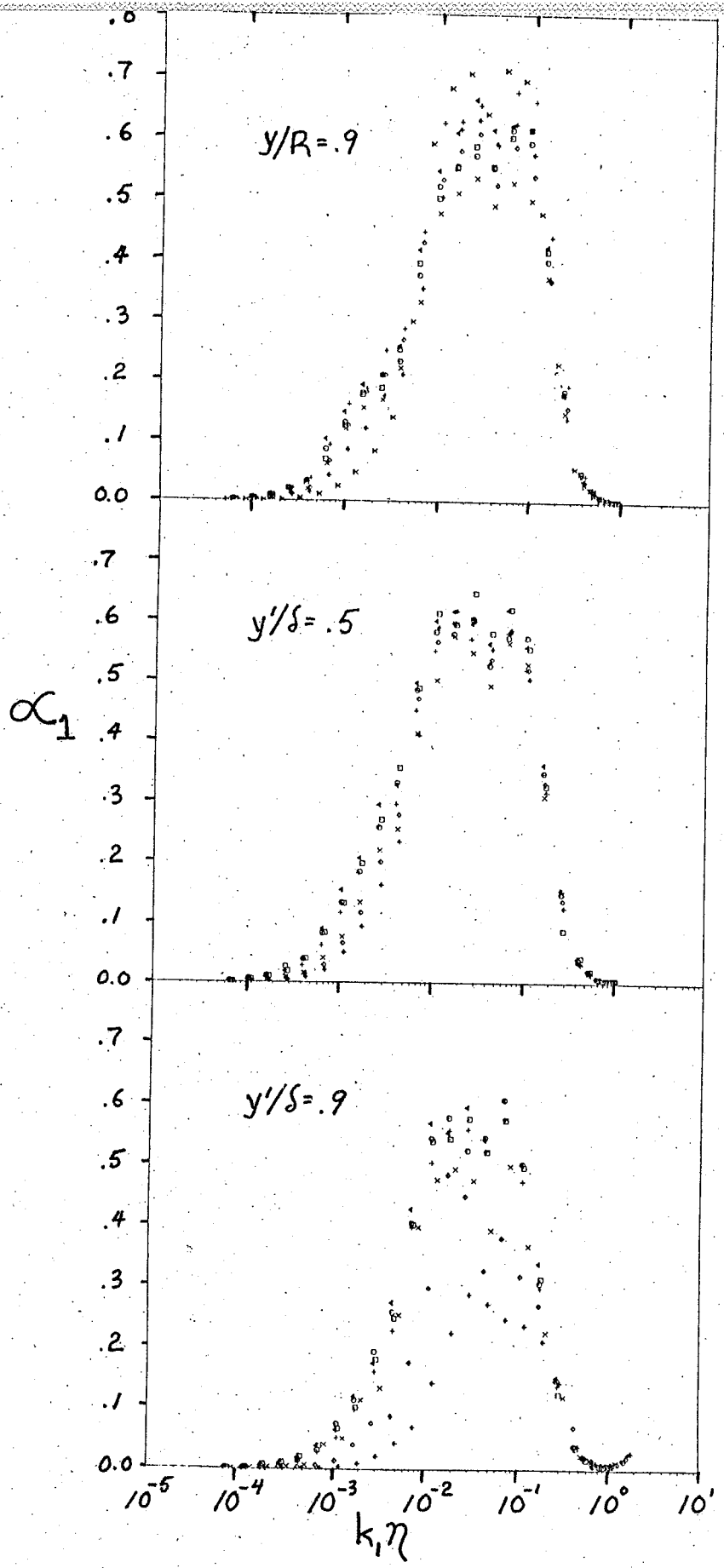

Figure 56. Kolmogorov inertial subrange constant, α_1 (eqn. 7.1); Re = 54900. Symbols as for figure 50.

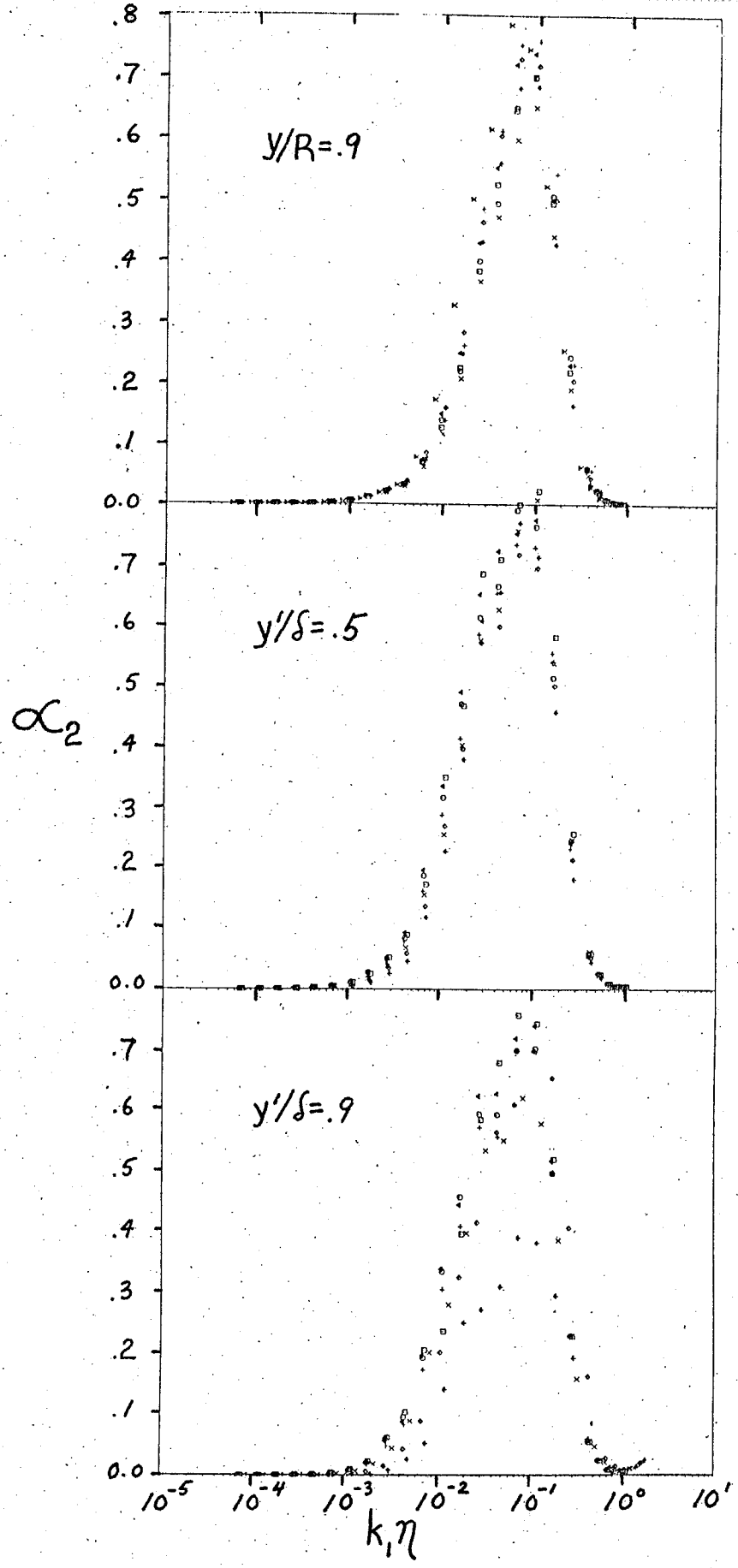

Figure 57. Kolmogorov inertial subrange constant, α_2 (eqn. 7.1); Re = 54900. Symbols as for figure 50.

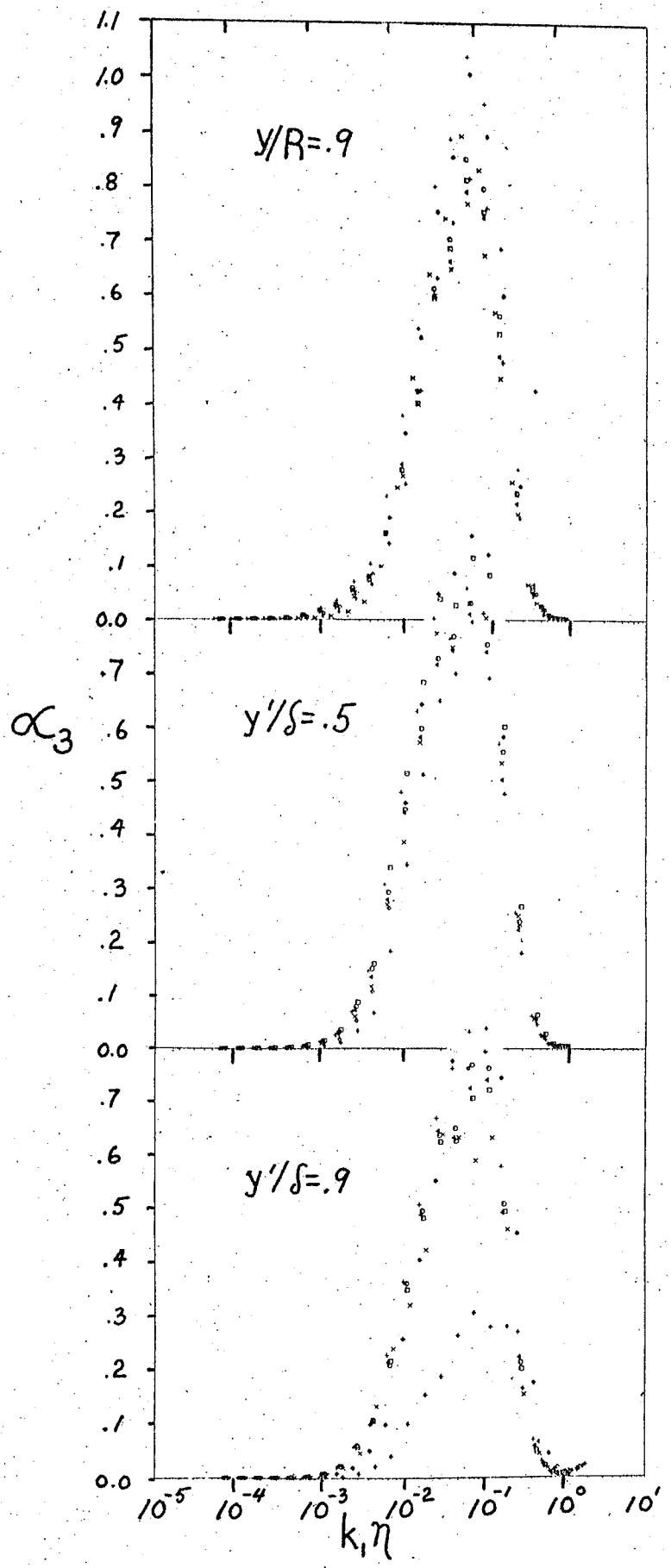

Figure 58. Kolmogorov inertial subrange constant, α_3 (eqn. 7.1); Re = 54900. Symbols as for figure 50.

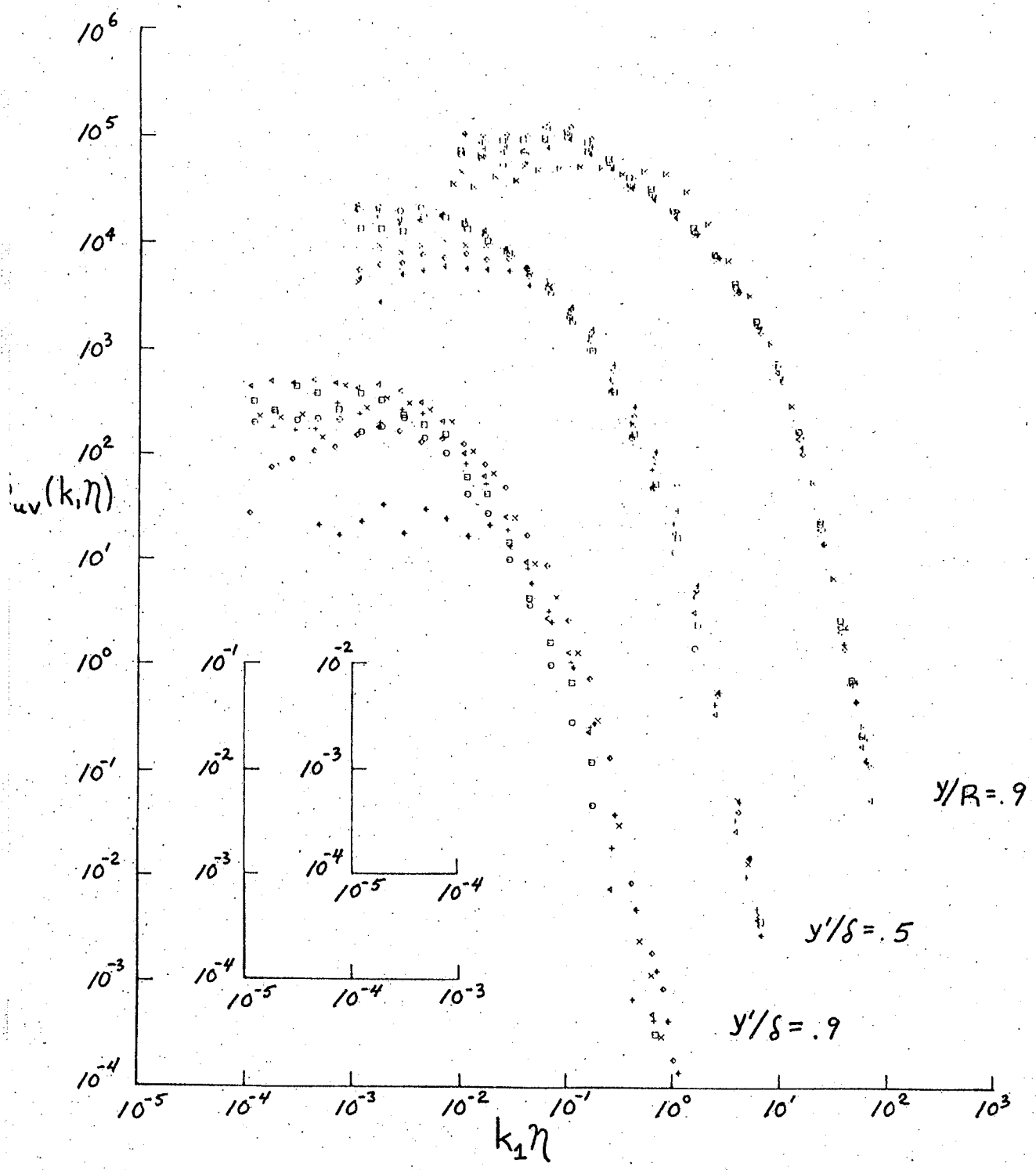

Figure 59. Normalized one dimensional cross spectral density, $\Phi_{uv}(k_1\eta)$; Re = 54900; symbols as for figure 50.

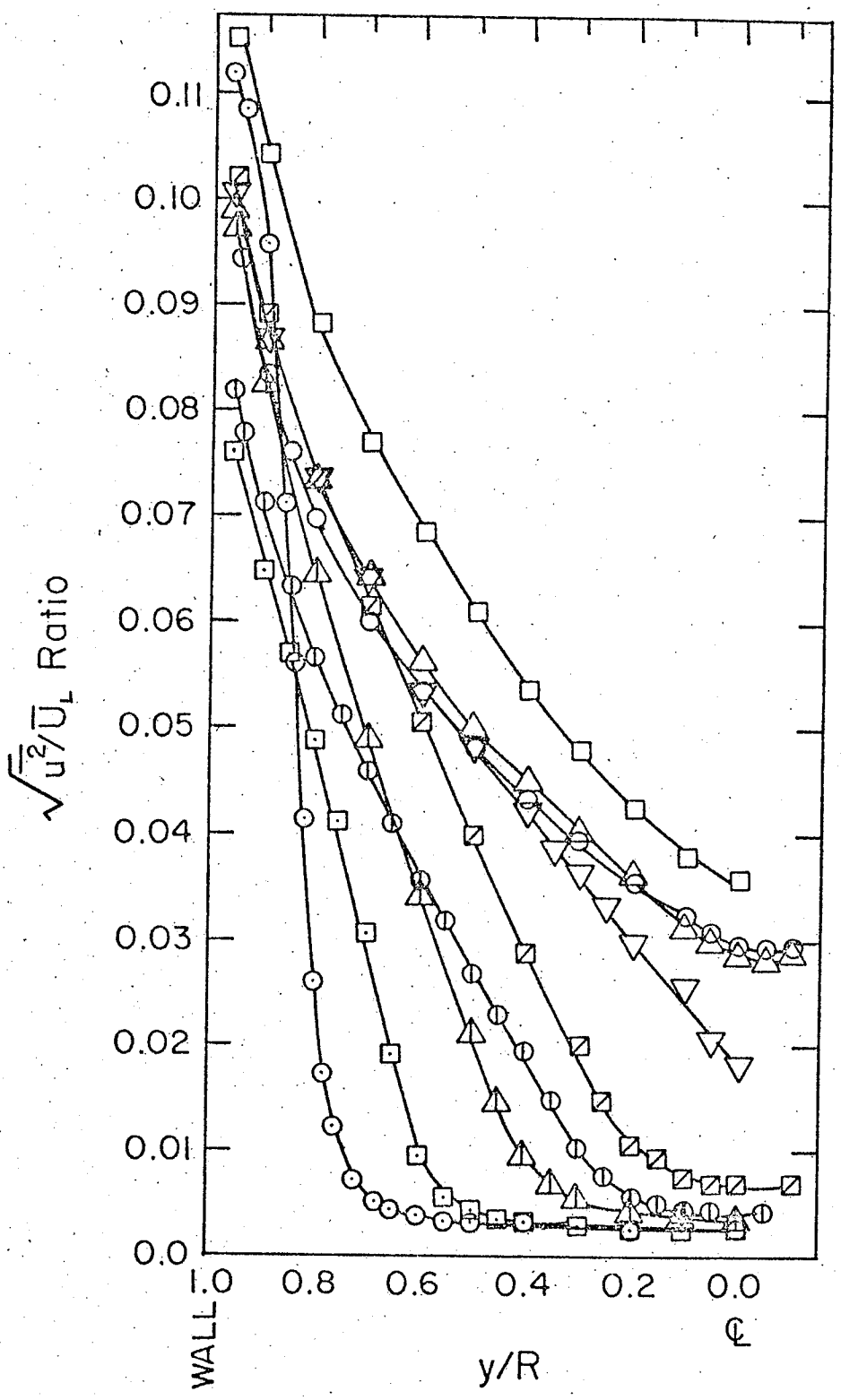

Figure 60. Nondimensionalized turbulence intensity profiles, $\sqrt{u^2}/\bar{U}_L$; Re = 54900; symbols as for figure 87.

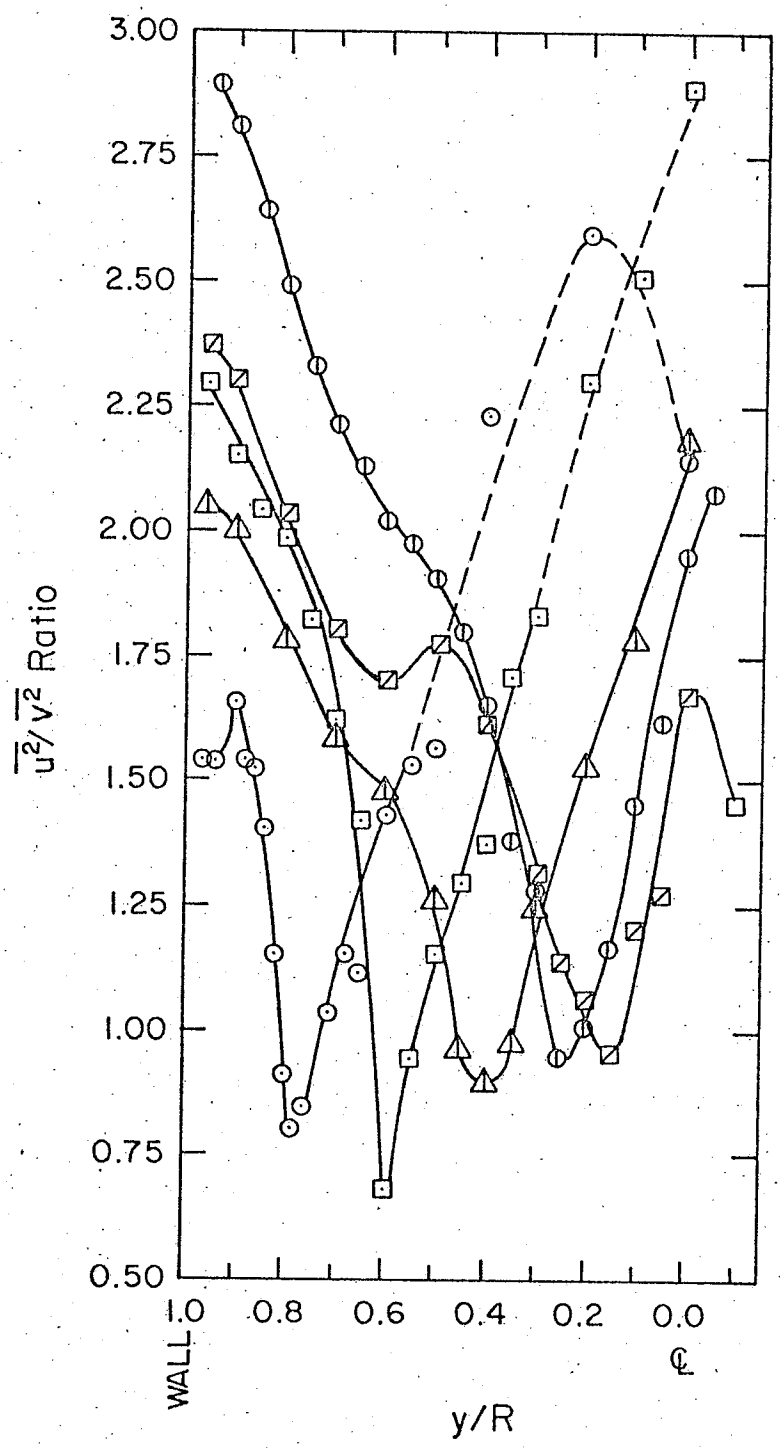

Figure 61. Ratio of longitudinal to radial turbulence intensity profiles, $\overline{u^2}/\overline{v^2}$; Re = 54900; symbols as for figure 87.

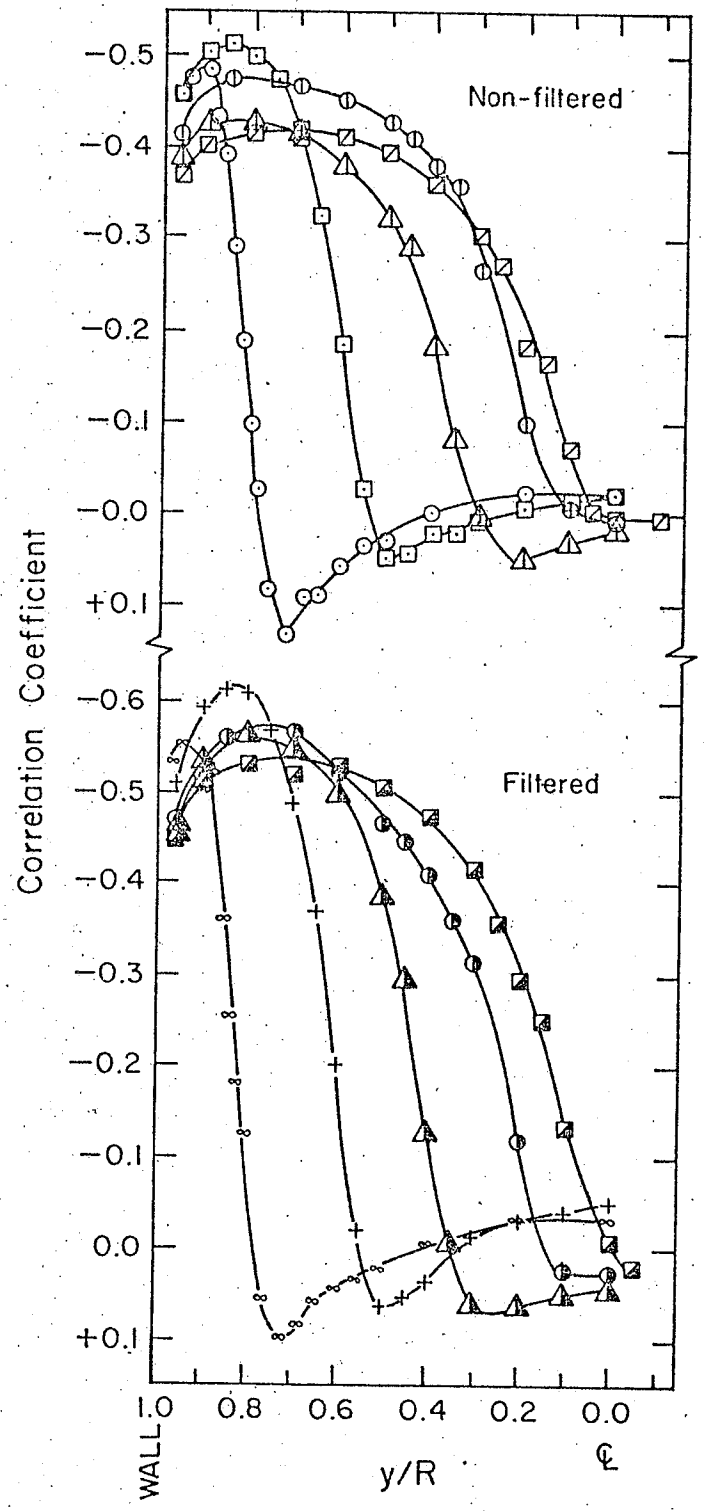

Figure 62. Correlation coefficient profiles in the interaction region, filtered and nonfiltered; Re = 54900; symbols as for figures 87 and 88.

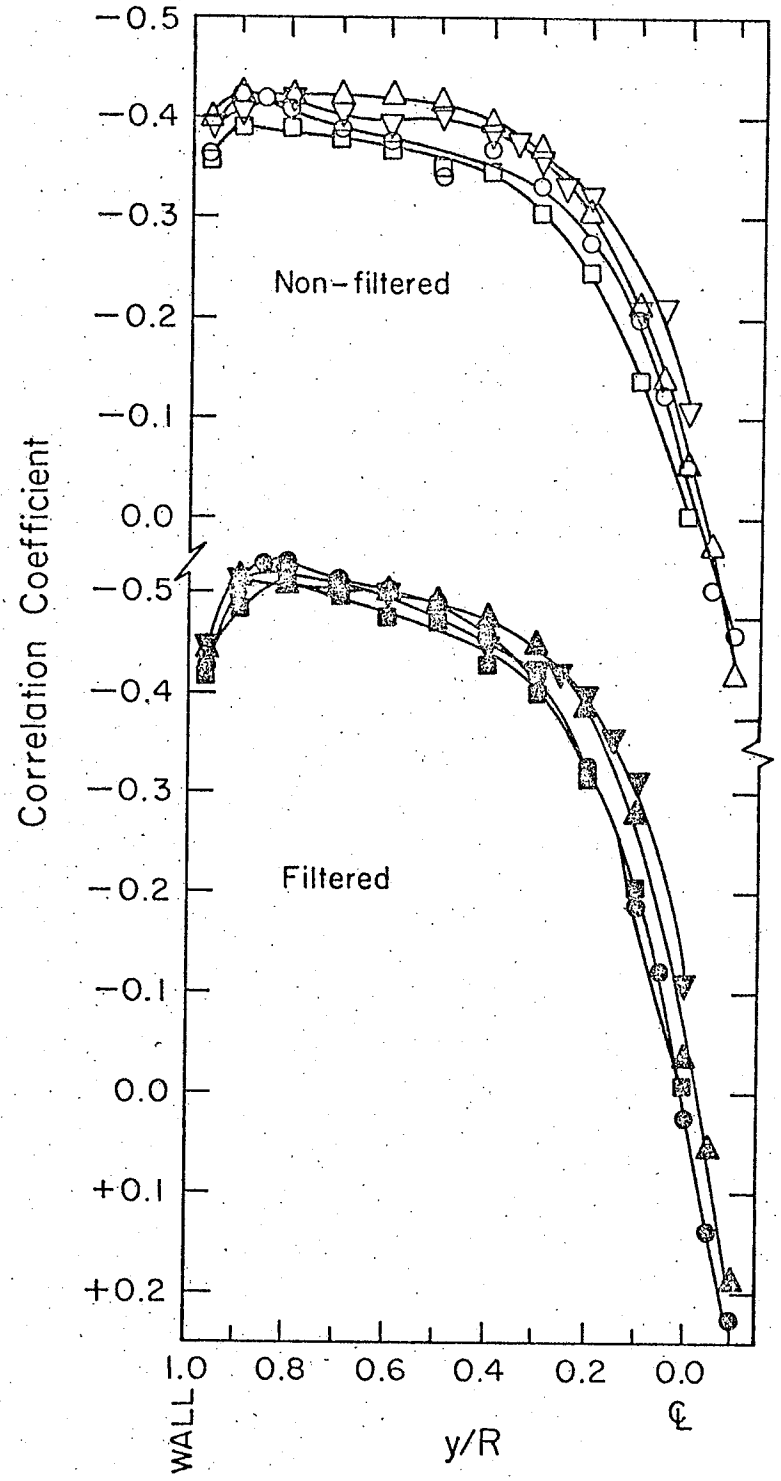

Figure 63. Correlation coefficient profiles in the recovery region, filtered and nonfiltered; Re = 54900; symbols as for figures 87 and 88.

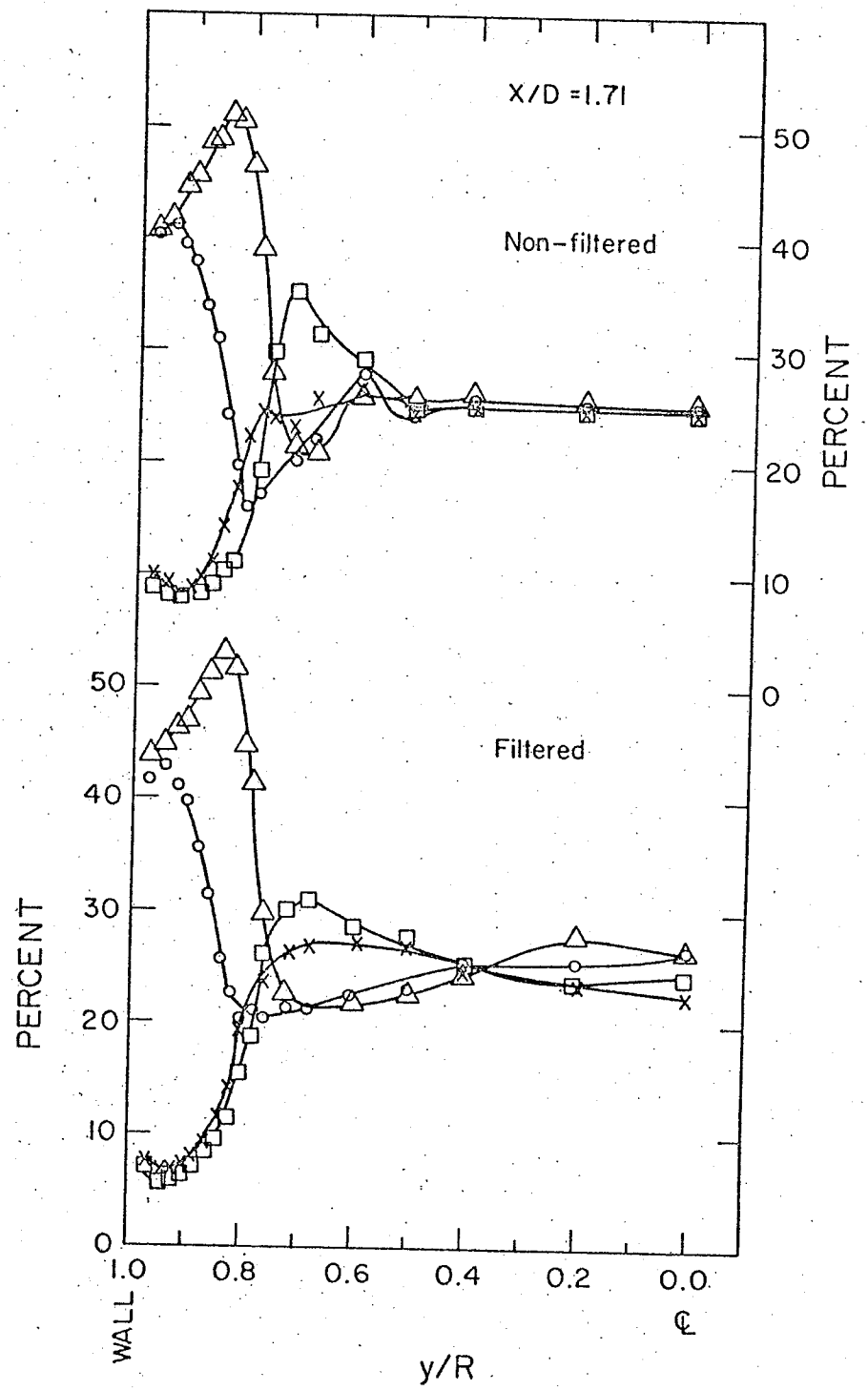

Figure 64. Quadrant conditioned Reynolds stresses for filtered and non-filtered u and v; x/D = 1.71; Re = 54900; Δ, u_-v_+; O, u_+v_-; □, u_+v_+; X, u_-v_-.

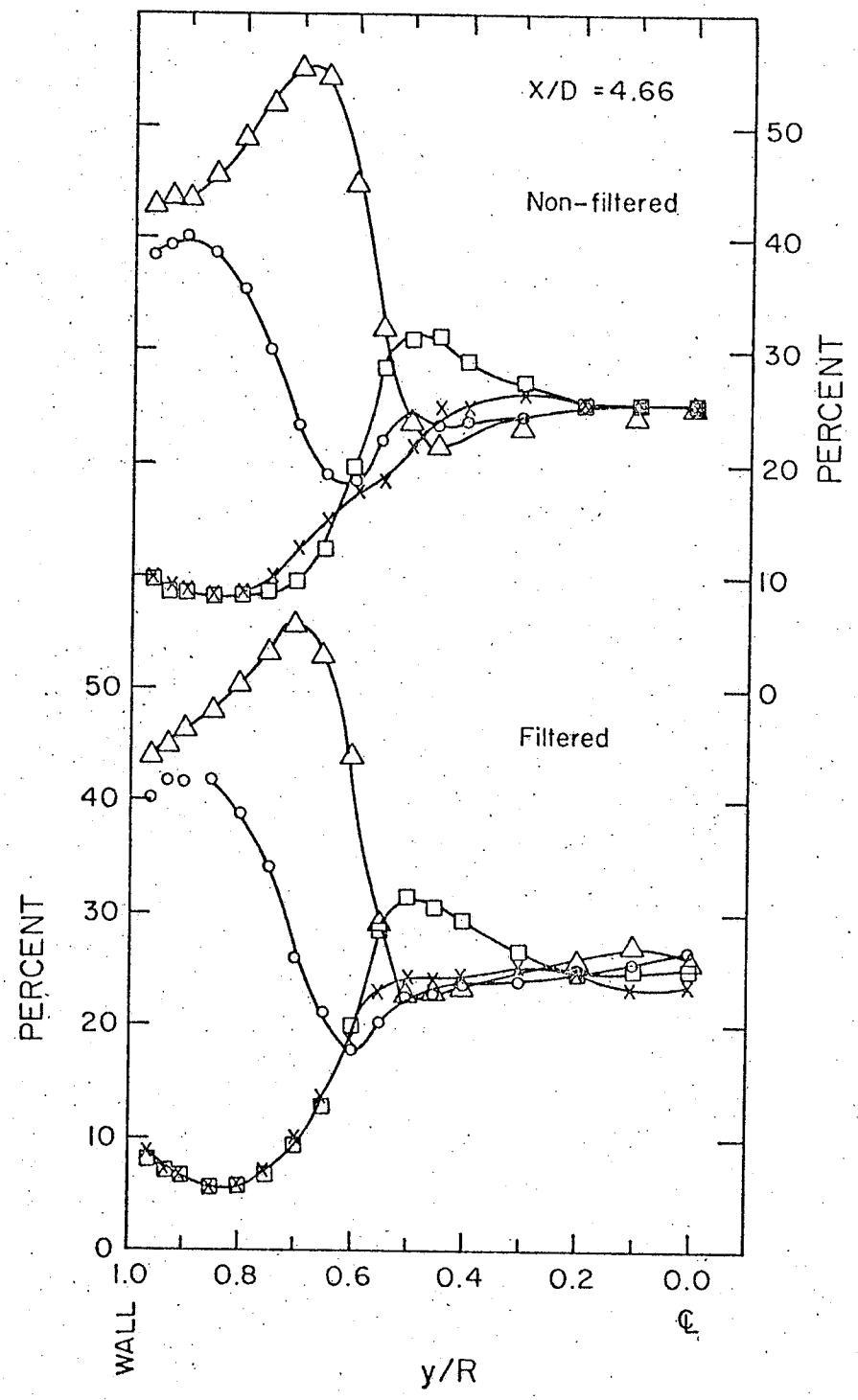

Figure 65. Quadrant conditioned Reynolds stresses for filtered and non-filtered u and v; x/D = 4.66; Re = 54900; symbols as for figure 64.

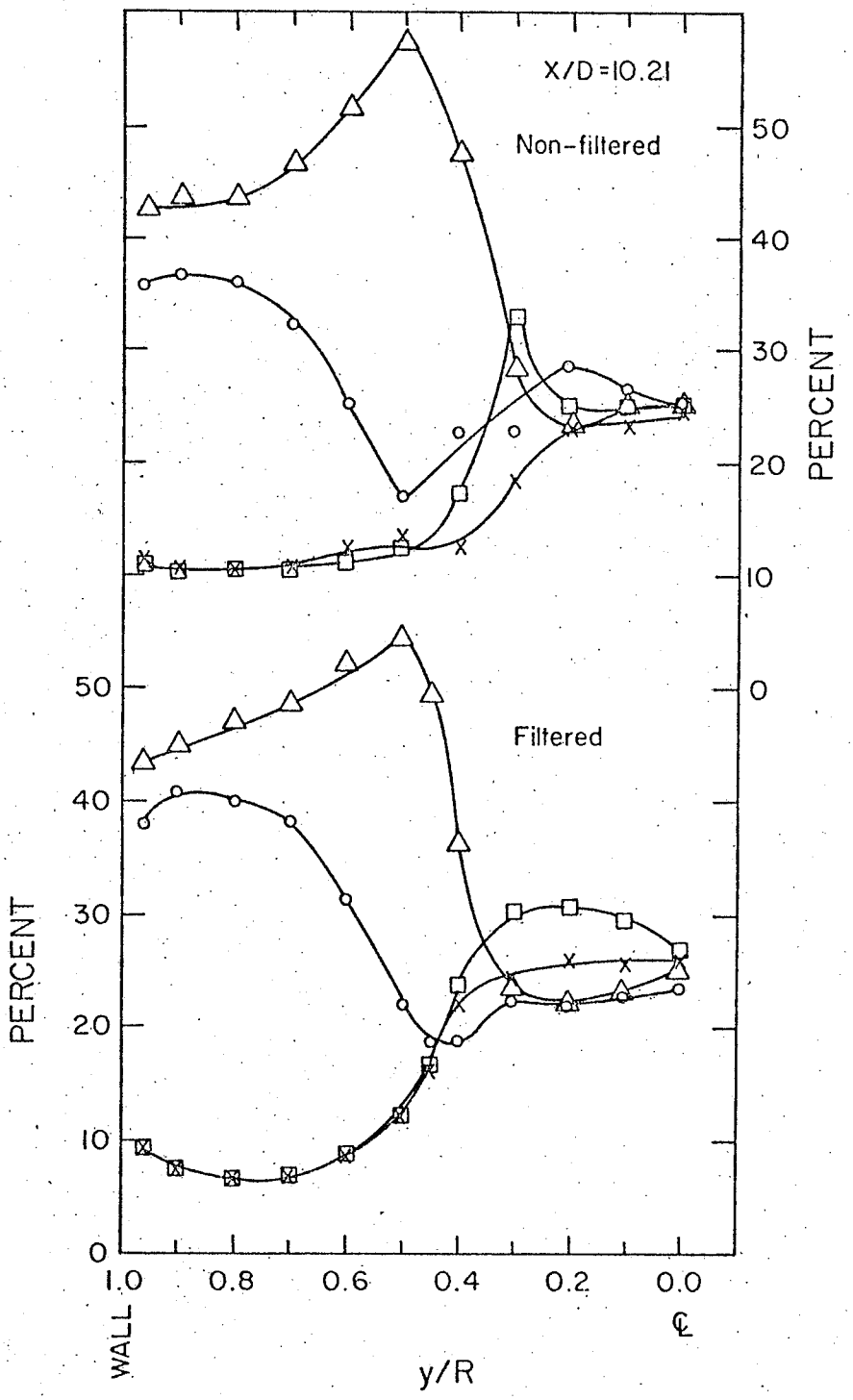

Figure 66. Quadrant conditioned Reynolds stresses for filtered and non-filtered u and v; x/D = 10.21; Re = 54900; symbols as for figure 64.

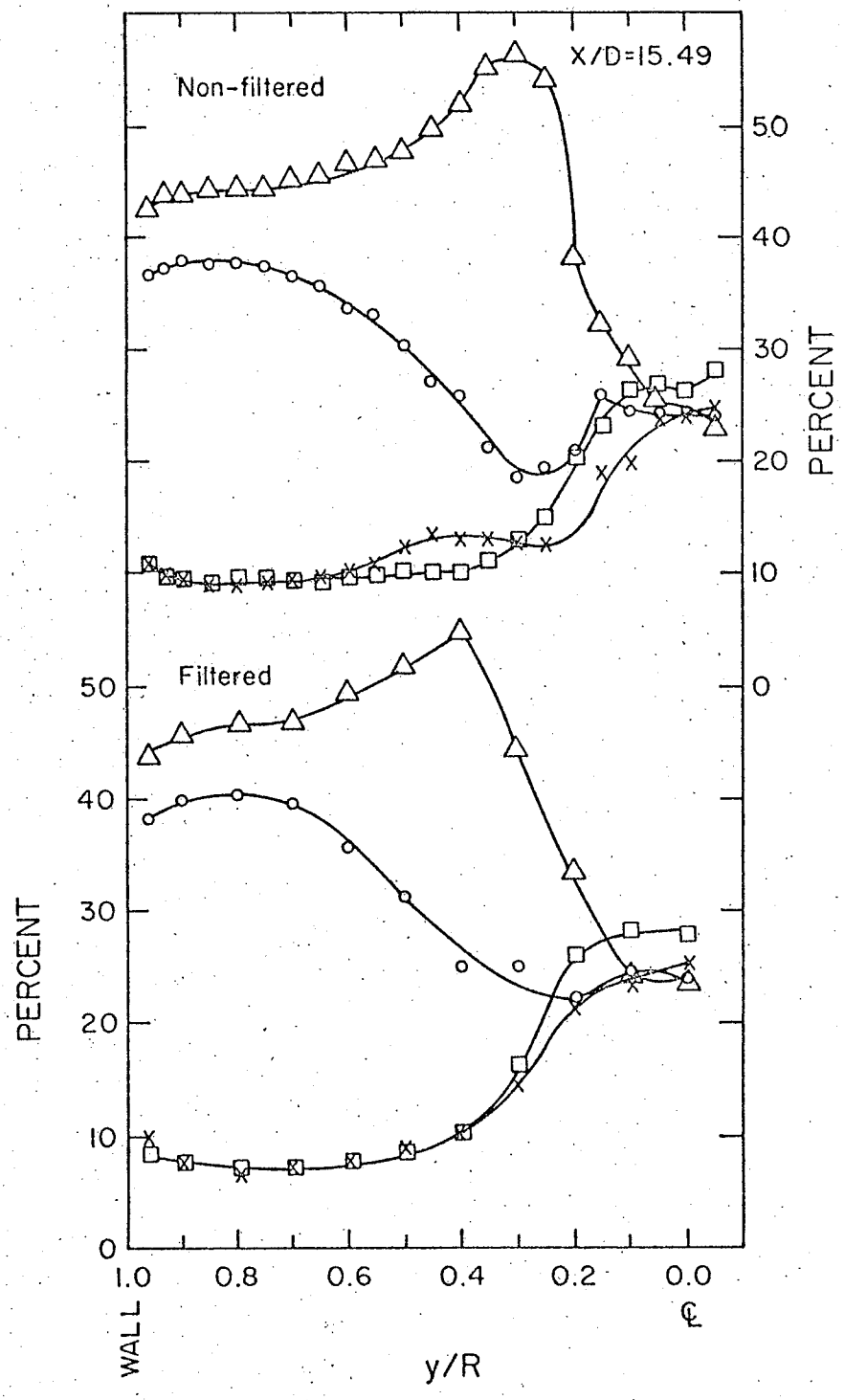

Figure 67. Quadrant conditioned Reynolds stresses for filtered and non-filtered u and v; x/D = 15.49; Re = 54900; symbols as for figure 64.

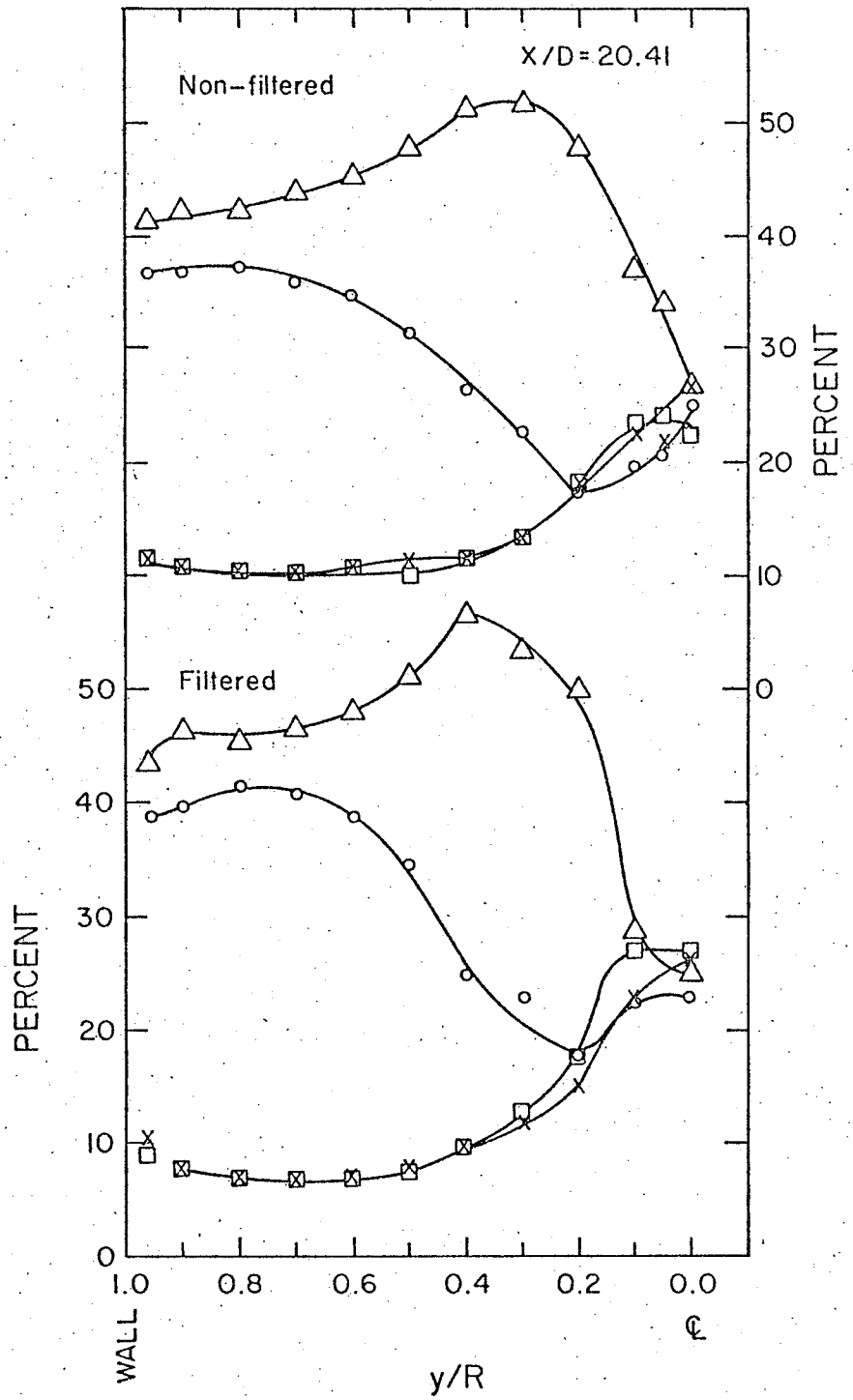

Figure 68. Quadrant conditioned Reynolds stresses for filtered and non-filtered u and v; x/D = 20.41; Re = 54900; symbols as for figure 64.

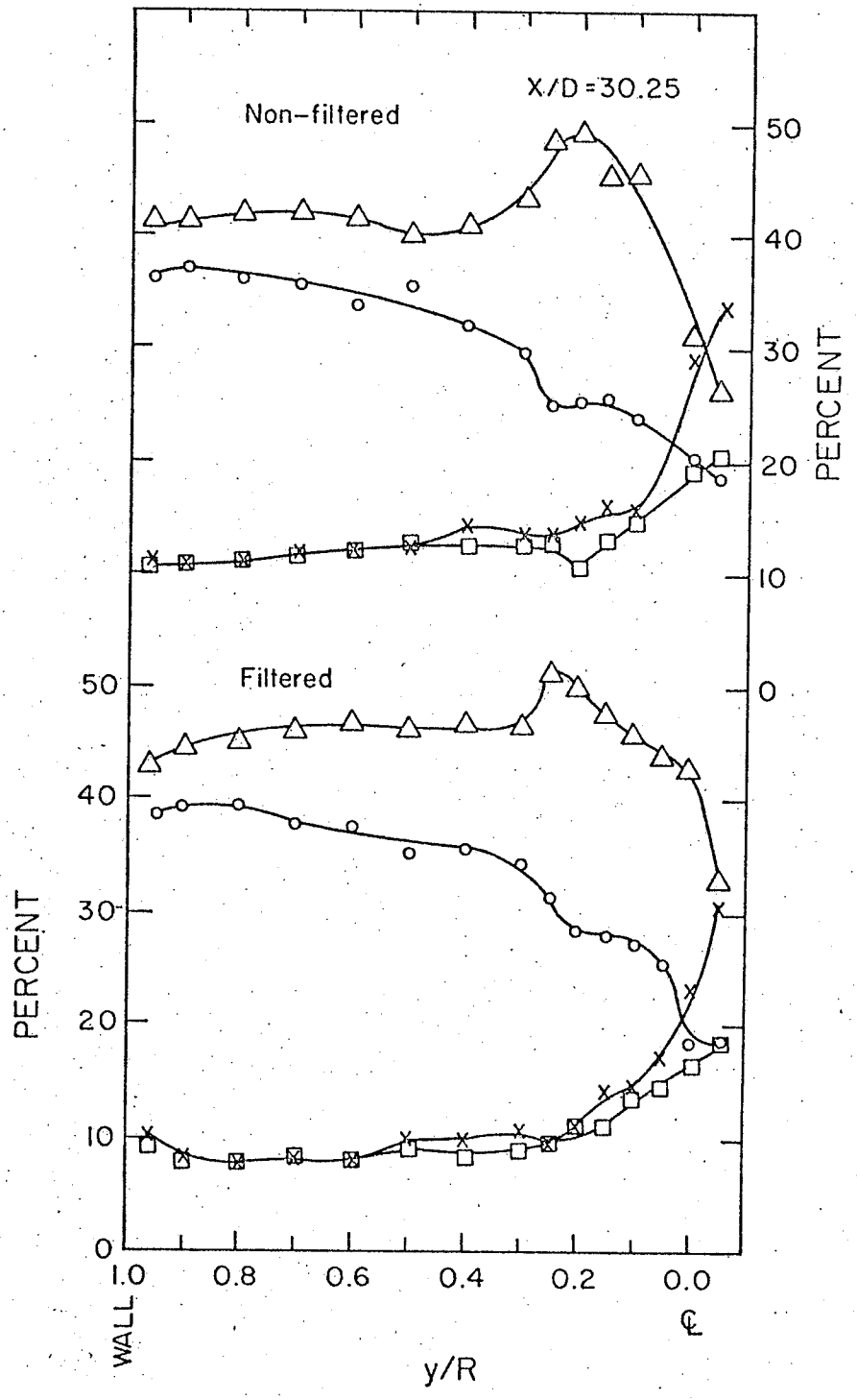

Figure 69. Quadrant conditioned Reynolds stresses for filtered and non-filtered u and v; x/D = 30.25; Re = 54900; symbols as for figure 64.

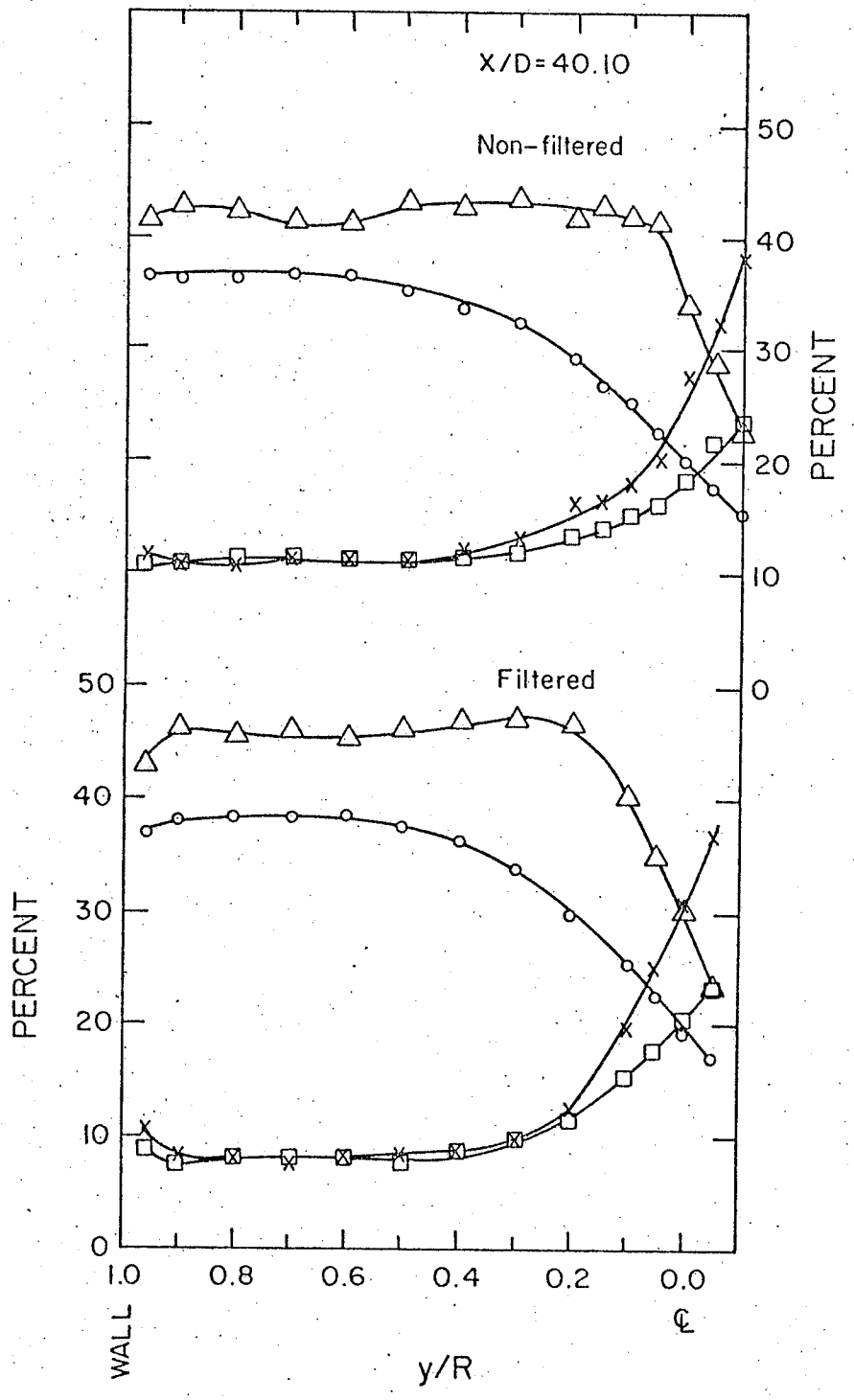

Figure 70. Quadrant conditioned Reynolds stresses for filtered and non-filtered u and v; x/D = 40.10; Re = 54900; symbols as for figure 64.

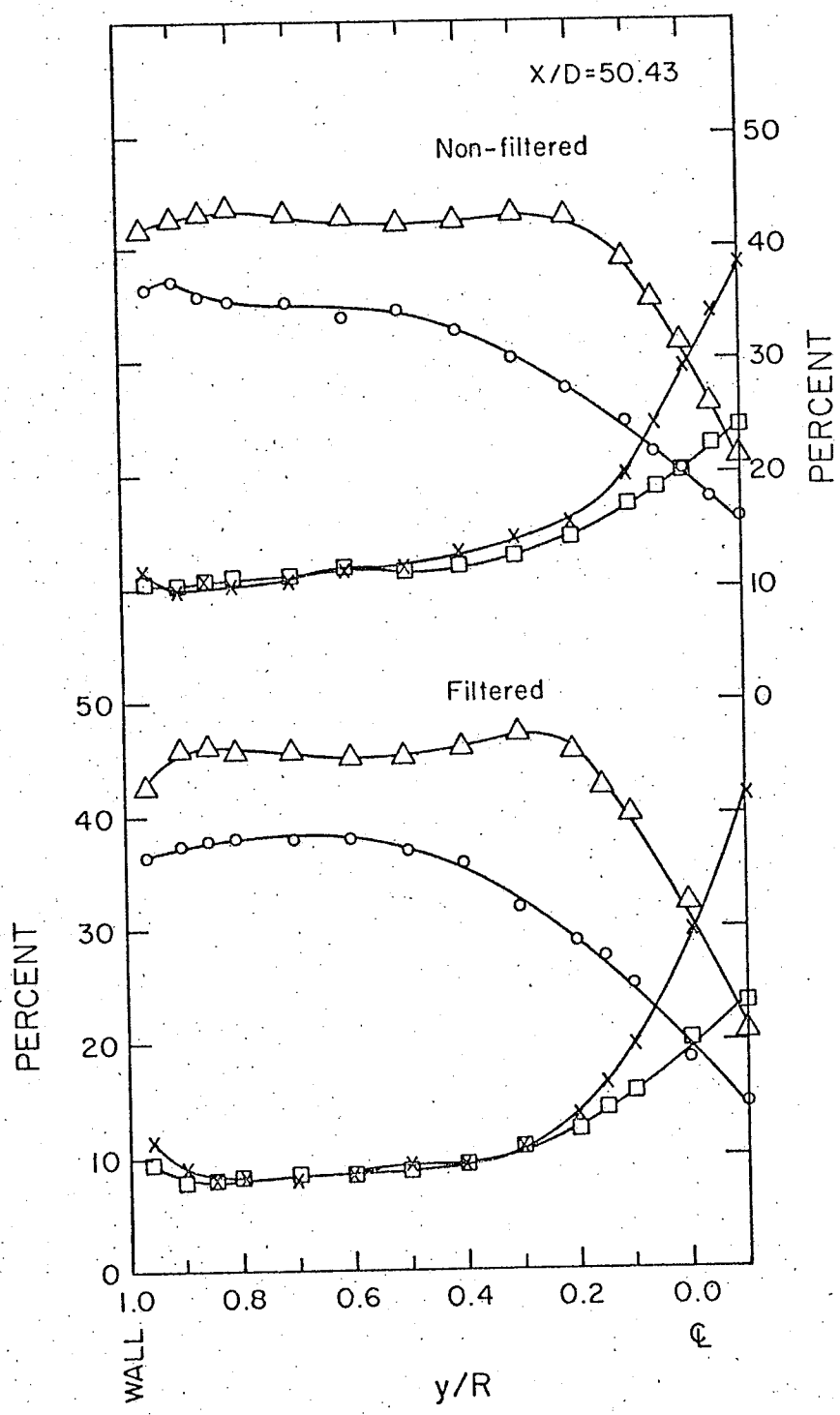

Figure 71. Quadrant conditioned Reynolds stresses for filtered and non-filtered u and v; x/D = 50.43; Re = 54900; symbols as for figure 64.

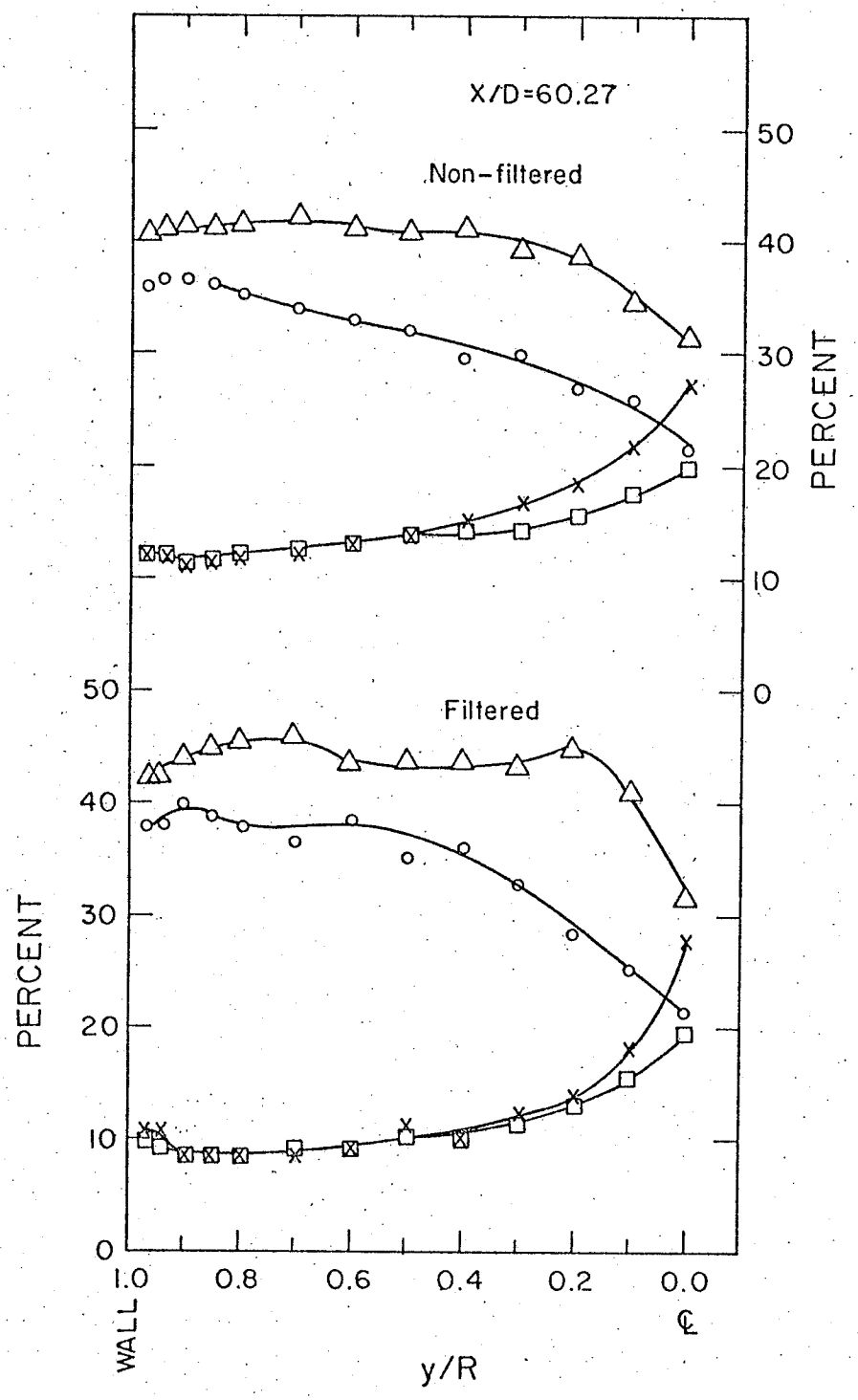

Figure 72. Quadrant conditioned Reynolds stresses for filtered and non-filtered u and v; x/D = 60.27; Re = 54900; symbols as for figure 64.

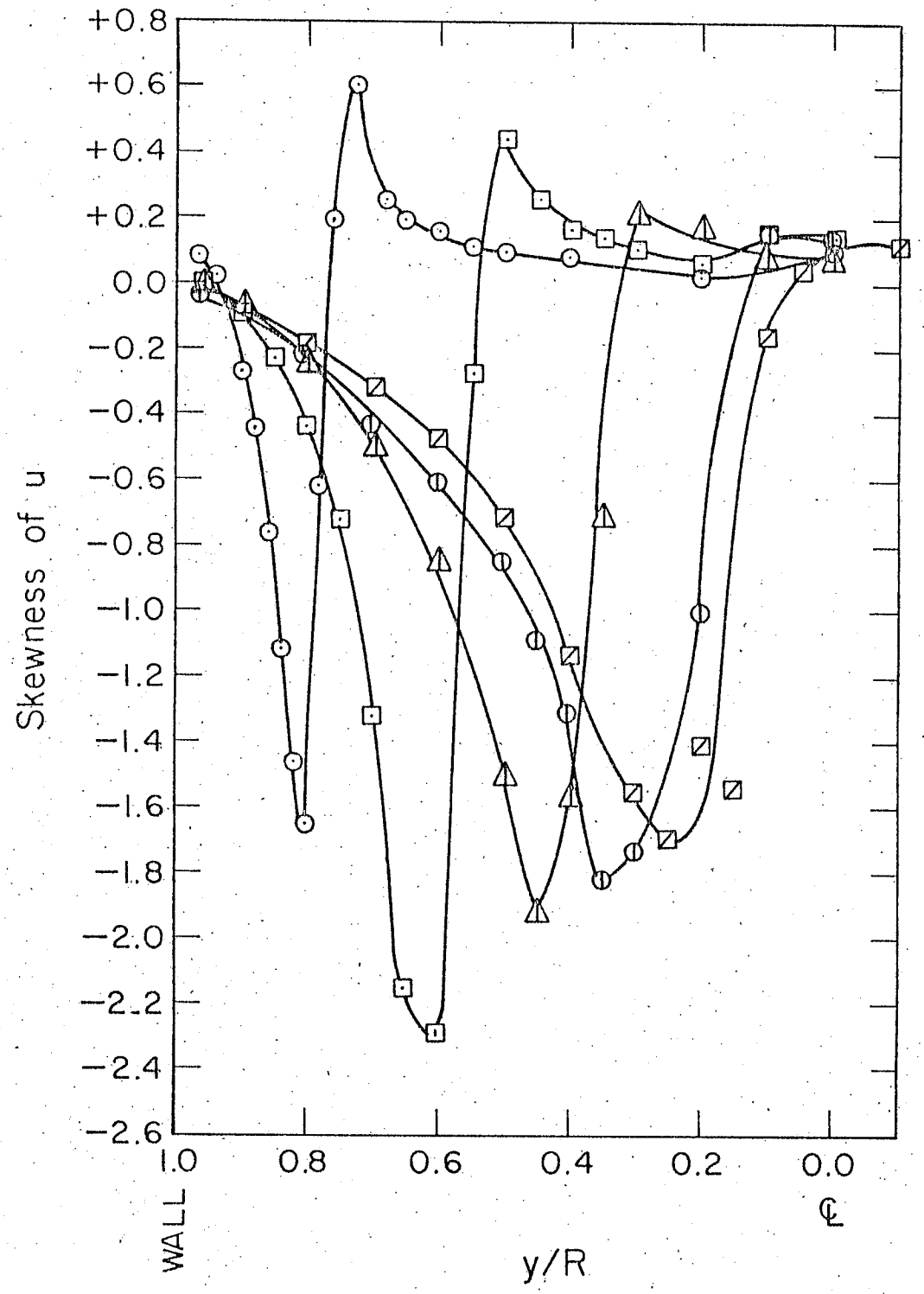

Figure 73. Skewness of nonfiltered u in the interaction region, S_u; Re = 54900; symbols as for figure 87.

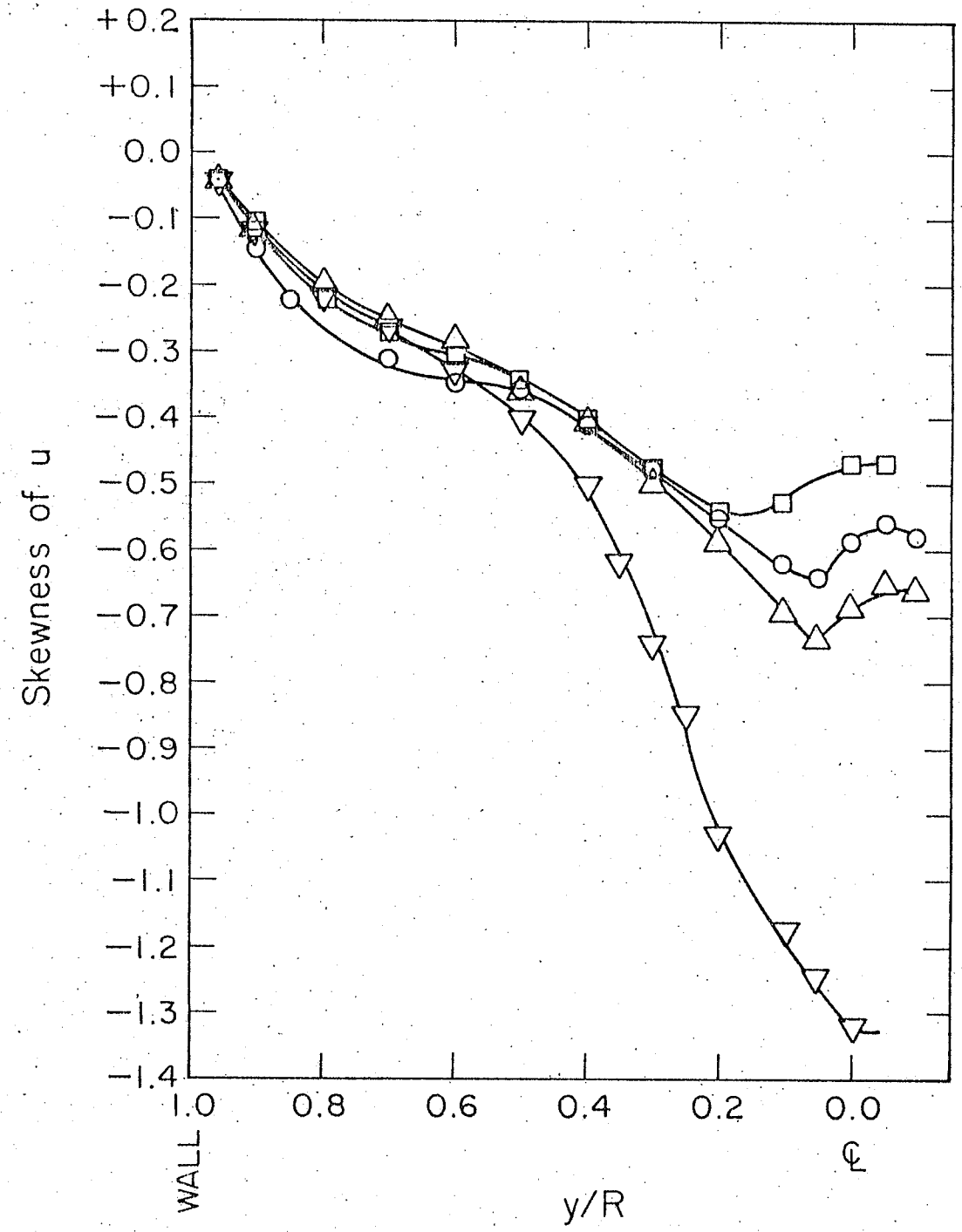

Figure 74. Skewness of nonfiltered u in the recovery region, S_u; Re = 54900; symbols as for figure 87.

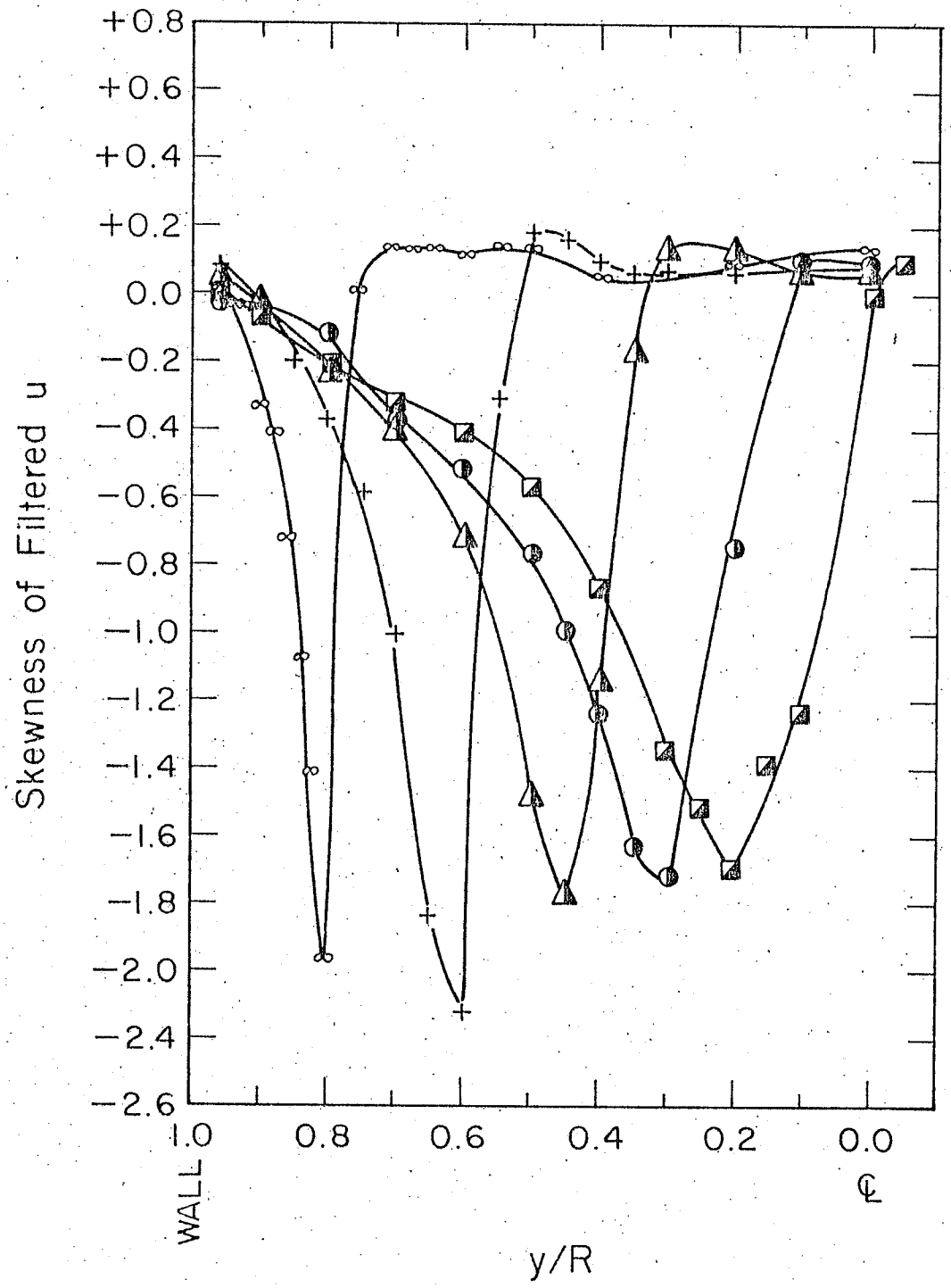

Figure 75. Skewness of filtered u in the interaction region, S_u; Re = 54900; symbols as for figure 88.

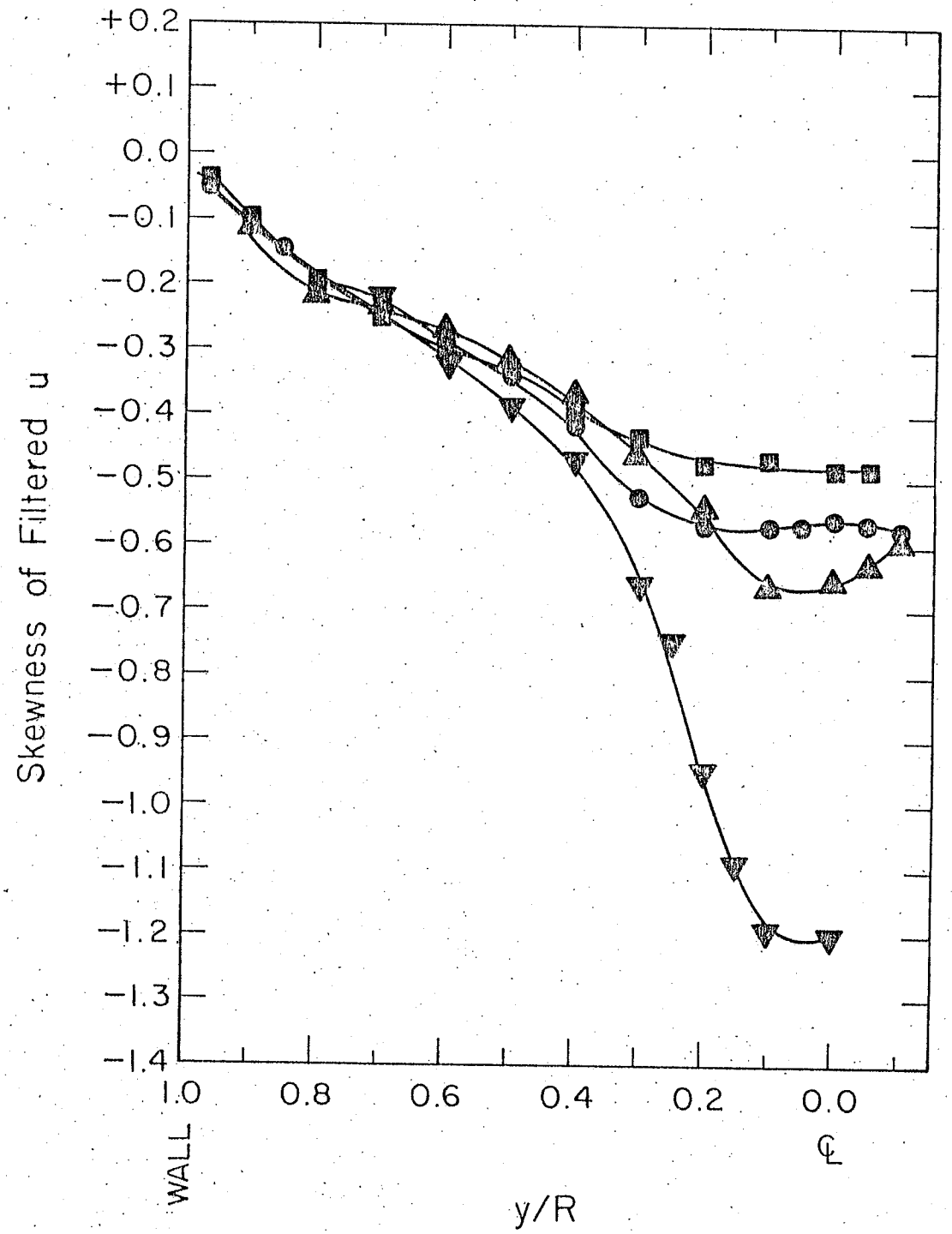

Figure 76. Skewness of filtered u in the recovery region, S_u; Re = 54900; symbols as for figure 88.

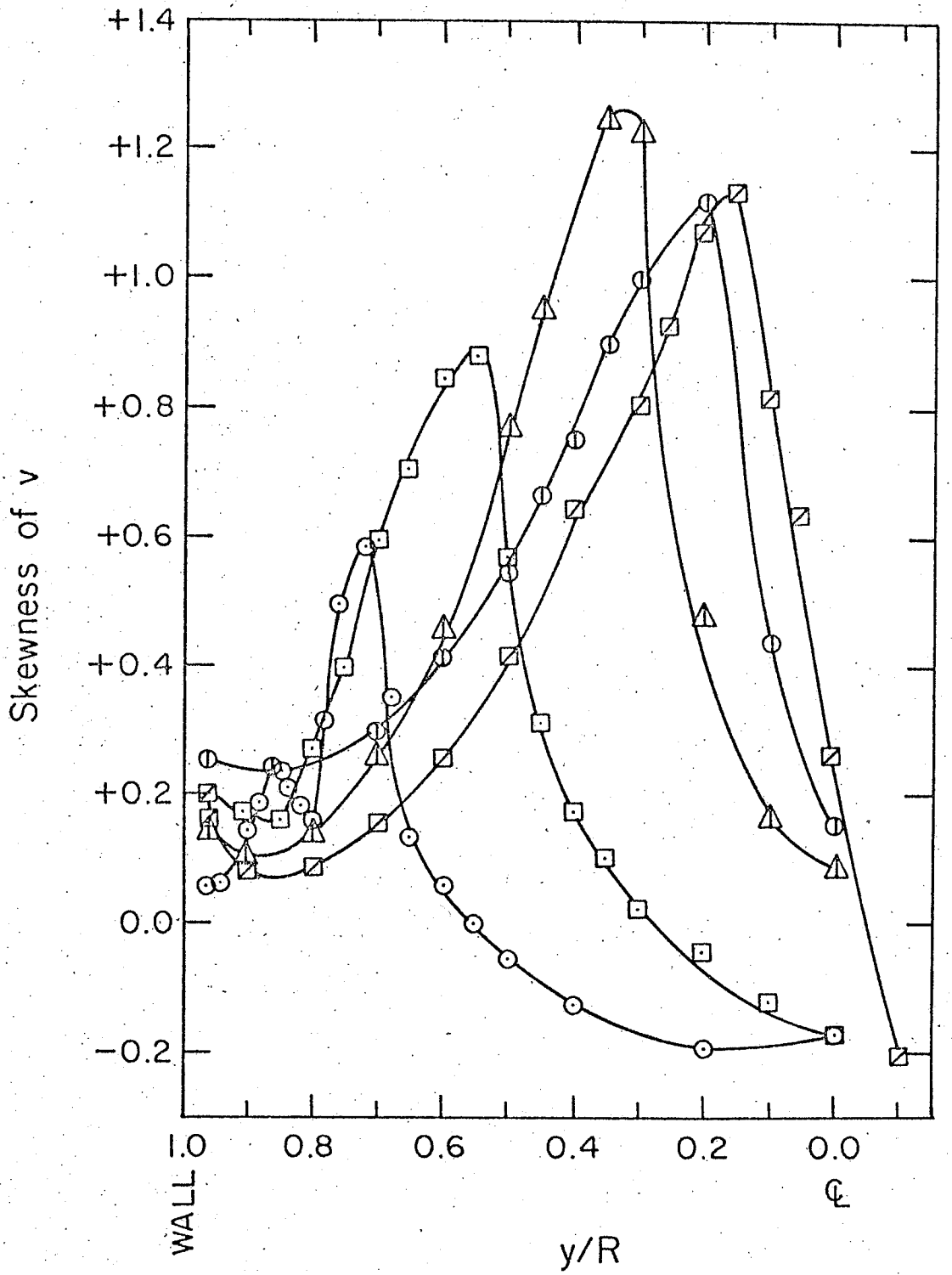

Figure 77. Skewness of nonfiltered v in the interaction region, S_v; Re = 54900; symbols as for figure 87.

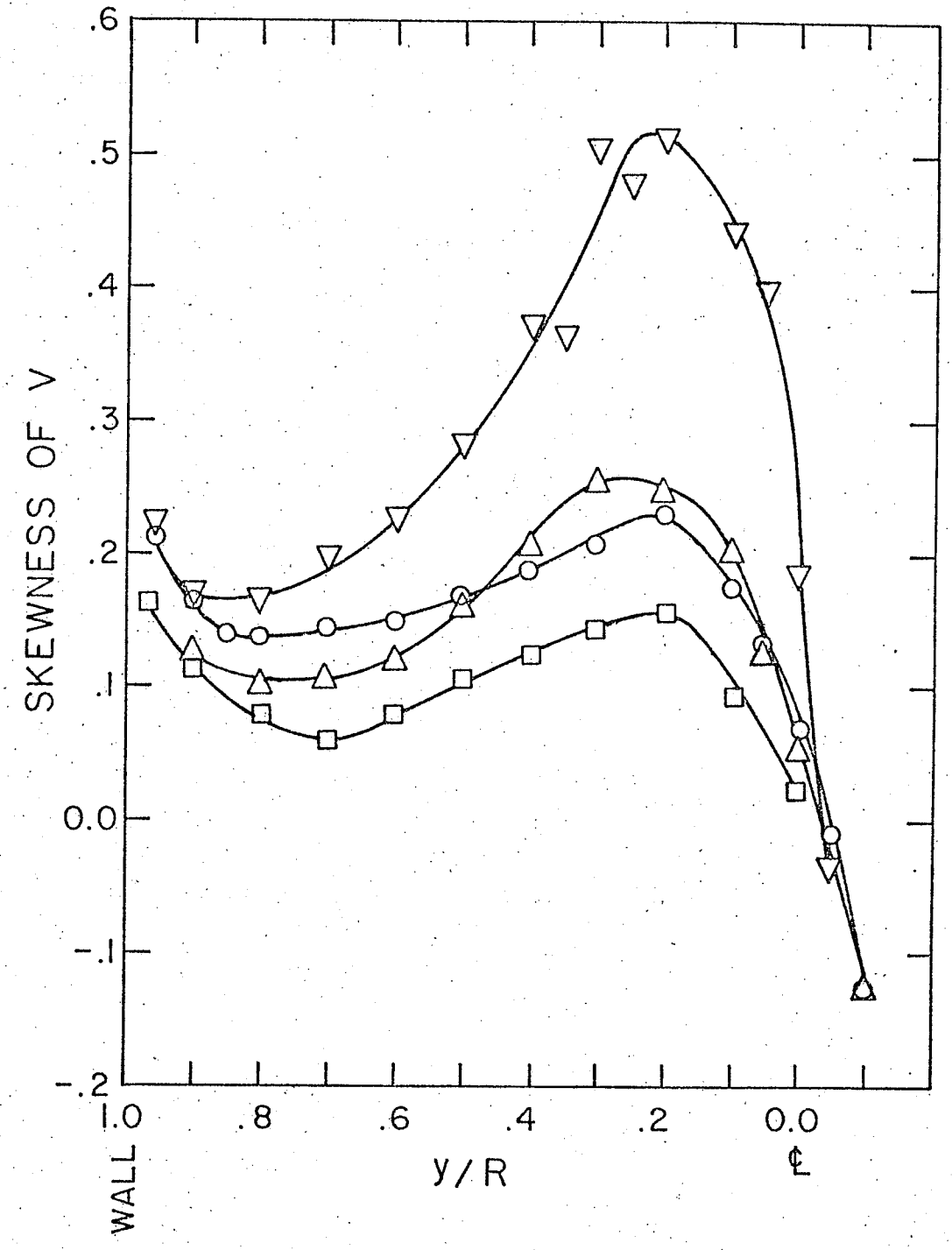

Figure 78. Skewness of nonfiltered v in the recovery region. S_v; Re = 54900; symbols as for figure 87.

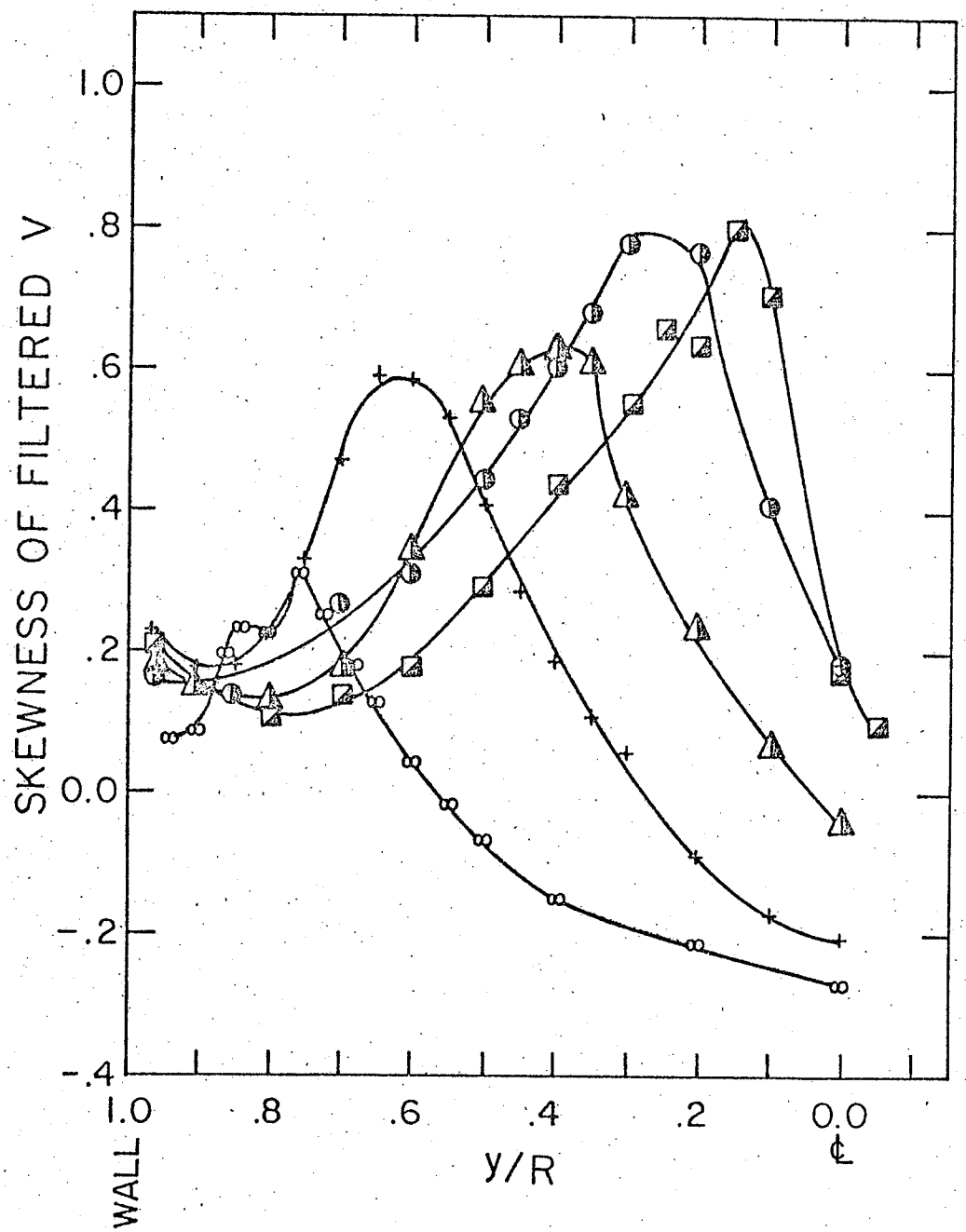

Figure 79. Skewness of filtered v in the interaction region, S_v; Re = 54900; symbols as for figure 88.

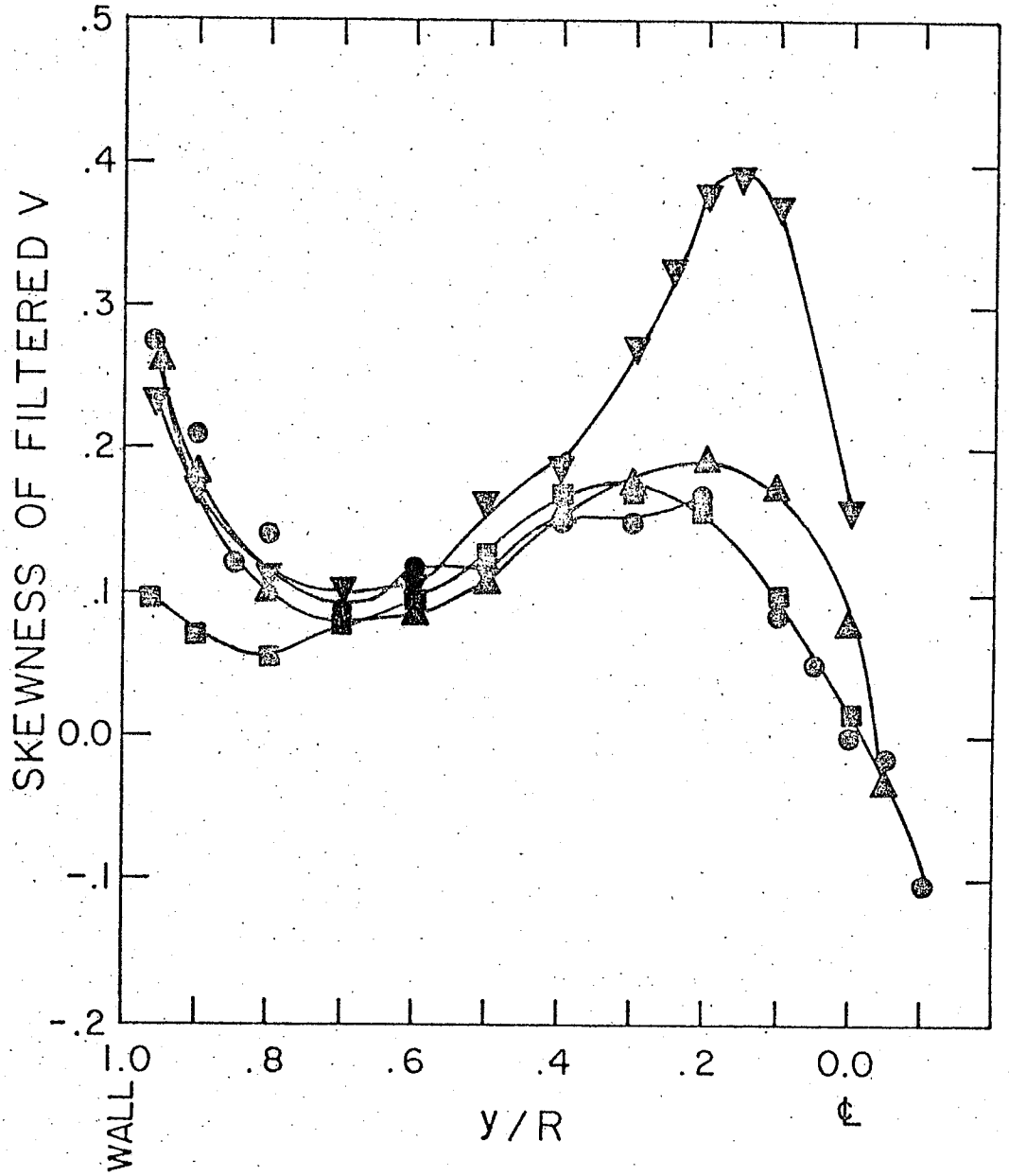

Figure 80. Skewness of filtered v in the recovery region, S_v; Re=54900; symbols as for figure 88.

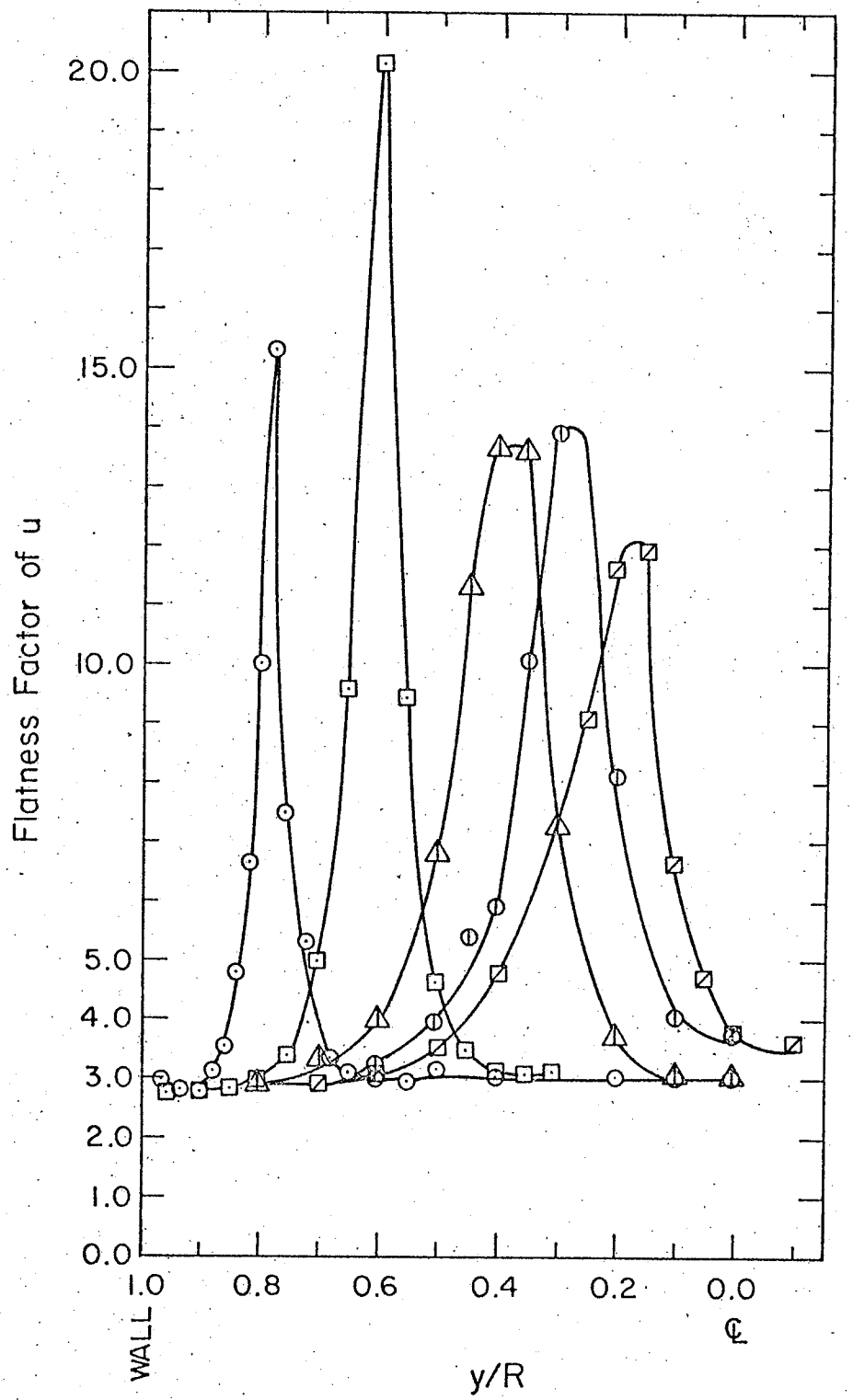

Figure 81. Flatness factor of nonfiltered u in the interaction region F_u; Re = 54900; symbols as for figure 87.

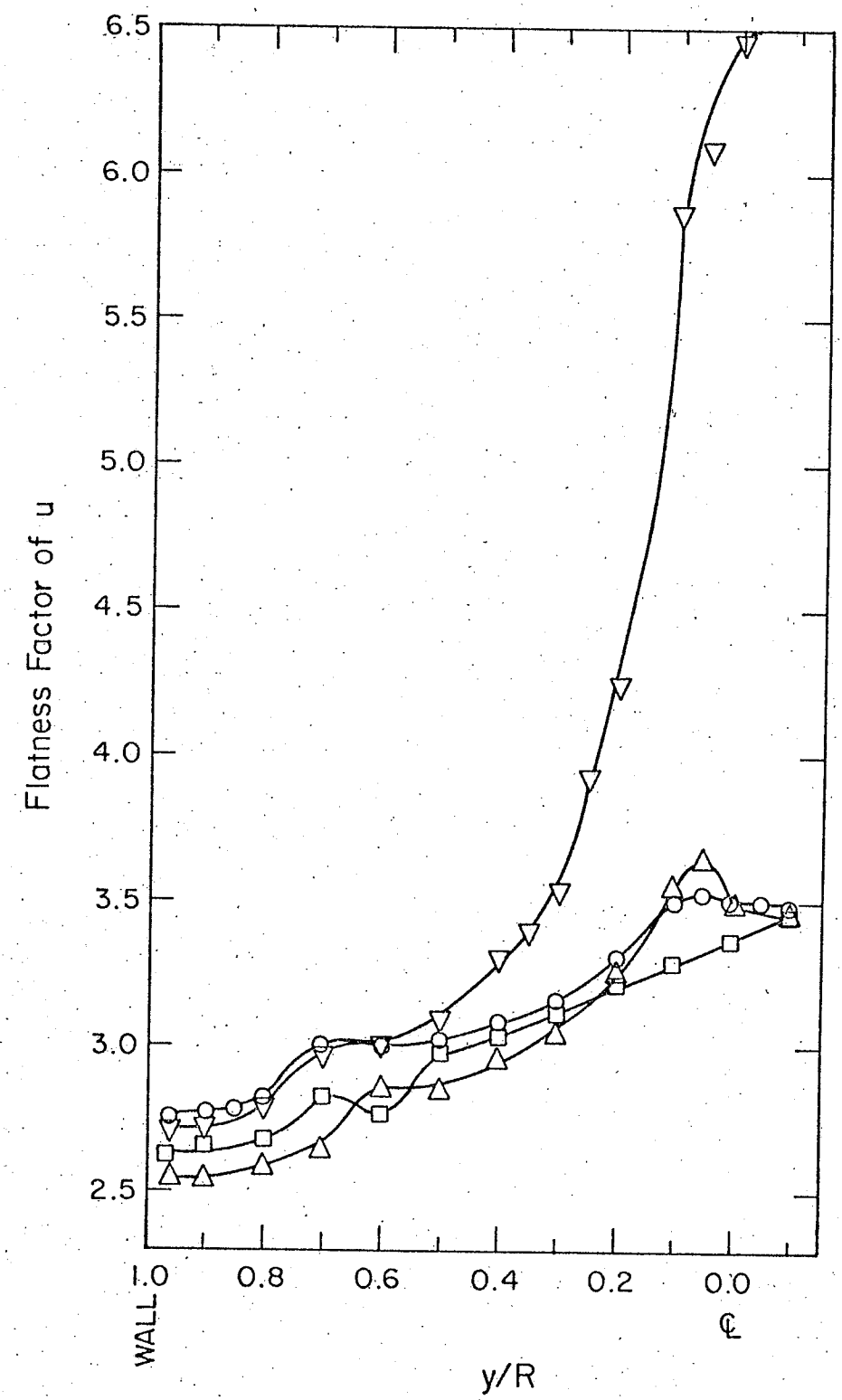

Figure 82. Flatness factor of nonfiltered u in the recovery region, F_u; Re = 54900; symbols as for figure 87.

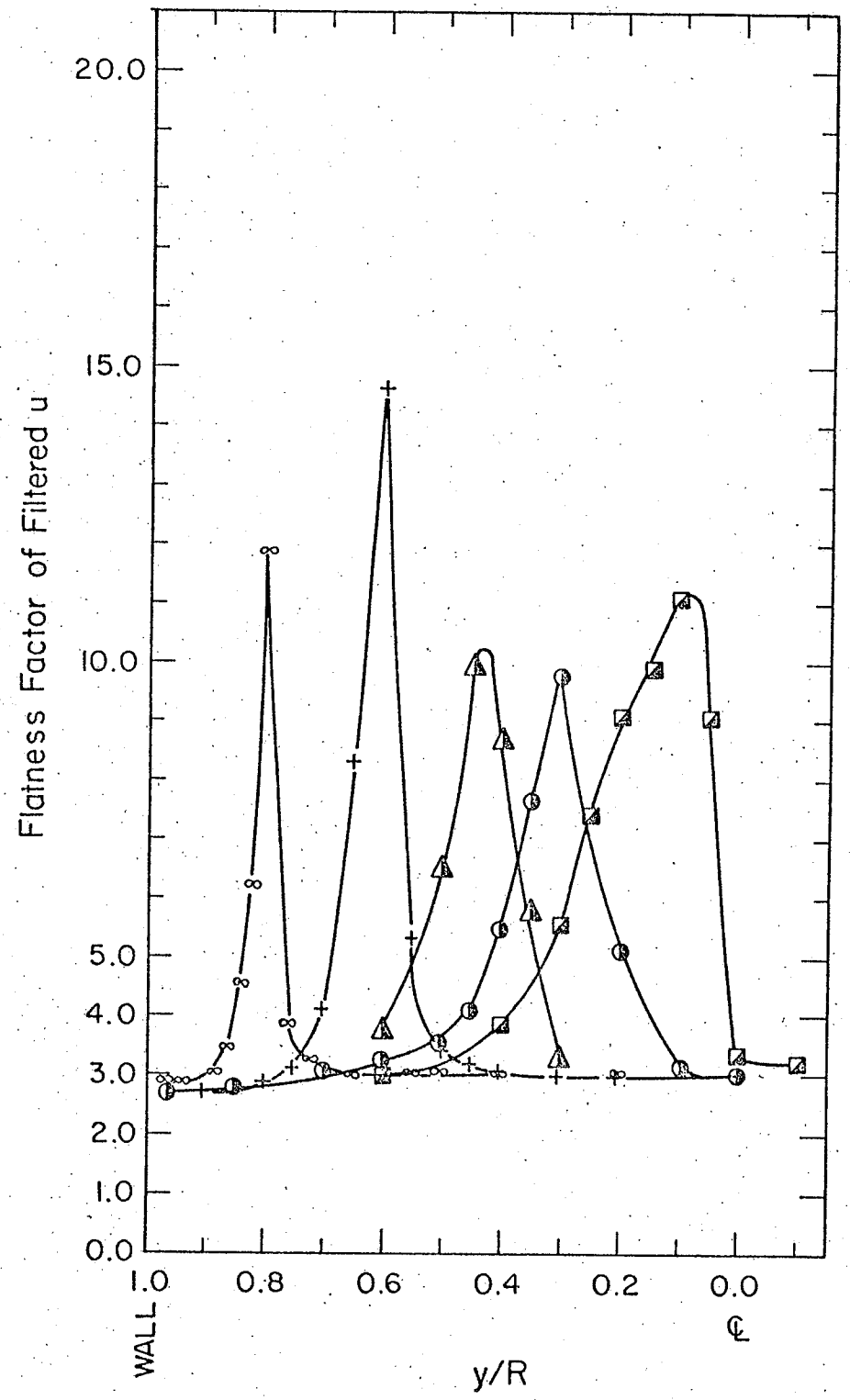

Figure 83. Flatness factor of filtered u in the interaction region, F_u; Re = 54900; symbols as for figure 88.

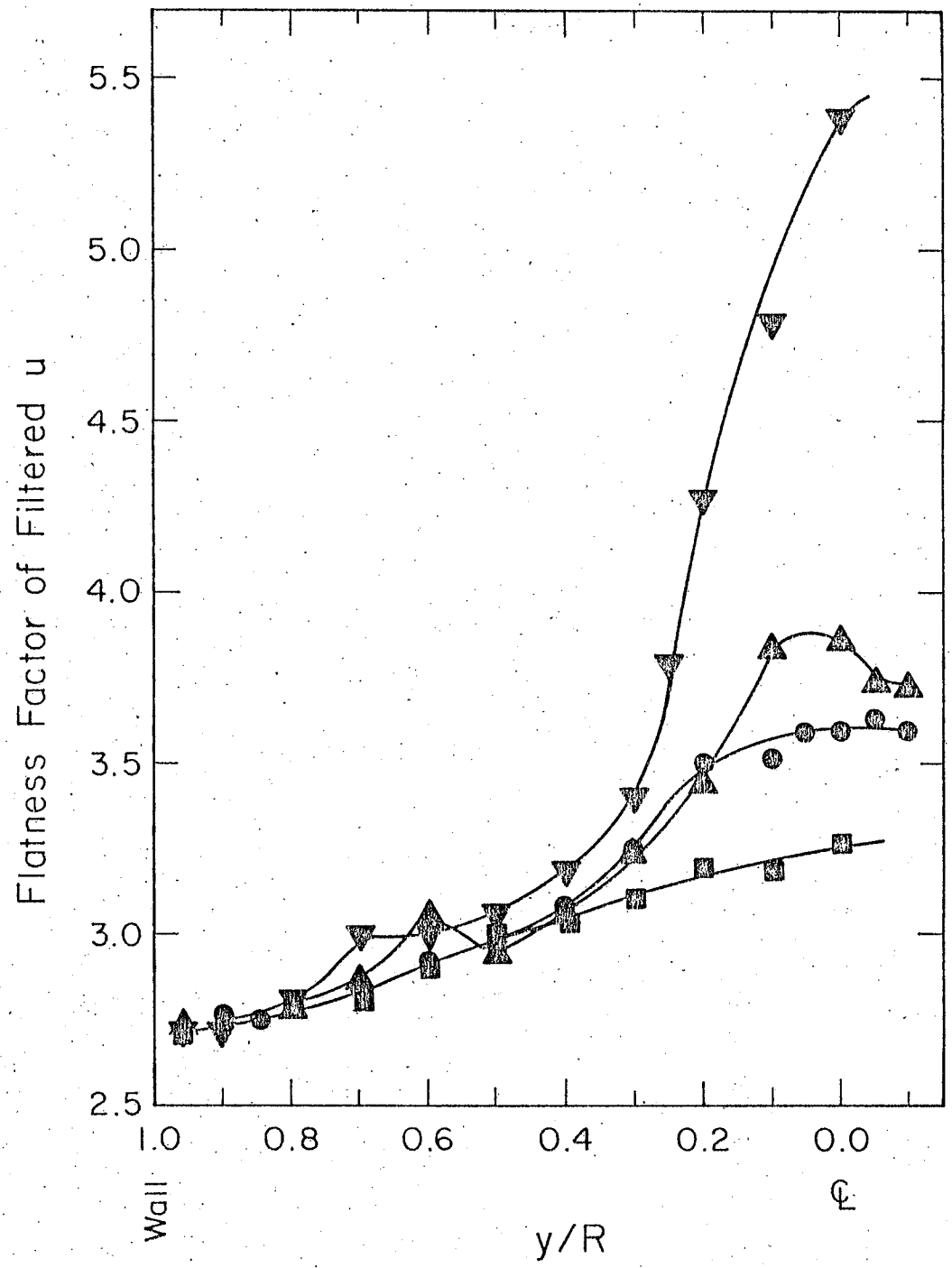

Figure 84. Flatness factor of filtered u in the recovery region, F_u; Re = 54900; symbols as for figure 88.

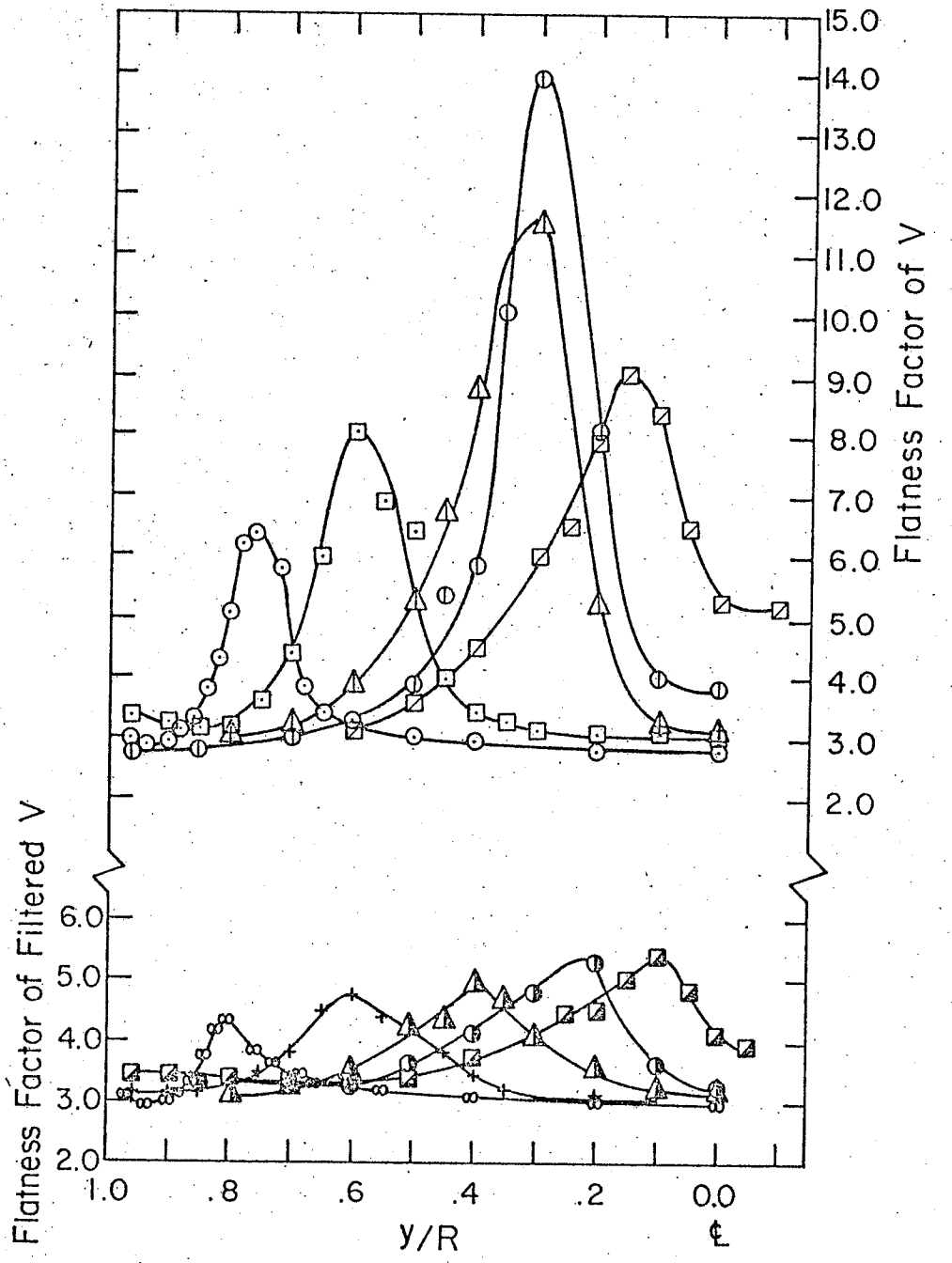

Figure 85. Flatness factor of v, F_v, filtered and nonfiltered, in the interaction region; Re = 54900; symbols as for figures 87 and 88.

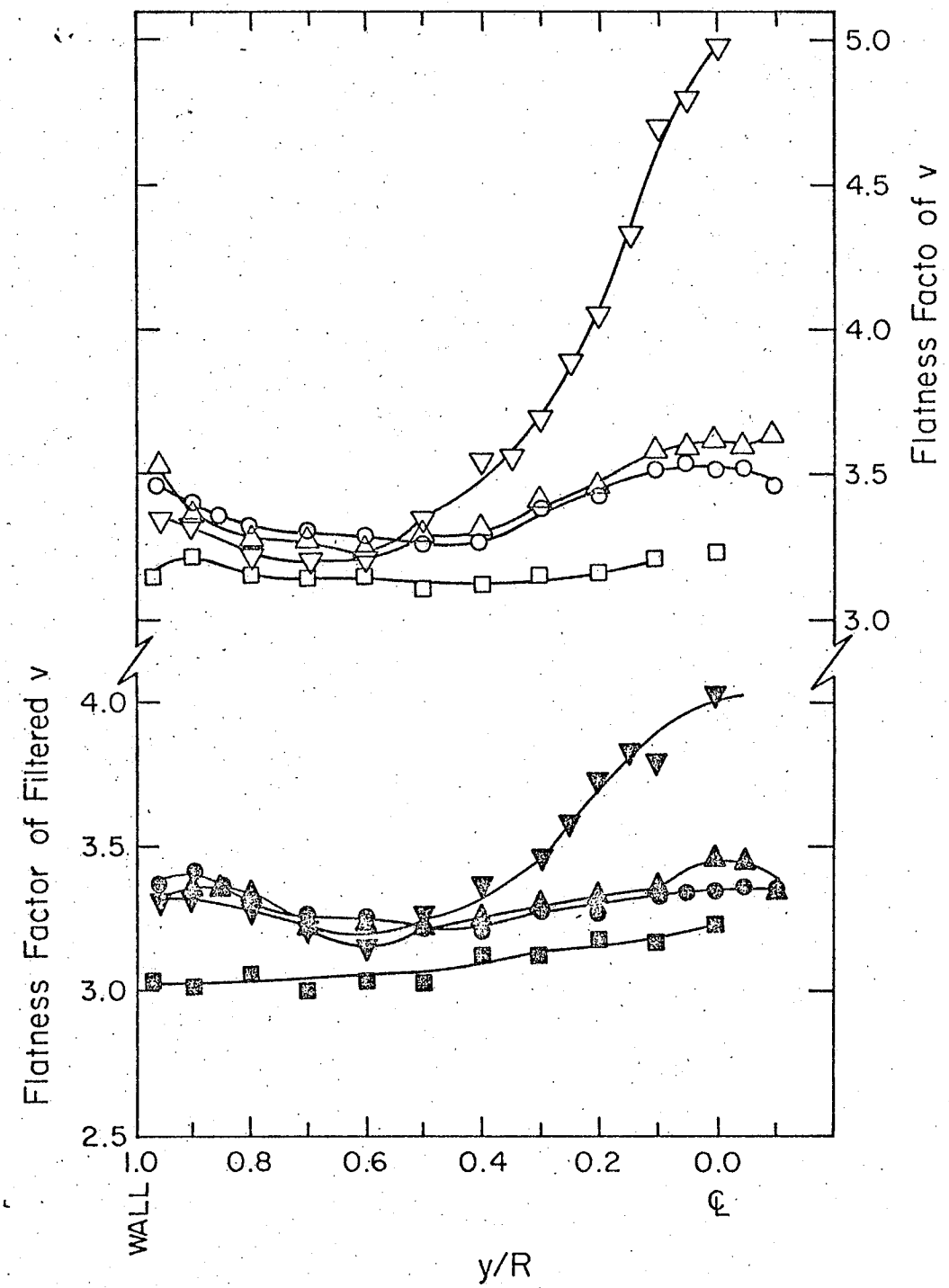

Figure 86. Flatness factor of v, F_v, filtered and nonfiltered, in the recovery region; Re = 54900; symbols as for figures 87 and 88.

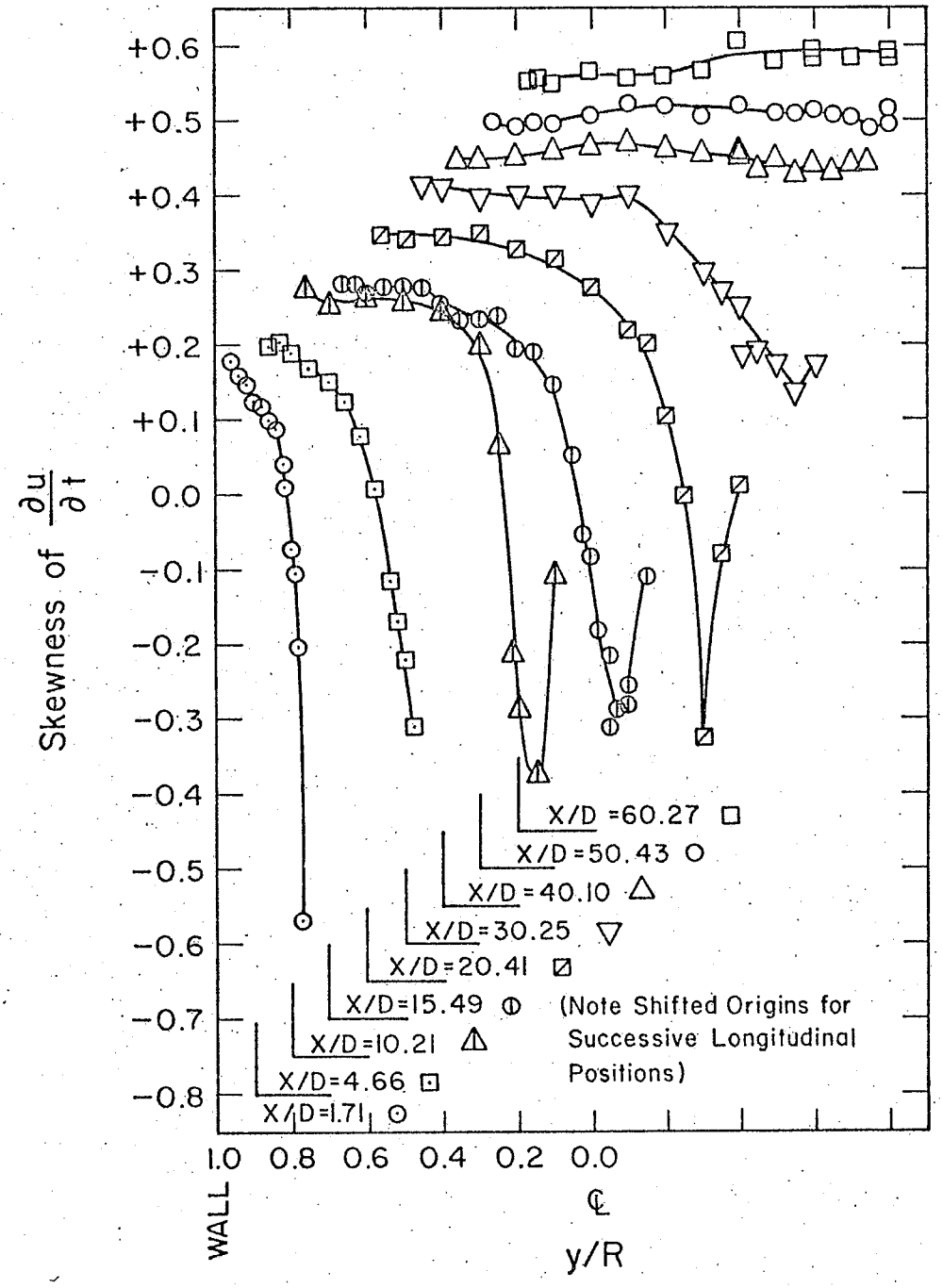

Figure 87. Skewness of time derivative for nonfiltered u, (S coefficient); Re = 54900.

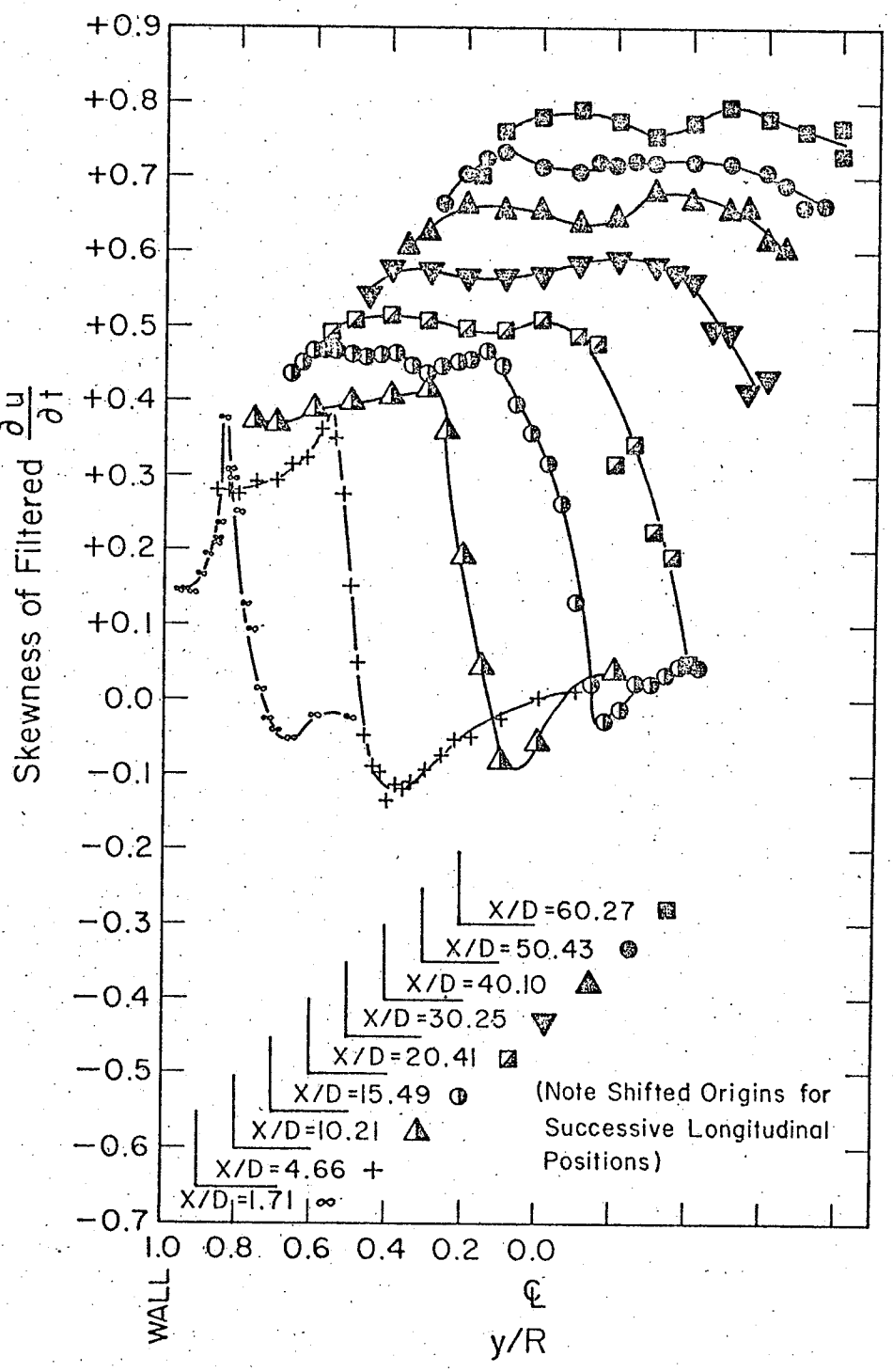

Figure 88. Skewness of time derivative for filtered u, (S coefficient); Re = 54900.

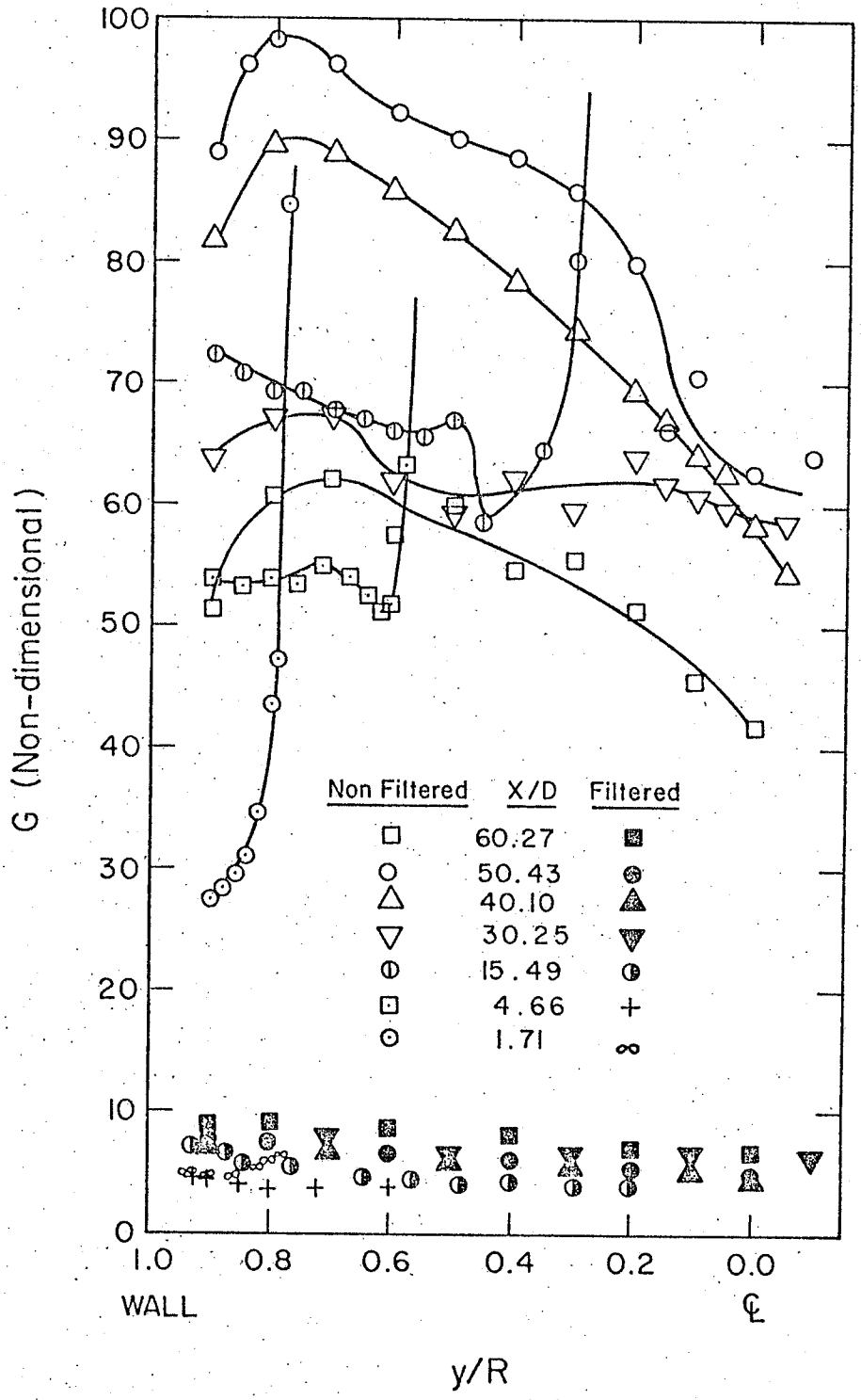

Figure 89. Nondimensionalized second time derivative G coefficient for filtered and nonfiltered u (eqn 8.5); Re = 54900.

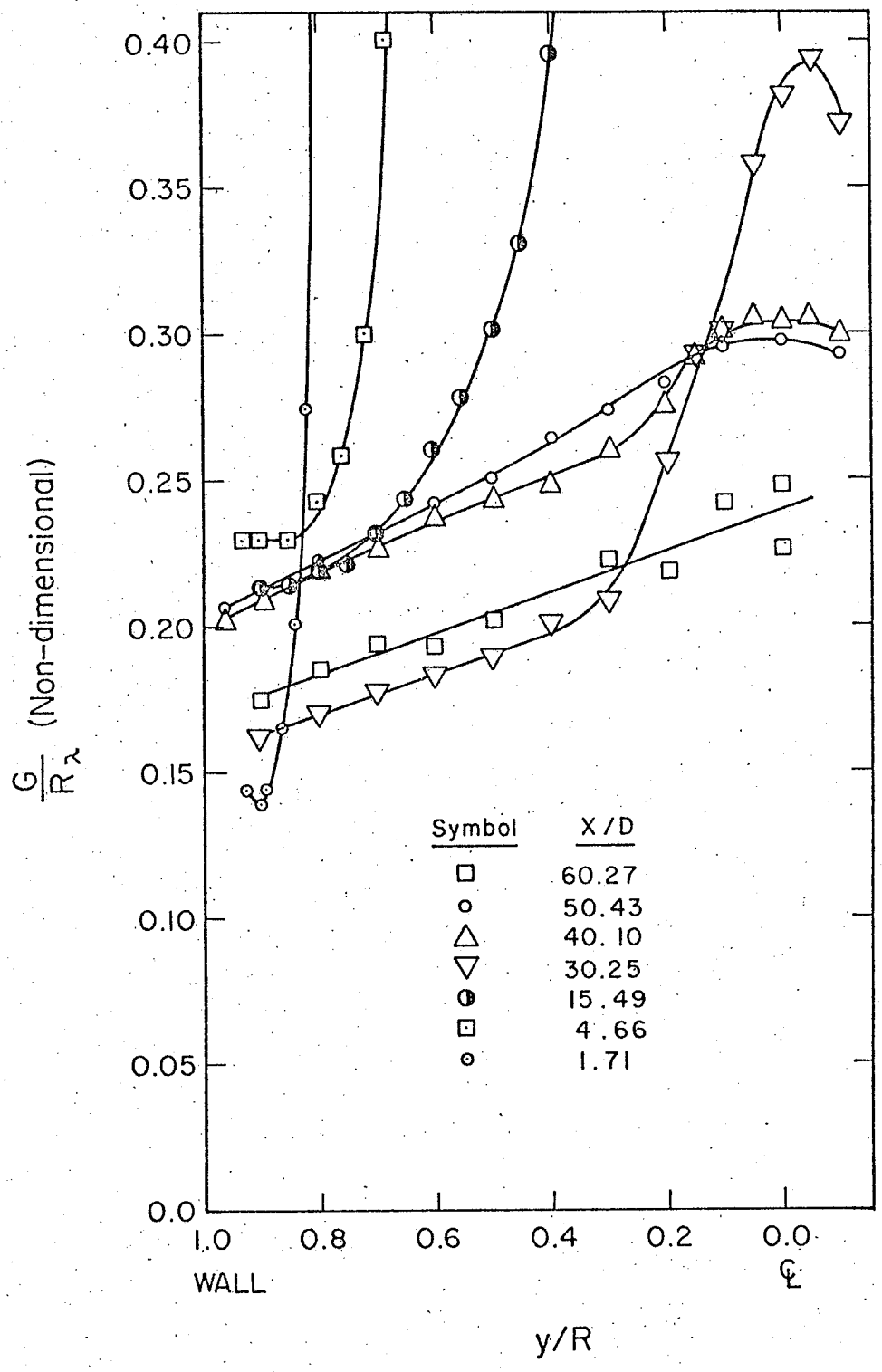

Figure 90. Nondimensional coefficient G/R_λ; (eqn 8.6); Re = 54900.

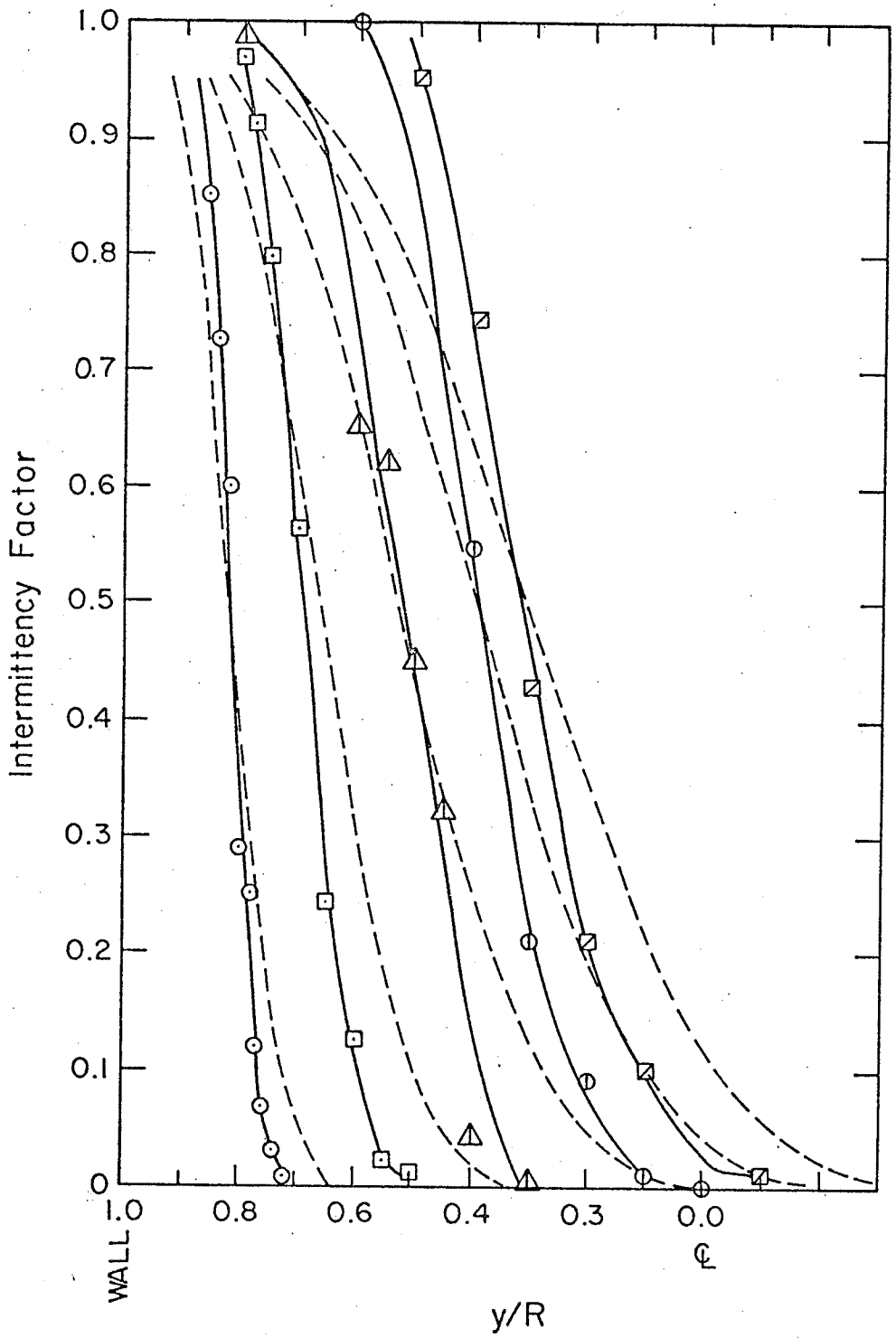

Figure 91. Intermittency factor estimate, γ. Dashed lines computed from eqn. 8.7 Re = 54900; symbols as for figure 87.

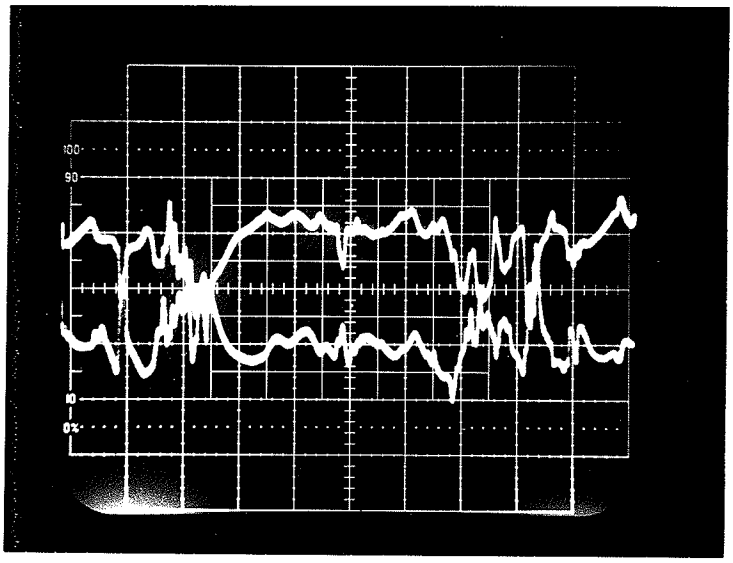

Figure 92(A) (See Table 3)

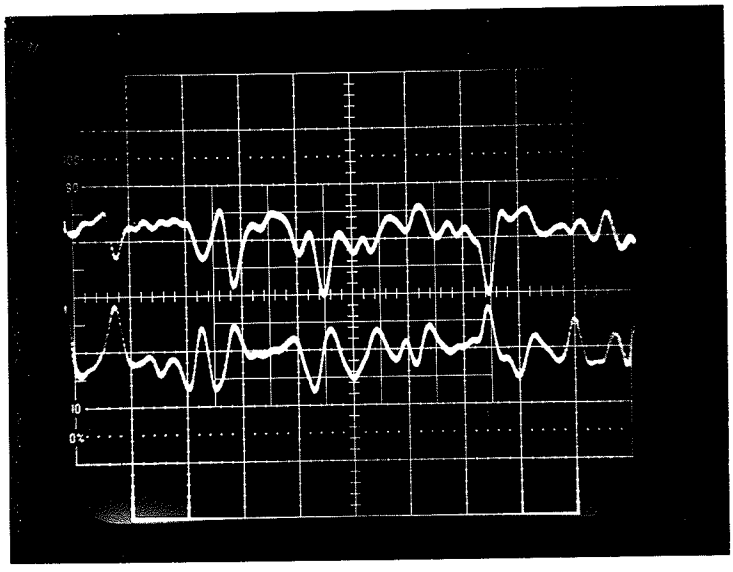

Figure 92(B) (See Table 3)

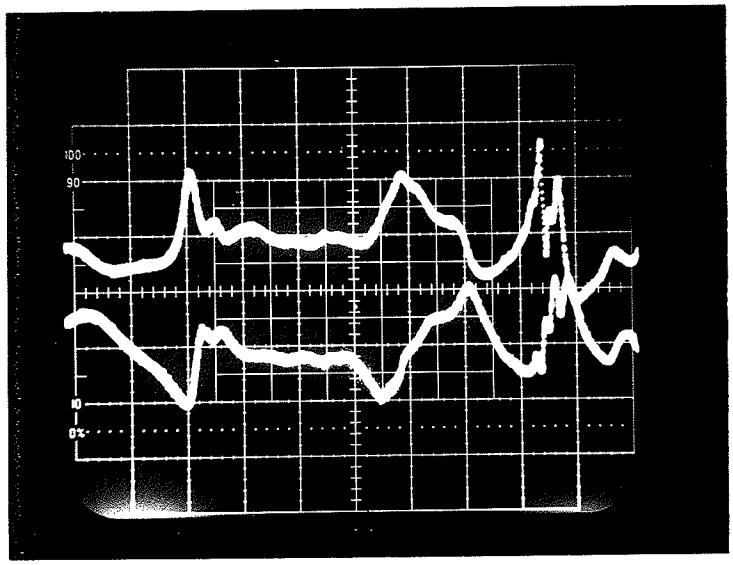

Figure 92(C) (See Table 3)

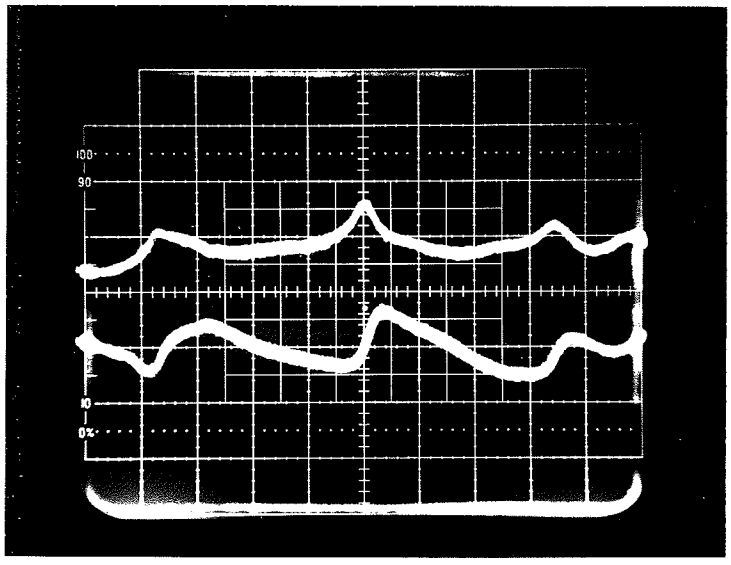

Figure 92(D) (See Table 3)

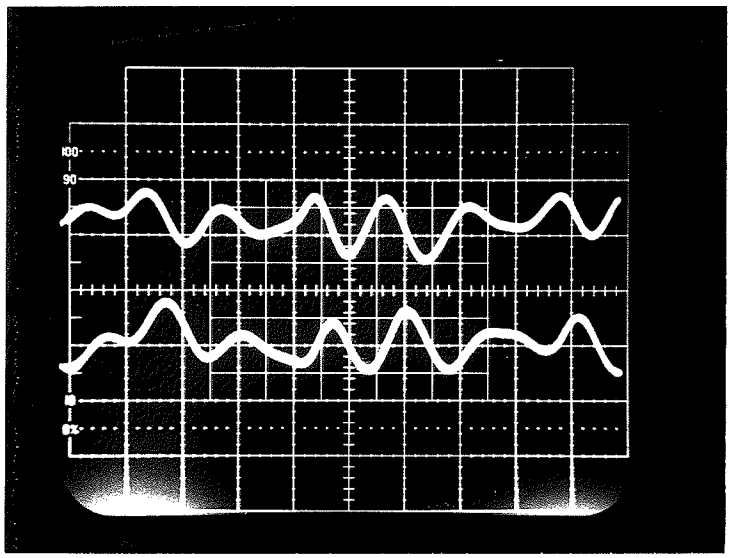

Figure 92(E) (See Table 3)

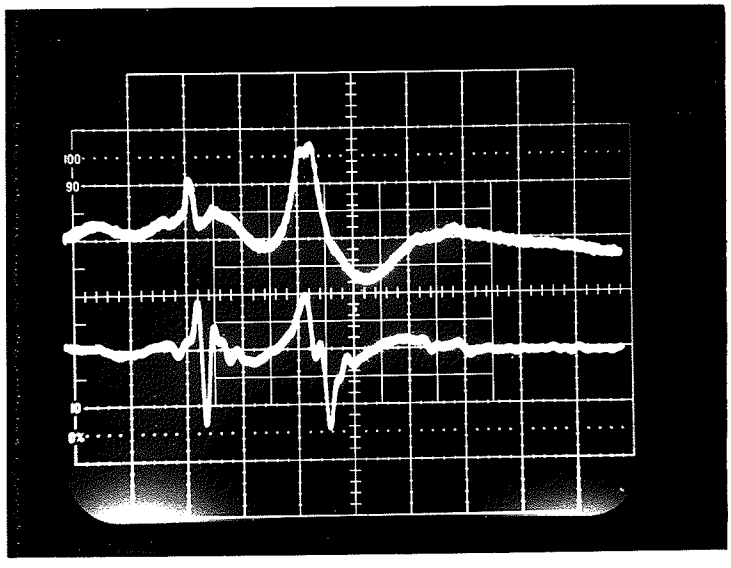

Figure 92(F) (See Table 3)

V I T A

JAMES KEITH REICHERT

Date of Birth: June 8th, 1949
Place of Birth: St. Boniface, Manitoba
Citizenship: Canadian

EDUCATION: Elementary and Jr. High education in Winnipeg School Division schools. Senior matriculation from West Kildonan Collegiate. Entered the Faculty of Science at The University of Manitoba in September, 1966, taking liberal arts subjects plus major programs in Mathematics and Physics. Dean's Honour Roll 1968 and 1969. Awarded B.Sc. in May, 1969. May, 1971, completed a two-year pre-M.Sc. program in Department of Physics, The University of Manitoba. September, 1971, entered M.Sc. program in Mechanical Engineering studying heat transfer and fluid mechanics. Awarded M.Sc. in February, 1974. Financial support through an N.R.C. Postgraduate Scholarship.

EMPLOYMENT:

Summer 1974	- Armaments Division, Defence Research Establishment, Val Cartier, P.Q.
Summers 1972 and 1971	- Whiteshell Nuclear Research Establishment, Atomic Energy of Canada.
Summer 1970	- Texaco Exploration Co. of Canada.
Summers 1969 and 1968	- Meteorological Branch, Canada Department of Transport.